La maurocalcine : substance naturelle d'intérêt thérapeutique

Céline Tisseyre

UNIVERSITÉ DE GRENOBLE

THÈSE

Pour obtenir le grade de

DOCTEURE DE L'UNIVERSITÉ DE GRENOBLE

Spécialité : **Biotechnologie**

Présentée par

Céline Tisseyre

Thèse dirigée par **Michel de Waard**

Préparée au sein de **l'Institut des Neurosciences de Grenoble**
et de l'**Ecole Doctorale Chimie et Sciences du Vivant**

La maurocalcine : substance naturelle d'intérêt thérapeutique

Thèse soutenue publiquement le **12 mai 2014**,
Devant le jury composé de :

M. Stefan Nonchev
Professeur de l'Université Joseph Fourier, Président

Mme Sandrine Sagan
Directrice du Laboratoire des BioMolécules, UPMC, Rapporteuse

M. Denis Servent
Directeur de recherche au Laboratoire de toxinologie moléculaire et biotechnologies, Rapporteur

Mme Muriel Cuendet
Professeure Associée à l'Ecole des Sciences Pharmaceutiques de l'Université de Genève, Examinatrice

M. Michel De Waard
Directeur de recherche à l'Institut des Neurosciences de Grenoble, Directeur de thèse

"Dans la vie, rien n'est à craindre, tout est à comprendre."

Marie Skłodowska-Curie

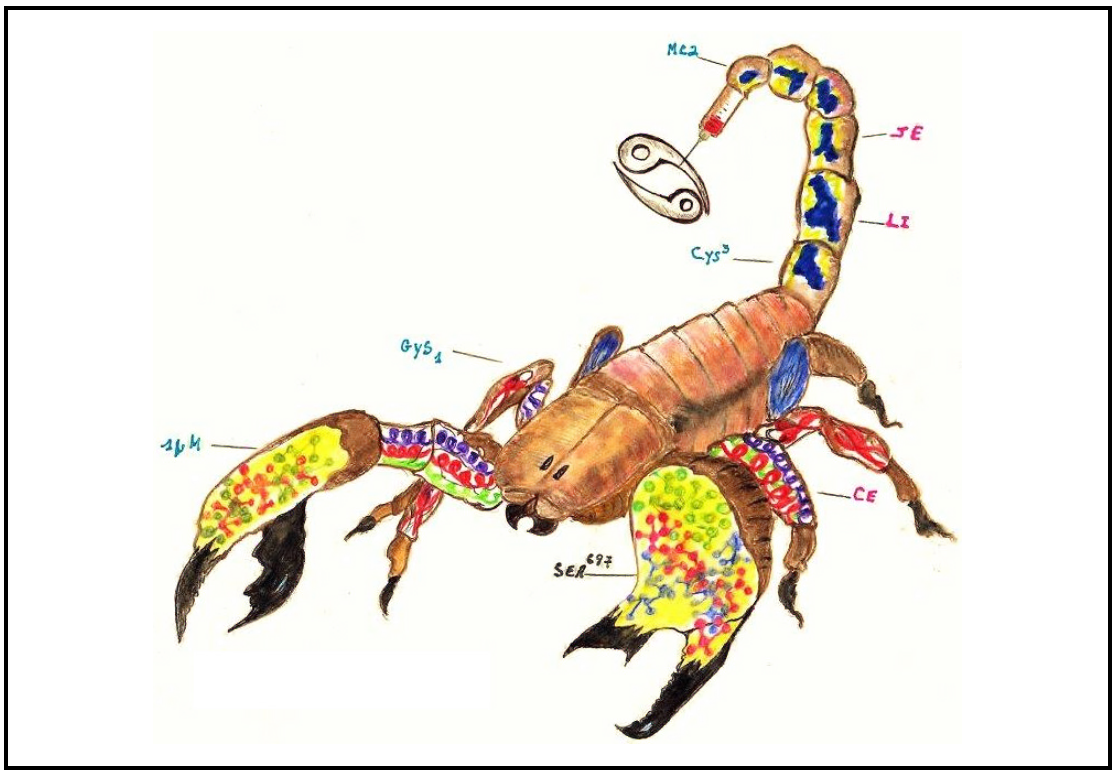

Maurocalcina cancerum luctanti

Ph. T.

Remerciements

Avant toute chose, je me dois de remercier **Michel De Waard** pour m'avoir accueillie au sein de son équipe, et permis de définir avec lui un sujet prolifique à la croisée de nos centres d'intérêt respectifs. Merci de m'avoir donné cette opportunité, sans laquelle il est évident que rien de tout ceci n'aurait eu lieu.

Ce travail est le fruit de nombreuses collaborations et je ne peux citer l'ensemble des personnes avec lesquelles j'ai travaillé, mais je souhaiterais remercier **Chantal Rémy**, **Régine Farion** et **Catherine Ghezzi** pour leur conseil scientifique, leur aide technique ainsi que pour leur précieux soutien moral.

Je tiens à remercier les membres de ce jury pour avoir accepté d'évaluer l'ensemble de mon travail, notamment les rapporteurs **Denis Servent** et **Sandrine Sagan** pour leurs remarques avisées.

Je remercie tout particulièrement **Stefan Nonchev** pour m'avoir fait l'honneur de présider le jury après m'avoir accompagnée avec pédagogie et bienveillance tout au long de mon parcours universitaire. Vos encouragements ne sont pas étrangers à ma persévérance, et je vous en remercie !

Je voudrais remercier les étudiantes de l'équipe : **Lucie**, **Marwa**, **Elodie** et **Nadia** (même si tu es passée du côté obscur du postdoc avant de nous rejoindre !) pour toutes les discussions scientifiques constructives qu'on a pu avoir, mais surtout pour toutes celles au cours desquelles la science a été dramatiquement absente ! Je n'ai qu'un regret : vous avoir attendues pendant plus d'un an. Je vous souhaite le meilleur pour la suite, et beaucoup de mots fléchés à venir !

Un grand merci à **Nath** pour son soutien administratif et amical. Les pauses-café prises sur ta terrasse vont me manquer !

Lucie... **Lucy**. **Lucy**, ça a été un plaisir de travailler avec toi et je suis ravie que ce soit toi qui prennes la suite de ce projet qui aura tellement compté pour moi. Bientôt tu devras toi aussi passer le relais et je te souhaite de tout cœur d'avoir le plaisir de le faire avec quelqu'un d'aussi agréable et intéressant que toi, sur le plan scientifique mais aussi et surtout en dehors. Encore une fois, bon courage pour la suite, tu y es presque ! Il ne te reste "plus" qu'à inspirer un grand coup et te dire : *"Allons-y !"*.

Ces quelques années passées au sein du GIN n'auraient pas été les mêmes sans les belles rencontres que j'ai pu y faire ; elles ont été nombreuses mais je pense surtout à **Mathilde** et **Anouk**, qui sont devenues des amies. Quel que soit l'endroit où vos projets vous mènent, que la vie soit belle et que le vent vous porte !

Agata, my Dear, you deserve *at least* an acknowledgment in English. Thank you so much for your help as well as all the chats, the laughs and the climbing tips. I wish you all the best and truly hope we'll meet again soon !

Les amitiés au sein du labo sont vitales lors d'une thèse, mais celles qui nous soutiennent en dehors le sont au moins tout autant. Je remercie chaleureusement celles qui m'ont apporté d'innombrables moments d'évasion comme autant de bulles d'oxygène qui m'auront, paradoxalement, permis de garder un peu les pieds sur terre : **Amandine**, **Chlox** (♡ LMF ♡), **Gaufrette** (et le petit coquin), **Odile** (et Clément), **Sarah** et **Tiffany**. Merci pour toutes ces soirées, ces fous rires, ces interminables discussions hautement intellectuelles (hem hem), philosophiques (si si, c'est arrivé !) et toujours ô combien salvatrices.

Matthias (ma Cocotte), **Marion** (ma Zette). Mes amis de toujours. Comment vous oublier ? Merci d'être là, tout simplement.

Je tiens à remercier ma famille ainsi que tous les proches qui ont été présents lors de la soutenance. Vous voir à mes côtés en ce jour si spécial m'a beaucoup touchée, grâce à vous je me suis sentie entourée et soutenue dans cette toute dernière épreuve, et je suis heureuse d'avoir pu partager ce moment avec vous !

Un immense merci à **mes parents** pour leur soutien inconditionnel et leurs encouragements constants. Il va de soi que je n'aurais jamais pu en arriver là sans vous, et je tiens à vous remercier d'avoir tout fait pour que cette thèse soit possible ! Merci d'avoir toujours cru en moi plus que je n'aurais osé le faire.

Parfois, il est des choses sur lesquelles il est inutile de mettre des mots et j'ai la chance incroyable de partager ça avec mes sœurs **Lise** et **Jéromine**... Merci pour votre soutien sans faille et la confiance que vous avez toujours eue en moi ! Je tiens à ce que vous sachiez cependant que vous ne serez jamais aussi fières de moi que je ne le suis déjà de vous...

Enfin, merci à toi, mon **Rémi**. Merci pour ton soutien, si précieux. Merci pour ton aide, tes conseils, ton humour, ta sérénité légendaire... Sans toi cette aventure n'aurait pas eu la même saveur, et elle aurait été tellement moins belle ! Merci pour tout, donc, et n'oublie jamais que *zouk la sé sel médikaman nou ni (sa kon sa)* ! ♡ ♡ ♡

Liste des principales abréviations

Antp	Antennapedia
CPP	Cell Penetrating Peptide
GBM	Glioblastoma Multiform
HGF	Hepatocyte Growth Factor
hsp90	heat shock protein 90
HUVEC	Human Umbilical Vein Endothelial Cells
ICK	Inhibitor Cystine Knot
MCa	Maurocalcine
μ-CTX	μ-conotoxines
RMN	Résonance Magnétique Nucléaire
RyR	Ryanodine Receptor
scFv	Single Chain Fragment Variant
Tat	Trans-Activator of Transcription protein
VGCC	Voltage-Gated Calcium Channel
VGKC	Voltage-Gated Potassium Channel
VGSC	Voltage-Gated Sodium Channel

Table des matières

Table des figures

Liste des tableaux

Première partie

Introduction

Chapitre 1

Introduction

1.1 Les produits naturels en thérapeutique

Depuis toujours, les produits naturels (métabolites secondaires) jouent un rôle prépondérant dans la découverte de nouvelles molécules thérapeutiques, mais l'intérêt qu'on leur porte est en déclin depuis l'avènement du criblage à haut débit et de la protéomique (Harvey, 2008). Néanmoins, ils contribuent au développement de la moitié des drogues nouvellement mises sur le marché (Newman & Cragg, 2012).

Le premier document écrit attestant de pratiques thérapeutiques basées sur les substances naturelles a été estimé vieux d'environ 4600 ans, et décrit l'utilisation d'un millier de composés dérivés de plantes en Mésopotamie (Cragg & Newman, 2013; Dias *et al.*, 2012). Il s'agit notamment d'huiles de cyprès (*Cupressus sempevirens*), cèdre (plusieurs espèces de *Cedrus*), réglisse (*Glycyrrhiza glabra*), myrrhe (plusieurs espèces de *Commiphora*) et pavot somnifère (*Papaver somniferum*). Ces molécules sont toujours en usage pour le traitement d'affections diverses telles que la toux, le rhume, les infections parasitaires ou bien encore l'inflammation (Cragg & Newman, 2013). Historiquement, on peut citer plusieurs dérivés de métabolites secondaires de plantes utilisés à des fins thérapeutiques : l'aspirine (anti-inflammatoire dérivé de la saliciline, elle-même issue de l'écorce du saule pleureur *Salix alba*), la morphine (analgésique dérivé de l'opium issu du pavot somnifère *P. somniferum*), la quinine (anti-malarial isolé de l'écorce du quinquina *Cinchona succirubra*) (Dias *et al.*, 2012)... Plus récemment, un nouvel antitumoral a été mis en évidence : il s'agit du paclitaxel, inhibiteur du fuseau mitotique extrait de l'écorce de l'if *Taxus brevifolia* utilisé dans le traitement du cancer de l'ovaire, cancer du sein et cancer du poumon non à petites cellules (Kingston, 2007).

Les plantes ne sont pas les seuls organismes à produire des composés pharmacologiquement intéressants. En effet, les microorganismes ont eux aussi permis la découverte de molécules thérapeutiques, l'exemple le plus célèbre étant celui du champignon *Penicillium notatum* à partir duquel a été extraite la pénicilline (Dias *et al.*, 2012; Spratt, 2012). Les venins constituent également un immense réservoir de molécules d'intérêt : citons à titre d'exemple celui du cône *Conus magnus*, qui contient la conotoxine à l'origine de l'analgésique ziconotide (Dias *et al.*, 2012; Mayer *et al.*, 2010). Les toxines animales sont de puissants outils thérapeutiques pour lesquels une description détaillée au sein de ce manuscrit s'impose.

1.2 Les toxines animales

1.2.1 Modes d'action

La Nature a recours aux toxines animales pour deux mécanismes fondamentaux, qui sont la défense et la prédation. La haute affinité de ces molécules pour leur cible ainsi que leur stabilité *in vivo* leur confèrent un intérêt thérapeutique certain. Il est possible de les classer non pas selon leur organisme d'origine mais relativement à leur mode d'action. La plupart des toxines animales ayant un effet sur les canaux ioniques, j'ai choisi de présenter ici leurs principaux modes d'action selon le type de canal ainsi que quelques exemples pour chaque cas.

Toxines se liant aux canaux sodiques

Les canaux sodiques voltage-dépendants ou VGSCs (voltage-gated sodium channels) sont impliqués dans la propagation du signal nerveux et dans la contraction des myocytes. En effet, ces protéines transmembranaires sont sensibles au potentiel de membrane et perméables (ou non) aux ions sodium (Catterall, 2000; Waszkielewicz *et al.*, 2013). Certaines toxines animales ont la capacité de se fixer à ces canaux, influant ainsi sur le devenir du message nerveux ou sur l'activation électrique du myocarde et entraînant le plus souvent une paralysie. On peut différencier ces toxines selon qu'elles bloquent, qu'elles activent ou qu'elles stabilisent le canal.

Les μ-conotoxines (μ-CTX) sont de petits peptides (16 à 26 acides aminés) contenant trois ponts disulfure et issus du venin de cônes. Ces peptides bloquent les VGSCs,

inhibant ainsi le relargage de sodium (Knapp *et al.*, 2012). Certaines de ces toxines sont responsables de la paralysie des proies des cônes, mais elles sont étudiées pour leurs propriétés analgésiques (Zhang *et al.*, 2007).

La toxine Lqh issue du venin de *Leiurus quinquestriatus hebraeus* fait partie des α-toxines de scorpion, polypeptides (61 à 67 résidus) comprenant quatre ponts disulfure et une structure secondaire β α β β . Ces toxines modifient la dépendance au voltage des VGSCs, ce qui a pour effet de ralentir leur inactivation et donc de stabiliser leur ouverture (Ma *et al.*, 2012).

Toxines se liant aux canaux potassiques

Les canaux potassiques comprennent les canaux voltage-dépendants (voltage-gated potassium channels, VGKCs), les canaux activés par le calcium, les canaux à rectification interne et les canaux potassiques de repos. Ils sont présents dans bon nombre de types cellulaires, notamment les myocytes et les neurones (Waszkielewicz *et al.*, 2013). La perturbation de leur fonctionnement peut donc entraîner une paralysie, ou une arythmie cardiaque parfois mortelle.

L'apamine est un peptide de 18 acides aminés issu du venin de l'abeille mellifère *Apis mellifera*, et dont la structure comporte deux ponts disulfure (van Rietschoten *et al.*, 1975). Cette toxine bloque de façon très spécifique les canaux potassiques calcium-dépendants de faible conductance (small conductance calcium-activated potassium channels ou canaux SK) (Hugues *et al.*, 1982; Jenkinson, 2006).

Si l'apamine est la seule toxine animale connue pour bloquer spécifiquement les canaux SK, les toxines de scorpions sont réputées pour leur capacité à bloquer une grande partie des canaux potassiques. On peut notamment citer la maurotoxine (*Scorpio maurus palmatus*), peptide de 34 acides aminés et possédant 4 ponts disulfure, qui se lie à plusieurs canaux potassiques voltage-dépendants (Kharrat *et al.*, 1996) ainsi qu'aux canaux calcium-dépendants de faible conductance (SK) (Kharrat *et al.*, 1996; Regaya *et al.*, 2004) ou de conductance intermédiaire (IK) (Castle *et al.*, 2003; Regaya *et al.*, 2004).

Toxines se liant aux canaux calciques

On distingue deux types de canaux calciques, selon que leur activation dépend d'un ligand ou du voltage. Les canaux calciques voltage-dépendants (voltage-gated calcium channels, VGCCs) sont présents à la membrane des cellules excitables et jouent

un rôle dans de nombreuses fonctions biologiques telles que la transmission synaptique ou la contraction musculaire. Ils sont ouverts lors de la dépolarisation de la membrane, ce qui entraîne un relargage d'ions Ca^2+. Certains canaux ioniques étant sensibles au calcium, ils peuvent donc être indirectement activés par l'ouverture de canaux calciques (Waszkielewicz *et al.*, 2013). Les ions calcium étant impliqués dans de nombreuses fonctions cellulaires, les canaux calciques voltage-dépendants peuvent être considérés comme des transducteurs du signal électrique en message chimique et jouent donc un rôle crucial dans la régulation de certains mécanismes. Par conséquent, la fixation de toxines aux canaux calciques peut avoir des effets considérables.

Les ω-conotoxines ciblent certains canaux calciques voltage-dépendants et font partie des premières toxines de cône à avoir été caractérisées (McCleskey *et al.*, 1987; Terlau & Olivera, 2004; Pringos *et al.*, 2011). Les canaux ciblés par les ω-conotoxines étant impliqués dans les mécanismes de nociception, ces toxines sont étudiées pour leurs propriétés analgésiques (Terlau & Olivera, 2004; Lewis *et al.*, 2012; Hannon & Atchison, 2013).

Le venin de l'araignée *Agelenopsis aperta* contient divers peptides dont les ω-agatoxines, qui sont des antagonistes présynaptiques des VGCCs et dont la spécificité de fixation varie en fonction de la toxine considérée (Pringos *et al.*, 2011). Ces neurotoxines permettent donc une meilleure caractérisation des propriétés des VGCCs ainsi que de leur rôle dans le relargage de neurotransmetteur.

La maurocalcine est l'un des composants du venin du scorpion *Scorpio maurus palmatus* et cible le récepteur à la ryanodine (RyR), un canal calcique intracellulaire (Fajloun *et al.*, 2000). Les caractéristiques structurales et fonctionnelles de la maurocalcine seront développées plus loin.

Toxines se liant aux canaux chlorure

Les canaux chlorure sont encore méconnus, mais on sait qu'ils sont impliqués dans différentes fonctions physiologiques telles que la régulation du volume, la prolifération et la migration cellulaires (Ransom *et al.*, 2001). Comme tous les canaux ioniques, certains sont activés par le voltage, d'autres par la fixation d'un ligand.

La chlorotoxine, initialement issue du venin du scorpion *Leiurus quinquestriatus*, se fixe entre autres aux canaux chlorure (DeBin *et al.*, 1993). Cette fixation entraîne l'internalisation du complexe, réduisant ainsi le nombre de canaux disponibles et sup-

primant le courant ionique (Deshane *et al.*, 2003).

Le venin du scorpion *Buthus martenzii* Karsch contient une toxine semblable à la chlorotoxine, la BmKCTa, capable elle aussi de se fixer aux canaux chlorure et de les inactiver (Fu *et al.*, 2007).

Toxine	Origine	Mode d'action	Référence
μ-conotoxines	Venin de cônes	Bloquent les VGSCs et inhibent le relargage de sodium	Zhang *et al.* 2007
Lqh	Venin du scorpion *Leiurus quinquestriatus hebraeus*	Modifie la dépendance au voltage des VGSCs et stabilise leur ouverture	Ma *et al.* 2012
Apamine	Venin de l'abeille mellifère *Apis mellifera*	Bloque les canaux SK (small conductance VGKCs)	Jenkinson *et al.* 2006
Maurotoxine	Venin du scorpion *Scorpio maurus palmatus*	Bloque les VGKCs ainsi que les canaux SK et IK (conductance intermédiaire)	Regaya *et al* 2004
ω-conotoxines	Venin de cônes	Ciblent les VGCCs	Hannon *et al.* 2013
ω-agatoxines	Venin de l'araignée *Agelenopsis aperta*		Pringos *et al.* 2011
Maurocalcine	Venin du scorpion *Scorpio maurus palmatus*	Cible le canal calcique intracellulaire RyR	Fajloun *et al.* 2000
Chlorotoxine	Venin du scorpion *Leiurus quinquestriatus*	Cible les canaux chlorure, entraîne leur internalisation et inhibe le courant ionique	Deshane *et al.* 2003
BmKCTa	Venin du scorpion *Buthus martenzii* Karsch	Cible et inactive les canaux chlorure	Fu *et al.* 2007

TABLE 1 – Quelques toxines animales et leurs modes d'action

1.2.2 Applications thérapeutiques

Les toxines animales ayant des effets variés sur les fonctions cellulaires selon le récepteur qu'elles ciblent, elle peuvent donner lieu à diverses applications thérapeutiques. Les propriétés antalgiques des ω-conotoxines ont par exemple été exploitées pour permettre la mise en place d'un nouvel analgésique, le ziconotide (commercialisé sous le nom de Prialt) (McGivern, 2007). Ce peptide n'ayant pas (ou presque) la capacité de traverser la barrière hémato-encéphalique, il est nécessaire de recourir à une administration intrathécale. Le ziconotide est donc réservé au traitement de douleurs chroniques intenses.

La plupart des médicaments dérivés de produits naturels utilisés de nos jours ont été développés à partir de toxines de plantes ou de microorganismes, mais de plus en plus de toxines animales sont étudiées pour leurs propriétés thérapeutiques. C'est le cas par exemple de la chlorotoxine, présente dans le venin du scorpion *Leiurus quinquestriatus* et qui possède la capacité de cibler les cellules tumorales gliales. En effet, la chlorotoxine cible les canaux chlorure surexprimés dans plusieurs types de cancers, mais également la MMP2 (matrix metalloproteinase 2), surexprimée dans les gliomes (Graf *et al.*, 2012). En 2005 déjà, une étude clinique avait montré que le peptide TM-601, un analogue synthétique de la chlorotoxine, était en mesure de se fixer de façon spécifique aux cellules tumorales et ce plus de 6 jours après l'injection (le peptide ne s'étant pas fixé étant lui totalement éliminé au bout de 48 h) (Hockaday *et al.*, 2005). Le peptide TM-601 présente donc un intérêt pour l'imagerie et / ou le traitement des tumeurs gliales (selon les cargos qui lui sont associés), c'est pourquoi il continue à être l'objet d'études cliniques.

Certaines toxines animales ne font pas encore l'objet d'essais cliniques mais sont néanmoins activement étudiées. C'est évidemment le cas de la maurocalcine, dont les caractéristiques seront détaillées plus loin, mais également celui de la melittine. La melittine, peptide de 26 acides aminés, est, tout comme l'apamine, l'un des constituants du venin de l'abeille mellifère *Apis mellifera* (Gauldie *et al.*, 1976). Contrairement à de nombreuses toxines animales, elle ne cible pas de canal ionique mais s'associe toutefois à la membrane plasmique, induisant sa destruction *via* la formation de pores (van den Bogaart *et al.*, 2008). Les propriétés cytotoxiques de la melittine sont étudiées pour la mise en place de thérapies anticancéreuses : Soman *et al.* ont notamment montré en 2009, après avoir inclus le peptide dans la couche lipidique externe

d'un nanovecteur afin de mieux maîtriser sa toxicité, que cette construction était en mesure d'inhiber la croissance de différentes tumeurs chez la souris (mélanome allogreffé et cancer du sein xénogreffé) (Soman *et al.*, 2009).

La capacité de la melittine à former des pores dans la membrane plasmique est également exploitée dans la lutte contre le VIH. En 2013, Hood *et al.* ont publié une étude au cours de laquelle ils se sont intéressés aux effets d'une nanoparticule couplée à plusieurs molécules de melittine ainsi qu'à des "butoirs" (Hood *et al.*, 2013). Le complexe s'est révélé capable de limiter l'infection tout en épargnant les cellules saines environnantes grâce aux "butoirs" : la chimère reste à distance des cellules, mais le VIH, plus petit, s'immisce entre deux "butoirs" et se retrouve ainsi en contact avec la melittine. La toxine peut dès lors former des pores dans l'enveloppe du virus, entraînant ainsi sa destruction. Cette découverte pourrait donner lieu à la création d'un gel vaginal permettant de limiter fortement la primo-infection, mais également de développer une nouvelle thérapie administrée par injection intraveineuse et particulièrement indiquée pour les cas d'infections résistantes aux drogues.

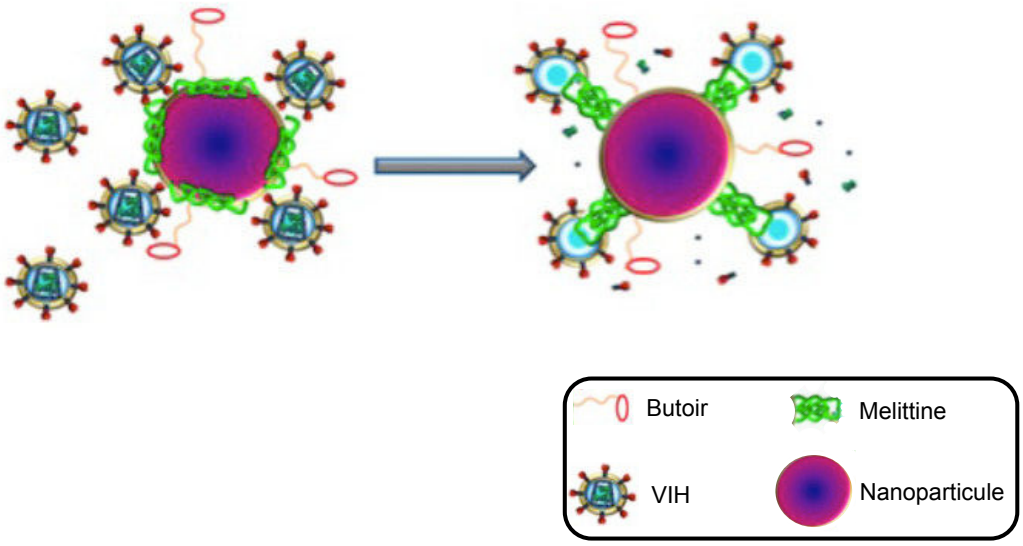

Figure 1 – Possible application thérapeutique de la melittine dans la lutte contre le VIH (d'après Hood *et al.* (2013))

1.3 La maurocalcine et autres peptides vecteurs

1.3.1 Les peptides de pénétration cellulaire

Historique

Les peptides de pénétration cellulaire ou CPP (cell-penetrating peptides) sont de petits peptides d'une dizaine à une trentaine d'acides aminés en moyenne, et dont la charge nette est positive de par la présence d'un grand nombre de résidus lysine ou arginine. Les CPP ont la capacité de délivrer des cargos au sein des cellules sans altérer la membrane plasmique. Cette caractéristique présente un intérêt thérapeutique certain puisque l'action de nombreuses drogues est restreinte par le fait qu'elles atteignent difficilement le milieu intracellulaire. Toutefois, cet intérêt est limité par l'absence de sélectivité cellulaire des CPP. En effet, s'ils voient leur capacité de pénétration varier en fonction du type cellulaire étudié, ils sont néanmoins capables d'atteindre un grand nombre de compartiments intracellulaires différents. Ceci peut s'expliquer par l'absence de récepteur cellulaire connu pour la plupart des CPP, à l'exception de ceux issus de protéines fonctionnelles.

Le premier CPP a avoir été découvert est la protéine Tat (trans-activatrice de la transcription) du VIH-1 (virus de l'immunodéficience humaine). En 1988, Frankel et Pabo ont démontré la capacité de Tat à traverser la membrane plasmique et s'accumuler au sein du noyau (Frankel & Pabo, 1988). La protéine Tat native est formée de 86 acides aminés et possèdent deux résidus lysine et six résidus arginine qui forment une région fortement basique (Arya *et al.*, 1985; Sodroski *et al.*, 1985). Sa séquence minimale nécessaire à l'internalisation a été mise en évidence en 1997 et confirmée par la suite : elle comprend une dizaine d'acides aminés situés au niveau du fragment 48-60 de la séquence native (Vives *et al.*, 1997; Wender *et al.*, 2000).

Initialement, il a été montré que Tat s'internalisait par des voies indépendantes de l'endocytose puisque sa pénétration n'était pas affectée par une incubation à 4°C (Vives *et al.*, 1997) ou par l'utilisation d'inhibiteurs de l'endocytose (Suzuki *et al.*, 2002). Des données plus récentes ont cependant démontré que Tat empruntait des voies endocytaires et que les résultats précédents pouvaient être attribués à des artéfacts expérimentaux (Richard *et al.*, 2003). En effet, la pénétration de Tat est sensible à l'ajout d'inhibiteurs de l'endocytose (Richard *et al.*, 2003) et ce CPP colocalise avec la transferrine, marqueur connu de l'endocytose dépendante de la clathrine (Richard *et al.*, 2005). Toutefois, comme pour tous les CPP, la pénétration de Tat au sein des cellules

dépend du cargo qui lui est associé ainsi que de sa concentration extracellulaire.

L'autre CPP de référence est la pénétratine, correspondant à la troisième hélice α de l'homéodomaine codé par le gène *Antennapedia* (Antp) de la drosophile (Qian *et al.*, 1989; Gehring *et al.*, 1994). En effet, cette hélice longue de 16 acides aminés est nécessaire à la pénétration cellulaire de la protéine Antp (Derossi *et al.*, 1994).

L'internalisation de la pénétratine est indépendante de l'énergie puisqu'elle peut avoir lieu à 4°C (Joliot *et al.*, 1991), elle ne dépend également pas totalement des voies endocytaires (Derossi *et al.*, 1996). Le résidu tryptophane en position 48 ainsi que la structure en hélice α sont en revanche cruciaux pour la pénétration de ce CPP (Derossi *et al.*, 1994, 1996). Derossi et ses collaborateurs ont démontré qu'aucun récepteur chiral n'était impliqué dans l'internalisation de la pénétratine puisque l'analogue synthétisé à partir d'acides aminés D possède les mêmes propriétés de pénétration cellulaire (Derossi *et al.*, 1996).

Certains CPP ne sont pas simplement dérivés d'un produit naturel mais composés de plusieurs fragments de peptides. C'est le cas notamment du transportan, molécule chimère comprenant la partie N-terminale du neuropeptide galanine liée *via* une lysine au peptide mastoparan issu du venin de guêpe (Pooga *et al.*, 1998). L'internalisation du transportan semble indépendante de l'énergie et d'un transporteur (Pooga *et al.*, 2001). En couplant ce CPP à des molécules d'or, Padari *et al.* ont montré qu'il pénétrait dans les cellules par endocytose et translocation (Padari *et al.*, 2005).

MPG et Pep-1 sont deux CPP chimères amphipathiques et de structures similaires. En effet, tous deux ont en commun le domaine hydrophile dérivé de la séquence de localisation nucléaire de l'antigène T du virus simien SV40. Le domaine hydrophobe de MPG est dérivé de la glycoprotéine 41 du VIH, celui de Pep-1 est une séquence riche en tryptophane. L'internalisation de ces deux CPP semble indépendante des voies endocytaires (Morris *et al.*, 1997, 2001).

Certains CPP peuvent également être des toxines animales, c'est le cas par exemple de la crotamine, issue du venin du serpent *Crotalus durissus terrificus*. Ce peptide de 42 acides aminés est riche en résidus basiques ainsi qu'en cystéines, impliquées dans la formation de trois ponts disulfure (Kerkis *et al.*, 2004). La crotamine s'accumule au sein des cellules à partir de faibles concentrations extracellulaires (10 nM) et ne nécessite pas une incubation prolongée puisqu'on la détecte à partir de 5 minutes (pour un maximum atteint à 3 h) . Elle possède en outre une localisation nucléaire et son inter-

nalisation dépend des voies endocytaires puisqu'elle est inhibée à basse température (Kerkis *et al.*, 2004).

L'imperatoxine fait elle aussi partie des toxines animales considérées comme des CPP. Cette toxine, initialement isolée du venin du scorpion *Pandinus imperator*, cible les récepteurs à la ryanodine (RyR, canaux calciques situés à la membrane du réticulum endoplasmique). Pour atteindre sa cible, l'imperatoxine franchit la membrane plasmique et cette capacité n'est pas inhibée par le couplage à un cargo (Gurrola *et al.*, 2010). Cette toxine possède des similarités séquentielles et structurales avec la maurocalcine, dont les caractéristiques seront détaillées plus loin.

	Peptide vecteur	Origine	Séquence	Référence
CPP naturels	Tat (48-60)	Protéine Tat du VIH-1	GRKKRRQRRRPPQ	Vives *et al.* 1997
	Pénétratine	Protéine Antennapedia de la drosophile	RQIKIWFQNRRMKWKK	Derossi *et al.* 1994
CPP chimères	Transportan	Galanine + Mastoparan	GWTLNSAGYLLGKINLKA LAALAKKIL	Pooga *et al.* 1998
	MPG	NLS de SV40 + glycoprotéine 41 du VIH	GALFLGWLGAAGSTMGA WSQPPKKKRKV	Morris *et al.* 1997
	Pep-1	NLS de SV40 + sq riche en tryptophane	KETWWETWWTEWSQPK KKRKV	Morris *et al.* 2001
CPP dérivés de toxines animales	Crotamine	Venin de *Crotalus durissus terrificus*	YKQCHKKGGHCFPKEKI CLPPSSDFGKMDCRWR WKCCKKGSG	Kerkis *et al.* 2004
	Imperatoxine	Venin de *Pandinus imperator*	GDCLPHLKRCKADNDCC GKKCKRRGTNAEKRCR	Gurrola *et al.* 2010

TABLE 2 – Quelques peptides de pénétration cellulaire

Voies d'entrée dans la cellule

Il n'existe pas de consensus en ce qui concerne les modalités de pénétration des CPP au sein des cellules. Néanmoins, deux types d'internalisation sont admis : il s'agit de la translocation et de l'endocytose. Un CPP emprunte l'une ou l'autre de ces voies (et parfois les deux) selon sa nature et celle du cargo qu'il transporte.

La translocation

La translocation directe est un mécanisme d'internalisation indépendant de l'énergie (Pooga *et al.*, 1998) qui peut suivre différents schémas. Les plus connus sont le modèle de barrel-stave et celui de carpet.

Selon le modèle de barrel-stave, les peptides se lient à la membrane plasmique et s'oligomérisent sous forme de pores. Ce type d'internalisation requiert une structure peptidique particulière : présence d'une hélice α amphiphatique ou hydrophobe, et / ou de feuillets β (Shai & Oren, 2001).

Dans le modèle de carpet, les peptides s'accumulent à la surface de la membrane plasmique sur toute leur longueur (jusqu'à atteindre une concentration limite) et la recouvrent à la manière d'un tapis. L'accumulation de peptides induit une perturbation locale de la membrane plasmique, entraînant la formation de pores transitoires et permettant de ce fait l'internalisation des peptides (Shai & Oren, 2001). Contrairement au modèle de barrel-stave, le modèle de carpet ne nécessite pas une structure peptidique particulière ou la formation de canaux structurés.

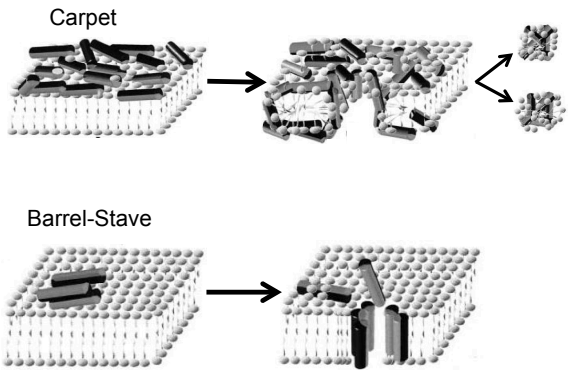

Figure 2 – Illustration de la translocation selon les modèles de carpet et barrel-stave (d'après Shai & Oren (2001))

L'endocytose

A l'inverse de la translocation, l'endocytose dépend de l'énergie, mais elle suit elle aussi différents schémas : la phagocytose est utilisée par les cellules pour l'internalisation de grosses particules, tandis que la pinocytose est réservée aux solutés.

La phagocytose est particulière aux cellules spécialisées que sont les macrophages, les neutrophiles et les cellules dendritiques, à qui elle permet l'assimilation de particules volumineuses qui seront ensuite détruites. Ce mécanisme d'internalisation met en jeu des récepteurs membranaires (permettant la reconnaissance de la particule à détruire). L'activation de ces récepteurs entraîne un réarrangement de la membrane plasmique qui s'évagine autour de la particule, formant un phagosome qui sera internalisé. Le phagosome fusionne au sein de la cellule avec des vésicules lytiques, conduisant ainsi à la destruction de la particule (Conner & Schmid, 2003).

La pinocytose est réalisée par tous les types cellulaires et se décline en quatre processus majeurs : la macropinocytose, l'endocytose dépendante de la clathrine, l'endocytose dépendante de la cavéoline, et l'endocytose "clathrine et cavéoline indépendante". Lors de la macropinocytose, l'internalisation se fait par le biais de vésicules hétérogènes de grande taille, les macropinosomes. Ce type d'endocytose intervient dans la plupart des internalisations de fluides (Conner & Schmid, 2003).

L'endocytose dépendante de la clathrine représente l'essentiel de l'activité de pinocytose. La clathrine est un trimère d'hétérodimères assemblés sous forme de triskèle. Les triskèles polymérisent en hexagones ou pentagones formant des cages, et n'interagissent avec la membrane plasmique que par le biais d'adaptateurs, tels que la protéine AP2. Lors de l'internalisation, la membrane plasmique s'invagine et la vésicule en formation est recouverte, au niveau cytoplasmique, d'un manteau de clathrine. Le détachement de la vésicule du reste de la membrane plasmique a lieu grâce aux molécules de dynamine qui induisent sa fission à la base. Le manteau de clathrine se désassemble alors, et la vésicule nouvellement formée fusionne avec un endosome précoce (Boucrot & McMahon, 2011).

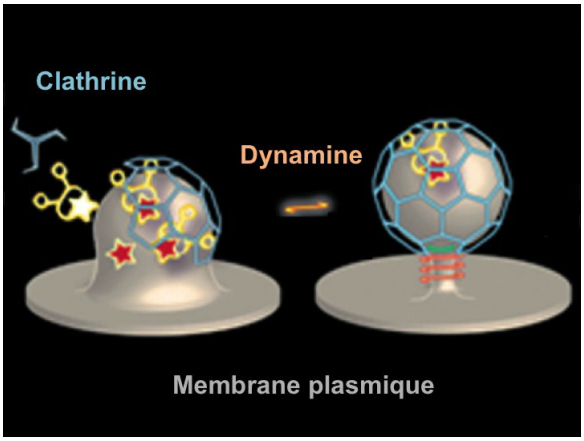

Figure 3 – Modèle classique de la formation d'une vésicule de clathrine (d'après Boucrot & McMahon (2011))

La cavéoline est une protéine formant plusieurs boucles transmembranaires et impliquée dans la formation de cavéoles, structures membranaires en forme de fiole riches en cholestérol et sphingolipides. L'endocytose dépendante de la cavéoline dépend également de la présence de cholestérol au niveau de la membrane plasmique, et est impliquée dans l'internalisation de l'albumine, du récepteur à l'insuline, des toxines responsables du choléra et du tétanos, ou encore de certains virus. De la même façon que pour l'endocytose dépendante de la clathrine, la dynamine est impliquée dans le détachement des vésicules de la membrane plasmique (Kumari *et al.*, 2010).

Même si la clathrine et la cavéoline sont responsables d'une grande partie de l'activité de pinocytose, elles ne sont pas impliquées dans tous les processus d'internalisation. En effet, d'autres protéines peuvent conduire à la formation de vésicules. C'est le cas par exemple des flotillines et des tétraspanines, ces dernières permettant une endocytose ne dépendant pas du niveau de cholestérol membranaire (Kumari *et al.*, 2010).

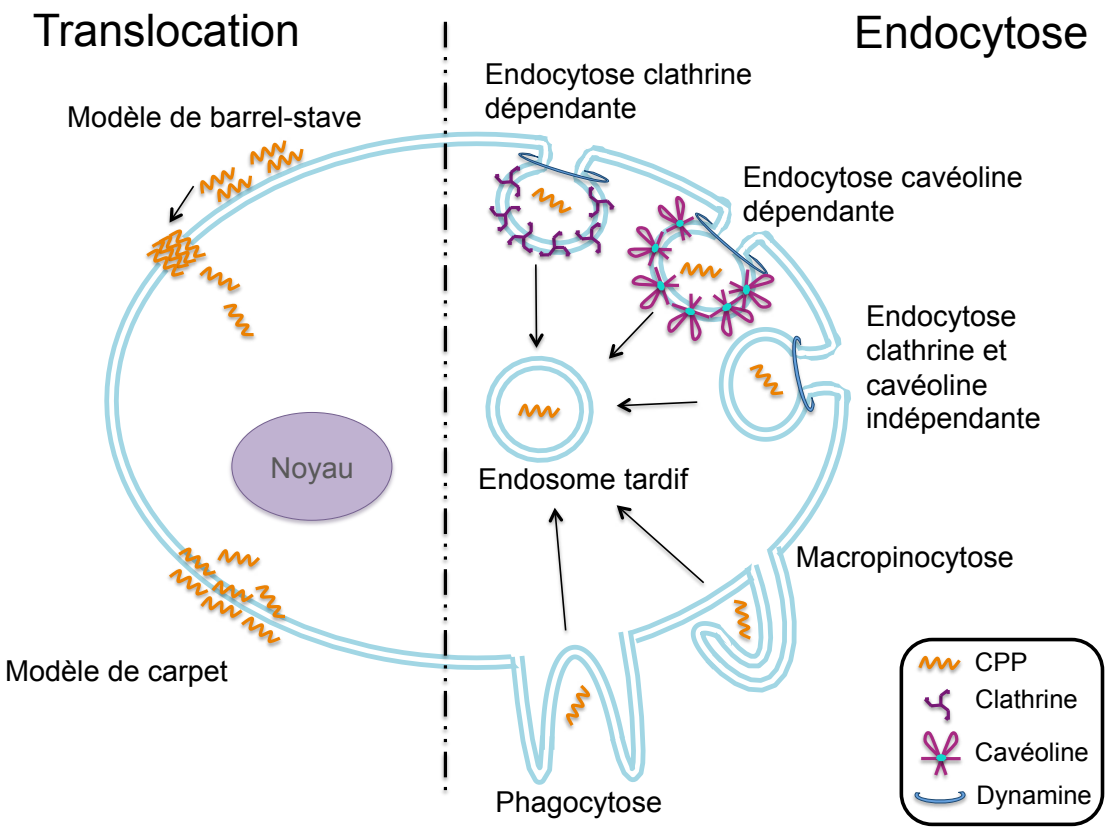

Figure 4 – Principales voies d'internalisation des CPP

Applications thérapeutiques

La perméabilité relative de la membrane plasmique à certaines drogues, limitant drastiquement leur capacité à atteindre leur cible, constitue un obstacle majeur à la mise en place de nouvelles stratégies thérapeutiques. Le recours à de hautes doses permet parfois de pallier ce problème, mais il présente le risque d'effets secondaires accrus. Les CPP en tant que vecteurs de ces molécules dans le milieu intracellulaire représentent donc la solution la plus optimale (Heitz *et al.*, 2009). Un CPP peut être considéré comme un vecteur d'intérêt s'il répond aux critères suivants : rapidité d'accumulation intracellulaire à de faibles doses, absence de toxicité et capacité de délivrer le cargo de façon à ce qu'il atteigne sa cible, ce dernier critère pouvant être lié à un relargage endosomal rapide.

Couplage de cargos aux CPP

Différentes stratégies peuvent être mises en place pour le couplage entre le peptide vecteur et son cargo, selon leur nature. En effet, la molécule à transporter peut limiter l'internalisation induite par le CPP, tout comme le peptide peut interférer avec l'action thérapeutique de la drogue. Plusieurs sortes de liaisons sont donc susceptibles d'être mises en place, et il est possible de les classer en deux groupes distincts selon qu'elles ont un caractère covalent ou non.

La liaison disulfure représente la majorité des liaisons covalentes et possède l'avantage d'être clivée après l'internalisation, laissant plus de liberté au cargo pour atteindre sa cible (Mohandessi *et al.*, 2012). Il est également possible de lier le CPP et son cargo directement lors de la synthèse, mais la liaison peptidique ainsi formée peut altérer l'activité pharmacologique du cargo (Temsamani & Vidal, 2004). Les autres liaisons covalentes (maleimide par exemple) impliquent quant à elles la présence d'un linker entre le CPP et son cargo.

Les liaisons non covalentes comprennent les liaisons électrostatiques et les liaisons streptavidine-biotine. Les liaisons électrostatiques sont souvent utilisées pour la délivrance de siRNA, ceux-ci étant chargés négativement alors que les CPP sont chargés positivement (Shiraishi & Nielsen, 2011). La liaison streptavidine-biotine implique une modification chimique du cargo et de son vecteur, mais la très forte affinité existant entre la streptavidine et la biotine confère une grande stabilité au complexe.

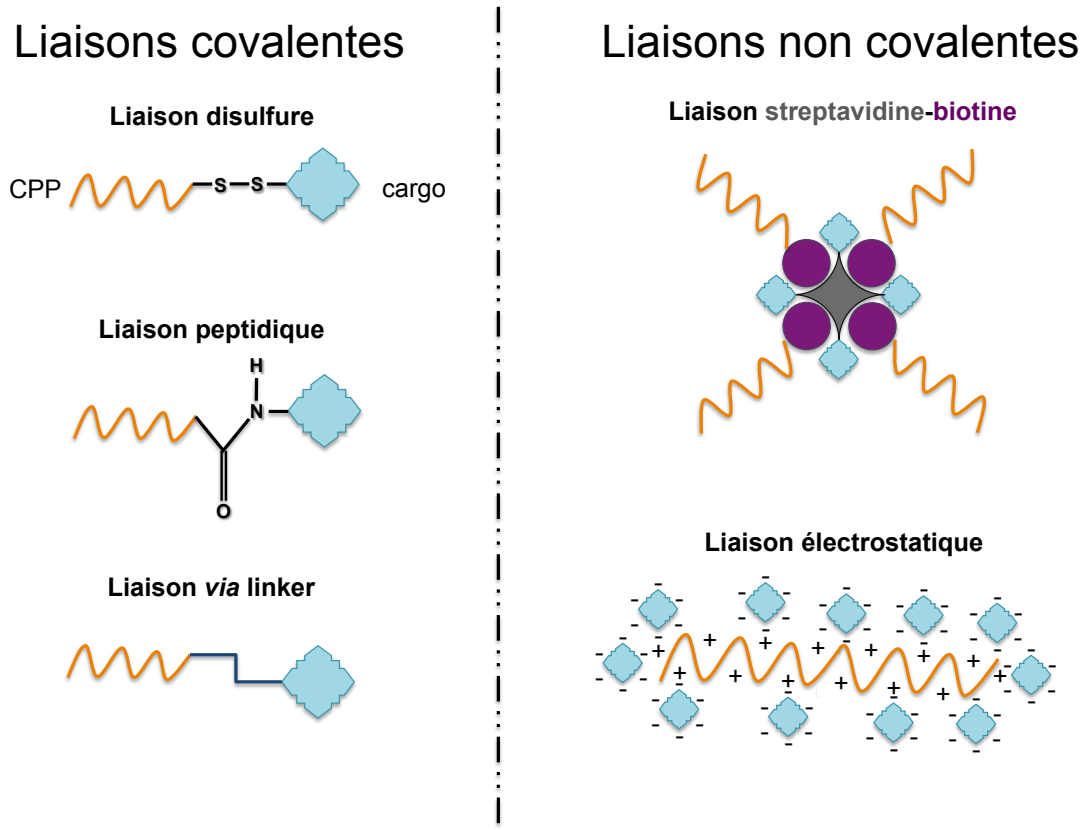

Figure 5 – Méthodes de couplage de cargos aux CPP

Délivrance de siRNA

Les siRNA (small interfering RNA, ARN interférents) inhibent l'expression d'un gène en s'hybridant au mRNA (ARN messager) correspondant, ce qui interfère avec le processus de traduction. Ils représentent donc un intérêt thérapeutique considérable mais certains obstacles restent à surmonter avant l'application clinique, notamment l'internalisation cellulaire. En effet, la membrane plasmique n'est que très peu perméable aux acides nucléiques (Margus *et al.*, 2012). Les CPP peuvent apporter une réponse partielle en assurant la délivrance cytoplasmique des siRNA, et de nombreuses études vont dans ce sens.

En 2013, Mehta et ses collaborateurs ont réalisé le couplage du CPP Tat_{48-60} au siRNA spécifique du gène *hsp90*α (heat shock protein) impliqué dans la croissance tumorale et surexprimé dans le cas de glioblastome multiforme (GBM). Ce couplage a consisté en la mise en présence du peptide chargé positivement et du siRNA chargé négativement, conduisant à la formation de liaisons électrostatiques. Le complexe ainsi formé à été ajouté au milieu de culture de cellules humaines tumorales (GBM) ou non (astrocytes), en association avec un antibiotique. Cette étude a démontré l'efficacité d'un tel traitement, l'inhibition de la croissance tumorale étant directement liée à la réduction de l'expression de *hsp90*α et la toxicité étant spécifique aux cellules tumorales. Le knockdown de *hsp90*α après administration du complexe a été confirmé *in vivo* sur un modèle murin (Mehta *et al.*, 2013).

Délivrance de protéines et de peptides

La délivrance de protéines ou de peptides peut être intéressante de par l'activité intrinsèque de molécules exogènes, ou encore pour pallier l'absence ou la mutation de composés endogènes. Afin de permettre une meilleure internalisation d'agents antitumoraux, Lim *et al.* se sont intéressés à la buforine II, analogue de la buforine I, peptide issu du tissu stomacal du crapaud *Bufo bufo gargarizans* (Park *et al.*, 1996). Ce nouveau peptide, BR2, a été couplé à une protéine, fragment simple chaîne d'anticorps (scFv, single chain fragment variant) dirigé contre le proto-oncogène *K-ras*. Ce complexe a été obtenu *via* l'expression par *E. Coli* du gène codant pour la molécule chimère. Le peptide BR2 s'est révélé capable de s'internaliser de façon spécifique dans les cellules tumorales *in vitro* (cancer du col de l'utérus humain, cancer du côlon humain et mélanome murin), sans présenter de toxicité pour les cellules saines à de faibles concentrations. Le couplage du fragment scFv anti *K-ras* à BR2, en permettant son accumulation intracytoplasmique, a permis la réduction significative de la viabilité des cellules tumorales (Lim *et al.*, 2013).

Cantelmo et ses collaborateurs se sont eux penchés sur l'intérêt de l'utilisation de CPP pour la délivrance d'un peptide de synthèse imitant le site de fixation de Met, récepteur du HGF (hepatocyte growth factor), tous deux étant impliqués dans la croissance et l'invasion tumorales. Le peptide Met a été directement couplé au CPP Tat durant la synthèse, et les effets du complexe Tat-Met ont été évalués *in vitro* sur des cellules endothéliales de la veine de cordon ombilical humain (HUVEC, human umbilical

vein endothelial cells), ainsi qu'*in vivo* sur des tumeurs xénogreffées de sarcome de Kaposi (tumeur induite par le HHV-8, human herpesvirus-8) chez la souris nude. *In vitro*, Tat-Met inhibe la prolifération, la migration, l'invasion et la formation de structure semblables aux capillaires par les cellules endothéliales. *In vivo*, ce complexe limite l'angiogénèse ainsi que la croissance et la vascularisation tumorales (Cantelmo *et al.*, 2010).

Délivrance d'agents de contraste ou de fluorochromes

Les CPP peuvent également être couplés à divers agents de contraste pour l'imagerie par résonance magnétique ou à des fluorochromes, afin de pallier l'écueil que représente leur faible capacité d'internalisation cellulaire. Olson et ses collaborateurs ont par exemple créé une molécule chimère composée d'une nanoparticule couplée à un CPP de synthèse ainsi qu'à plusieurs molécules de cyanine 5 (fluorochrome) et plusieurs molécules de gadolinium (agent de contraste pour l'IRM). Grâce à l'utilisation de CPP activables en présence de MMP-2 et MMP-9 (matrix metalloproteinases, suractivées dans de nombreux cancers), ce complexe permet la détection d'amas de cellules tumorales de taille supérieure à 200 µm. Cette sonde multimodale permet une détection précise des tumeurs par IRM, la présence de CPP entraînant l'accumulation massive de gadolinium au sein du cytoplasme, ce qui conduit à un signal plus puissant et qui permet des acquisitions de plus longue durée. De plus, la présence de la cyanine 5 laisse la possibilité à une étape de chirurgie assistée par fluorescence, technique précise permettant une résection fine des tumeurs (Olson *et al.*, 2010).

Peptide vecteur	Cargo	Application(s)	Référence
Tat (48-60)	siRNA spécifique du gène *hsp90α*	Inhibition de la croissance tumorale (glioblastome)	Mehta *et al.* 2013
	Peptide Met (cible le HGF)	Inhibition de l'angiogénèse, de la vascularisation tumorale et de la formation de métastases	Cantelmo *et al.* 2010
BR2	scFv dirigé contre *K-ras*	Induction de la mort de cellules tumorales	Lim *et al.* 2013
CPP synthétique et activable en présence de MMP-2 et MMP-9	Nanoparticule couplée à plusieurs molécules de Cy5 et plusieurs molécules de gadolinium	Détection précise des tumeurs par IRM (gadolinium) et résection chirurgicale fine (Cy5)	Olson *et al.* 2010

TABLE 3 – Exemples de complexes CPP-Cargo et leurs applications

1.3.2 La maurocalcine

Historique

La maurocalcine (MCa) a été identifiée pour la première fois en 2000, après avoir été extraite du venin du scorpion *Scorpio maurus palmatus*. Cette toxine est composée de 33 acides aminés qui s'organisent selon une structure comprenant trois ponts disulfure. Elle possède une forte analogie de séquence (82%) avec l'imperatoxine A, peptide issu du venin du scorpion *Pandinus imperator* (Fajloun *et al.*, 2000). La maurocalcine ne représentant que 0,5% des protéines présentes dans le venin de *Scorpio maurus palmatus*, l'étude de ses propriétés requiert une synthèse chimique.

La MCa possède une singularité structurale en cela qu'elle ne se replie selon aucun des motifs consensus habituellement retrouvés dans les toxines de scorpions (repliement α/β par exemple). En revanche, les trois ponts disulfure entraînent la formation d'un motif ICK (inhibitor cystine knot), également présent dans les μ-conotoxines et qui confère une grande stabilité au peptide. Ces ponts s'organisent de la façon suivante : Cys^{3}-Cys^{17}, Cys^{10}-Cys^{21} et Cys^{16}-Cys^{32} (Fajloun *et al.*, 2000).

La détermination de la structure de la MCa par spectroscopie RMN (résonance magnétique nucléaire) en solution a confirmé la présence du motif ICK et mis en évidence trois feuillets β comprenant respectivement les acides aminés 9 à 11, 20 à 23 et 30 à 33 (Mosbah *et al.*, 2000).

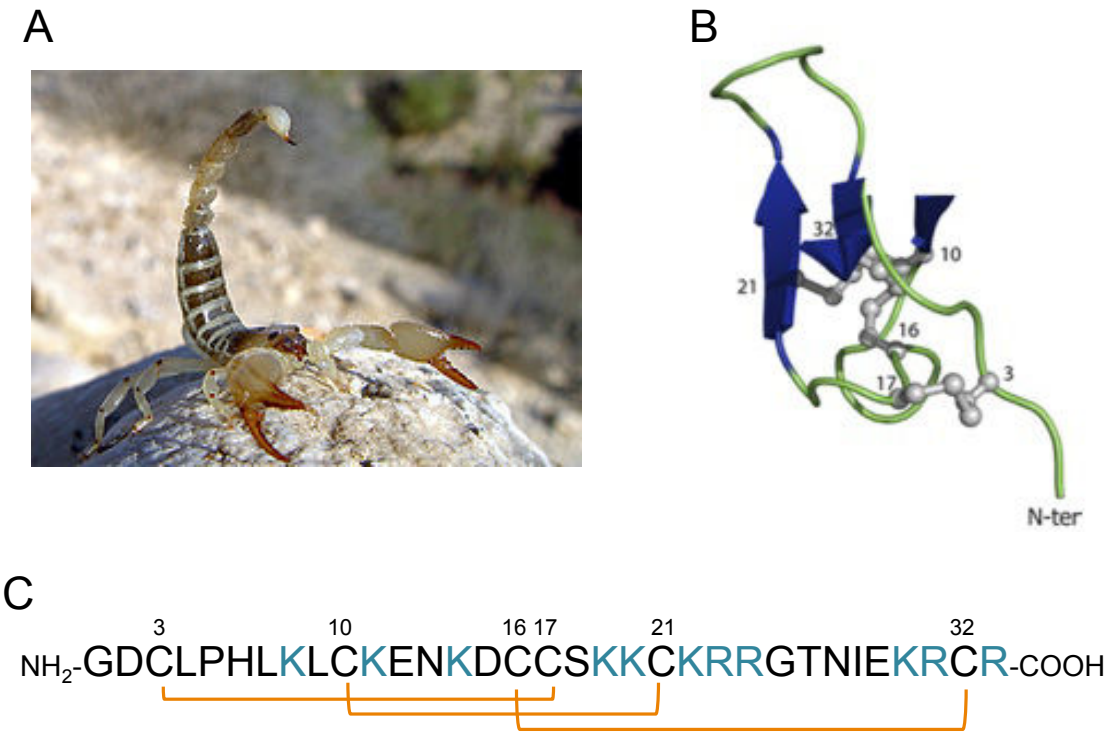

Figure 6 – (A) *Scorpio maurus palmatus,* (B) Structure 3-D de la MCa (d'après Poillot *et al.* (2010)), (C) Séquence de la MCa

Propriétés pharmacologiques

Du fait de sa similarité avec l'imperatoxine A, connue pour agir sur les RyR (récepteurs de la ryanodine), les études concernant la maurocalcine se sont d'abord intéressées à sa possible interaction avec ces récepteurs ainsi qu'aux effets en découlant.

La MCa reconnaît deux isoformes du RyR, récepteur à la ryanodine situé à la membrane du réticulum sarcoplasmique (réticulum endoplasmique lisse des cellules musculaires) : le RyR1, principalement présent dans les cellules de muscles squelettiques ainsi que le RyR2, spécifique aux cellules du myocarde (Altafaj *et al.*, 2007). Ce type de canal calcique doit son nom à sa forte affinité pour la ryanodine (alcaloïde retrouvé dans différentes plantes) et est composé de quatre sous-unités transmembranaires. Les RyR sont impliqués dans le relargage cytoplasmique d'ions calcium par le réticulum sarcoplasmique, nécessaire à la contraction musculaire. L'activation du RyR nécessite la fixation d'ions calcium sur sa partie cytoplasmique et peut être déclenchée par la ryanodine, l'ATP, la caféine ou encore la maurocalcine (Esteve *et al.*, 2003).

Lorsqu'elle se fixe au RyR1, la MCa stabilise son ouverture, facilitant ainsi la fixation de la ryanodine qui se lie préférentiellement au récepteur lorsqu'il est en conformation ouverte. Cette fixation de la MCa diminue également le seuil d'activation du RyR1 (qui s'ouvre donc à des concentrations en ions calcium moins élevées) et augmente son seuil d'inactivation (l'effet inhibiteur du Ca^{2+} survient donc à des concentrations plus élevées) (Esteve *et al.*, 2003). Cette succession d'évènements conduit par conséquent à un relargage massif de calcium par le réticulum sarcoplasmique.

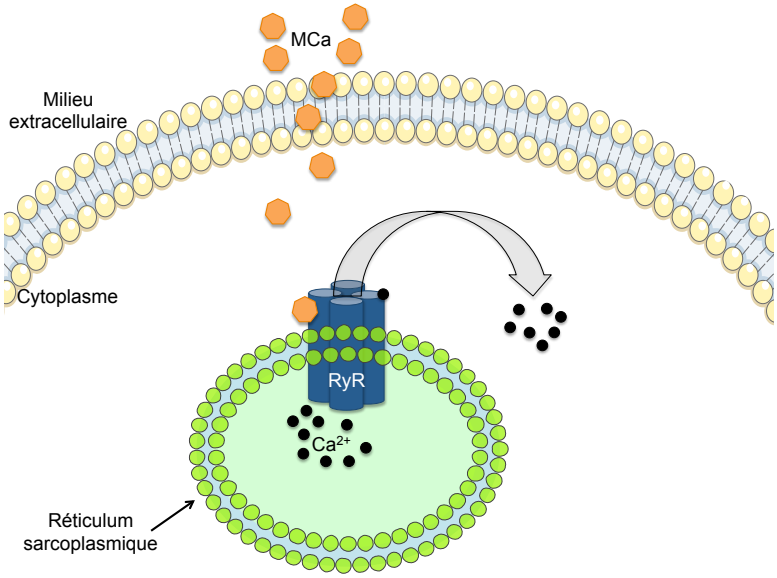

Figure 7 – Relargage de Ca^{2+} après fixation de la MCa sur le RyR

Propriétés de pénétration cellulaire

Afin d'atteindre sa cible, la MCa doit nécessairement franchir la membrane plasmique. Cette toxine possède donc des propriétés de pénétration cellulaire, qui font l'objet de nombreuses études depuis plusieurs années déjà.

En 2005, Estève *et al.* ont couplé la MCa au fluorochrome Cy3 *via* une liaison streptavidine/biotine (*cf* ***Couplage de cargos aux CPP***) afin de pouvoir suivre son entrée dans des cellules de différentes lignées par microscopie confocale. La capacité de la MCa à s'internaliser a été testée dans différentes conditions : à température normale ou à 4°C (afin de s'affranchir de l'effet de mécanismes dépendant de l'énergie), et en présence ou non d'inhibiteurs d'endocytose.

Cette étude a montré que l'internalisation de la MCa était indépendante des voies endocytaires puisque cette toxine est capable de franchir la membrane plasmique à faible température et en présence d'inhibiteurs de l'endocytose. L'hypothèse de la translocation comme voie majeure d'entrée de la MCa dans la cellule est confirmée par le relargage quasi-immédiat de calcium (après une minute d'incubation seulement), l'endocytose ne permettant pas une internalisation aussi rapide (Esteve *et al.*, 2005).

La prévalence de la translocation comme voie d'entrée de la MCa dans les cellules a été confirmée par Boisseau *et al.*, qui ont aussi montré que l'internalisation de cette toxine avait lieu de façon dose-dépendante. Leur étude a également mis en évidence le rôle du potentiel de membrane, la pénétration de la MCa étant diminuée après dépolarisation de la membrane plasmique (Boisseau *et al.*, 2006). Ces caractéristiques d'internalisation étant communes aux CPP, la maurocalcine est considérée comme un nouveau peptide de pénétration cellulaire.

Par ailleurs, il est à noter que la présence d'acides aminés basiques dans la structure de la MCa native joue un rôle prépondérant dans son interaction avec la membrane plasmique. En effet, la suppression d'un seul de ces acides aminés diminue la forte affinité de la MCa pour les lipides chargés négativement, or cette affinité est primordiale à la translocation de la toxine dans les cellules (Mabrouk *et al.*, 2007).

La MCa possède la capacité de s'internaliser à de faibles concentrations extracellulaires et sans qu'une incubation longue soit nécessaire. Cependant, ses propriétés pharmacologiques, même si elles ne s'appliquent pas à tous les types cellulaires, sont à éviter pour une application *in vivo*. C'est pourquoi plusieurs études ont été (et sont encore) consacrées à la mise au point d'un analogue de la maurocalcine dépourvu d'effet pharmacologique. On peut par exemple citer la maurocalcine linéaire, qui conserve tous les acides aminés de la structure native sauf les cystéines (remplacées par des résidus Abu, acide aminobutyrique), ce qui inhibe la formation de ponts disulfure et donc le repliement du peptide. Une cystéine surnuméraire a été ajoutée en N-terminal afin de permettre le couplage de cargos, mais puisqu'elle est unique au sein de la structure, la molécule reste linéaire. Cet analogue, MCa_{Abu}, conserve des propriétés de pénétration cellulaire (bien que légèrement inférieures à celles de la MCa native), n'a aucun effet pharmacologique, et possède donc l'avantage d'être en mesure de se fixer à un cargo (Ram *et al.*, 2008a).

Si l'analogue linéaire est plus facile à synthétiser et n'est pas en mesure de se lier au RyR, il présente néanmoins le désavantage d'une moins grande stabilité *in vivo* par rapport à un peptide possédant une structure repliée. Afin de conserver les avantages d'une toxine foldée tout en s'affranchissant de son activité pharmacologique, un variant de la maurocalcine a été synthétisé à partir d'acides aminés D (la toxine native étant composée d'acides aminés L). Ce peptide est appelé "D-MCa", en opposition à la "L-MCa". La D-MCa conserve les propriétés de pénétration de la L-MCa quasi-intactes, n'a aucune activité pharmacologique et possède l'avantage d'une plus grande stabilité *in vivo* par rapport à l'analogue linéaire (Poillot *et al.*, 2010).

Malgré les propriétés de pénétration cellulaire remarquables de la MCa, la fixation d'un cargo peut influencer l'internalisation du complexe. Ram *et al.* ont par exemple montré que la MCa couplée à la streptavidine (pour la formation d'un complexe avec le fluorochrome Cy5 lui-même lié à la biotine) ne favorisait pas la translocation mais au contraire s'internalisait majoritairement *via* la macropinocytose. Ceci est probablement dû au fait que la streptavidine est en mesure de se lier simultanément à quatre molécules de MCa. En effet, le complexe ainsi formé est de taille imposante, mais il est également probable qu'il ne permette pas une interaction optimale de la toxine avec la membrane plasmique (Ram *et al.*, 2008b).

Couplage de cargos à la MCa

Bien que ce ne soit pas leur fonction première, les molécules couplées à la MCa afin de permettre sa détection (et notamment la streptavidine, impliquée dans la liaison aux fluorochromes et de masse supérieure à celle de la toxine) ont permis de mettre en évidence la capacité de la maurocalcine à induire l'internalisation des cargos qui lui sont greffés (Esteve *et al.*, 2005).

Partant de ce constat, Aroui *et al.* se sont inspirés des travaux de Ram et de ses collaborateurs pour la création d'un complexe formé par le peptide MCa_{Abu} couplé *via* une liaison covalente (grâce à sa cystéine surnuméraire) à un cross-linker, lui-même lié à la doxorubicine. La doxorubicine est un agent antitumoral applicable à plusieurs types de cancer, mais son action est limitée par la fréquente apparition d'une résistance de la part des cellules tumorales après une certaine durée de traitement. Cette résistance intervient principalement sous la forme d'une augmentation de l'extrusion de la drogue. Grâce aux propriétés de pénétration et d'accumulation cellulaire de la maurocalcine, le complexe MCa_{Abu}-doxorubicine a pu "contourner" le mécanisme de résistance et resensibiliser *in vitro* une lignée de cellules tumorales de sein. Néanmoins, cette molécule chimère s'est montrée légèrement moins efficace que la doxorubicine seule dans le cas de cellules sensibles, ce qui suggère de limiter son utilisation aux cancers chimiorésistants (Aroui *et al.*, 2009).

La maurocalcine est utile pour la délivrance intracellulaire de molécules thérapeutiques, mais elle peut également être un outil d'internalisation de molécules servant à l'imagerie. La toxine native a notamment été couplée à différentes nanoparticules luminescentes ou quantum dot (QD), *via* une liaison streptavidine-biotine. Chaque QD émettant à une longueur d'onde particulière, les différents complexes obtenus ont permis le marquage de différents types de leucocytes : monocytes/macrophages et lymphocytes T. La présence de ces sondes chimères au sein du cytoplasme des cellules ne s'est pas révélée toxique *in vitro*. Les cellules marquées ont ensuite été réinjectées *in vivo* dans un modèle murin d'athérosclérose, l'évolution de la maladie étant caractérisée par l'infiltration de leucocytes. Cette technique a permis la détection précise de lésions athérosclérotiques formées et en cours de formation, ainsi qu'une meilleure compréhension de l'implication des différents types de leucocyte dans ce processus (Jayagopal *et al.*, 2009).

La maurocalcine est donc un produit naturel aux propriétés de pénétration et d'accumulation cellulaires puissantes, et particulièrement approprié pour l'internalisation de divers cargos. Cet outil reste néanmoins perfectible et certains de ses analogues se sont révélés comme des alternatives prometteuses. C'est dans ce contexte que s'inscrit mon travail de thèse.

Deuxième partie

Résultats

Chapitre 2

Article 1 : Incidence de la linéarisation et de la troncation de la maurocalcine sur la pénétration cellulaire

2.1 Introduction

Comme nous avons pu le voir dans l'introduction générale, la maurocalcine native (L-MCa) ainsi que son énantiomère (D-MCa) possèdent des propriétés de pénétration cellulaire et sont de ce fait considérées comme des nouveaux peptides de pénétration cellulaire (CPP). Cependant, si la D-MCa présente l'avantage de n'avoir, contrairement à la molécule native, aucune activité pharmacologique, sa synthèse reste complexe du fait de la présence de trois ponts disulfure et de sa taille relativement importante (33 acides aminés). De plus, la présence de ponts disulfure dans la structure d'un peptide, bien que lui conférant une plus grande stabilité *in vivo*, rend son couplage avec des cargos plus délicat. En effet, l'ajout d'une cystéine surnuméraire lors de la synthèse peptidique tend à interférer avec le processus de repliement. Cependant, la fonction thiol de cette cystéine est nécessaire au couplage avec des cargos *via* une liaison disulfure ou maleimide.

Au sein de l'équipe, une stratégie a donc été mise au point en 2008 : la synthèse d'un peptide conservant une séquence de 33 acides aminés mais dépourvu de ponts disulfure (Ram, Weiss 2008). Pour ce faire, les résidus cystéine à l'origine de ces ponts (Cys1-Cys4 Cys2-Cys5 et Cys3-Cys6) ont été remplacés par des groupements acide 2-aminobutyrique, inhibant de ce fait tout repliement. Ce peptide linéaire possède éga-

lement la capacité de pénétrer dans les cellules, mais de façon bien moins efficace que les molécules repliées. Cet analogue est donc avantageux en ce qui concerne la synthèse mais reste à améliorer en terme d'efficacité de pénétration cellulaire.

Nous avons donc cherché à identifier de nouveaux analogues de la MCa, plus faciles à synthétiser que la molécule native mais qui conserveraient ses propriétés de pénétration remarquables. Pour ce faire, nous avons testé différents variants linéaires tronqués et synthétisés avec une cystéine surnuméraire afin de permettre le couplage d'un cargo.

Cell Biology:

Small Efficient Cell-penetrating Peptides Derived from Scorpion Toxin Maurocalcine

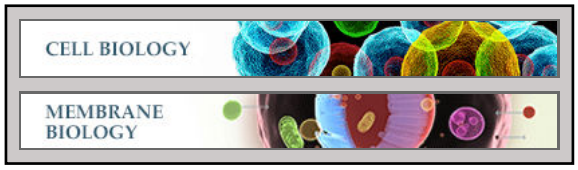

Cathy Poillot, Hicham Bichraoui, Céline Tisseyre, Eloi Bahemberae, Nicolas Andreotti, Jean-Marc Sabatier, Michel Ronjat and Michel De Waard

J. Biol. Chem. 2012, 287:17331-17342.
doi: 10.1074/jbc.M112.360628 originally published online March 20, 2012

THE JOURNAL OF BIOLOGICAL CHEMISTRY VOL. 287, NO. 21, pp. 17331–17342, May 18, 2012

Small Efficient Cell-penetrating Peptides Derived from Scorpion Toxin Maurocalcine*[S]

Received for publication, March 9, 2012 Published, JBC Papers in Press, March 20, 2012, DOI 10.1074/jbc.M112.360628

Cathy Poillot[‡§], Hicham Bichraoui[‡§1], Céline Tisseyre[‡§1], Eloi Bahemberae[‡§], Nicolas Andreotti[¶], Jean-Marc Sabatier[¶], Michel Ronjat[‡§], and Michel De Waard[‡§‖2]

From [‡]INSERM U836, Grenoble Neuroscience Institute, Site Santé La Tronche, Chemin Fortuné Ferrini, BP 170, 38042 Grenoble Cedex 9, France, the [§]Université Joseph Fourier, 38041 Grenoble, France, [¶]INSERM UMR1097, Luminy, 13288 Marseille, France, and [‖]Smartox Biotechnologies, Biopolis, 5 Avenue du Grand Sablon, 38700 La Tronche, France

Background: This study aimed at developing a new set of maurocalcine-derived cell-penetrating peptides from truncation.
Results: Several truncated peptides were designed and evaluated for Cy5 dye cell penetration.
Conclusion: All truncated peptides are competitive cell-penetrating peptides, many of them comparing favorably well with TAT.
Significance: Maurocalcine-derived truncated cell-penetrating peptides differ in their properties, enlarging the potential fields of applications.

Maurocalcine is the first demonstrated example of an animal toxin peptide with efficient cell penetration properties. Although it is a highly competitive cell-penetrating peptide (CPP), its relatively large size of 33 amino acids and the presence of three internal disulfide bridges may hamper its development for *in vitro* and *in vivo* applications. Here, we demonstrate that several efficient CPPs can be derived from maurocalcine by replacing Cys residues by isosteric 2-aminobutyric acid residues and sequence truncation down to peptides of up to 9 residues in length. A surprising finding is that all of the truncated maurocalcine analogues possessed cell penetration properties, indicating that the maurocalcine is a highly specialized CPP. Careful examination of the cell penetration properties of the truncated analogues indicates that several maurocalcine-derived peptides should be of great interest for cell delivery applications where peptide size matters.

Maurocalcine (MCa)[3] is a 33-mer peptide that was initially isolated from the venom of a Tunisian chactid scorpion, *Scorpio maurus palmatus* (1). The toxin belongs to a family of peptide that folds according to an inhibitor cystine knot motif and thus contains three disulfide bridges with a Cys^1-Cys^4, Cys^2-Cys^5, and Cys^3-Cys^6 connecting pattern (2). The solution structure, as defined by ^{1}H NMR, illustrates that MCa contains three β-strands (strand 1 from amino acid residues 9–11, strand 2 from 20–23, and strand 3 from 30–33). One distinctiveness of MCa is the fact that it is greatly enriched in basic amino acid residues. Of the 33 amino acids that compose MCa, 12 of them are basic, most of them represented by Lys residues. Interestingly, the β-strands of MCa encompass most of the basic domains (see Fig. 1*A*). MCa turned to be of interest to our research group for several reasons. First, it is an exquisite pharmacological activator of the ryanodine receptor type 1 (RyR1) from skeletal muscle because it promotes high Po gating modes and long lasting subconductance states of the ion channel (3, 4). On myotubes, application of MCa rapidly induces Ca^{2+} release from the sarcoplasmic reticulum (SR) (5), a result further confirmed by positive effect of MCa on the release of Ca^{2+} from purified SR vesicles (3, 5). The interaction of MCa with RyR1 has been witnessed by increased [^{3}H]ryanodine binding onto purified RyR1 (3, 5). The binding site for MCa on RyR1 has also been mapped and shown to correspond to domain(s) that have a predicted localization within the cytoplasm (6). Second, similarly to imperatoxin A (7) for which this was first noted, MCa has an interesting sequence homology with the II–III loop of the L-type calcium channel $Ca_v1.1$ subunit over a domain that is slightly larger than the second β-strand of MCa (see Fig. 1*A*) (5). This loop is predominantly involved in excitation-contraction coupling through direct molecular interactions with RyR1 (6, 8). This homology has been a source of inspiration to an understanding of how toxins may interfere with the process of excitation-contraction coupling (4, 8, 9). Third, and this is the scope of this paper, MCa has been shown to act as a cell-penetrating peptide (CPP) (10). This discovery stemmed from earlier criticisms that MCa may not be an activator of RyR1 because peptide toxins were not known to cross the plasma membrane, which would be required here to bind to RyR1. Studies that were undertaken to demonstrate the ability of MCa to reach its target showed that (i) MCa triggers Ca^{2+} release from the SR a few seconds after its application in the extracellular medium (5) and (ii) intracellular accumulation of fluorescent-streptavidin occurs if it incubated first with biotinylated MCa (10). Since these pioneering studies, MCa or analogues thereof proved powerful vectors for the cell entry of proteins, peptides (11),

* This work was supported by grants from Technology pour la Santé (Program TIMOMA2 of the Commissariat à l'Energie Atomique) and from Agence Nationale pour la Recherche PNANO (Programs SYNERGIE and NanoFret). Mass spectrometry analyses were performed by the Centre d'Investigation Clinique of Grenoble under the direction of Dr. Michel Sève.
[S] This article contains supplemental Figs. 1 and 2.
[1] Both authors contributed equally to this work.
[2] To whom correspondence should be addressed. Tel.: 33-4-56-52-05-63; Fax: 33-4-56-52-06-37; E-mail: michel.dewaard@ujf-grenoble.fr.
[3] The abbreviations used are: MCa, maurocalcine; Abu, 2-aminobutyric acid; CPP, cell-penetrating peptide; F, folded; Fmoc, *N*-(9-fluorenyl)methoxycarbonyl; MTT, 3-(4,5-dimethylthiazol-2-yl)-2,5-diphenyltetrazolium bromide; RyR, ryanodine receptor; SR, sarcoplasmic reticulum; UF, unfolded.

nanoparticles, or drugs such as doxorubicin (12–15). Although the mode of cell penetration of MCa may vary according to cargo nature, cell type, or chemical linkage employed, the data gathered so far suggest that the peptide may enter cells according to two priming steps onto the plasma membrane: first an interaction with proteoglycans with an affinity in the micromolar range, followed by a second interaction with negatively charged lipids which occurs with greater affinity (16, 17). The mode of cell entry of MCa is not altered by the absence of proteoglycans, but simply reduced quantitatively, suggesting that proteoglycans do not orient the mode of cell penetration. Two modes seem to concur to MCa cell entry, as far as observed, one related to macropinocytosis and another to membrane translocation. The balance between both modes of entry was found correlated to cargo nature and the type of MCa analogue used. It is of great interest to pursue the study of MCa as CPP despite the wealth of new CPP sequences that are discovered yearly. Among the competitive advantage of MCa over other CPP sequences are the facts that it has almost no associated toxicity *in vitro* and *in vivo*, penetrates into cells at very low concentrations, and is extremely stable *in vivo* upon intravenous injection (over 24 h).[4]

Although MCa appears as an elaborate and efficient CPP, its pharmacological properties represent a serious hindrance while envisioning *in vitro* and *in vivo* applications. In addition, because of its length (33 amino acid residues) and the presence of three disulfide bridges, MCa is a relatively difficult to synthesize CPP, compared with other CPPs, and would benefit from a downsizing approach. Several strategies have been employed successfully in the past to overcome one or both of these issues. The first strategy was based on single-point mutations of the MCa sequence. This strategy preserved the disulfide bridges and the three-dimensional structure of the analogues. Overall, mutations affected more seriously the pharmacology of MCa than the cell penetration properties (18). Many of the amino acids involved in RyR1 binding and pharmacology were located within the cluster of basic amino acids that presented sequence homology with the L-type $Ca_v1.1$ channel. Some of these residues, but not all, were also important for cell penetration properties. Hence, several analogues could be defined that kept close to intact cell penetration properties while entirely losing their pharmacological action (MCa R24A for instance). Some other analogues were actually better than MCa itself for cell penetration, suggesting that pairs of mutations, aiming at disrupting pharmacology and improving penetration, may be used in the future to define still better CPP analogues of MCa. The second strategy, which has yield success, is based on the chemical synthesis of D-MCa, an analogue entirely based on the use of D-amino acids. This peptide is a mirror image of the natural L-MCa but, like other D-CPPs, preserves its cell penetration properties while losing entirely its ability to interact with RyR1 (19). This method has several advantages. It no longer is sensitive to proteases that may be an additional advantage for *in vivo* experiments where the half-life of the circulating peptide matters. It is also possible to improve this analog by introducing point mutations shown previously to improve cell penetration (19). In these two strategies, although being effective, one may argue that (i) the peptides are still among the longest CPP known to date, implying increased costs of production, and (ii) the yield of production of these peptides is hampered by the folding process. Also, the use of peptides with internal disulfide bridges, despite have advantageous features in term of stability *in vivo*, makes chemical coupling of these CPPs to cargoes more complicated (difficulty to add extra Cys residues to the peptides for instance without interfering with the correct folding process). The third strategy that was used to circumvent one of this criticism was the chemical synthesis of an MCa analog in which all internal Cys residues were replaced by isosteric 2-aminobutyric acid residues (11). The resulting peptide was still 33-mer long but one step in production was saved by avoiding the folding process. In addition, an extra-Cys residue could be added to the N terminus of the peptide to favor simplified cargo grafting on this CPP analogue. This peptide, termed here C-$MCa_{UF1–33}$ (C for extra-Cys, UF for unfolded, and 1–33 for its length; see Fig. 1*B*) no longer has any secondary structures, but efficiently penetrates into cells. Interestingly also, the peptide completely lacks pharmacological activity, indicating that folding and secondary structures are essential for binding onto RyR1. Although this peptide is an efficient CPP, it remains less potent than MCa in its folded version, suggesting that further optimization should be brought to this analogue. Such optimization appears feasible on the basis of the fact that MCa fulfills three different functions (pharmacology, obligation to resemble the L-type channel, and cell penetration). We reasoned that because only cell penetration was the quality we searched for, the peptide could be further simplified and novel analogues be designed.

In this study, we undertook to identify new more potent MCa analogues with three criteria in mind. First, these analogues should be shorter than the folded version of MCa (MCa_F) or the unfolded version (MCa_{UF}). Second, these peptides should be designed to better delimitate the domains of MCa responsible for cell penetration. Third, we should be able to design analogues with extra free SH functions for cargo grafting. We present several new analogues that have highly potent cell penetration capabilities, while losing pharmacological activity, preserving lack of cell toxicity, and with facilitated cargo grafting. This new generation of MCa analogues is predicted to have bright futures for CPP applications *in vitro* and *in vivo*.

EXPERIMENTAL PROCEDURES

Reagents—*N*-α-Fmoc-L-amino acid, Wang-Tentagel resin, and reagents used for peptide syntheses were obtained from Iris Biotech. Solvents were analytical grade products from Acros Organics. Cy5 maleimide mono-reactive dye was purchased from GE Healthcare.

Solid Phase Peptide Syntheses—Chemical syntheses of MCa analogues were performed as described previously (19). Briefly, analogues of MCa were chemically synthesized by the solid phase method (20) using an automated peptide synthesizer (CEM© Liberty). Peptide chains were assembled stepwise on 0.24 meq of Fmoc-D-Arg-Pbf-Wang-Tentagel resin using 0.24 mmol of Fmoc L-amino acid derivatives. The side chain pro-

[4] C. Poillot, H. Bichraoui, C. Tisseyre, E. Bahemberae, N. Andreotti, J.-M. Sabatier, M. Ronjat, and M. De Waard, unpublished data.

tecting groups were: Trityl for Cys and Asn; *tert*-butyl for Ser, Thr, Glu, and Asp; Pbf for Arg; and *tert*-butylcarbonyl for Lys. Reagents were at the following concentrations: Fmoc-amino acids (0.2 M Fmoc-AA-OH in dimethylformamide), activator (0.5 M 2-(1H-benzotriazole-1-yl)-1,1,3,3-tetramethyluronium hexafluorophosphate in dimethyformamide), activator base (2 M diisopropylethylamine in *N*-methyl-pyrrolidone) and deprotecting agent (5% piperazine/0.1 M 1-hydroxybenzotriazole in dimethyformamide), as advised by PepDriver (CEM©). After peptide chain assembly, resins were treated 4 h at room temperature with a mixture of TFA/water/triisopropylsilan/dithiothreitol (DTT) (92.5/2.5/2.5/2.5). The peptide mixtures were then filtered, and the filtrates were precipitated by adding cold *t*-butylmethyl ether. The crude peptides were pelleted by centrifugation (10,000 × *g*, 15 min), and the supernatants were discarded. MCa analogues were purified by HPLC using a Vydac C18 column (218TP1010, 25 × 10 cm). Elutions of the peptides were performed with a 10–60% acetonitrile linear gradient containing 0.1% TFA. The purified fractions were analyzed by analytical RP-HPLC (Vydac C18 column 218TP104, 25 × 4.6 cm). All analogues were characterized by MALDI-TOF mass spectrometry.

Labeling of Peptide with Cy5—Each peptide was labeled with Cy5 according to the manufacturer's protocol (GE Healthcare). Peptides were dissolved at 1 mg/ml in 0.1 M Na_2CO_3 buffer, pH 9.3. 300 μl of the solubilized peptides was added to Cy5-maleimide-containing tubes. The mixtures were incubated for 2 h at room temperature and then purified by HPLC using an analytical Vydac C18 column. Elution of the Cy5-labeled peptides was performed with a 10–60% acetonitrile linear gradient containing 0.1% TFA. The pure peak fractions were lyophilized and peptides quantified by UV spectrophotometer at 649 nm.

Cell Culture—Chinese hamster ovary (CHO) and F98 cell lines (from ATCC) were maintained at 37 °C in 5% CO_2 in F-12 nutrient medium (Invitrogen) supplemented with 10% (v/v, CHO) or 2% (v/v, F98) heat-inactivated fetal bovine serum (Invitrogen) and 100 units/ml streptomycin and penicillin (Invitrogen).

MTT Assay—Cells were seeded into 96-well micro plates at a density of ~8×10^4 cells/well. After 2 days of culture, the cells were incubated for 24 h at 37 °C with MCa analogues at a concentration of 10 μM. Control wells containing cell culture medium alone or with cells, both without peptide addition, were included in each experiment. 0.1% saponin was used as toxic agent for comparison. The cells were then incubated with MTT for 30 min. Conversion of MTT into purple colored MTT formazan by the living cells indicates the extent of cell viability. The crystals were dissolved with dimethyl sulfoxide, and the optical density was measured at 540 nm using a microplate reader (Biotek ELx-800; Mandel Scientific Inc.) for quantification of cell viability. All assays were run in triplicate.

Confocal Microscopy—For analysis of the subcellular localization of MCa-Cy5 analogues in living cells, cell cultures were incubated with the fluorescent peptides for 2 h and then washed with phosphate-buffered saline (PBS) alone. The plasma membrane was stained with 5 μg/ml rhodamine-conjugated concanavalin A (Molecular Probes) for 5 min. Cells were washed once more. Live cells were then immediately analyzed by confocal laser scanning microscopy using a Leica TCS-SPE operating system. Rhodamine (580 nm) and Cy5 (670 nm) were sequentially excited, and emission fluorescence was collected in z-confocal planes of 10–15-nm steps.

Fluorescence-activated Cell Sorting—CHO cells were incubated with various concentrations of Cy5-labeled peptides in F-12K culture medium without serum at 37 °C for 2 h. The cells were then washed with PBS to remove excess extracellular peptide and treated with 1 mg/ml trypsin (Invitrogen) for 5 min at 37 °C to detach cells from the surface and centrifuged at 200 × *g* before suspension in PBS. For experiments with the macropinocytosis inhibitor, amiloride, CHO cells were initially washed with F-12K and preincubated for 30 min at 37 °C with 1 mM amiloride (Sigma). The cells were then incubated for 2 h at 37 °C with 1 μM Cy5-MCa analogues. For all of these experimental conditions, flow cytometry analyses were performed with live cells using a Becton Dickinson FACS LSR II flow cytometer (BD Biosciences). Data were obtained and analyzed using FCS express software (De Novo). Live cells were gated by forward/side scattering from a total of 10,000 events.

Preparation of Heavy SR Vesicles—Heavy SR vesicles were prepared following the method of Kim *et al.* (21). Protein concentration was measured by the Biuret method.

[^{3}H]Ryanodine Binding Assay—Heavy SR vesicles (1 mg/ml) were incubated at 37 °C for 2 h in an assay buffer composed of 10 nM [^{3}H]ryanodine, 150 mM KCl, 2 mM EGTA, 2 mM $CaCl_2$ (pCa = 5), and 20 mM MOPS, pH 7.4. Truncated MCa analogues were added prior to the addition of heavy SR vesicles. [^{3}H]Ryanodine bound to heavy SR vesicles was measured by filtration through Whatman GF/B glass filters followed by three washes with 5 ml of ice-cold washing buffer composed of 150 mM NaCl, 20 mM HEPES, pH 7.4. [^{3}H]Ryanodine retained on the filters was measured by liquid scintillation. Nonspecific binding was measured in the presence of 80 μM unlabeled ryanodine. The data are presented as mean ± S.E. Each experiment was performed in triplicate.

Statistical Analyses—All data are given as mean ± S.D. for n number of observations, and statistical significance (p) was calculated using Student's t test.

RESULTS

Nonfolded Truncated Maurocalcine Peptides Are Efficient CPPs—Fig. 1*A* illustrates the primary structure of MCa with its secondary structures (β-strands) and its pattern of disulfide bridges. This peptide will be termed MCa_F, for folded (F) MCa. An earlier report has demonstrated that replacing the six internal cysteine residues of MCa by Abu residues results in a pharmacologically inert and unfolded (UF) CPP (MCa_{UF1-33}, Fig. 1*B*). This peptide loses its secondary structures (11). Because this project aims at identifying shorter CPP sequences based on MCa_{UF1-33} sequence by the delivery of Cy5 cargo, we first determined where at the N terminus (C-MCa_{UF1-33}) or C terminus (MCa_{UF1-33}-C) the cargo could be best grafted after addition of an extra cysteine residue (C) (Fig. 1*B*). As shown, both vector-cargo complexes Cy5-C-MCa_{UF1-33} and MCa_{UF1-33}-C-Cy5 penetrated efficiently within CHO cells, as estimated by confocal microscopy (Fig. 1*C*) or by FACS (Fig. 1*D*). At 3 μM, a slightly better cell penetration was observed with Cy5 localized

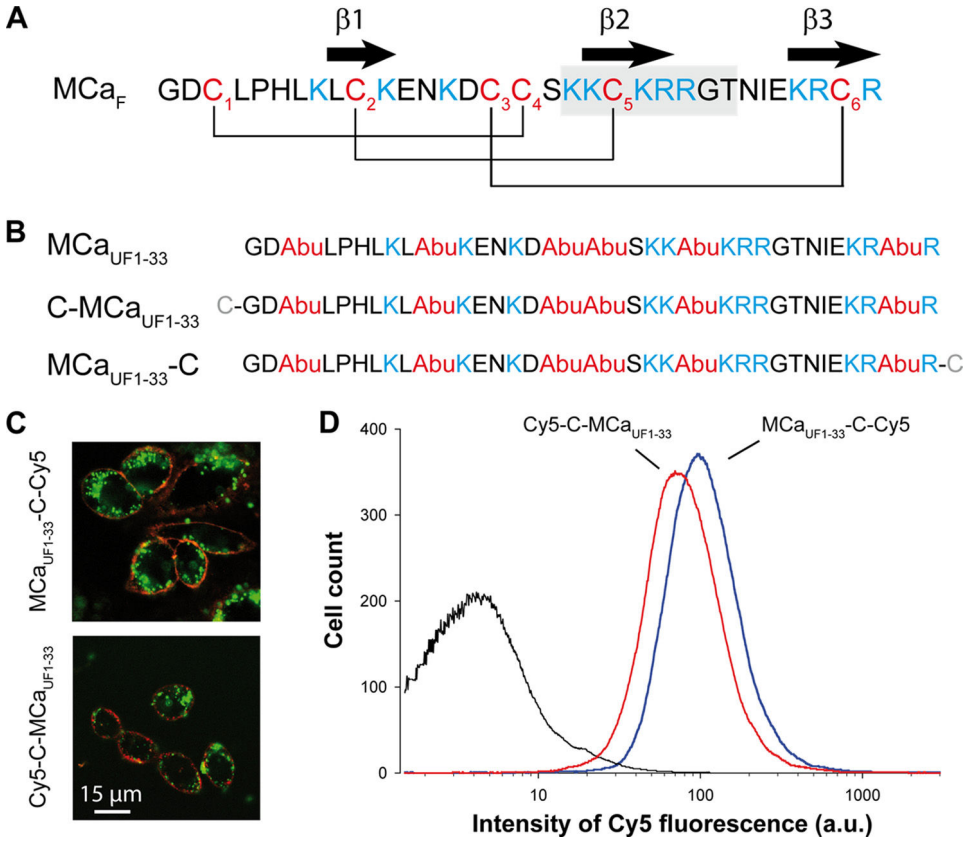

FIGURE 1. **Efficacy of cargo penetration as function of grafting position on MCa$_{UF1-33}$.** *A*, amino acid sequence of MCa$_F$ in single-letter code. The positions of half-cystine residues are *highlighted* in *red*. Cys residues are *numbered*, and basic amino acids are *highlighted* in *blue*. Secondary structures (β-strands) are indicated by *arrows*. The *gray box* is the sequence of homology of MCa with the dihydropyridine-sensitive Ca$_v$1.1 channel. *B*, amino acid sequences of unfolded MCa analogues in single-letter code. Cys residues are replaced by isosteric 2-aminobutyric acid residues (*Abu*, in *red*) to form MCa$_{UF1-33}$. An additional N-terminal (C-MCa$_{UF1-33}$) or C-terminal (MCa$_{UF1-33}$-C) Cys residue was added in two novel analogues competent for cargo grafting (shown in *gray*). *C*, confocal microscopy images illustrating cell penetration of Cy5-C-MCa$_{UF1-33}$ and MCa$_{UF1-33}$-C-Cy5 (*green labeling*). Plasma membranes are labeled with concanavalin A-rhodamine (in *red*). CHO cells were incubated 2 h with 1 μM peptide concentration. *D*, comparison of cell penetration efficacy between Cy5-C-MCa$_{UF1-33}$ and MCa$_{UF1-33}$-C-Cy5 as determined by FACS. CHO cells were incubated for 2 h with 3 μM peptide, washed and treated 5 min by 1 mg/ml trypsin before quantification of intracellular fluorescence. *a.u.*, arbitrary unit.

at the C terminus of MCa$_{UF1-33}$, but this difference was not significant. Because chemical syntheses of truncated MCa$_{UF1-33}$ analogues was facilitated by adding the extra cysteine residue at the C terminus of the sequence rather than at the N terminus, we kept on working on the basis of MCa$_{UF1-33}$-C sequence. Nevertheless, these data indicate for the first time that cargo grafting on the CPP MCa$_{UF1-33}$ can be performed likewise at both extremities of the sequence.

Next, we designed a series of truncated MCa$_{UF}$-C peptides comprising either a C-terminal truncation (three analogues: MCa$_{UF1-20}$-C, MCa$_{UF1-15}$-C, and MCa$_{UF1-9}$-C), a N-terminal truncation (7 analogues: MCa$_{UF8-33}$-C, MCa$_{UF11-33}$-C, MCa$_{UF14-33}$-C, MCa$_{UF18-33}$-C, MCa$_{UF20-33}$-C, MCa$_{UF22-33}$-C, and MCa$_{UF25-33}$-C), and Both N- and C-terminal truncations (2 analogues: MCa$_{UF6-25}$-C and MCa$_{UF14-25}$-C) (Fig. 2*A*). All of these analogues were then labeled with Cy5 to investigate their cell penetration properties. Every one of these peptides has been designed in such a way that the cargo would be removed from the peptide upon trypsin cleavage. This was useful for the FACS experiments in which the fluorescence associated to the cells is measured after trypsin treatment, thereby potentially removing the cargo from peptides that would eventually be associated with the outer part of the plasma membrane. The net positive charges of the peptides were drastically different, ranging from 0 (MCa$_{UF1-15}$-C and MCa$_{UF1-9}$-C) to +8 (MCa$_{UF8-33}$-C). However, many of the peptides contained a percentage of positively charged residues equal (MCa$_{UF-25-33}$-C) or superior to MCa$_F$ or MCa$_{UF1-33}$ (8 of 12 analogues). Three analogues had a lower percentage of basic residues than MCa$_F$ (all three C-terminal truncated analogues, MCa$_{UF1-20}$-C, MCa$_{UF1-15}$-C, and MCa$_{UF1-9}$-C).

We first evaluated by FACS the fluorescence accumulation within CHO cells that occurred after a 2 h incubation with 3 μM positively charged MCa peptides (net charge ≥ +5; Fig. 2*B*). This first study revealed several unexpected findings. First, all of the charged peptides (8 tested) demonstrated CPP properties. These peptides all had the K^{22}R^{23}R^{24} sequence in common, a cluster of basic amino acid residues shown to contribute to the dose efficacy of cell penetration of MCa$_F$ in an earlier study (18). Interestingly, removing the last 8 C-terminal amino acids of MCa had little impact on the cell penetration properties (if one compares MCa$_{UF14-25}$-C with MCa$_{UF14-33}$-C). Similarly, the removal of the amino acid region His^6-Asn^{13} did not drastically change cell penetration properties (MCa$_{UF6-25}$-C *versus* MCa$_{UF14-25}$-C). Second, all peptides appeared to behave better than the reference peptide MCa$_{UF1-33}$-C, suggesting that

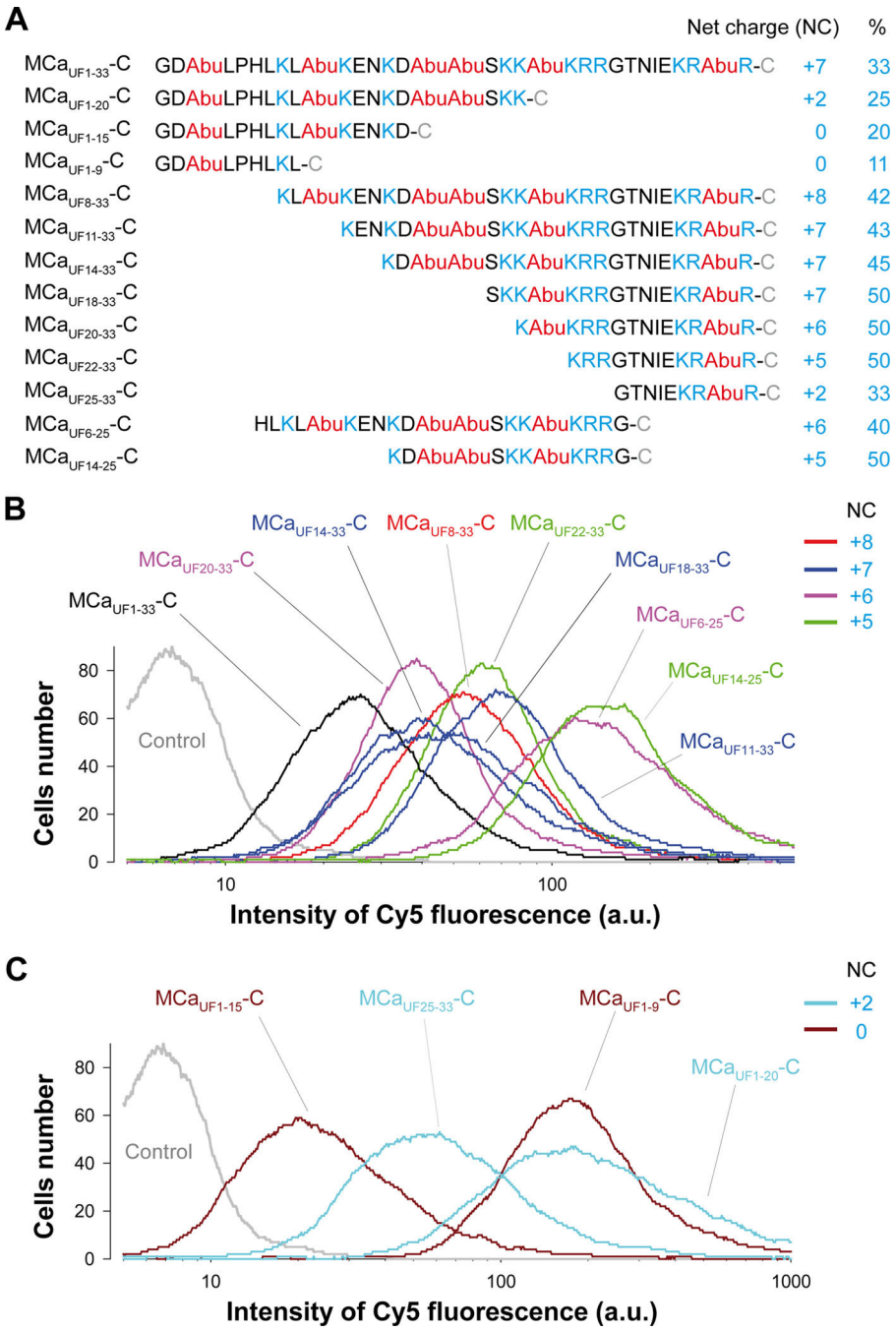

FIGURE 2. **Primary structure of truncated MCa$_{UF}$ analogues and comparison of cell penetration efficacies.** *A*, primary structures of truncated MCa$_{UF}$-C analogues and determination of their net positive charge and percentage of basic amino acid residues within the sequence. A total of 12 truncated MCa$_{UF}$-C analogues were produced (three with truncations in C terminus, seven in N terminus, and two in both N and C termini). Positively charged residues are in *blue* (His residues were not counted), whereas Abu residues that replace Cys residues are in *red*. *B*, comparative cell penetration efficacy of all MCa$_{UF}$-C-Cy5 truncated analogues that possess a net positive charge $\geq +5$. Code colors: *red* (net charge +8), *blue* (+7), *pink* (+6), and *green* (+5). The nontruncated MCa$_{UF1-33}$-C-Cy5 analogue is shown as reference (*black line*) for the efficacy of cell penetration of all analogues. Experimental conditions: CHO cell incubation with 1 μM concentration of each analogue for 2 h and fluorescence quantification by FACS. *a.u.*, arbitrary unit. *C*, same as *B* but for truncated MCa$_{UF}$-C-Cy5 analogues with positive net charge $\leq +2$.

sequence truncation of MCa$_{UF}$ may represent a potent strategy to define more efficient CPPs. Less positively charged peptides were also tested for their ability to penetrate into CHO cells (Fig. 2*C*). No less surprisingly, all peptides showed CPP properties, including two peptides with no net positive charge (MCa$_{UF1-9}$-C and MCa$_{UF1-15}$-C). MCa$_{UF1-9}$-C appeared as a better CPP than MCa$_{UF1-15}$-C, suggesting that the Abu^{10}-Asp^{15} region introduces no competitive advantage and confirming results shown in Fig. 2*B*. This may represent an inhibitory region because of the presence of Glu^{12} and Asp^{15}, two negatively charged residues. The finding that mutation of Glu^{12} to Ala enhances cell penetration of both MCa$_{F}$ (18) and MCa$_{UF}$ (11) further supports this conclusion. MCa$_{UF25-33}$-C turned out to have CPP properties also, even though this sequence did not confer a competitive advantage to other MCa CPP analogues as shown in Fig. 2*B*. Two additional experiments were conducted

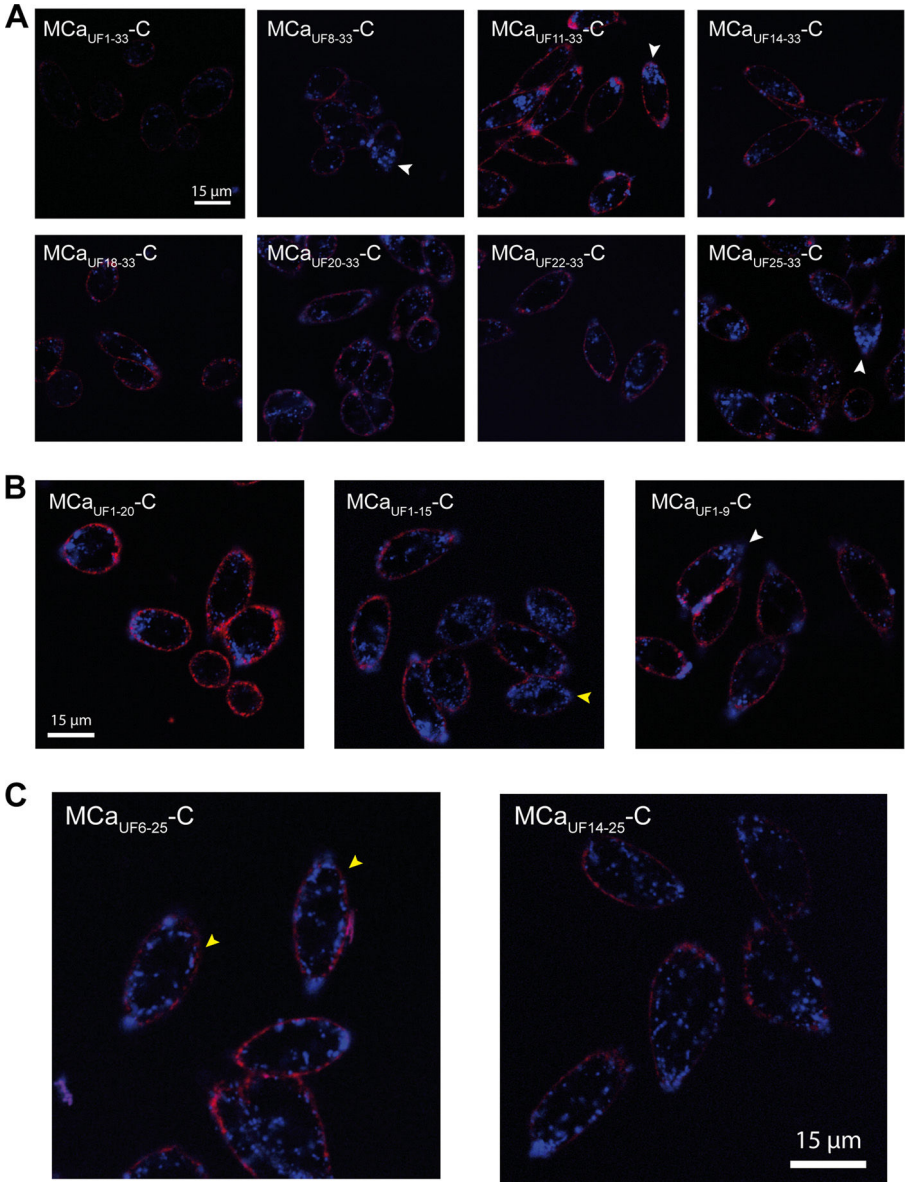

FIGURE 3. **All truncated MCa$_{UF}$-C-Cy5 vector-cargo complexes have resembling intracellular distributions.** *A*, intracellular distribution of N-terminal truncated MCa$_{UF}$ analogues. *B*, intracellular distribution of C-terminal truncated MCa$_{UF}$ analogues. *C*, intracellular distribution of N- and C-terminal truncated MCa$_{UF}$ analogues. CHO cells were incubated for 2 h with 3 μM MCa$_{UF}$-C-Cy5 vector-cargo complexes, before extensive washing, membrane labeling with rhodamine-conjugated concanavalin A, and live cell confocal microscopy imaging. Cy5 is in *blue*, and rhodamine is in *red*. *White arrows* illustrate a tendency for a preferential apical localization of the Cy5 dye. *Yellow arrows* illustrate the tendency for a subplasma membrane labeling of the Cy5 dye.

to confirm the specificity of these findings. First, a truncated charybdotoxin peptide was synthesized (ChTx$_{UF1-12}$-C) in which the internal Cys residue was replaced by Abu and an additional C-terminal Cys residue added for Cy5 labeling, as for our MCa$_{UF}$ analogues (supplemental Fig. 1*A*). As shown by confocal microscopy, ChTx$_{UF1-12}$-C was unable to deliver the Cy5 cargo at a higher concentration of 5 μM. Second, we also designed two MCa$_{UF}$ peptides in which, instead of using Abu derivatives, we mutated internal Cys residues by Ala residues. As shown, both MCa$_{UF1-9(Ala)}$-C and MCa$_{UF14-25(Ala)}$-C worked well for Cy5 delivery into CHO cells, demonstrating that Abu residues were not responsible by themselves for the cell penetration properties of the peptides (supplemental Fig. 1, *B* and *C*). Ala residues were, however, not fully equivalent to Abu residues as dose-response curve was slightly better for MCa$_{UF14-25(Ala)}$-C than for MCa$_{UF14-25}$-C, further arguing that Abu residues were not central to the cell penetration properties of truncated MCa$_{UF}$ peptides (supplemental Fig. 1*D*). The overall message from this first study is that all truncated MCa$_{UF}$ analogues can behave as CPPs at the concentration tested. The findings suggest that MCa is a peptide fully specialized to achieve cell penetration including in domains that are not highly charged.

Intracellular Distribution of All Truncated MCa$_{UF}$ Analogues Bears Resemblance to That of Full-length MCa$_{UF}$—Although all truncated derivatives of MCa$_{UF1-33}$ show cell penetration properties according to the FACS analyses, we examined whether there were differences in intracellular distribution among these peptides. This question was investigated by confocal microscopy after 2 h of peptide accumulation into CHO cells (Fig. 3). Interestingly, all peptides showed very sim-

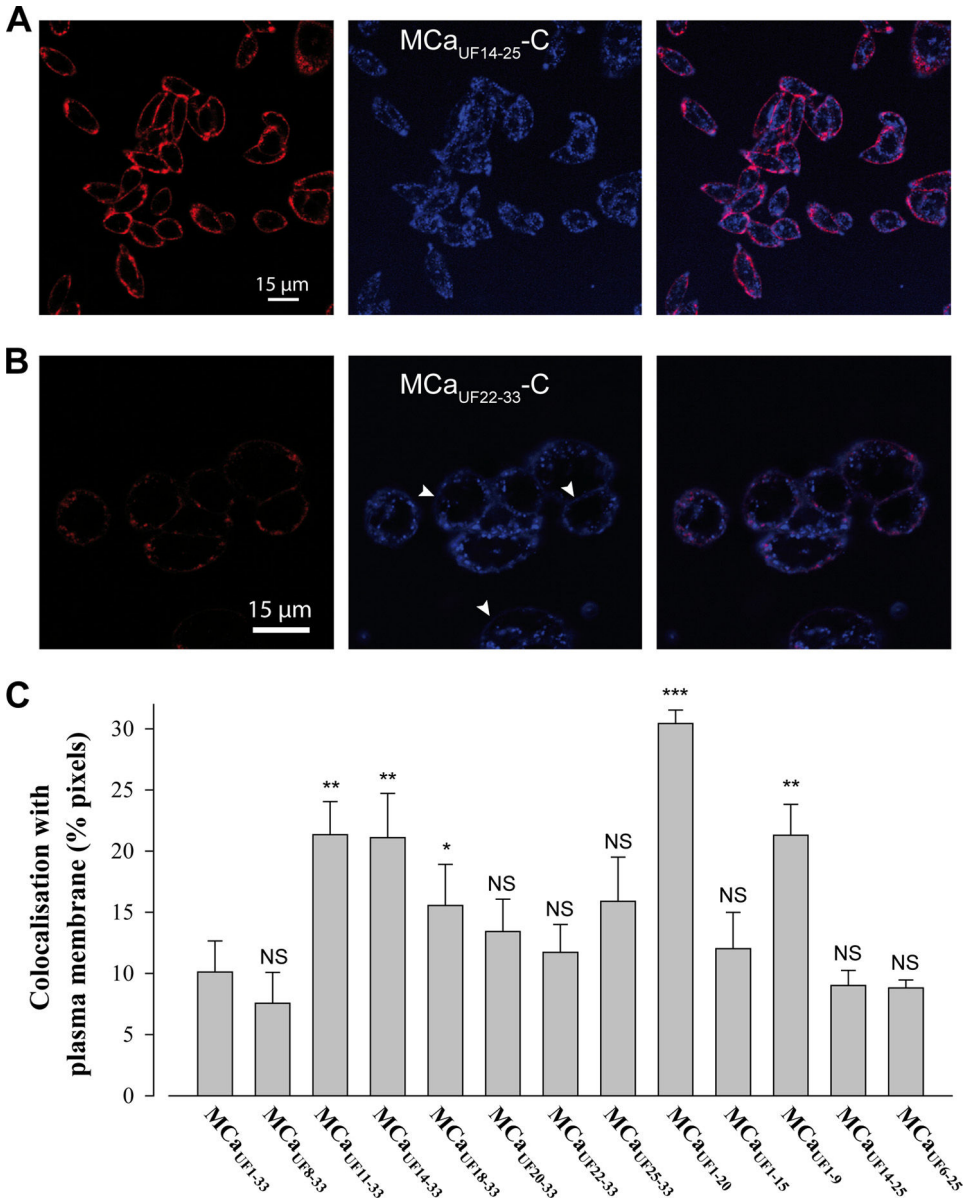

FIGURE 4. **Membrane staining is diffuse whereas intracellular staining is punctuated.** *A*, lower magnification image of CHO cells stained with 3 μM MCa$_{UF14-25}$-C-Cy5 that illustrates a predominant subplasma membrane rim-like distribution. *B*, diffuse membrane staining of CHO cells by MCa$_{UF22-33}$-C-Cy5. *White arrows* indicate domains of the plasma membrane where the diffuse staining of the peptide-cargo complex is the most evident. *C*, extent of colocalization of the Cy5-labeled peptides with the rhodamine-labeled plasma membrane. *NS*, nonsignificant; *, ≤0.1; **, ≤0.05; and ***, ≤0.001.

ilar intracellular distributions, although the degree of accumulated cell fluorescence varied somewhat with peptide sequences. In confirmation of the FACS results, the peptide that appeared to penetrate the least was the full-length unfolded MCa, MCa$_{UF1-33}$-C-Cy5 (Fig. 3*A*). The vast majority of the fluorescence appears in punctuate dots within the cells. In many cases, these dots appear at higher concentrations within one pole of the cell (see labeling of MCa$_{UF8-33}$-C-Cy5, MCa$_{UF11-33}$-C-Cy5, MCa$_{UF25-33}$-C-Cy5, and MCa$_{UF1-9}$-C-Cy5, for instance). On various occasions also, all of the peptides tend to present a subplasma membrane distribution, forming a rim of smaller circumference than the concanavalin A labeling itself. This subplasma membrane rim localization was more evident for CHO cells labeled with MCa$_{UF14-25}$-C-Cy5 as illustrated in Fig. 4*A*. Finally, more rarely, a direct plasma membrane labeling by the peptide-cargo complex was observable (Fig. 4*B*). This type of labeling could be observed with N-terminal truncated vectors exclusively and was most evident for MCa$_{UF22-33}$-C-Cy5. The staining of the plasma membrane was always diffuse in contrast to intracellular staining which was mainly punctuated. Diffuse membrane labeling was also observed for MCa$_{UF25-33}$-C-Cy5 and MCa$_{UF20-33}$-C-Cy5, two peptides that differ from 2 to 3 amino acids of MCa$_{UF22-33}$-C-Cy5. It was difficult to evidence for the other vector-cargo complexes. We propose that this staining coincides with an alteration of the duration of peptide plasma membrane residency for these truncated MCa$_{UF}$ analogues. The lower occurrence of this diffuse staining for the other truncated variants may reflect faster internalization by endocytosis and/or membrane translocation. Globally, these effects reflect cell entry and distribu-

tion tendencies that were hard to quantify, and they should therefore be interpreted with caution.

In an attempt to better apprehend peptide behavior at the plasma membrane, we quantified the extent of Cy5/rhodamine staining colocalization. Rhodamine-positive staining was also Cy5-positive for 63–86% of the pixels (best performing peptides were $MCa_{UF14-33}$-C-Cy5, $MCa_{UF18-33}$-C-Cy5, $MCa_{UF20-33}$-C-Cy5, and $MCa_{UF22-33}$-C-Cy5; data not shown). This finding indicates that the peptides invade large membrane areas and that membrane interaction is not limited to small specialized surface areas. In contrast, Cy5-positive pixels were rhodamine-positive to far more variable extents (Fig. 4*C*). For instance, 10.1 ± 2.6% of MCa_{UF1-33}-C-Cy5, the reference compound, was colocalized with the plasma membrane indicator. Despite the fact that short plasma membrane staining times were used (few minutes), a fraction of the colocalization that is quantified also corresponds to intracellular staining following ongoing endocytosis. Nevertheless, this result indicates that this peptide does not remain stuck within the plasma membrane during its 2-h incubation with CHO cells. It thus indicates relatively fast cell penetration. Many of the other peptides, however, behaved differently from MCa_{UF1-33}-C-Cy5. Indeed, several peptides show surprisingly higher colocalization with rhodamine (21.3 ± 2.6% for $MCa_{UF11-33}$-C-Cy5 and 30.4 ± 1.4% for MCa_{UF1-20}-C-Cy5, for instance). These higher values of colocalization indicate that some peptides remain for longer periods of time or at higher concentration within the plasma membrane. Alternatively, these peptides may rely more heavily on endocytosis for cell penetration and are present within intracellular organelles to which subsequent endocytotic vesicles that contain rhodamine labeling will fuse. Peptides most concerned by these behaviors were $MCa_{UF11-33}$-C-Cy5 and $MCa_{UF14-33}$-C-Cy5, which contained two or one of the CPP inhibitory negative charges (Glu^{12} and Asp^{15}), and MCa_{UF1-9}-C-Cy5 and MCa_{UF1-20}-C-Cy5, which were poorly charged peptides.

Amiloride Sensitivity of Cell Penetration of Truncated MCa_{UF} Analogues—In earlier studies, we have demonstrated that the cell entry of MCa_{UF1-33} was largely sensitive to amiloride. Because amiloride is an exquisite blocker of macropinosomes (22–24), this suggested a predominant macropinocytosis mechanism for its cell penetration (17). However, it was likely that such a predominant reliance on macropinocytosis was also conferred by the cargo type transported (streptavidin in that report). We therefore conducted an in-depth analysis of the amiloride sensitivity of the various truncated MCa_{UF} peptides with Cy5 as cargo and quantified by FACS the degree of cell penetration inhibition. Fig. 5*A* illustrates the amiloride sensitivity of four different truncated peptides. As shown, amiloride inhibits the cell penetration of MCa_{UF1-33}-C-Cy5 by 19.6% and of MCa_{UF1-15}-C-Cy5 by 39%. The finding that amiloride blocks to a far lesser extend the penetration of Cy5 compared with that of streptavidin (17) when MCa_{UF1-33} is the vector indicates the influence of the cargo nature on the mechanism of cell entry. Surprisingly, amiloride was found to enhance rather than inhibit the cell penetration of $MCa_{UF20-33}$-C-Cy5 and $MCa_{UF18-33}$-C-Cy5 (Fig. 5*A*). Preserving the plasma membrane from undergoing macropinocytosis may free surface areas for enhanced peptide translocation through the membrane. The effect of amiloride was always associated with a sharpening of the fluorescence intensity distribution in the *x* axis (see, for instance MCa_{UF1-15}-C-Cy5), reflecting reduced cell heterogeneity for the mechanisms underlying peptide penetration. The amiloride sensitivity of cell penetration was further investigated for all truncated MCa_{UF} peptides, and the results are presented in Fig. 5*B*. Four peptides showed higher amiloride sensitivity than MCa_{UF1-33}-C-Cy5 ($MCa_{UF11-33}$-C-Cy5, $MCa_{UF25-33}$-C-Cy5, MCa_{UF1-15}-C-Cy5, and $MCa_{UF14-25}$-C-Cy5). All other peptides showed reduced amiloride sensitivities or a tendency for greater cell penetration under the effect of amiloride. We conclude that the Cy5 cargo does not promote macropinocytosis as the main route of peptide entry and that truncation of MCa_{UF} may lead to analogues that rely to a lesser extent on macropinocytosis for cell entry.

Comparative Dose-dependent Cell Penetration of MCa_{UF} Analogues—Although we compared the properties of cell penetration of truncated peptides at rather mild concentrations, we also aimed at comparing the dose dependence of cell penetration of these peptides by FACS (Fig. 6). One example of such an analysis is shown for peptide MCa_{UF8-33}-C-Cy5 in Fig. 6*A*. 33 μM was the highest concentration that could be tested on CHO cells, and obviously cell penetration did not show any sign of saturation for cell incubation times with this peptide of 2 h. The dose-dependent cell penetrations were compared for all N-terminal truncated peptides (Fig. 6*B*), C-terminal truncated peptides (Fig. 6*C*), and double truncated analogues (Fig. 6*D*) with the same settings. These analyses confirm that MCa_{UF1-33}-C-Cy5 is the least performing cell-penetrating peptide. Most truncated peptides show detectable cell penetration at concentrations ≥1 μM. One remarkable exception to this rule was noticeable. MCa_{UF1-9}-C-Cy5 shows an unusual dose-dependent penetration with detectable cell penetration at 10 nM and only small progressive increases in fluorescence intensity with higher peptide concentrations (Fig. 6*C*). This peptide was therefore the best performing peptide for cell penetration at low concentrations. Finally, additional information that could be taken from these analyses is that the peptides differed significantly with regard to the maximal extent of cell penetration. Among the N-terminal truncated MCa_{UF} analogues, $MCa_{UF18-33}$-C-Cy5 performed drastically better than the other truncated peptides (Fig. 6*B*). The difference in cell penetration among $MCa_{UF11-33}$-C-Cy5 and $MCa_{UF18-33}$-C-Cy5 resides in the removal of the KENKDAbuAbu sequence which we presume is inhibitory to some extent because of the presence of Glu^{12} and Asp^{15}. Among the C-terminal truncated peptides, MCa_{UF1-20}-C-Cy5 was performing as well as MCa_{UF8-33}-C-Cy5, and although not tested at higher concentrations, MCa_{UF1-9}-C-Cy5 would be expected to perform still better. Finally, for N- and C-terminal truncated analogues, the best peptide turns out to be $MCa_{UF14-25}$-C-Cy5, which yields the greatest fluorescence accumulation at 33 μM compared with all other truncated MCa_{UF} analogues. Whereas all of these peptides performed quite well, we were curious to compare them with a classical CPP under similar experimental conditions. Cell penetration was observed for TAT-C in CHO cells, and the dose-response curve was equivalent or even less favorable for TAT than for many MCa_{UF} peptides (supplemental Fig. 1, *E*

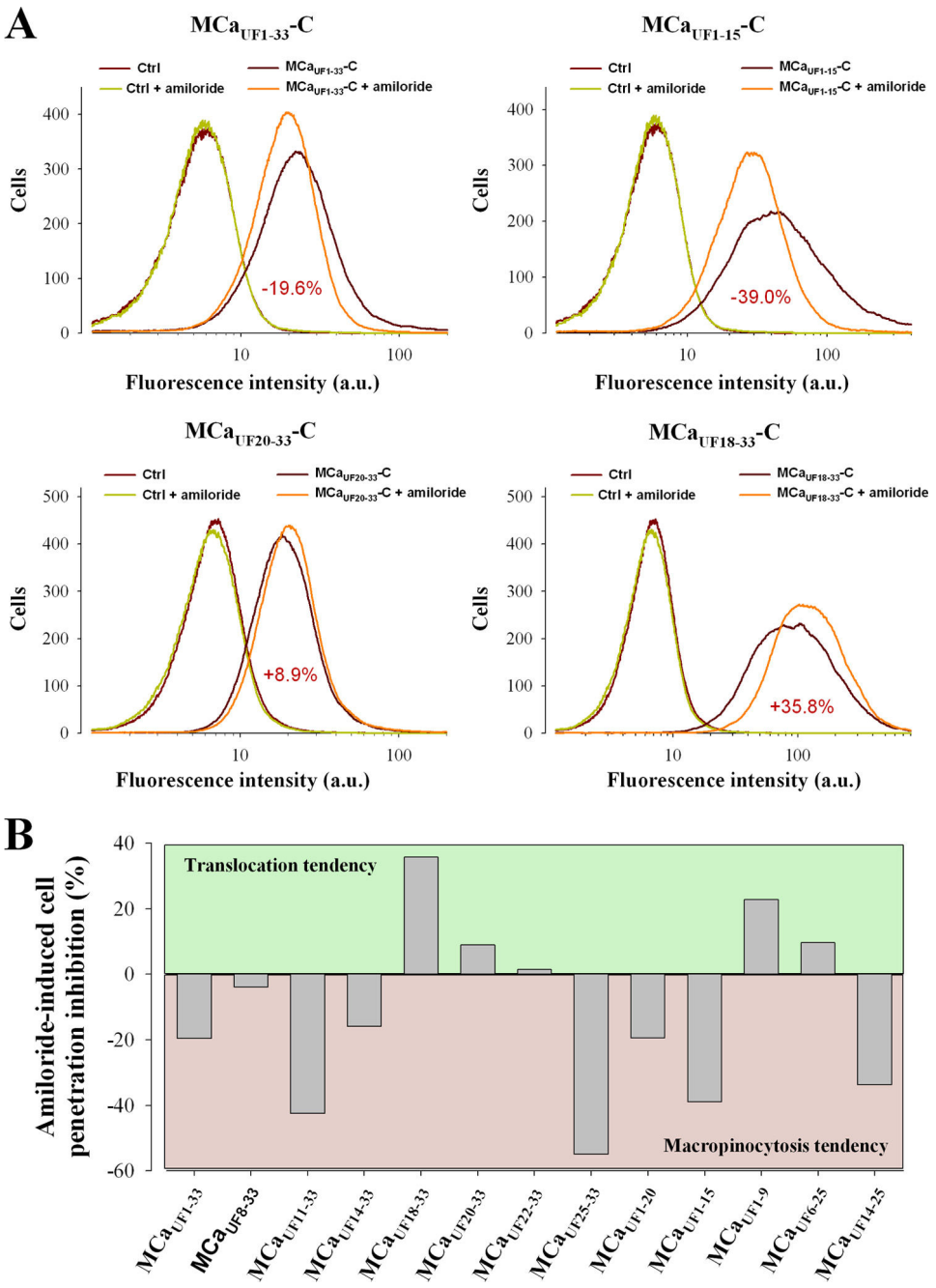

FIGURE 5. **Amiloride sensitivity of truncated MCa$_{UF}$ peptide cell entry.** *A*, representative FACS analyses of the effect of 5 mM amiloride on MCa$_{UF1-33}$-C-Cy5 (*upper left*), MCa$_{UF1-15}$-C-Cy5 (*upper right*), MCa$_{UF20-33}$-C-Cy5 (*lower left*), and MCa$_{UF18-33}$-C-Cy5 (*lower right*) entries. *Numbers* in *red* represent average decrease or increase in peptide entry upon amiloride treatment. Cells were treated for 2 h with 3 μM peptide concentration with or without 5 mM amiloride. *a.u.*, arbitrary unit. *B*, average effect of amiloride on mean cell entry of the truncated peptides. Positive values reflect increase in cell entries, whereas negative values indicate reduction in cell penetration.

and *F*). This was further largely confirmed when comparing the vector properties of TAT-C and MCa$_{UF1-9}$-C in yet another cell type, the glioma F98 rat cell line (supplemental Fig. 2). 3 μM MCa$_{UF1-9}$-C proved better than TAT-C at 3 and 10 μM.

Truncated MCa$_{UF}$ Peptides Lack Pharmacological Effects and Are Predominantly Nontoxic—An earlier report has shown that MCa$_{UF1-33}$ is unable to interact with the MCa target, RyR1 (11). This is due to the loss of secondary structures because of the lack of internal disulfide bridging. We did therefore expect that truncated analogues of MCa$_{UF}$ should also be pharmacologically inert. This hypothesis was challenged by testing the ability of the Cy5-free peptides to stimulate [^{3}H]ryanodine binding (Fig. 7*A*). As shown, contrary to MCa$_F$, which contains secondary structures and disulfide bridges, none of the peptides we designed had an effect on [^{3}H]ryanodine binding.

Finally, the peptides were challenged for their toxicity by incubating CHO cells with 1 or 10 μM peptide concentrations for an extended duration (24 h) that far exceeds the duration challenged for cell penetration (Fig. 7*B*). A 10 μM peptide concentration was generally slightly more toxic than 1 μM, except for MCa$_{UF14-25}$-C. At 1 μM, toxicity never exceeded 8%, and significances of these effects were negligible. In contrast, toxic-

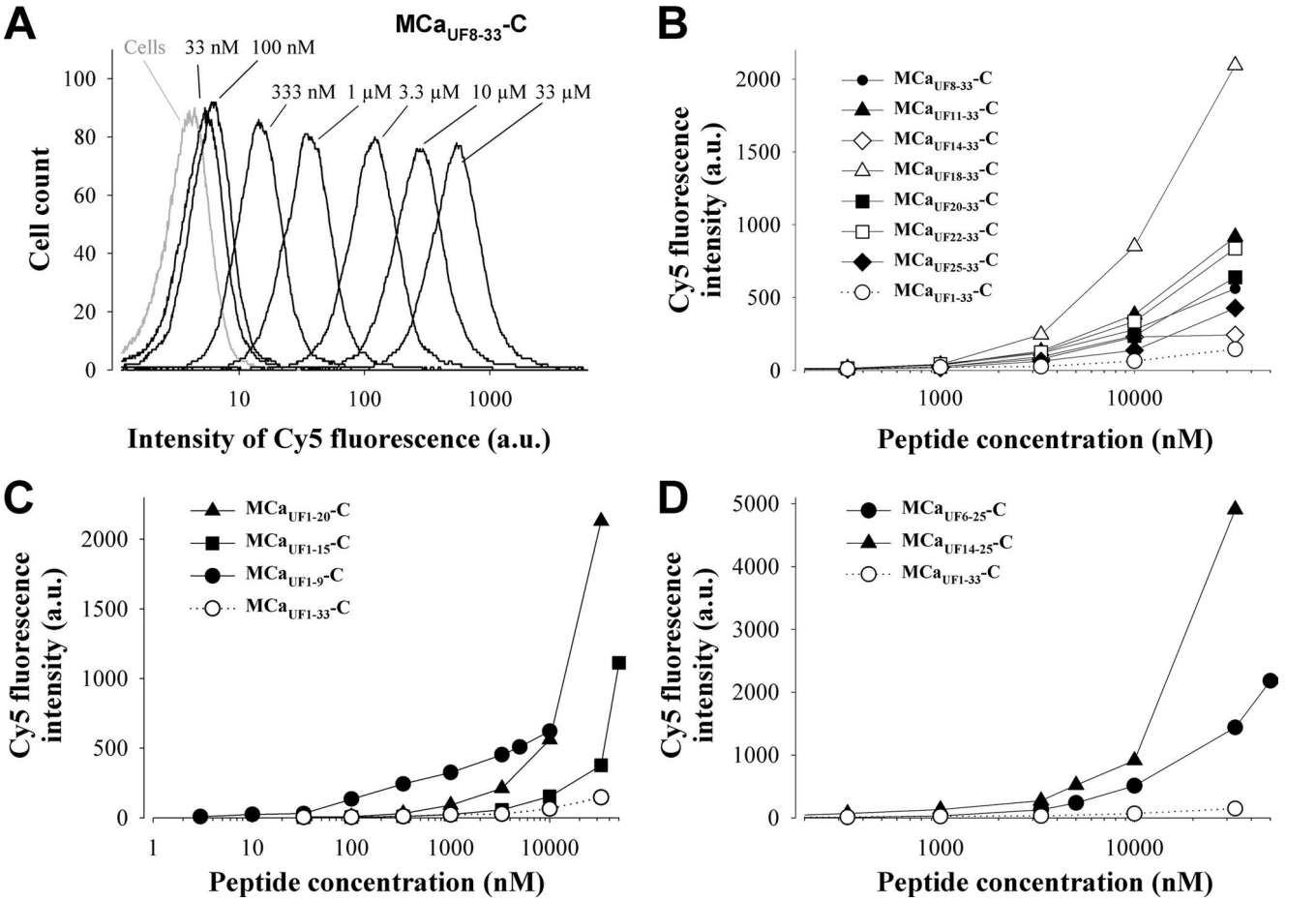

FIGURE 6. **Dose-dependent cell penetration of truncated MCaUF peptides.** *A*, representative example of the dose-dependent cell penetration of MCa_{UF8-33}-C -Cy5 in CHO cells as analyzed by FACS. The peptide was incubated for 2 h with the cells before analyses. There was no saturation of cell entry for a concentration up to 33 μM. *B*, dose-dependent cell penetration of N-terminal truncated MCa_{UF} peptides compared with MCa_{UF1-33}-C-Cy5 (*open circles*, *dotted line*). *a.u.*, arbitrary unit. *C*, dose-dependent cell penetration of C-terminal truncated MCa_{UF} peptides. *D*, dose-dependent cell penetration of N- and C-terminal truncated MCa_{UF} peptides. Note the increase in scale for the penetration of these two peptides.

ity could reach 20% at 10 μM peptide concentration, and these effects had higher significance. Most peptides behaved equally well or better than MCa_{UF1-33}-C, indicating that truncation did not enhance cell toxicity of the peptides.

DISCUSSION

MCa_F is a rather large and complex CPP with its three disulfide bridges which makes its use in *in vitro* and *in vivo* applications more delicate because of production yield (peptide with correct disulfide bridging) and cargo coupling (thiol groups are for the moment difficult to use). One may also argue that the size of the peptide introduces additional synthesis cost compared with other popular in use CPPs such as Tat and penetratin. Whereas size and folding most likely add a competitive advantage for *in vivo* applications because of peptide stability issues, it may be of interest to derive small CPPs from MCa that could have a broader use than MCa itself. The study we conducted not only aimed at defining these smaller MCa-derived CPP sequences, but also provided interesting clues on how MCa may have evolved for cell penetration. The most surprising finding from this study was therefore that all of the analogues we defined could be considered as CPPs, which suggests that MCa is a highly specialized sequence for the purpose of cell penetration. Although evidently none of the peptides could compete with MCa_F itself for cell penetration, it is nevertheless obvious that many of the truncated MCa_{UF} peptides are better CPPs than MCa_{UF1-33} itself. These findings lead to two general conclusions. First, folding and disulfide bridging appear to be prerequisites to properly optimizing the CPP potential of all of the MCa domains. It is highly likely that the secondary structures triggered by disulfide bridging play a key role in that respect. We therefore believe that it would be worthwhile to design additional MCa analogues presenting both truncations (like in the present study) and 1 to 2 disulfide bridges to regain some of the secondary structures that confer a competitive advantage to MCa_F for cell penetration. Second, the fact that all of the truncated sequences are CPPs that possess different properties and efficacies suggests that there is further room for MCa cell penetrating optimization. In this study, our data indicate that the amino acid region Lys^{11}-Ser^{18} would be an ideal target for mutagenesis. Glu^{12} mutation has already been shown to improve cell penetration on various analogues (11, 18). We now sense that Asp^{15} may also represent an excellent target for further optimization of MCa properties. Double mutagenesis may be an option. However, it will be essential to determine whether the disulfide bridging and folding ability of the native peptide is not affected by this procedure. Truncated MCa_{UF}

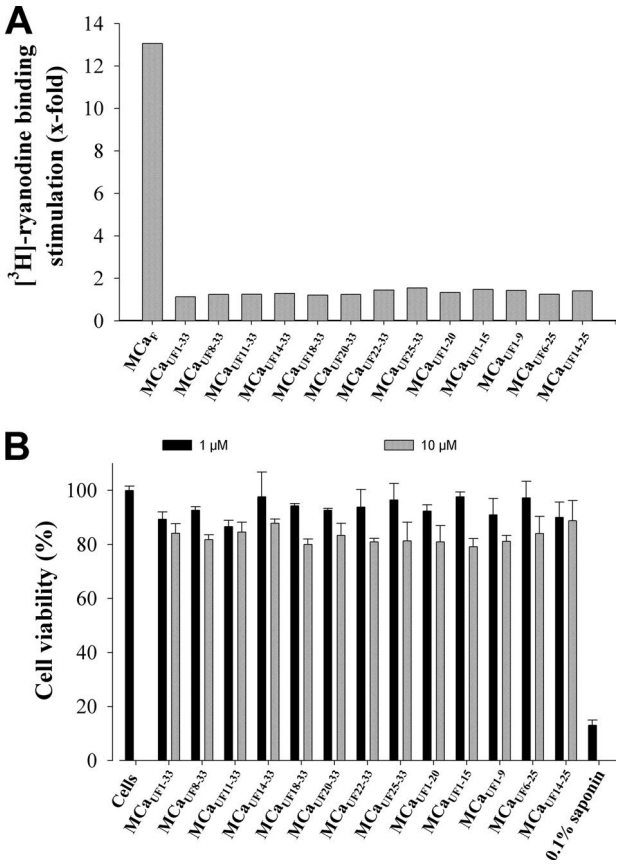

FIGURE 7. **Lack of pharmacological effects of the truncated peptides and reduced cell toxicity.** *A*, effect of MCa_F, MCa_{UF1-33}, and truncated MCa_{UF} peptides on [^{3}H]ryanodine binding. Data are expressed as -fold increase in binding induced by the peptides. *B*, effect of 1 and 10 μM MCa_{UF1-33} and truncated MCa_{UF} peptides on CHO cell viability. Peptides were incubated for 24 h with the cells *in vitro*.

peptides may also benefit from further mutagenesis of negatively charged residues, such as MCa_{UF1-20}. It is noteworthy that another well behaving truncated CPP, $MCa_{UF18-33}$, also contains a Glu residue at position 29 that could represent another target for mutagenesis and peptide optimization. This is also the case for MCa_{UF1-9} that contains an Asp residue at position 2.

Several other findings of this report merit some comments. First, we demonstrate that cargo coupling can occur at the N terminus as well as the C terminus of MCa, enhancing the flexibility of cargo coupling to our vectors. Second, although it is obvious that most of our truncated MCa_{UF} analogues remain heavily basic, we also found out that poorly charged MCa peptides could behave as efficient CPPs. This is the case for MCa_{UF1-9} which is one of our best performing CPPs, especially if one wishes to work with low CPP concentrations. Third, small size CPPs can be derived from MCa_{UF}, MCa_{UF1-9}, and $MCa_{UF25-33}$ being our smallest peptides. Although we did not test greater truncation, it is not impossible that still smaller CPPs might be designed on the basis of MCa sequence. Fourth, the truncated MCa_{UF} analogues differ somewhat in their mode of cell penetration, some being more prone to enter cells by macropinocytosis than others. Various peptides were even insensitive to amiloride application, suggesting that macropinocytosis did not contribute at all to their entry. We cannot exclude at this stage that these peptides rely on modes of endocytosis other than macropinocytosis. This is suggested by the punctuate nature of intracellular Cy5 fluorescence distribution. How reliably a punctuate distribution reveals endocytosis is however not known, and one cannot rule out also that this distribution is due to peptide aggregation with or without lipid components. When plasma membrane distribution could be observed, large diffuse staining was evident, indicating that when peptides encountered the membrane no such aggregation occurred. In any case, many of the peptides had distribution that mostly differed from plasma membrane labeling (including these membranes that had undergone endocytosis), indicating that peptide intracellular distribution may not necessarily colocalize with the plasma membrane components. Refined studies will be required, however, to define how much of the peptides enter cells by direct membrane translocation *versus* endocytosis.

In conclusion, we identified several interesting lead CPPs based on MCa_{UF} truncation strategy. This is the case for $MCa_{UF18-33}$ (macropinocytosis entry-independent), MCa_{UF1-9} (penetrates better at low concentration), and $MCa_{UF14-25}$ (yields the greatest cell entry of the dye). These peptides are easy to produce, yield good cell penetration, and we should be able to further improve their cell penetrating characteristics by mutagenesis or by reintroducing one disulfide bridge to restore some of the secondary structures. Although the scope of this study was not to compare our mini-MCa with other popular CPPs, we were surprised to find out that many of the MCa_{UF} vectors behaved far better than TAT for the transport of Cy5, both in CHO and F98 cells. It may be argued that the field does not require many more CPP sequences. However, a significant fraction of the ongoing research is based on the use of TAT, which no longer appears as the most competitive peptide. Also, increasing evidence suggests that CPP sequences differ in their cell type targeting properties, which will undoubtedly represent an important feature to exploit when it comes to developing *in vivo* applications. Other essential parameters for *in vivo* applications will be the peptide stability upon intravenous or intraperitoneal injection. In that respect, we found out that MCa is a particularly stable peptide with and without disulfide bridges.[4] These still "hidden" aspects of the CPP features may be advantageously exploited later on if the number of known CPPs is high. The advantages of using smaller CPPs over MCa_F remains to be investigated as one may of course argue also that they require higher concentrations and possibly longer incubation times for effectiveness, two factors that may lead to spurious signaling events *in vivo*.

REFERENCES

1. Fajloun, Z., Kharrat, R., Chen, L., Lecomte, C., Di Luccio, E., Bichet, D., El Ayeb, M., Rochat, H., Allen, P. D., Pessah, I. N., De Waard, M., and Sabatier, J. M. (2000) Chemical synthesis and characterization of maurocalcine, a scorpion toxin that activates Ca^{2+} release channel/ryanodine receptors. *FEBS Lett.* **469,** 179–185
2. Mosbah, A., Kharrat, R., Fajloun, Z., Renisio, J. G., Blanc, E., Sabatier, J. M., El Ayeb, M., and Darbon, H. (2000) A new fold in the scorpion toxin family, associated with an activity on a ryanodine-sensitive calcium channel. *Proteins* **40,** 436–442
3. Chen, L., Estève, E., Sabatier, J. M., Ronjat, M., De Waard, M., Allen, P. D., and Pessah, I. N. (2003) Maurocalcine and peptide A stabilize distinct

subconductance states of ryanodine receptor type 1, revealing a proportional gating mechanism. *J. Biol. Chem.* **278,** 16095–16106
4. Lukács, B., Sztretye, M., Almássy, J., Sárközi, S., Dienes, B., Mabrouk, K., Simut, C., Szabó, L., Szentesi, P., De Waard, M., Ronjat, M., Jóna, I., and Csernoch, L. (2008) Charged surface area of maurocalcine determines its interaction with the skeletal ryanodine receptor. *Biophys. J.* **95,** 3497–3509
5. Estève, E., Smida-Rezgui, S., Sarkozi, S., Szegedi, C., Regaya, I., Chen, L., Altafaj, X., Rochat, H., Allen, P., Pessah, I. N., Marty, I., Sabatier, J. M., Jona, I., De Waard, M., and Ronjat, M. (2003) Critical amino acid residues determine the binding affinity and the Ca^{2+} release efficacy of maurocalcine in skeletal muscle cells. *J. Biol. Chem.* **278,** 37822–37831
6. Altafaj, X., Cheng, W., Estève, E., Urbani, J., Grunwald, D., Sabatier, J. M., Coronado, R., De Waard, M., and Ronjat, M. (2005) Maurocalcine and domain A of the II–III loop of the dihydropyridine receptor Cav 1.1 subunit share common binding sites on the skeletal ryanodine receptor. *J. Biol. Chem.* **280,** 4013–4016
7. Gurrola, G. B., Arévalo, C., Sreekumar, R., Lokuta, A. J., Walker, J. W., and Valdivia, H. H. (1999) Activation of ryanodine receptors by imperatoxin A and a peptide segment of the II–III loop of the dihydropyridine receptor. *J. Biol. Chem.* **274,** 7879–7886
8. Szappanos, H., Smida-Rezgui, S., Cseri, J., Simut, C., Sabatier, J. M., De Waard, M., Kovács, L., Csernoch, L., and Ronjat, M. (2005) Differential effects of maurocalcine on Ca^{2+} release events and depolarization-induced Ca^{2+} release in rat skeletal muscle. *J. Physiol.* **565,** 843–853
9. Pouvreau, S., Csernoch, L., Allard, B., Sabatier, J. M., De Waard, M., Ronjat, M., and Jacquemond, V. (2006) Transient loss of voltage control of Ca^{2+} release in the presence of maurocalcine in skeletal muscle. *Biophys. J.* **91,** 2206–2215
10. Estève, E., Mabrouk, K., Dupuis, A., Smida-Rezgui, S., Altafaj, X., Grunwald, D., Platel, J. C., Andreotti, N., Marty, I., Sabatier, J. M., Ronjat, M., and De Waard, M. (2005) Transduction of the scorpion toxin maurocalcine into cells: evidence that the toxin crosses the plasma membrane. *J. Biol. Chem.* **280,** 12833–12839
11. Ram, N., Weiss, N., Texier-Nogues, I., Aroui, S., Andreotti, N., Pirollet, F., Ronjat, M., Sabatier, J. M., Darbon, H., Jacquemond, V., and De Waard, M. (2008) Design of a disulfide-less, pharmacologically inert, and chemically competent analog of maurocalcine for the efficient transport of impermeant compounds into cells. *J. Biol. Chem.* **283,** 27048–27056
12. Aroui, S., Brahim, S., De Waard, M., Bréard, J., and Kenani, A. (2009) Efficient induction of apoptosis by doxorubicin coupled to cell-penetrating peptides compared to unconjugated doxorubicin in the human breast cancer cell line MDA-MB 231. *Cancer Lett.* **285,** 28–38
13. Aroui, S., Brahim, S., Hamelin, J., De Waard, M., Bréard, J., and Kenani, A. (2009) Conjugation of doxorubicin to cell-penetrating peptides sensitizes human breast MDA-MB 231 cancer cells to endogenous TRAIL-induced apoptosis. *Apoptosis* **14,** 1352–1365
14. Aroui, S., Brahim, S., Waard, M. D., and Kenani, A. (2010) Cytotoxicity, intracellular distribution and uptake of doxorubicin and doxorubicin coupled to cell-penetrating peptides in different cell lines: a comparative study. *Biochem. Biophys. Res. Commun.* **391,** 419–425
15. Aroui, S., Ram, N., Appaix, F., Ronjat, M., Kenani, A., Pirollet, F., and De Waard, M. (2009) Maurocalcine as a nontoxic drug carrier overcomes doxorubicin resistance in the cancer cell line MDA-MB 231. *Pharm. Res.* **26,** 836–845
16. Boisseau, S., Mabrouk, K., Ram, N., Garmy, N., Collin, V., Tadmouri, A., Mikati, M., Sabatier, J. M., Ronjat, M., Fantini, J., and De Waard, M. (2006) Cell penetration properties of maurocalcine, a natural venom peptide active on the intracellular ryanodine receptor. *Biochim. Biophys. Acta* **1758,** 308–319
17. Ram, N., Aroui, S., Jaumain, E., Bichraoui, H., Mabrouk, K., Ronjat, M., Lortat-Jacob, H., and De Waard, M. (2008) Direct peptide interaction with surface glycosaminoglycans contributes to the cell penetration of maurocalcine. *J. Biol. Chem.* **283,** 24274–24284
18. Mabrouk, K., Ram, N., Boisseau, S., Strappazzon, F., Rehaim, A., Sadoul, R., Darbon, H., Ronjat, M., and De Waard, M. (2007) Critical amino acid residues of maurocalcine involved in pharmacology, lipid interaction and cell penetration. *Biochim. Biophys. Acta* **1768,** 2528–2540
19. Poillot, C., Dridi, K., Bichraoui, H., Pêcher, J., Alphonse, S., Douzi, B., Ronjat, M., Darbon, H., and De Waard, M. (2010) D-Maurocalcine, a pharmacologically inert efficient cell-penetrating peptide analogue. *J. Biol. Chem.* **285,** 34168–34180
20. Merrifield, R. B. (1969) Solid-phase peptide synthesis. *Adv. Enzymol. Relat. Areas Mol. Biol.* **32,** 221–296
21. Kim, D. H., Ohnishi, S. T., and Ikemoto, N. (1983) Kinetic studies of calcium release from sarcoplasmic reticulum *in vitro*. *J. Biol. Chem.* **258,** 9662–9668
22. West, M. A., Bretscher, M. S., and Watts, C. (1989) Distinct endocytotic pathways in epidermal growth factor-stimulated human carcinoma A431 cells. *J. Cell Biol.* **109,** 2731–2739
23. Veithen, A., Cupers, P., Baudhuin, P., and Courtoy, P. J. (1996) v-Src induces constitutive macropinocytosis in rat fibroblasts. *J. Cell Sci.* **109,** 2005–2012
24. Meier, O., Boucke, K., Hammer, S. V., Keller, S., Stidwill, R. P., Hemmi, S., and Greber, U. F. (2002) Adenovirus triggers macropinocytosis and endosomal leakage together with its clathrin-mediated uptake. *J. Cell Biol.* **158,** 1119–1131

2.2 Conclusion

Les douze variants tronqués de la MCa que nous avons testés au cours de cette étude possèdent tous des propriétés de pénétration cellulaire et ce où que se situe la partie de la séquence tronquée (en N-terminal, C-terminal ou les deux). Ceci suggère que la grande capacité de la MCa à être internalisée est liée au fait que plusieurs parties de sa séquence possèdent des propriétés de pénétration cellulaire. Nous avons également pu mettre en évidence le fait que la troncation de la molécule linéaire représente un avantage, puisque les variants tronqués sont tous plus efficaces que le peptide linéaire possédant la séquence complète. Il est à noter que tous ces petits peptides ne présentent aucune activité pharmacologique ni de toxicité majeure.

L'un des variants de la MCa les plus remarquables est le petit peptide linéaire composé des neuf premiers acides aminés (MC$a_{\mathrm{UF1-9}}$). En effet, si l'on remarque la pénétration de la majorité des autres variants lorsqu'ils atteignent une concentration d'environ 1 µM dans le milieu extracellulaire, le peptide MC$a_{\mathrm{UF1-9}}$ est détecté à partir de 100 nM. Ceci lui confère un avantage non négligeable, l'efficacité à dose minimale étant un critère d'importance dans le domaine des peptides de pénétration cellulaire. Le petit peptide MC$a_{\mathrm{UF1-9}}$ est donc un nouveau CPP dont il semble primordial de continuer à évaluer les propriétés.

Chapitre 3

Article 2 : Propriétés de pénétration cellulaire d'un petit variant tronqué de la maurocalcine

3.1 Introduction

Puisque, comme nous l'avons démontré dans l'article précédent, le variant MC$a_{\mathrm{UF1-9}}$ de la maurocalcine peut être considéré comme un nouveau CPP, nous avons cherché à évaluer plus en détail ses propriétés de pénétration cellulaire. Pour ce faire, nous l'avons comparé à plusieurs CPP de référence : la protéine Tat (transactivatrice de la transcription du génome du VIH), la pénétratine (dérivée d'un facteur de transcription de l'homéodomaine du gène Antennapedia de la drosophile) et un séquence poly-R (polyarginine). Nous avons également essayé de déterminer l'importance des différentes partie de sa structure en testant les propriétés de pénétration cellulaire de plusieurs de ses analogues.

La séquence de MC$a_{\mathrm{UF1-9}}$ comprenant une histidine accessible à la protonation, nous nous sommes également intéressés à sa sensibilité au pH ainsi qu'à celle de ses variants. En effet, une meilleure pénétration à pH acide présente un avantage dans le cas de cellules tumorales *in vivo*, pour lesquelles le pH environnant est relativement bas (Cardone *et al.*, 2005).

Pharmaceuticals **2013**, *6*, 320-339; doi:10.3390/ph6030320

OPEN ACCESS

pharmaceuticals

ISSN 1424-8247

www.mdpi.com/journal/pharmaceuticals

Article

Cell Penetration Properties of a Highly Efficient Mini Maurocalcine Peptide

Céline Tisseyre [1,2,3,†], Eloi Bahembera [1,2,3,†], Lucie Dardevet [1,2,3], Jean-Marc Sabatier [4], Michel Ronjat [1,2,3] and Michel De Waard [1,2,4,5,*]

[1] Unité Inserm U836, Grenoble Institute of Neuroscience, Université Joseph Fourier, La Tronche, Chemin Fortuné Ferrini, Bâtiment Edmond Safra, 38042 Grenoble Cedex 09, France

[2] Labex Ion Channel Science and Therapeutics, Nice, France

[3] Université Joseph Fourier, Grenoble, France

[4] Inserm U1097, Parc scientifique et technologique de Luminy, 163, avenue de Luminy, 13288 Marseille cedex 09, France

[5] Smartox Biotechnology, Biopolis, 5 Avenue du Grand Sablon, 38700 La Tronche, France

[†] These authors contributed equally to this work.

[*] Author to whom correspondence should be addressed; E-Mail: michel.dewaard@ujf-grenoble.fr; Tel.: +33-4-56-52-05-63; Fax: +33-4-56-52-06-37.

Received: 23 February 2013; in revised form: 6 March 2013 / Accepted: 7 March 2013 / Published: 18 March 2013

Abstract: Maurocalcine is a highly potent cell-penetrating peptide isolated from the Tunisian scorpion *Maurus palmatus*. Many cell-penetrating peptide analogues have been derived from the full-length maurocalcine by internal cysteine substitutions and sequence truncation. Herein we have further characterized the cell-penetrating properties of one such peptide, MCa_{UF1-9}, whose sequence matches that of the hydrophobic face of maurocalcine. This peptide shows very favorable cell-penetration efficacy compared to Tat, penetratin or polyarginine. The peptide appears so specialized in cell penetration that it seems hard to improve by site directed mutagenesis. A comparative analysis of the efficacies of similar peptides isolated from other toxin members of the same family leads to the identification of hadrucalcin's hydrophobic face as an even better CPP. Protonation of the histidine residue at position 6 renders the cell penetration of MCa_{UF1-9} pH-sensitive. Greater cell penetration at acidic pH suggests that MCa_{UF1-9} can be used to specifically target cancer cells *in vivo* where tumor masses grow in more acidic environments.

Keywords: maurocalcine; hadrucalcin; toxin; cell penetrating peptide; F98 cells; glioma; analogs

1. Introduction

Maurocalcine (MCa) is a 33 amino acid residue peptide that was isolated in 2000 from the venom of the Tunisian chactid scorpion *Scorpio maurus palmatus* [1]. It folds according to an 'Inhibitor Cystine Knot' (ICK) motif [2] and contains three disulfide bridges connected by the following pattern: C_1-C_4, C_2-C_5 and C_3-C_6 [3]. Based on high amino acid sequence and pharmacological target similarities, MCa belongs to a larger family of scorpion toxins that also includes imperatoxin A (from *Pandinus imperator*) [4], opicalcine 1 and opicalcine 2 (from *Opistophthalmus carinatus*) [5], hemicalcin [6] and hadrucalcin [7]. All these peptides act on ryanodine receptors resulting in pharmacological activation. These receptors are calcium channels located in the membrane of the endoplasmic reticulum. They control Ca^{2+} release from internal stores and therefore a large number of cell functions [7–10]. Binding of MCa on the ryanodine receptor type 1 occurs on protein cytoplasmic domains. Because MCa acts within seconds, once applied to the extracellular medium, it was soon obvious that it had to cross the plasma membrane very efficiently in order to activate the ryanodine receptor [11]. An additional curiosity of MCa lies into the fact that there is an intriguing sequence homology with a domain of the L-type voltage-gated calcium channel from the skeletal muscle (domain A). This channel lies in the plasma membrane, while domain A is found underneath the membrane in the cytoplasm within a loop that has been recognized as extremely important for the process of excitation-contraction coupling [12,13]. While the role of domain A in excitation-contraction coupling is still unclear, it is however surprising and stimulating to observe that peptides containing domain A sequence act with quite a lot of similarities to MCa on the ryanodine receptor type 1 [14,15]. According to the ^{1}H-NMR solution structure, MCa is rigidly structured by the three disulfide bridges and contains three β-strands, comprising the following stretches of amino acid residues: 9–11 (strand 1), 20–23 (strand 2), and 30–33 (strand 3). MCa has an incredibly stable structure since it cannot be denatured, even at high temperatures up to 100 °C or extreme pH values [16]. Interestingly, the peptide is highly enriched in basic amino acid residues, more than a third of the amino acids being either lysine (seven out of 33) or arginine residues (four out of 33). The histidine residue at position 6 is susceptible, depending of the environmental pH, to introduce an additional positive charge to the peptide by protonation. Interestingly, stretches of positively charged residues seem to confound with the three MCa β-strands. The 3D structure of MCa also strikingly highlights the asymmetrical distribution of the positive charges at its surface: one face is highly basic, while the opposite face is rather hydrophobic. If, in addition, one depicts the amino acid residues important for the ryanodine receptor activation [17], then it appears that the peptide can be schematically represented with three domains: one hydrophobic head that tops the peptide, a larger second face, mainly basic, and a third side domain that contains the pharmacophore (Figure 1A).

Besides its Ca^{2+} channel activity, MCa is also used as a cell-penetrating peptide (CPP). Its properties have been investigated in detail. It was soon discovered that MCa could act as vector for the cell penetration of a variety of cargoes, including proteins [11], peptides [18], small dyes [16,19],

drugs [20–23] or nanoparticles [24,25]. The mechanism of cell penetration most likely includes a combination of membrane translocation (direct passage to the cytoplasm) and endocytosis, mostly macropinocytosis (indirect access to the cytoplasm through leakage from late endosomes) [16,19,26,27].

Figure 1. The hydrophobic domain of MCa is an efficient CPP. (**A**) Schematic representation of MCa 3D structure. The hydrophobic domain (from amino acid residue 1 to 9) is shown on top. Residues are in yellow. Shown also are the basic face (basic amino acid residues are in blue or in pink) and the pharmacophore (residues identified as interacting with the ryanodine receptor are in red or in pink). Pink residues belong both to the pharmacophore and the basic face. (**B**) Confocal microscopy images illustrating the penetration of four different peptides labeled with Cy5 at various concentrations into glioma F98 cells (blue color). Incubation times were 2 h for each peptide/concentration. Images were taken immediately after washout of the extracellular peptide. The plasma membrane is labeled with concanavalin-A-rhodamine (red color). (**C**) Dose-dependent penetration of each peptide-cargo complex in F98 cells as assessed by flow cytometry. A control Cys-Cy5 is also provided. (**D**) Absence of cell penetration of 33 µM Cys-Cy5 (a single Cys residue linked to Cy5—abbreviated C-Cy5) evaluated by confocal microscopy. (**E**) Lack of cell penetration of 3 µM $ChTx_{UF1-12}$-C-Cy5 as determined by confocal microscopy (right panel). Quantitative analysis of F98 $ChTx_{UF1-12}$-C-Cy5 fluorescence as determined by flow cytometry. Internalization of the $ChTx_{UF1-12}$-C-Cy5 peptide is lower than TAT-C-Cy5 but not negligible.

Figure 1

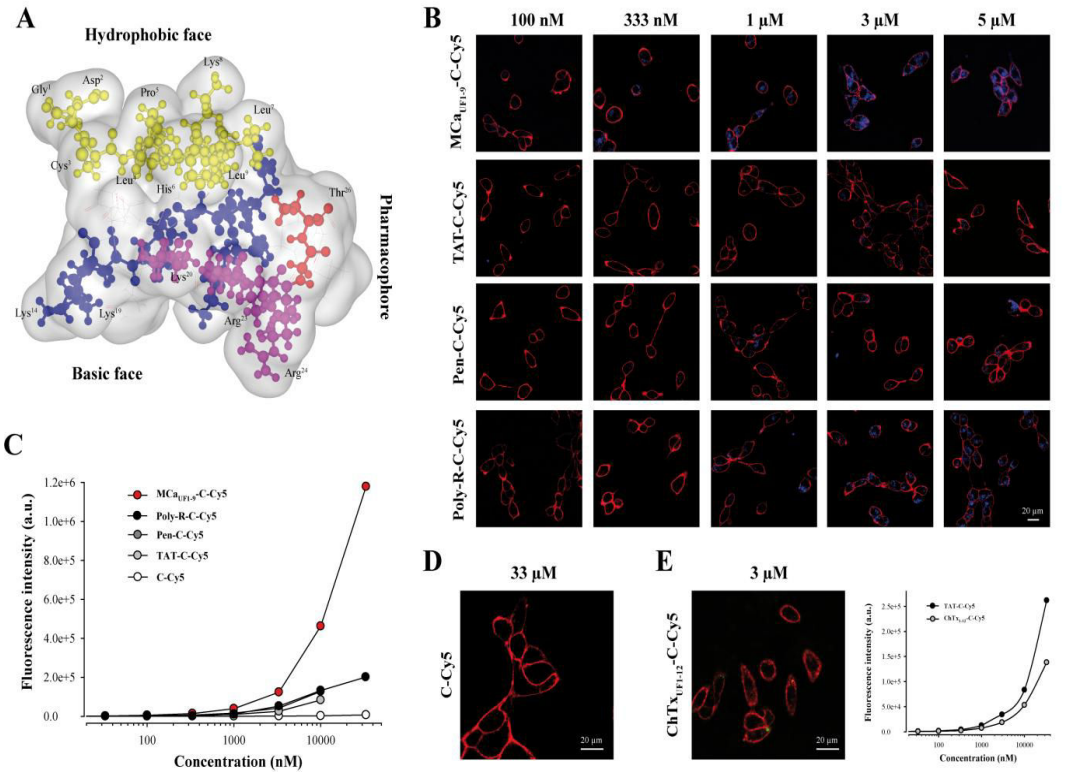

Even if the mechanism(s) of penetration of CPP are subject to debate [28,29], because of the rapidity of action of MCa on the ryanodine receptor, it appears clearly that one way of penetration of

MCa can be membrane translocation. Furthermore, MCa has the ability to bind onto glycosaminoglycans, including heparin and heparan sulfates, with micromolar affinity. However, cell penetration still occurs according to both mechanisms of penetration in cells devoid of glycosaminoglycans, suggesting that glycosaminoglycans do not preferentially direct MCa's cell penetration towards endocytosis [26]. In contrast, these cell surface receptors appear to be helpful as peptide sinks for increased peptide delivery into cells. More relevant to cell penetration is the fact that MCa binds to a number of membrane lipids, mostly negatively charged ones [26,27], as observed for other CPP [28]. Binding seems to occur with higher affinity (100 nM) in close agreement with the concentration of MCa required for cell penetration. In addition, MCa analogues that penetrate better than wild-type MCa also exhibit a greater affinity for membrane lipids and *vice versa*. Endocytosis becomes predominant with some large cargoes. Conversely, small cargoes seem to have less interference with a translocation mode of entry of CPP. These observations tend to indicate that endocytosis may become the preferential mode of cell entry of MCa if coupled to bulky cargoes that are expected to increase the duration of residency at the plasma membrane. However, although MCa is an extremely efficient vector for cell penetration of impermeable cargoes, it is of limited usefulness in its native conformation. Indeed, complex disulfide bridging may hamper the attachment of some cargoes. The size of the CPP is greater than those used in the literature. Finally, the native pharmacological activity is generally undesirable for most applications, so like other CPPs before, modification of the native MCa was made in order to ease its use *in vivo* as a new delivery system [30]. Canceling MCa's pharmacological activity turned out to be quite simple due to the fact that structural requirements involved in binding onto the ryanodine receptor are more stringent than for cell penetration. Several chemical strategies turned out to be successful including point mutations [17], blocking MCa's folding by preventing disulfide bridge formation [18], and producing a D-diastereomer MCa [16]. The second strategy had the advantage to produce a MCa analogue that was simpler to produce since the oxidation/folding step was no longer necessary. However, the resulting peptide turned out to be slightly less efficient in cell penetration than the folded/oxidized MCa, indicating that the correct positioning in space of the various structural determinants of MCa is important to optimize cell penetration. In addition, the unfolded MCa CPP was still thirty three amino acid residues in length. Quite recently, in an attempt to further delimitate the cell penetrating properties of MCa to smaller sequences, a number of unfolded truncated MCa-derived peptides were synthesized and assessed for cell penetration properties [19]. Surprisingly, all truncated peptides turned out to be more efficient than the unfolded full-length MCa for cell penetration, suggesting that each structured domain within the folded/oxidized MCa may provide a specific contribution to the cell penetration of the wild-type peptide. The shortest peptides were nine residues in length and included both the N-terminal and the C-terminal sequences. One of the peptides, $MCa_{UF1\text{-}9}$, stood out as atypical since the net charge of the peptide was 0 and its cell penetration properties differed to some extent from the significantly more basic other MCa-derived truncated peptides. Penetration of this peptide occurred at polarized ends of CHO cells. The peptide also showed greater residency times within the plasma membrane. Its penetration did not rely at all on macropinocytosis for cell entry (at least when coupled to a dye as cargo). Finally, penetration of this peptide occurs at lower extracellular concentrations than the more basic peptides derived from MCa [19]. Altogether the properties of $MCa_{UF1\text{-}9}$ seemed interesting enough to warrant a more in-depth investigation of its cell penetration properties. We therefore

compare herein the properties of this peptide to well-reputed CPP (Tat, penetratin and poly-R) or analogous peptides derived from other toxins of the calcin family. We investigated the properties of a number of point mutated MCa_{UF1-9} analogues, and more specifically the pH-sensitivity of its penetration in order to design pH-sensitive CPP. The data point to new very powerful CPP with unprecedented efficacies and demonstrate the pH-sensitivities of several of our analogues for cell penetration.

2. Results and Discussion

2.1. A Peptide Derived from the Hydrophobic Face of MCa Behaves as a Highly Competitive CPP

A schematic representation of MCa illustrates that the amino acid sequence 1 to 9 tops the rest of the peptide (yellow residues) and defines an independent more hydrophobic face (Figure 1A). The opposite side of the peptide is highly basic (blue and pink residues) and defines therefore a basic face. Some of the residues involved in binding onto the ryanodine receptor have been defined in the past [17]. They include important residues such as Arg^{23} and Arg^{24} and define the pharmacophore side (residues in red and in pink). Therefore the pharmacophore and basic regions overlap to some degree.

We compared the efficacy of MCa_{UF1-9} for cell penetration within the glioma rat cell line F98 to other very popular peptides, comprising TAT, penetratin (Pen) and poly-Arg (poly-R). All peptides included an additional C-terminal Cys residue that was labeled with the Cy5 fluorochrome which served the purpose of cargo in this study. Of note, the extra Cys residue in MCa_{UF1-9}-C-Cy5 is at its natural position as in the folded/oxidized MCa (Cys^{10}) where it is linked to Cys^{21} by a disulfide bridge. In contrast, Cys^3 of MCa_{UF1-9} was replaced by an isosteric 2-aminobutyric acid (Abu) residue to avoid mislabeling by Cy5 in the middle of the sequence. A series of confocal microscopy images were taken immediately after a 2 h incubation of F98 cells with various concentrations of the four peptides tested (MCa_{UF1-9}-C-Cy5, TAT-C-Cy5, Pen-C-Cy5 and poly-R-C-Cy5). As shown, cell penetration of MCa_{UF1-9}-C-Cy5 is perceptible at concentrations as low as 100 nM, whereas none of the other peptides showed penetration at this concentration (Figure 1B). Penetration was then dose-dependent for all peptides. It was more marked at 333 nM for MCa_{UF1-9}-C-Cy5 and started to show up for Poly-R-C-Cy5, while still absent for TAT-C-Cy5 and Pen-C-Cy5. At 1 µM all peptides showed some degree of penetration, the least efficient peptide being TAT-C-Cy5. At 5 µM, F98 cells incubated with TAT-C-Cy5 showed levels of fluorescence that were more or less comparable to those obtained with MCa_{UF1-9}-C-Cy5 at 333 nM. These data qualitatively indicated that MCa_{UF1-9}-C-Cy5 behaved better than those three popular CPP as far as F98 cells are concerned. Similar results were obtained with CHO cells indicating that these differences in performances between the four peptides do not depend on the cell type studied (data not shown). With regard to cell distribution of the peptides, we did not notice any obvious differences in distribution suggesting that the peptides may all borrow the same mechanisms of cell penetration. However, a more complete investigation on this issue is needed before one comes to a firm conclusion. To more quantitatively compare the CPP, we investigated fluorescence levels by flow cytometry (Figure 1C). The data confirmed the confocal microscopy analyses showing that MCa_{UF1-9}-C-Cy5 behaves more potently than other CPP. The following order of penetration efficiency was observed: MCa_{UF1-9}-C-Cy5 >> Poly-R-C-Cy5 = Pen-C-Cy5 > TAT-C-Cy5. At 10 µM, MCa_{UF1-9}-C-Cy5

penetrates 5.5-fold better than TAT-C-Cy5, 3.6-fold better than Pen-C-Cy5, and 3.5-fold better than Poly-R-C-Cy5.

2.2. Randomly Defined Control Peptides Delimit the Threshold Level of an Acceptable Cell Penetration

Our data also illustrate that the control linker-cargo, a single Cys residue linked to Cy5 (C-Cy5), does not penetrate at all into F98 cells (at concentrations up to 33 µM), demonstrating the peptide specificity of cell entry (Figure 1C and D). Another control was also tested, based on a fragment of charybdotoxin (ChTx), a voltage-gated potassium channel blocker, not known previously for cell penetration aptitude. The peptide encompasses the 12 first amino acids of ChTx. Internal Cys residues were replaced by Abu, an additional Cys residue was added at the C-terminus and the resulting peptide labeled with Cy5 as well to yield $ChTx_{UF1\text{-}12}$-C-Cy5. Confocal microscopy images do not show any evidence of cell penetration if F98 cells are incubated 2 h with 3 µM $ChTx_{UF1\text{-}12}$-C-Cy5 (Figure 1E). However, if a more sensitive and quantitative approach is taken to examine the levels of fluorescence, it becomes obvious that F98 cells take up a defined amount of $ChTx_{UF1\text{-}12}$-C-Cy5. This is unlikely to represent the level of binding of this peptide to some cell-surface potassium channels as this fragment is not known to bind potassium channels. In contrast, it may indicate the propensity of some cell types to internalize peptides that present even low affinity for the plasma membrane. A comparison with our least-performing peptide TAT-C-Cy5 indicates that $ChTx_{UF1\text{-}12}$-C-Cy5 is less efficient than TAT-C-Cy5, although significant. At 10 µM, the cell entry of this non-conventional CPP is 1.57-fold less than TAT. These findings may question the relevance of some studies reporting the discovery of "new" CPP or alternatively may suggest that $ChTx_{UF1\text{-}12}$ can also be considered as a poorly performing CPP.

2.3. Pharmacological Blockade of Endocytosis in F98 Cells Affects Poorly $MCa_{UF1\text{-}9}$ Cell Entry

Punctiform distribution of $MCa_{UF1\text{-}9}$-C-Cy5 may be interpreted as a cell entry that is mainly based on a form of endocytosis. This point was assessed by FACS analyses using various drugs at the 2 h cell entry timepoint of 1 µM $MCa_{UF1\text{-}9}$-C-Cy5 in F98 cells. We tested amiloride, a macropinocytosis inhibitor, methyl-β-cyclodextrin to deplete membrane cholesterol and inhibit lipid raft-dependent pathways, nocodazole to prevent microtubule formation, and cytochalasin D to stop F-actin elongation, required for macropinocytosis and clathrin-dependent endocytosis [31]. Amiloride only affected $MCa_{UF1\text{-}9}$-C-Cy5 cell entry in F98 cells very mildly, with an average inhibition of 27% indicating an entry partly based on macropinocytosis (Figure 2).

The 18.5% inhibition observed by cytochalasin D, while being non-significant, was in agreement with the contribution of macropinocytosis to the cell entry of the peptide. Quite surprisingly, both methyl-β-cyclodextrin and nocodazole produced 24.7 and 48.9% increases in the cell entry of $MCa_{UF1\text{-}9}$-C-Cy5. The lack of inhibition by methyl-β-cyclodextrin indicates that caveolae-mediated endocytosis is not involved in the entry of this peptide. The observed increase in cell penetration may indicate on the contrary that one preferential route of cell entry by translocation may be in lipid rafts. Preventing the loss of lipid rafts by blocking endocytosis at this level would increase the surface area devoted to lipid rafts and hence peptide entry.

Figure 2. Effect of endocytosis inhibitors on MCa_{UF1-9} peptide penetration in F98 cells. (**A**) Representative FACS data showing the effect of amiloride (red curve), cytochalasine D (yellow curve), methyl-β-cyclodextrine (blue curve) and nocodazole (green curve) on 1 µM MCa_{UF1-9}-C-Cy5 cell entry (black curve). (**B**) Average fluorescence intensities for the cell entry of 1 µM MCa_{UF1-9}-C-Cy5 in F98 cells without and with endocytosis inhibitors. * $p \leq 0.1$.

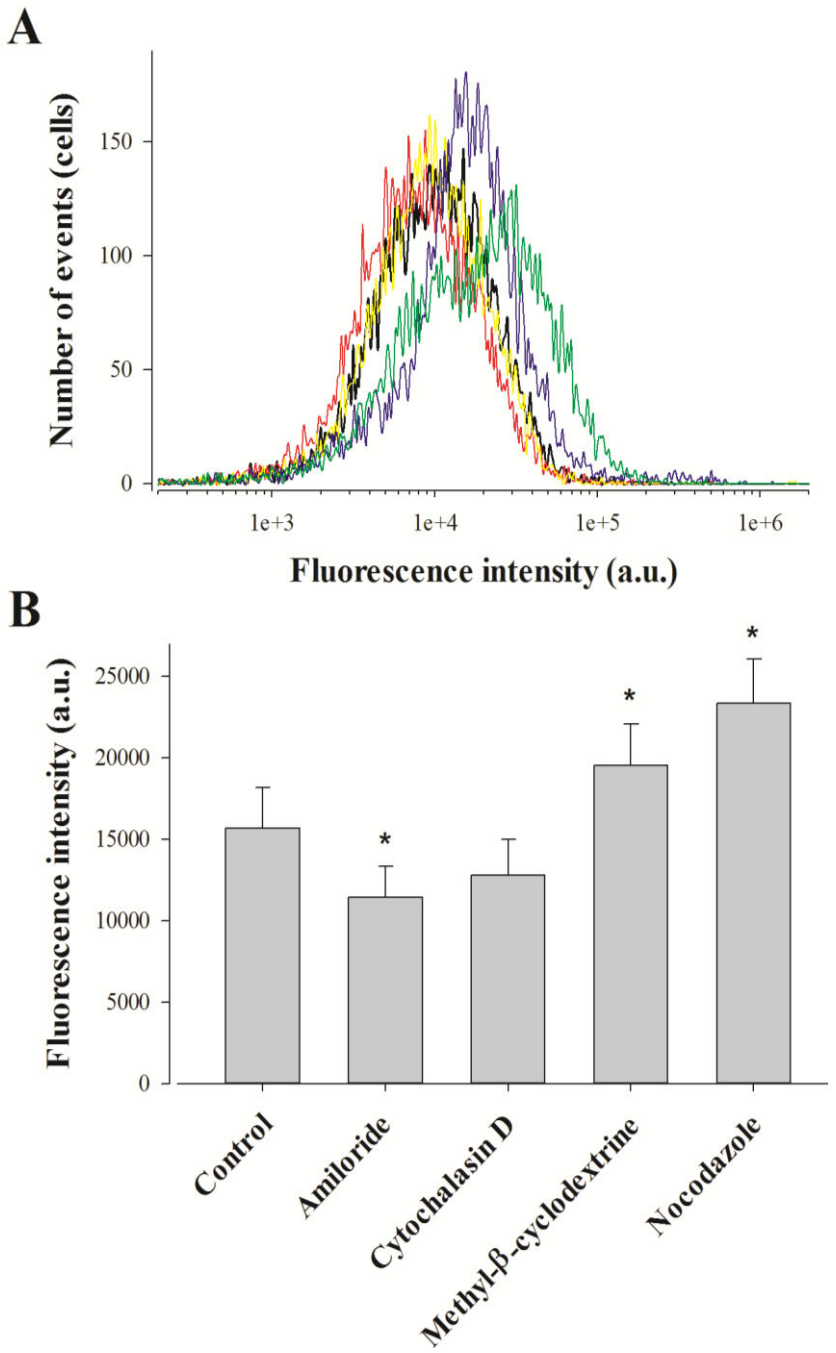

Similarly, it is possible that microtubules hinder cell penetration explaining why blocking their formation may help peptide entry to this large extent. These observations demonstrate that while the intracellular distribution of MCa_{UF1-9}-C-Cy5 in F98 cells looks punctiform, this is not necessarily the consequence of a cell entry by endocytosis.

2.4. Point Mutation of MCa_{UF1-9} Fails to Optimize The Cell Penetrating Properties of This Peptide

Next, we attempted to design a number of MCa_{UF1-9} peptide analogues in order to get some hints on what structural determinants may be important for the efficacy of this peptide in cell penetration. At the N-terminal side of Cys^3 (replaced by Abu) of MCa_{UF1-9}, there are two residues that appear of minor importance (Gly^1 and Asp^2). Removing these two residues yields MCa_{UF3-9}. As shown, MCa_{UF3-9}-C-Cy5 still accumulates very well in F98 cells (Figure 3A,B).

Figure 3. Structural determinants of MCa_{UF1-9} peptide penetration. (**A**) Confocal images illustrating the penetration of 3 µM MCa_{UF3-9}-C-Cy5, $MCa_{UF1-9(W3)}$-C-Cy5, $MCa_{UF1-9(Q3)}$-C-Cy5 or $MCa_{UF1-9(A3)}$-C-Cy5 into F98 cells. 2 h incubation time before washout and imaging. (**B**) Effect of N-terminal peptide truncation on cell penetration efficacy of MCa_{UF1-9}-C-Cy5 as assessed by flow cytometry. (**C**) Effect of point mutation at position 3 on the cell penetration efficacy of MCa_{UF1-9}-C-Cy5. (**D**) Confocal images illustrating the penetration of 3 µM single or double point mutated MCa_{UF1-9}-C-Cy5 peptide into F98 cells. (E) Effect of single point mutations on the cell penetration efficacy of MCa_{UF1-9}-C-Cy5 as assessed by flow cytometry.

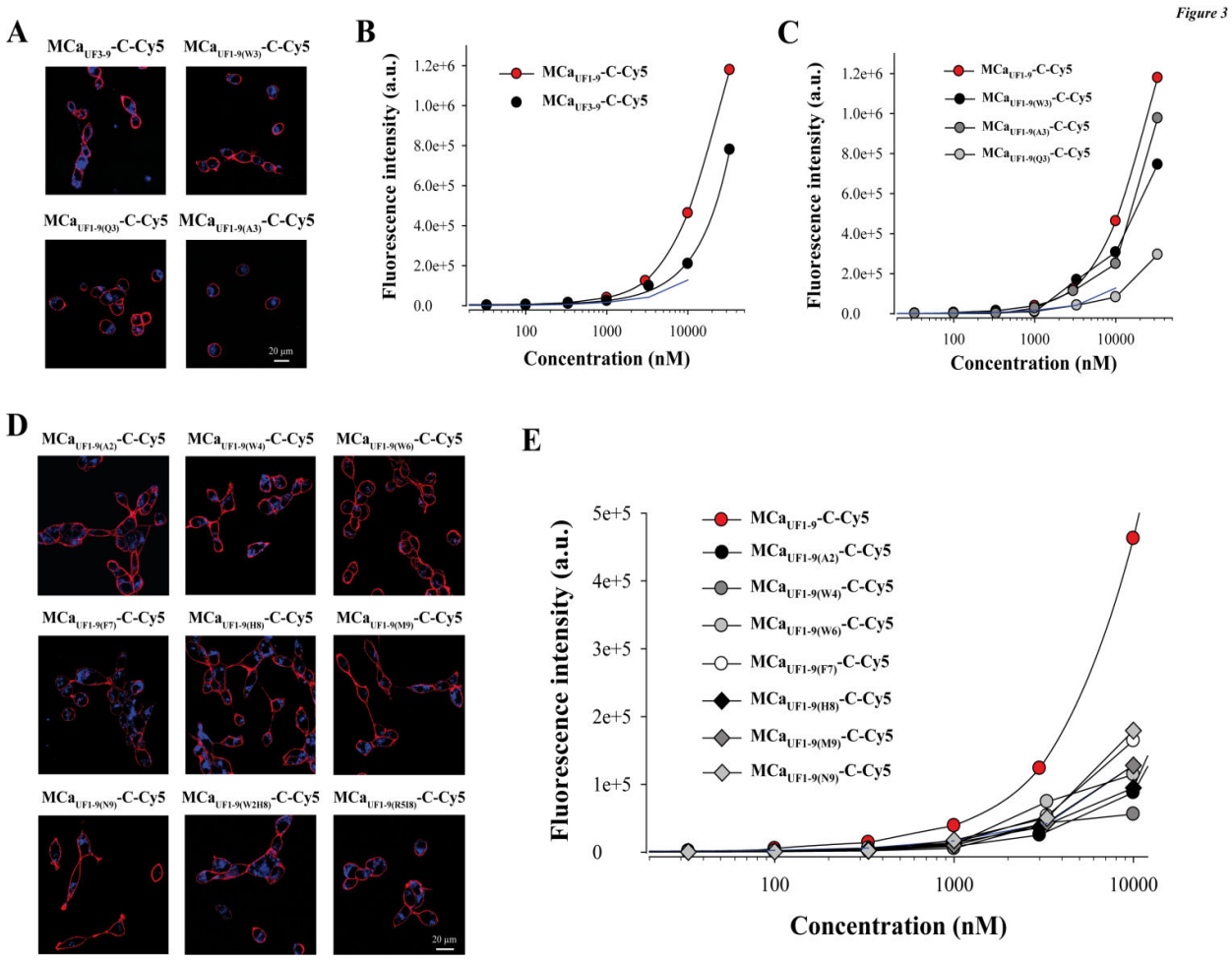

At the quantitative level, there was a 1.25-decrease in cell penetration efficacy at 3 µM, indicating that these two residues were most likely not essential for cell penetration. This deletion brings the size of this efficient CPP down to seven amino acid residues which is remarkably short. At position 3 of the

wild-type MCa there is normally a Cys residue that engages itself into a disulfide bridge. The lateral chain of this residue is therefore not exposed towards the outside face of the molecule and is unlikely to play a role in cell penetration. MCa_{UF1-9} contains an Abu residue instead of a Cys residue and the peptide is quite efficient for cell penetration. We nevertheless probed this position by replacing the Abu residue by Trp, Gln or Ala. As shown, none of these replacements at position 3 within MCa_{UF1-9}-C-Cy5 hindered the cell penetration of these analogues (Figure 3A). At 3 µM, $MCa_{UF1-9(W3)}$-C-Cy5 penetrated 1.36-fold better than MCa_{UF1-9}-C-Cy5, while $MCa_{UF1-9(A3)}$-C-Cy5 penetrated 1.08-fold less well, indicating little variations (Figure 3C). In contrast, when Gln was put at position 3 in the sequence, the resulting $MCa_{UF1-9(Q3)}$-C-Cy5 peptide behaved similarly to TAT but 2.94-fold less well than MCa_{UF1-9}-C-Cy5 suggesting that a Gln may hinder the cell penetration process. Next, we made a series of single (seven peptide) or double (two peptide) point mutated analogues to probe the functional importance of these MCa residues. As shown, all mutated MCa_{UF1-9}-C-Cy5 analogues produced evident cell penetration at 3 µM, indicating that none of the substitutions were powerful enough to fully prevent cell penetration (Figure 3D). However, according to flow cytometry analyses, none of the mutated peptides performed better than MCa_{UF1-9}-C-Cy5 (Figure 3E). Taking TAT-C-Cy5 as a standard, $MCa_{UF1-9(A2)}$-C-Cy5, $MCa_{UF1-9(W4)}$-C-Cy5 and $MCa_{UF1-9(H8)}$-C-Cy5 behaved slightly less well. In contrast, $MCa_{UF1-9(F7)}$-C-Cy5 and $MCa_{UF1-9(M9)}$-C-Cy5 still behaved better than TAT-C-Cy5. Double mutants ($MCa_{UF1-9(W2H8)}$-C-Cy5 and $MCa_{UF1-9(R5I8)}$-C-Cy5 were also closely similar to TAT-C-Cy5 (not shown). Overall, these data indicate that MCa_{UF1-9} peptide has been optimized for cell penetration with many amino acid residues playing an important role for cell entry. At this stage it would be difficult to point to one single residue as being more important than another one within the sequence.

2.5. Analogous Hydrophobic Domains of Other Toxin Members of the Calcin Family Are Also Excellent CPP

The inability to produce MCa_{UF1-9} peptides with greater cell penetration efficacies tends to indicate that sequence variation of this hydrophobic domain needs to be considered more cautiously to design optimized peptides. Interestingly, MCa belongs to a larger family of peptides that have, most of them, never been assessed for cell penetration. Results have been presented indicating that imperatoxin A also behaves as a CPP [32]. All these peptides are structured similarly to MCa, with a similar hydrophobic face topping a more basic face (Figure 4A). All peptides that have been tested are also active on the ryanodine receptor [6,7,33], indicating the presence of a similar pharmacophore. A close examination of the amino acid sequence of the hydrophobic domain reveals only minor sequence diversity among these peptides (Figure 4B). The nine first residues of hemicalcin are identical to MCa. Imperatoxin A, opicalcin 1 and opicalcin 2 differ from MCa only by residue 9 (an arginine instead of a leucine residue).

The most differing peptide sequence is the one derived from hadrucalcin with two extra N-terminal residues. Interestingly, the sequence SerGluLys replaces the Gly^1 residue of MCa, but Asp^2 of MCa is conserved. Also, four internal substitutions are noticeable. Leu^4, Pro^5, Lys^8 and Leu^9 of MCa are substituted by Iso, Lys, Gln and Arg, respectively. Finally, Had_{UF1-11} has an additional basic amino acid compared to MCa_{UF1-9}. We next evaluated the ability of these peptides to accumulate into F98 cells. At 1 µM, it was obvious, according to confocal imaging, that Imp_{UF1-9}-C-Cy5 (equivalent to

Opi1$_{UF1-9}$-C-Cy5 or Opi2$_{UF1-9}$-C-Cy5) is less efficient for cell penetration than MCa$_{UF1-9}$-C-Cy5 and Had$_{UF1-11}$-C-Cy5 (Figure 4D). Interestingly, a similar deletion of the two first amino terminal residues of Had$_{UF1-9}$-C-Cy5 yielded a peptide, MCa$_{UF3-11}$-C-Cy5 with excellent penetration capabilities. Evaluation of dose-dependent penetration by flow cytometry demonstrated that Imp$_{UF1-9}$-C-Cy5 penetrates quantitatively in a similar way than TAT-C-Cy5. For the first time, we also show that Had$_{UF1-11}$-C-Cy5 and Had$_{UF3-11}$-C-Cy5 both penetrate better than MCa$_{UF1-9}$-C-Cy5 (Figure 4C).

Figure 4. Cell penetration properties of the hydrophobic domains of toxins from the calcin family. (**A**) Real or modeled 3D structures of MCa (PDB access code 1C6W), imperatoxin A (access code 1IE6), hemicalcin (model), opicalcin 1 (model), opicalcin 2 (model) and hadrucalcin (model). Residues in blue describe the hydrophobic domain investigated in this study. Red residues are all amino acids that differ from MCa's amino acid sequence. Residues in green are cystine residues. (**B**) Amino acid sequences of the hydrophobic domains of each member of the calcin family. The third Cys residue is systematically replaced by Abu in our synthetic peptides and is represented in grey color. Residues in blue are those that differ from MCa$_{UF1-9}$ amino acid sequence. This sequence alignment defines three groups of peptides with similar N-terminal sequences. (**C**) Comparative cell penetration efficacies of the peptides derived from members of the calcin family as assessed by dose-response curves from flow cytometry data. TAT-C-Cy5 data are indicated by a blue dashed line for comparison. (**D**) Confocal images illustrating the cell penetration of each peptide of the calcin family after incubation of 1 µM of the peptides with F98 cells during 2 h. A significantly lower cell penetration is observed for Imp$_{UF1-9}$-C-Cy5 compared to the two hadrucalcin-derived peptides (Had$_{UF1-11}$-C-Cy5 and Had$_{UF3-11}$-C-Cy5).

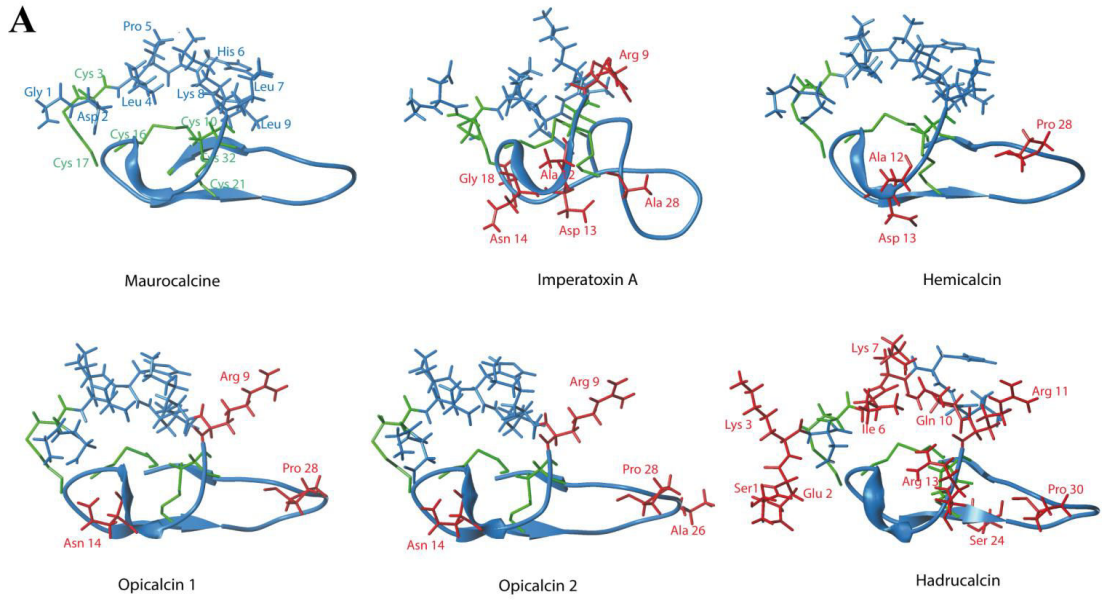

Figure 4. *Cont.*

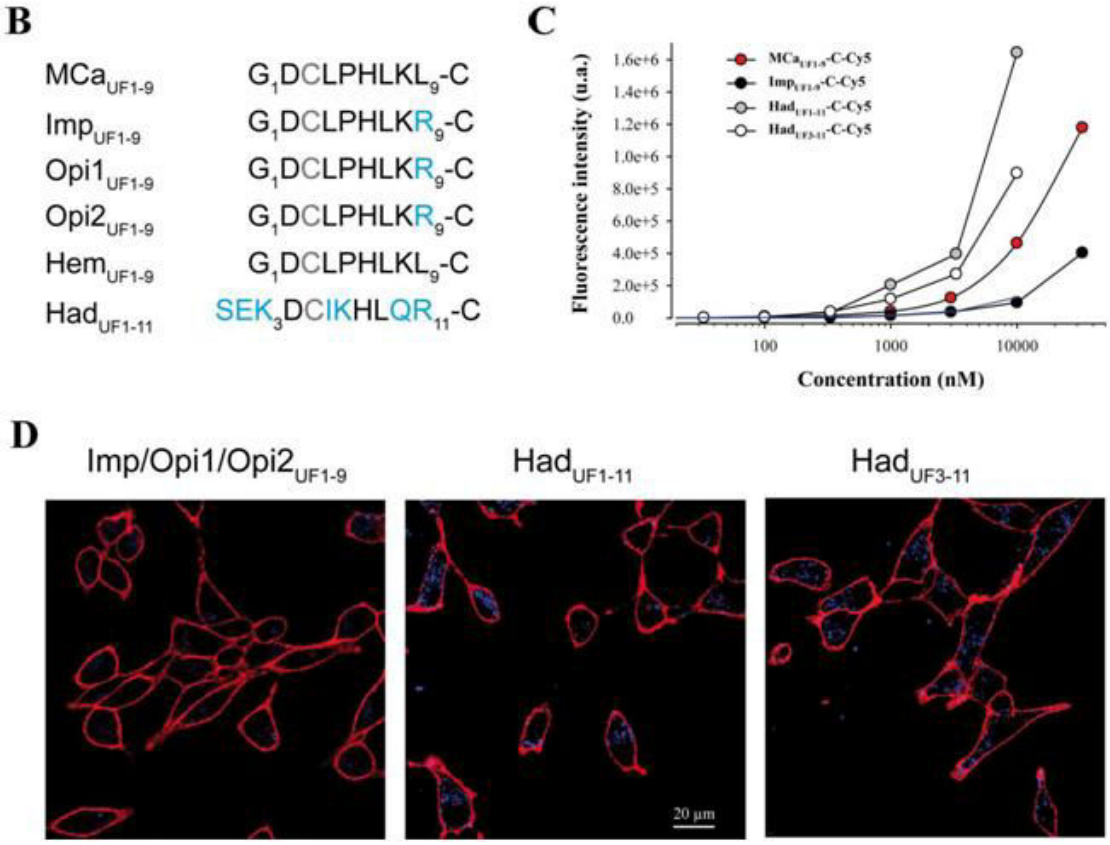

This indicates that a series of very selective set of amino acid substitutions are required to improve MCa_{UF1-9} cell penetration properties. They also demonstrate that the calcin family can accommodate some variation in cell penetration efficacy for the activation of the ryanodine receptor. Nevertheless, it remains to be investigated whether the additional basic face and pharmacophore region are necessary to improve the characteristics of cell penetration of imperatoxin A, opicalcin 1 or opicalcin 2. In any case, it is obvious that Had_{UF1-11} is a remarkable cell penetration peptide by the extent of its efficacy compared to the popular peptides challenged in Figure 1.

2.6. Cell Penetration of MCa_{UF1-9} is pH-sensitive Owing to the Presence of an His Residue in its Amino Acid Sequence

Close examination of the amino acid sequence of MCa reveals that it contains a histidine residue at position 6. This residue is therefore also present in MCa_{UF1-9}. According to Figure 2 data, this histidine residue contributes to some extent to the cell penetration efficacy of MCa_{UF1-9}-C-Cy5. The imidazole sidechain of histidine has a pKa of approximately 6.0, while overall the pKa of the amino acid is 6.5. However, this value is susceptible to be influenced by the direct amino acid environment of this residue. In any case, it can be considered that at physiological conditions, relatively small changes in pH value is susceptible to alter the average charge of MCa_{UF1-9}. At a pH value lower than 6, the imidazole ring is essentially protonated. Protonation of the His residue at position 6 may affect the cell penetration efficacy of MCa_{UF1-9}-C-Cy5. To test this idea, the extracellular pH value was varied between 5.0 and 8.0 during the 2 h incubation of F98 cells with MCa_{UF1-9}-C-Cy5 and the total

accumulated fluorescence level evaluated by FACS. The data were normalized to the value at pH 5.0. As shown, decreasing pH values results in higher fluorescence values and therefore greater accumulation of the peptide in F98 cells (Figure 5A).

A fit of the data with a decreasing exponential suggests that the peptide enters into F98 cells with a 2.8-fold lower efficacy than at acidic pH values. Half of this decrease in efficacy occurs for a variation in pH from 5.0 to 5.7 indicating that the pKa value of this histidine residue within MCa_{UF1-9}-C-Cy5 may be close to 5.7. The involvement of His^6 in this pH-dependence of the cell penetration of the peptide is demonstrated by the lack of pH-dependence in cell penetration of the mutant peptide $MCa_{UF1-9(W6)}$-C-Cy5 in which His^6 is replaced by Trp^6 (Figure 5B). Overall, these data indicate that protonation of His^6, provided by acidic environments, results in improved MCa_{UF1-9}-C-Cy5 cell delivery. In that respect, it is important to note that F98 cells are from rat glioma and that the extracellular pH within the glioma tumors masses in the brain has been predicted to be acidic [34]. Our finding therefore suggests that the MCa_{UF1-9} peptide may be useful to more specifically deliver anti-tumor drugs within glioma.

2.7. Long-Lasting Cell Retention of MCa_{UF1-9}

One property of CPP is that they enter quite rapidly into cells. However, the persistence of their intracellular accumulation is seldom looked after. We investigated this question with three peptides. We used MCa_{UF1-9}-C-Cy5, a non or poorly charged peptide depending on the protonation level of His^6, $MCa_{UF11-33}$-C-Cy5, a highly charged peptide mainly encompassing the two C-terminal thirds of MCa, and Had_{UF3-11}-C-Cy5 which is less hydrophobic than MCa_{UF1-9}-C-Cy5. One could expect that hydrophobic peptides may more readily escape from the cell interior than charged peptides. To test this idea, F98 cells were loaded 2 h with 1 µM of each of these peptides, extensively washed, maintained in culture for a variable duration (between 0 and 34 h, washout time), treated with trypsin and the fluorescence level remaining in the cells estimated by FACS (Figure 5C).

As shown and quite remarkably, the fluorescence levels of the accumulated peptides fade away only slowly with time indicating that the cell entry of the peptides are faster than their cell exit (Figure 5C,D). Time constant of half exit were estimated to be 5 h for MCa_{UF1-9}-C-Cy5, 8 h and 20 min for $MCa_{UF11-33}$-C-Cy5 and 16 h and 40 min for Had_{UF3-11}-C-Cy5. After 34 h, cells still contained 27, 21 and 23% of MCa_{UF1-9}-C-Cy5, $MCa_{UF11-33}$-C-Cy5 and Had_{UF3-11}-C-Cy5 fluorescence, respectively. These values are suspected to be higher in fact since 34 h is enough to register at least one cell division cycle. This property of persistence indicates that MCa_{UF1-9}, but also $MCa_{UF11-33}$ and Had_{UF3-11}, can be used both as CPP and retention agents for drugs that may freely enter into cells but would also freely escape from them. We have previously used such a property to fight against chemo-resistance of the breast tumor cell line MDA-MB-231 by coupling doxorubicin to a non-folded version of MCa [20,22,23]. Confocal microscopy images of the cell distribution of both peptides tested indicate that the distribution of the peptides does not evolve with washout time (Figure 5D). The distribution remains mostly punctiform (with an evolution towards what may seem smaller dots), internal and hardly invades the nucleus.

Figure 5. pH-dependence and persistence of the cell penetration of MCa_{UF1-9}-C-Cy5. (**A**) Effect of extracellular pH variation on the cell penetration efficacy of 1 µM MCa_{UF1-9}-C-Cy5 in F98 cells (2 h incubation). Mean of n = 3 experiments ± S.D. Mean FACS results were normalized before averaging. Data were fitted by a decreasing exponential of the type $y = y_0 + a.e^{-bx}$ where $y_0 = 0.36 \pm 0.05$, $a = 0.64 \pm 0.09$ and $b = 1.76 \pm 0.61$. (**B**) Effect of extracellular pH variation on the cell penetration of 1 µM MCa_{UF1-9}(W6)-C-Cy5 in F98 cells (2 h incubation). The pH-insensitive Trp^6 replaces the pH-sensitive His^6 in this mutant peptide. (**C**) Persistence of the fluorescence signal in F98 cells preincubated 2 h with 1 µM MCa_{UF1-9}-C-Cy5 (net charge 0 if His^6 is unprotonated, black symbol), the positively charged $MCa_{UF11-33}$-C-Cy5 (net charge +7, red symbol) or the mildly charged Had_{UF3-11}-C-Cy5 peptide (net charge +2 if His^8 is unprotonated, white symbol). FACS results were normalized to 1 at t=0 min at the start of the washout of the CPP. Data were fitted with a decreasing exponential function with $1/\tau = 0.20 \pm 0.01$ h^{-1} (MCa_{UF1-9}-C-Cy5), 0.12 ± 0.03 h^{-1} ($MCa_{UF11-33}$-C-Cy5) et 0.06 ± 0.02 h^{-1} (Had_{UF3-11}-C-Cy5), where τ is the time constant of the decrease in the mean cell fluorescence level. The non-decreasing fraction of fluorescence was equal to 0.27 ± 0.14 (MCa_{UF1-9}-C-Cy5), 0.21 ± 0.07 ($MCa_{UF11-33}$-C-Cy5) and 0.23 ± 0.13 (Had_{UF3-11}-C-Cy5). (**D**) Corresponding confocal images illustrating that the intracellular distribution of the peptides did not change with time. The 2.5-fold image enhancement also shows a close to complete lack of nucleus invasion by the peptides. The images also show that the two peptides do not differ in the type of intracellular distribution 3.5 h after washout of the extracellular peptides.

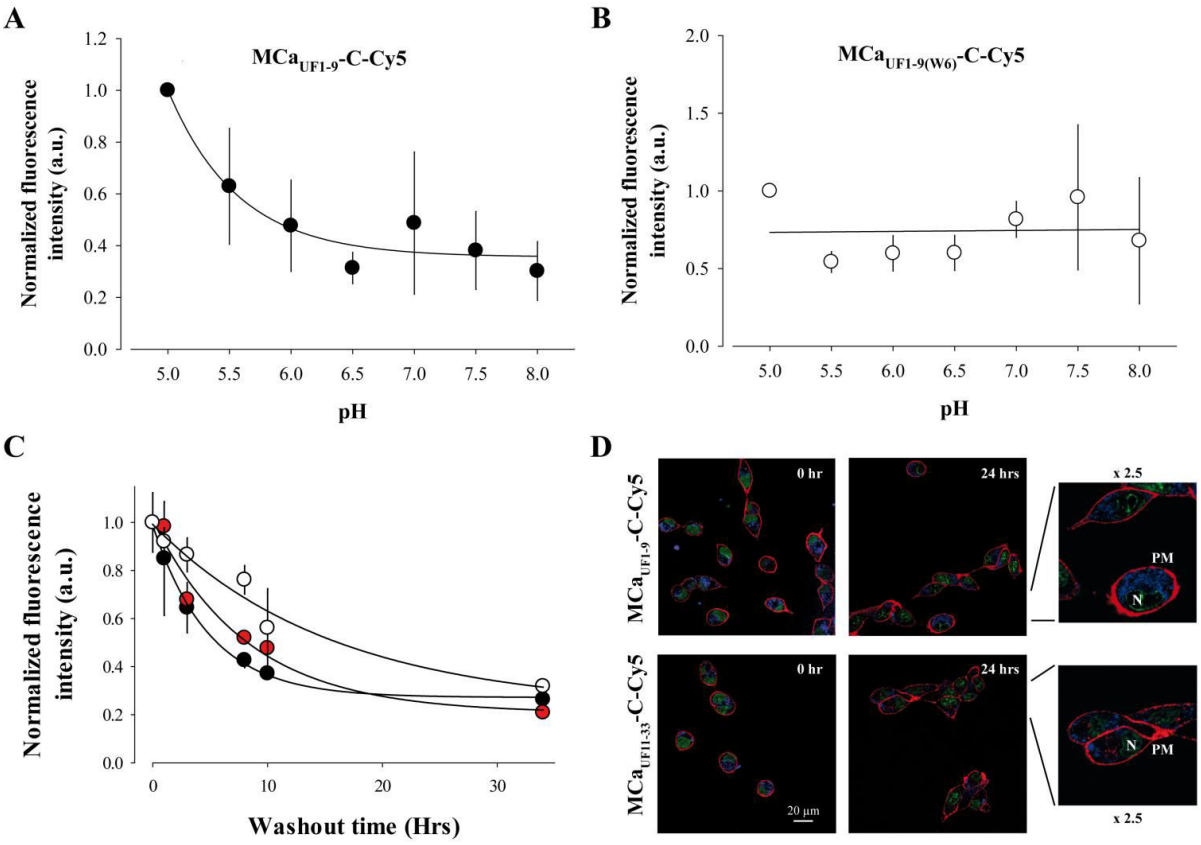

2.8. Discussion

While all MCa truncations and/or disruptions of disulfide bridges produce a loss of the 3D structure, MCa_{UF1-9} is more susceptible than other truncated peptides to preserve some of the structural characteristics that it may possess within the full-length MCa as it encloses by itself the entire hydrophobic face of MCa. At this stage, one may only speculate as to why MCa presents one hydrophobic face diametrically opposite to a highly charged basic face. It may present a strong advantage for the peptide if it has to deal with both a hydrophilic environment (extracellular space and cytoplasm) and a hydrophobic one (membrane lipids). Besides it may be essential to the mechanism of cell translocation if the peptide needs to cope with the amphiphilic nature of membrane lipids. The strong dipole moment of the peptide, resulting from the existence of these two different faces, probably orients the peptide in its interaction with the plasma membrane. The highly basic nature of MCa should also speed up the peptide entry through electrochemical attraction if one considers that it diffuses freely through the plasma membrane, in a similar way that Na^+ or Ca^{2+} ions would do when permeating through adequate ion channels while attracted by the inside negative membrane potential. Such a mechanism, if proven, would result in peptide accumulation against the concentration gradient. What the effect of a physical separation between these two peptide entities (hydrophobic face and basic face) might be on the cell penetration mechanism remains however unclear. One may notice at this point that MCa_{UF1-9}-C-Cy5 and $MCa_{UF11-33}$-C-Cy5 produce quite similar intracellular punctiform distributions in F98 cells arguing that they share nonetheless similar mechanisms of cell penetration. This was also the case for the other CPP investigated in this study (poly-R-C-Cy5, Tat-C-Cy5 and Pen-C-Cy5). It is of interest to note however that the cell distribution of fluorescent D-MCa, a full-length and well-structured analogue of MCa, is mostly diffuse [16] suggesting that combining the hydrophobic and basic faces of the molecule to shorten the residency time in the plasma membrane may represent a significant advantage in cell penetration.

The most interesting information that we could gather from our mutagenesis program of MCa_{UF1-9}-C-Cy5 was that the two first amino acid residues were the most dispensable for its penetration properties. This truncation approach led to the design of a 7-mer CPP that has greater potency than most popular CPPs on the market. Investigating the cell penetrating properties of peptides derived from the hydrophobic face of other peptides members of the calcin family turned out as a more interesting approach than mutagenesis. Most of these peptides differ by only a few amino acid residues, with the notable exception of hadrucalcin. Coherent with the mono-substitution we performed at amino acid 9 of MCa_{UF1-9}-C-Cy5, the cell penetration properties of Imp_{UF1-9}-C-Cy5, $Opi1_{UF1-9}$-C-Cy5 and $Opi2_{UF1-9}$-C-Cy5, all presenting Arg^9 instead of Leu^9, were reduced to some extent compared to MCa_{UF1-9}-C-Cy5. Remarkably, multiple amino acid substitution as demonstrated within Had_{UF1-11}-C-Cy5 resulted in an important and unexpected improvement of cell penetration. Similarly to MCa_{UF1-9}-C-Cy5, removing the two first N-terminal amino acid residues of Had_{UF1-11}-C-Cy5 produced a peptide with quite significant levels of cell penetration. The core of the sequence, the one we assume to be important for cell penetration (after Abu^3 in MCa_{UF1-9}), contains no less than 4 substitutions (Leu^4 by Ile, Pro^5 by Lys, Lys^8 by Gln, and Leu^9 by Arg). This indicates that quite elaborate alterations need to be done to MCa_{UF1-9} sequence to further improve it cell penetrating properties. In any case, these findings (i) define a novel CPP with unprecedented efficacy, and (ii)

open the door for the design of hadrucalcin/MCa chimeras 1 µM MCa_{UF1-9}-C-Cy5 fluorescence at any given concentration and never in terms of starting concentration at which cell entry was observed. These observations suggest that the affinity of these peptides for plasma membrane components remains unaltered.

Since we are interested in developing a number of applications in oncology for MCa analogues, we also investigated the role of His^6 in cell entry into the glioma F98 cells. Of great interest for future applications, we found that protonation of His^6, occurring at more acidic pH, but in a range compatible with pH values observed in glioma, produced a three-fold more potent peptide for cell penetration. We assume that protonated His^6 may form a salt bridge with Asp^2 in the non-structured MCa_{UF1-9}. It is likely that, without this salt bridge, the negative charge carried by Asp^2 may disfavor cell penetration of MCa_{UF1-9}. This observation on the importance of protonation in peptide cell penetration will be useful for the future design of new MCa analogues in which important basic amino acid residues may be substituted by His residues in order to further improve the tumor-selectivity of these potent CPP. Interesting positions will include Lys^{19}, Lys^{20}, Lys^{22} and Arg^{24} all shown to contribute to the cell penetration efficacy of the full length MCa [17].

3. Experimental

3.1. Reagents

N-α-Fmoc-L-aminoacids, Wang-Tentagel resin and reagents used for peptide syntheses were obtained from Iris Biotech (Marktredwitz, Germany). Solvents were analytical grade products from Acros Organics (Geel, Belgium). Cy5 maleimide mono-reactive dye was purchased from GE Healthcare (Saclay, France).

3.2. Peptide Syntheses

Chemical syntheses of truncated toxin peptides were performed as previously described [16]. Briefly, peptides were chemically synthesized by the solid-phase method [35] using an automated peptide synthesizer (CEM© Liberty 12, Matthews, NC, USA). Peptide chains were assembled stepwise on 0.24 meq of Fmoc-D-Arg-Pbf-Wang-Tentagel resin using 0.24 mmol of *N*-α-fluorenylmethyloxycarbonyl (Fmoc) L-amino-acid derivatives. The side-chain protecting groups were: trityl for Cys and Asn, *tert*-butyl for Ser, Thr, Glu and Asp, Pbf for Arg and *tert*-butylcarbonyl for Lys. Reagents were at the following concentrations: Fmoc-amino-acids [0.2 M Fmoc-AA-OH in dimethylformamide (DMF)], activator (0.5 M 2-(1H-benzotriazole-1-yl)-1,1,3,3-tetramethyluronium hexafluorophosphate in DMF), activator base [2 M diisopropylethylamine in N-methylpyrrolidone (NMP)] and deprotecting agent (5% piperazine/0.1 M 1-hydroxybenzotriazole in DMF), as advised by PepDriver (CEM©). After peptide chain assembly, resins were treated 4 h at room temperature with a mixture of trifluoroacetic acid/water/triisopropylsilane (TIS)/dithiothreitol (DTT) (92.5/2.5/2.5/2.5). The peptide mixtures were then filtered and the filtrates were precipitated by adding cold *tert*-butylmethyl ether. The crude peptides were pelleted by centrifugation (10,000 × *g*, 15 min) and the supernatants were discarded. Truncated toxin analogues were purified by HPLC using a Vydac C18 column (218TP1010, 25 × 10 cm). Elutions of the peptides were performed with a 10–60% acetonitrile

linear gradient containing 0.1% trifluoroacetic acid. The purified fractions were analyzed by analytical RP-HPLC (Vydac C18 column 218TP104, 25 × 4.6 cm). All analogues were characterized by MALDI-TOF mass spectrometry.

3.3. Peptide Labeling With Cy5

Each peptide was labeled with Cy5 according to the manufacturer's protocol (GE Healthcare). Peptides were dissolved at 200 µg/mL in 1 M $NaHCO_3$ buffer, pH 9.3. 500 µL of solubilized peptides were added to Cy5-maleimide containing tubes. The mixtures were incubated during 2 h at room temperature and then purified by HPLC using an analytical Vydac C18 column. Elution of the Cy5-labeled peptides was performed with a 5–90% acetonitrile linear gradient containing 0.1% trifluoroacetic acid. The pure peak fractions were lyophilized and peptides quantified by UV spectrophotometer at 650 nm.

3.4. Cell Culture

Undifferentiated malignant glioma rat (F98) cell line (from ATCC) was maintained at 37 °C in 5% CO_2 in DMEM/F-12 nutrient medium (Invitrogen, Cergy Pontoise, France) supplemented with 2% (v/v) heat-inactivated fetal bovine serum (Invitrogen) and 100 µg/mL streptomycine and 100 units/mL penicillin (Invitrogen).

3.5. Confocal Microscopy

For analysis of the cell entry of Cy5-labeled-truncated toxin peptides in living cells, cell cultures were incubated with the fluorescent peptides (in DMEM/F-12 nutrient medium only) for 2 h, and then washed twice with phosphate-buffered saline (PBS) alone. The plasma membrane was stained with 50 µg/mL rhodamine-conjugated concanavalin A (Invitrogen, Cergy Pontoise, France) for 5 min. Cells were washed once more. Live cells were then immediately analyzed by confocal laser scanning microscopy using a Zeiss LSM operating system. Rhodamine (561 nm) and Cy5 (633 nm) were sequentially excited and emission fluorescence were collected.

3.6. Fluorescence Activated Cell Sorting Analyses

F98 cells were incubated with various concentrations of Cy5-labeled peptides in DMEM/F-12 culture medium without serum at 37 °C for 2 h. The cells were then washed with PBS to remove excess extracellular peptide and treated with 0.48 mM versene (Invitrogen) for 5 min at 37 °C to detach cells from the surface, and centrifuged at 200 *g* in DMEM/F-12 culture medium before suspension in PBS. For experiments concerning endocytosis inhibitors, F98 cells were initially preincubated in DMEM/F-12 culture medium without serum for 30 min at 37 °C with different inhibitors of endocytosis: (i) 100 µM amiloride, (ii) 5 µg/mL cytochalasin D (10 µM), (iii) 20 µM nocodazole, or (iv) 5 mM methyl-β-cyclodextrin (all from Sigma, Lyon, France). The cells were then incubated for 2 h at 37 °C with 1 µM $MCa_{UF1\text{-}9}$-C-Cy5 in the presence of each drug. Flow cytometry analyses were performed with live cells using an Accuri C6 flow cytometer (BD Biosciences, Le Pont

de Claix, France). Data were obtained and analyzed using CFlow Sampler (BD Biosciences). Live cells were gated by forward/side scattering from a total of 10,000 events.

3.7. Molecular Modeling

Using Sybyl X 1.3 (Tripos Inc., St. Louis, MO, USA) and PDB structure of MCa (code 1C6W) and imperatoxin A (code 1IE6), we generated 3D models of opicalcin 1 and 2, hemicalcin and hadrucalcin. There is a sequence homology (76% up to 91%) between these proteins. Based on previous reports [6,7], we replaced some amino acid of MCa sequence to obtain the corresponding ones for the four different proteins. Several steps of minimization and control of the stereochemistry were performed to obtain a model for each molecule.

4. Conclusions

In this manuscript, we have demonstrated that $MCa_{UF1\text{-}9}$-C-Cy5 starts to show detectable penetration in glioma F98 cells at concentrations as low as 33 nM (5-fold increase over control) as detected by FACS. The process is visible at 100 nM by confocal microscopy and a comparative analysis reveals that it is highly competitive compared to TAT, penetratin or Poly-R CPP. One analogue turns out to be extremely competitive, $MCa_{UF3\text{-}9}$, owing to its performance, length and ease of synthesis. Nevertheless, we also demonstrate that engineered optimization of its cell penetrating properties is hard to achieve but that Mother Nature has provided an elegant solution to this problem by selecting itself the best amino acid substitutions under the form of new calcin analogues. In that respect, the hydrophobic domain of hadrucalcin outperforms that of MCa. We evidence for the first time the possibility to modulate peptide cell penetration by external pH provided that His residues are strategically incorporated within the amino acid sequence. This finding enlarges the potential application of these peptides to the treatment of glioma. Additionally, the observation that the residency time of these peptides in glioma F98 cells is quite long suggest that these peptides may be best used when injected once inside a solid tumor rather than by intravenous route.

Acknowledgements

We acknowledge financial support to MDW by Inserm and by the Nanofret grant and LabEx ICST of the Agence Nationale de la Recherche (ANR). MDW is a recipient of a contrat d'interface from Inserm and Grenoble Hospital. EB has a fellowship from ANR. We also thank the Région Rhône Alpes for the financial support of CT by an Emergence grant.

References

1. Fajloun, Z.; Kharrat, R.; Chen, L.; Lecomte, C.; di Luccio, E.; Bichet, D.; El Ayeb, M.; Rochat, H.; Allen, P.D.; Pessah, I.N.; *et al*. Chemical synthesis and characterization of maurocalcine, a scorpion toxin that activates Ca^{2+} release channel/ryanodine receptors. *FEBS Lett.* **2000**, *469*, 179–185.
2. Mouhat, S.; Jouirou, B.; Mosbah, A.; de Waard, M.; Sabatier, J.M. Diversity of folds in animal toxins acting on ion channels. *Biochem J.* **2004**, *378*, 717–726.

3. Mosbah, A.; Kharrat, R.; Fajloun, Z.; Renisio, J.G.; Blanc, E.; Sabatier, J.M.; El Ayeb, M.; Darbon, H. A new fold in the scorpion toxin family, associated with an activity on a ryanodine-sensitive calcium channel. *Proteins* **2000**, *40*, 436–442.
4. Zamudio, F.Z.; Gurrola, G.B.; Arevalo, C.; Sreekumar, R.; Walker, J.W.; Valdivia, H.H.; Possani, L.D. Primary structure and synthesis of imperatoxin A (iptx(a)), a peptide activator of Ca^{2+} release channels/ryanodine receptors. *FEBS Lett.* **1997**, *405*, 385–389.
5. Zhu, S.; Darbon, H.; Dyason, K.; Verdonck, F.; Tytgat, J. Evolutionary origin of inhibitor cystine knot peptides. *FASEB J.* **2003**, *17*, 1765–1767.
6. Shahbazzadeh, D.; Srairi-Abid, N.; Feng, W.; Ram, N.; Borchani, L.; Ronjat, M.; Akbari, A.; Pessah, I.N.; de Waard, M.; El Ayeb, M. Hemicalcin, a new toxin from the iranian scorpion hemiscorpius lepturus which is active on ryanodine-sensitive Ca^{2+} channels. *Biochem. J.* **2007**, *404*, 89–96.
7. Schwartz, E.F.; Capes, E.M.; Diego-Garcia, E.; Zamudio, F.Z.; Fuentes, O.; Possani, L.D.; Valdivia, H.H. Characterization of hadrucalcin, a peptide from hadrurus gertschi scorpion venom with pharmacological activity on ryanodine receptors. *Br. J. Pharmacol.* **2009**, *157*, 392–403.
8. Altafaj, X.; France, J.; Almassy, J.; Jona, I.; Rossi, D.; Sorrentino, V.; Mabrouk, K.; de Waard, M.; Ronjat, M. Maurocalcine interacts with the cardiac ryanodine receptor without inducing channel modification. *Biochem. J.* **2007**, *406*, 309–315.
9. Szappanos, H.; Smida-Rezgui, S.; Cseri, J.; Simut, C.; Sabatier, J.M.; de Waard, M.; Kovacs, L.; Csernoch, L.; Ronjat, M. Differential effects of maurocalcine on Ca^{2+} release events and depolarization-induced Ca^{2+} release in rat skeletal muscle. *J. Physiol.* **2005**, *565*, 843–853.
10. Gurrola, G.B.; Arevalo, C.; Sreekumar, R.; Lokuta, A.J.; Walker, J.W.; Valdivia, H.H. Activation of ryanodine receptors by imperatoxin A and a peptide segment of the II-III loop of the dihydropyridine receptor. *J. Biol. Chem.* **1999**, *274*, 7879–7886.
11. Esteve, E.; Mabrouk, K.; Dupuis, A.; Smida-Rezgui, S.; Altafaj, X.; Grunwald, D.; Platel, J.C.; Andreotti, N.; Marty, I.; Sabatier, J.M.; *et al*. Transduction of the scorpion toxin maurocalcine into cells. Evidence that the toxin crosses the plasma membrane. *J. Biol. Chem.* **2005**, *280*, 12833–12839.
12. Tanabe, T.; Beam, K.G.; Adams, B.A.; Niidome, T.; Numa, S. Regions of the skeletal muscle dihydropyridine receptor critical for excitation-contraction coupling. *Nature* **1990**, *346*, 567–569.
13. Tanabe, T.; Beam, K.G.; Powell, J.A.; Numa, S. Restoration of excitation-contraction coupling and slow calcium current in dysgenic muscle by dihydropyridine receptor complementary DNA. *Nature* **1988**, *336*, 134–139.
14. Altafaj, X.; Cheng, W.; Esteve, E.; Urbani, J.; Grunwald, D.; Sabatier, J.M.; Coronado, R.; de Waard, M.; Ronjat, M. Maurocalcine and domain a of the II-III loop of the dihydropyridine receptor $Ca_v1.1$ subunit share common binding sites on the skeletal ryanodine receptor. *J. Biol. Chem.* **2005**, *280*, 4013–4016.
15. Chen, L.; Esteve, E.; Sabatier, J.M.; Ronjat, M.; de Waard, M.; Allen, P.D.; Pessah, I.N. Maurocalcine and peptide a stabilize distinct subconductance states of ryanodine receptor type 1, revealing a proportional gating mechanism. *J. Biol. Chem.* **2003**, *278*, 16095–16106.

16. Poillot, C.; Dridi, K.; Bichraoui, H.; Pecher, J.; Alphonse, S.; Douzi, B.; Ronjat, M.; Darbon, H.; de Waard, M. D-maurocalcine, a pharmacologically inert efficient cell-penetrating peptide analogue. *J. Biol. Chem.* **2010**, *285*, 34168–34180.
17. Mabrouk, K.; Ram, N.; Boisseau, S.; Strappazzon, F.; Rehaim, A.; Sadoul, R.; Darbon, H.; Ronjat, M.; de Waard, M. Critical amino acid residues of maurocalcine involved in pharmacology, lipid interaction and cell penetration. *Biochim. Biophys. Acta* **2007**, *1768*, 2528–2540.
18. Ram, N.; Weiss, N.; Texier-Nogues, I.; Aroui, S.; Andreotti, N.; Pirollet, F.; Ronjat, M.; Sabatier, J.M.; Darbon, H.; Jacquemond, V.; *et al.* Design of a disulfide-less, pharmacologically-inert and chemically-competent analog of maurocalcine for the efficient transport of impermeant compounds into cells. *J. Biol. Chem.* **2008**, *283*, 27048–27056.
19. Poillot, C.; Bichraoui, H.; Tisseyre, C.; Bahemberae, E.; Andreotti, N.; Sabatier, J.M.; Ronjat, M.; de Waard, M. Small efficient cell-penetrating peptides derived from scorpion toxin maurocalcine. *J. Biol. Chem.* **2012**, *287*, 17331–17342.
20. Aroui, S.; Brahim, S.; de Waard, M.; Breard, J.; Kenani, A. Efficient induction of apoptosis by doxorubicin coupled to cell-penetrating peptides compared to unconjugated doxorubicin in the human breast cancer cell line MDA-MB 231. *Cancer Lett.* **2009**, *285*, 28–38.
21. Aroui, S.; Brahim, S.; de Waard, M.; Kenani, A. Cytotoxicity, intracellular distribution and uptake of doxorubicin and doxorubicin coupled to cell-penetrating peptides in different cell lines: A comparative study. *Biochem. Biophys. Res. Commun.* **2010**, *391*, 419–425.
22. Aroui, S.; Brahim, S.; Hamelin, J.; de Waard, M.; Breard, J.; Kenani, A. Conjugation of doxorubicin to cell penetrating peptides sensitizes human breast MDA-MB 231 cancer cells to endogenous trail-induced apoptosis. *Apoptosis* **2009**, *14*, 1352–1365.
23. Aroui, S.; Ram, N.; Appaix, F.; Ronjat, M.; Kenani, A.; Pirollet, F.; de Waard, M. Maurocalcine as a non-toxic drug carrier overcomes doxorubicin resistance in the cancer cell line MDA-MB 231. *Pharm. Res.* **2009**, *26*, 836–845.
24. Ram, N.; Texier-Nogues, I.; Pernet-Gallay, K.; Poillot, C.; Ronjat, M.; Andrieux, A.; Arnoult, C.; Daou, J.; de Waard, M. *In vitro* and *in vivo* cell delivery of quantum dots by the cell penetrating peptide maurocalcine. *Int. J. Biomed. Nanosci. Nanotechnol.* **2011**, *2*, 12–32.
25. Stasiuk, G.J.; Tamang, S.; Imbert, D.; Poillot, C.; Giardiello, M.; Tisseyre, C.; Barbider, E.L.; Fries, P.H.; de Waard, M.; Reiss, P.; Mazzanti, M. Cell-permeable ln(III) chelate-functionalized InP quantum dots as multimodal imaging agents. *ACS Nano* **2011**, *5*, 8193–8201.
26. Ram, N.; Aroui, S.; Jaumain, E.; Bichraoui, H.; Mabrouk, K.; Ronjat, M.; Lortat-Jacob, H.; de Waard, M. Direct peptide interaction with surface glycosaminoglycans contributes to the cell penetration of maurocalcine. *J. Biol. Chem.* **2008**, *283*, 24274–24284.
27. Boisseau, S.; Mabrouk, K.; Ram, N.; Garmy, N.; Collin, V.; Tadmouri, A.; Mikati, M.; Sabatier, J.M.; Ronjat, M.; Fantini, J.; *et al*. Cell penetration properties of maurocalcine, a natural venom peptide active on the intracellular ryanodine receptor. *Biochim. Biophys. Acta* **2006**, *1758*, 308–319.
28. Jones, A.T.; Sayers, E.J. Cell entry of cell penetrating peptides: Tales of tails wagging dogs. *J. Control. Release* **2012**, *161*, 582–591.
29. Lindgren, M.; Hallbrink, M.; Prochiantz, A.; Langel, U. Cell-penetrating peptides. *Trends Pharmacol. Sci.* **2000**, *21*, 99–103.

30. Lundberg, P.; Langel, U. A brief introduction to cell-penetrating peptides. *J. Mol. Recognit.* **2003**, *16*, 227–233.
31. Mano, M.; Teodosio, C.; Paiva, A.; Simoes, S.; Pedroso de Lima, M.C. On the mechanisms of the internalization of s4(13)-pv cell-penetrating peptide. *Biochem. J.* **2005**, *390*, 603–612.
32. Gurrola, G.B.; Capes, E.M.; Zamudio, F.Z.; Possani, L.D.; Valdivia, H.H. Imperatoxin A, a cell-penetrating peptide from scorpion venom, as a probe of Ca-release channels/ryanodine receptors. *Pharmaceuticals (Basel)* **2010**, *3*, 1093–1107.
33. El-Hayek, R.; Lokuta, A.J.; Arevalo, C.; Valdivia, H.H. Peptide probe of ryanodine receptor function. Imperatoxin A, a peptide from the venom of the scorpion pandinus imperator, selectively activates skeletal-type ryanodine receptor isoforms. *J. Biol. Chem.* **1995**, *270*, 28696–28704.
34. Garcia-Martin, M.L.; Herigault, G.; Remy, C.; Farion, R.; Ballesteros, P.; Coles, J.A.; Cerdan, S.; Ziegler, A. Mapping extracellular pH in rat brain gliomas *in vivo* by 1H magnetic resonance spectroscopic imaging: Comparison with maps of metabolites. *Cancer Res.* **2001**, *61*, 6524–6531.
35. Merrifield, R.B. Solid-phase peptide synthesis. *Adv. Enzymol. Relat. Areas Mol. Biol.* **1969**, *32*, 221–296.

3.2 Conclusion

Cette étude nous a permis de confirmer les remarquables propriétés de pénétration cellulaires de MC$a_{\mathrm{UF1-9}}$. En effet, ce peptide est plus efficace que les trois CPP de référence auxquels nous l'avons comparé ; à titre d'exemple, sa pénétration cellulaire à 10 µM est 5,5 fois supérieure à celle de Tat. De plus, nous n'avons pas été en mesure d'améliorer l'efficacité de ce peptide par de simples mutations : sa structure semble donc optimale en termes de pénétration cellulaire. Le petit peptide MC$a_{\mathrm{UF1-9}}$ a également, tout comme la MCa native, la capacité de s'accumuler au sein des cellules, et bien qu'il ne parvienne pas jusqu'au noyau, cette caractéristique en fait un vecteur de choix pour la délivrance de substances thérapeutiques.

Nous avons pu mettre en évidence la sensibilité de MC$a_{\mathrm{UF1-9}}$ au pH environnant, ses capacités de pénétration cellulaire étant accrues en milieu acide. Nous avons effectué ces tests sur une lignée de glioblastome murin (F98), puisqu'il a été établi que les cellules tumorales gliales possèdent un environnement légèrement acide (Garcia-Martin *et al.*, 2001). Ce CPP particulièrement efficace et favorisé par les milieux acides semble donc prometteur pour la délivrance de composés antitumoraux, mais ceci reste à confirmer sur d'autres lignées cellulaires *in vitro*, puis à évaluer *in vivo*.

Chapitre 4

Article 3 : Quantification de la pénétration cellulaire de la L-MCa *in vitro*

4.1 Introduction

Les chapitres précédents nous ont permis de mettre en évidence un variant tronqué de la maurocalcine, le petit peptide MC$a_{\mathrm{UF1-9}}$, comme nouveau peptide de pénétration cellulaire et vecteur d'intérêt pour la délivrance de substances thérapeutiques. Cependant, il est important de continuer à approfondir nos connaissances de la molécule native qui possède notamment l'avantage d'une plus grande stabilité *in vivo* du fait de la présence de ponts disulfure au sein de sa structure. De plus, si la MCa est la première toxine animale à avoir été reconnue comme peptide de pénétration cellulaire (Poillot 2010), ses propriétés restent à caractériser plus en détail.

Nous avons donc cherché à quantifier l'accumulation intracellulaire de la MCa *in vitro*. Pour ce faire, nous avons commencé par évaluer le volume moyen des cellules de notre modèle (la lignée de gliobastome murin F98). Nous avons ensuite synthétisé une MCa comprenant une tyrosine supplémentaire qui a permis le marquage du peptide à l'iode radioactive (I^{125}). La MCa étant mono-iodée, nous avons pu calculer précisément les quantités de peptide accumulées au sein des cellules puis relarguées au cours du temps.

Biochimica et Biophysica Acta xxx (2014) xxx–xxx

Contents lists available at ScienceDirect

Biochimica et Biophysica Acta

journal homepage: www.elsevier.com/locate/bbamcr

Quantitative evaluation of the cell penetrating properties of an iodinated Tyr-L-maurocalcine analog ☆

Céline Tisseyre [a,b], Mitra Ahmadi [b,c], Sandrine Bacot [b,c], Lucie Dardevet [a,b], Pascale Perret [b,c], Michel Ronjat [a,b], Daniel Fagret [b,c], Yves Usson [b,e], Catherine Ghezzi [b,c], Michel De Waard [a,b,d,*]

[a] INSERM, U836, Grenoble Institute of Neuroscience, LabEx Ion Channels, Science and Therapeutics, Grenoble, France
[b] Université Joseph Fourier, Grenoble, France
[c] INSERM, U1039, Radiopharmaceutiques Biocliniques, Grenoble, France
[d] Smartox Biotechnologies, Grenoble, France
[e] CNRS, UMR5525, TIMC-IMAG, Grenoble, France

ARTICLE INFO

Article history:
Received 3 January 2014
Received in revised form 27 February 2014
Accepted 17 March 2014
Available online xxxx

Keywords:
Maurocalcine
Cell penetrating peptide
Radioiodination
Quantitative evaluation
Drug delivery

ABSTRACT

L-Maurocalcine (L-MCa) is the first reported animal cell-penetrating toxin. Characterizing its cell penetration properties is crucial considering its potential as a vector for the intracellular delivery of drugs. Radiolabeling is a sensitive and quantitative method to follow the cell accumulation of a molecule of interest. An L-MCa analog containing an additional N-terminal tyrosine residue (Tyr-L-MCa) was synthesized, shown to fold and oxidize properly, and successfully radioiodinated to ^{125}I-Tyr-L-MCa. Using various microscopy techniques, the average volume of the rat line F98 glioma cells was evaluated at 8.9 to 18.9 × 10^{-7} μl. ^{125}I-Tyr-L-MCa accumulates within cells with a dose-dependency similar to the one previously published using 5,6-carboxyfluorescein-L-MCa. According to subcellular fractionation of F98 cells, plasma membranes keep less than 3% of the peptide, regardless of the extracellular concentration, while the nucleus accumulates over 75% and the cytosol around 20% of the radioactive material. Taking into account both nuclear and cytosolic fractions, cells accumulate intracellular concentrations of the peptide that are equal to the extracellular concentrations. Estimation of ^{125}I-Tyr-L-MCa cell entry kinetics indicate a first rapid phase with a 5 min time constant for the plasma membrane followed by slower processes for the cytoplasm and the nucleus. Once inside cells, the labeled material no longer escapes from the intracellular environment since 90% of the radioactivity remains 24 h after washout. Dead cells were found to have a lower uptake than live ones. The quantitative information gained herein will be useful for better framing the use of L-MCa in biotechnological applications. This article is part of a Special Issue entitled: Calcium Signaling in Health and Disease.

1. Introduction

Crossing cellular membranes represents a major hurdle in current drug development. Cell-penetrating peptides (CPP) are molecular vectors that enter cells and allow the intracellular delivery of a number of bioactive molecules such as drugs, peptides, proteins, oligonucleotides/cDNA/RNA, and nanoparticles [1–3]. Originally isolated from the venom of the scorpion *Scorpio maurus palmatus* [4], L-maurocalcine (L-MCa) is a highly basic, positively charged, 33-mer peptide that efficiently binds to the ryanodine receptor in skeletal muscles and promotes channel opening and calcium release from the sarcoplasmic reticulum. The binding site of L-MCa on the ryanodine receptor has been identified as cytoplasmic [5], suggesting that cytoplasmic application is required for its pharmacological effect. The fast kinetics (few seconds) at which extracellular application of L-MCa triggers internal Ca^{2+} release indicates that the peptide should be able to easily translocate through the plasma membrane [6]. According to ^{1}H NMR analysis, the peptide presents three disulfide bridges (Cys^{3}–Cys^{17}, Cys^{10}–Cys^{21} and Cys^{16}–Cys^{32}) and folds along an inhibitor cysteine knot pattern [4,7]. It contains three β-strands from amino acid residues 9–11 (strand 1), 20–23 (strand 2), and 30–33 (strand 3) with strands 2 and 3 forming an antiparallel β-sheet (Fig. 1A). Several lines of experimental evidence indicate that L-MCa is a member of the exponentially growing family of CPPs [6,8–13]. The peptide is highly efficient in entering a variety of cell types compared to other popular CPP such as TAT or penetratin. It presents a low toxicity profile (absence of toxicity at concentrations above 10 μM) [8], penetrates at lower concentrations [14], and efficiently accumulates into the cytoplasm which is a highly desirable feature for many biotechnological applications that require the use of CPP. Therefore, a quantitative

☆ This article is part of a Special Issue entitled: Calcium Signaling in Health and Disease.

* Corresponding author at: INSERM, U836, Grenoble Neuroscience Institute, Site Santé de la Tronche, Bâtiment Edmond J. Safra, 38042 Grenoble Cedex 09, France. Tel.: +33 456 520 563; fax: +33 456 520 637.
E-mail address: michel.dewaard@ujf-grenoble.fr (M. De Waard).

http://dx.doi.org/10.1016/j.bbamcr.2014.03.017
0167-4889/

assessment of the cell penetration properties of L-MCa is of great importance considering its potential as a vector for the improved delivery of therapeutic compounds. Radiolabeling represents the most sensitive and quantitative method to follow the quantitative entry of a cell penetrating peptide of interest. Radioiodination is a widely used method for radiolabeling of chemical compounds since the presence of iodine would poorly affects the structural properties of the molecule of interest. Specifically, ^{125}I radiolabeling is commonly performed for *in vitro* radioligand interaction and *in vivo* biodistribution studies [15,16]. For the purpose of radiolabeling of L-MCa, we synthesized an analog with an extra amino-terminal tyrosine residue, termed Tyr-L-MCa, that still possesses the pharmacological properties of wild-type L-MCa. Next, we quantitatively investigated the cell penetration properties of the radioiodinated Tyr-L-MCa using the rat F98 glioma cell line and a precise evaluation of cell volume by Digital Holographic Microscopy (DHM) or by confocal microscopy (CM). The results of the present study will be useful for future *in vivo* biodistribution studies of MCa.

2. Material and methods

2.1. Materials

N-α-Fmoc-L-amino acid, Wang-Tentagel resin and reagents used for peptide synthesis were obtained from Iris Biotech. Solvents were analytical grade products from Acros Organics. Acetonitrile was High Performance Liquid Chromatography (HPLC) gradient grade from Fischer Scientific and trifluoroacetic acid (purum ≥98%) from Fluka

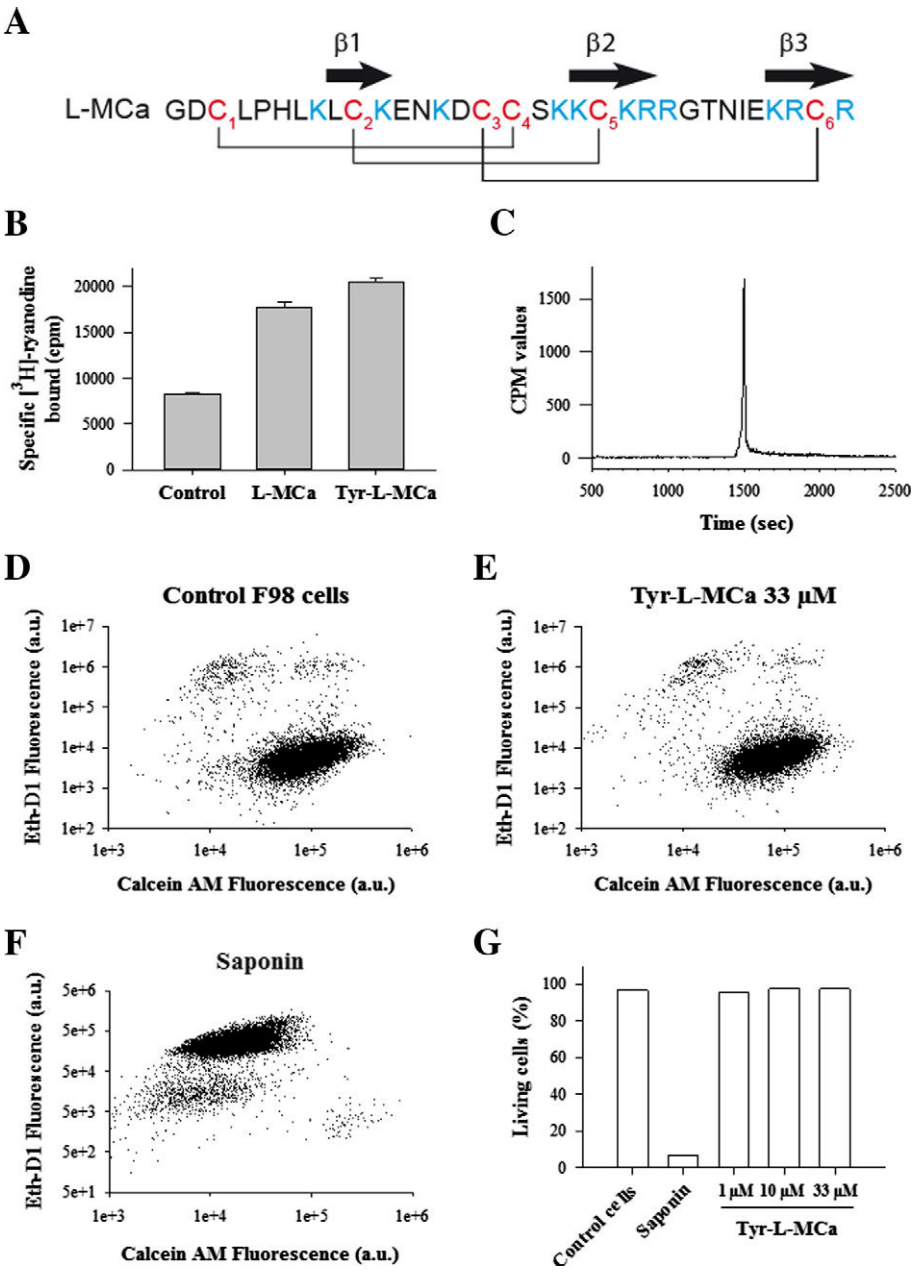

Fig. 1. Properties of the Tyr-L-MCa analog. (A) Primary structure of L-MCa. The disulfide bridge connectivity is shown by lines connecting the six semi-cystine residues. The positions of the three β-strands are indicated by arrows. Blue residues denote basic amino acids. (B) Stimulation of [^{3}H]-ryanodine binding onto SR vesicles. Experimentally, binding was performed at pCa = 5 which explains why L-MCa stimulation of binding is limited. No significant differences were observed between the efficacies of L-MCa and Tyr-L-MCa. (C) RP-HPLC profile of ^{125}I-Tyr-L-MCa after radiolabeling. Note the homogeneous labeling of the peptide by ^{125}I. (D) Cell viability assay by flow cytometry for control F98 cells. The ethidium-D1 fluorescence level measures cell death level. (E) Cell viability assay by flow cytometry for F98 cells after 2 h incubation with 33 µM Tyr-L-MCa. (F) Cell viability assay by flow cytometry for F98 cells after 5 min incubation with 0.1% saponin. Note the extensive cell death produced by saponin. (G) Proportion of live F98 cells for control, saponin and Tyr-L-MCa conditions.

Please cite this article as: C. Tisseyre, et al., Quantitative evaluation of the cell penetrating properties of an iodinated Tyr-L-maurocalcine analog, Biochim. Biophys. Acta (2014), http://dx.doi.org/10.1016/j.bbamcr.2014.03.017

and lactoperoxidase of bovine milk (80 IU/mg) were from Sigma-Aldrich, hydrogen peroxide 30% in water (w/w) from Carlo Erba and $Na^{125}I$ (3.7 GBq/ml) from Perkin Elmer. DMEM F-12 medium with or without phenol red, fetal bovine serum, Trypsin-EDTA, rhodamine-conjugated concanavalin A and live/dead viability/cytotoxicity kit were obtained from Invitrogen. Protease inhibitors (cOmplete Min, EDTA-free) were from Roche diagnostics.

2.2. Synthesis of Tyr-L-MCa by solid-phase

Tyr-L-MCa with an extra N-terminal tyrosyl residue was synthetized to allow L-MCa radioiodination. Chemical synthesis of Tyr-L-MCa was performed as previously described [17] with the following modifications. Briefly, Tyr-L-MCa was chemically synthesized by the solid-phase peptide synthesis (SPPS) method [18] using an automated peptide synthesizer (CEM© Liberty). The peptide chain was assembled stepwise on 0.24 mEq of Fmoc-L-Arg(Pbf)-Wang-Tentagel resin using 0.24 mmol of N-α-fluorenylmethyloxycarbonyl (Fmoc) L-amino-acid derivatives. The side-chain protecting groups were Trityl for Cys and Asn, *tert*-butyl for Ser and Tyr, Thr, Glu and Asp, Pbf for Arg, and *tert*-butylcarbonyl for Lys. Reagents were at the following concentrations: 0.2 M Fmoc-amino-acids (Fmoc-AA-OH in dimethylformamide (DMF)), 0.5 M activator (2-(1H-benzotriazole-1-yl)-1,1,3,3-tetramethyluronium hexafluorophosphate in DMF), 2 M activator base (diisopropylethylamine in N-methyl-pyrrolidone) and deprotecting agent (5% piperazine/0.1 M 1-hydroxybenzotriazole in DMF), as advised by PepDriver (CEM©). After peptide chain assembly, the resin was treated with a mixture of trifluoroacetic acid/water/triisopropylsilane/1,4-dithiothreitol (92.5/2.5/2.5/2.5) for 4 h at room temperature. The peptide mixture was then filtered to eliminate the resin and the filtrate was precipitated by adding cold *t*-butylmethyl ether. The crude peptide was pelleted by centrifugation (10,000 ×*g*, 15 min) and the supernatant was discarded. The crude and reduced Tyr-L-MCa was submitted to oxidation for disulfide bridge formation in 0.1 M Tris/HCl buffer at pH 8.2 during 3 days at room temperature. Oxidized/folded Tyr-L-MCa was then purified by HPLC using a Vydac C18 column (218TP1010, 250 × 10 mm). Elution of the peptide was performed with a 10–60% acetonitrile linear gradient containing 0.1% trifluoroacetic acid (TFA) over 40 min. The purity of the collected fraction was analyzed by reversed phase (RP)-HPLC using analytical C18 column (Vydac, 218TP104, 10 μm, 250 × 4.6 mm). Tyr-L-MCa was characterized by MALDI-TOF mass spectrometry. Samples were mixed 1:1 (v/v) with 10 mg/ml α-cyano-4-hydroxycinnamic acid (HCCA) before spotted onto a MALDI target plate. Mass spectrometry analyses were performed on a 4800 MALDI-TOF/TOF instrument (ABSciex). MS spectra were acquired in positive ion reflector mode over a mass range of 800–6000 m/z.

2.3. Radiolabeling of Tyr-L-MCa using lactoperoxidase

^{125}I-Tyr-L-MCa was prepared using a direct iodination procedure with lactoperoxidase/H_2O_2 system as oxidant. Briefly, 37 MBq of ^{125}I were added to 10 μg of Tyr-MCa in phosphate buffer (50 mM, pH 7.4). The reaction was allowed to proceed for 30 min at room temperature after addition of lactoperoxidase and H_2O_2 at a final concentration of 0.5 μM and 25 μM respectively. Radioiodinated Tyr-L-MCa was analyzed by HPLC immediately and radiochemical purity higher than 95% was achieved, thereby obviating the need for a purification step. A single peak of radioiodinated ^{125}I-Tyr-L-MCa was observed. The compound was stable for over 48 h. A similar labeling was performed with $Na^{127}I$ according to the same procedure. In these conditions, the compound was shown to be monoiodinated (not shown). The resulting compounds, ^{125}I-Tyr-L-MCa and ^{127}I-Tyr-L-MCa, were mixed in order to obtain a specific activity of 0.4 MBq/nmol of Tyr-L-MCa (activimeter Capintec). Hereafter, we shall speak about ^{125}I-Tyr-L-MCa although it reflects a mixture of ^{125}I-Tyr-L-MCa and ^{127}I-Tyr-L-MCa.

2.4. F98 glioma cell culture

All experiments were performed using the F98 glioblastoma cancer cell line (undifferentiated malignant glioma rat cell line from ATCC) maintained at 37 °C in 5% CO_2 in DMEM F-12 medium supplemented with 2% (v/v) heat-inactivated fetal bovine serum and 10,000 units/ml streptomycin and penicillin. Cells were platted on 24 well plates (Falcon; 700,000 cells/well) and grown 24 h until they reach 90% confluence.

2.5. Cell counting

To get a precise estimate of the cell number present in each well at the time where cell penetration experiments are performed with ^{125}I-Tyr-L-MCa, F98 cells were counted by flow cytometry analyses with live cells using a Becton Dickinson Accuri C6 flow cytometer (BD Biosciences). Data were obtained and analyzed using BD Accuri C6 software. Live cells were gated by forward/side scattering.

2.6. Evaluation of F98 cell death

Cells were incubated with or without various concentrations of Tyr-L-MCa during 2 h. Cells were washed with PBS and washes were conserved. They were then treated with 0.05% trypsin-EDTA for 5 min at 37 °C to detach them from the support. Cells were collected and resuspended in DMEM-F12 with 2% fetal bovine serum along with the initial washes. For one series of control cells, 0.1% saponin was added just before centrifugation to induce cell death. All cell conditions (control, Tyr-L-MCa and saponin) were centrifuged at 800 ×*g* during 5 min. The pellets were resuspended in 200 μl of staining mix according to Invitrogen recommendations. Cells were left in the dark for 15 min at room temperature before analyses by flow cytometry using the LIVE/DEAD® Viability/Cytotoxicity Kit of Invitrogen. This kit quickly discriminates live from dead cells by simultaneously staining with green-fluorescent calcein-AM to indicate intracellular esterase activity and red-fluorescent ethidium homodimer-1 to indicate loss of plasma membrane integrity. Similar results were obtained with ^{125}I-Tyr-L-MCa.

2.7. Estimation of F98 cell volume by Digital Holographic Microscopy or confocal microscopy

Digital Holographic Microscopy (DHM) is an interferometric technique that makes possible the imaging and measurement of the phase retardation through transparent biological specimen [19]. Because it is based on the interference of coherent light (lambda 658 nm) a high precision (nm order) can be obtained in optical thickness measurements. Under the hypothesis of invariance of the refractive index within the cytosol, it may be admitted that the measured optical thickness is a good estimate of the quantity of matter traversed by light [20]. Therefore, the average F98 cell volume was estimated by integrating the optical thickness over the projected area of each cell.

To evaluate the F98 cell volume by confocal microscopy, cell plasma membranes were stained with 50 μg/ml concanavalin A-rhodamine for 5 min. Next, cells were washed with phosphate buffered saline (PBS) and incubated in DMEM without phenol red. Live cells were then immediately analyzed by confocal laser scanning microscopy using a Zeiss LSM operating system. Rhodamine was sequentially excited (at 561 nm) and emission fluorescence (at 590 nm) was collected. Stacks of 17 to 22 confocal images were taken by steps of 1 μm on the z-axis to cover the entire depth of the cells. Globally, F98 cells were quite thick but some images of the stacks may not contain any information. Next, a dedicated Image J macro was developed to reconstruct the 3-D

Please cite this article as: C. Tisseyre, et al., Quantitative evaluation of the cell penetrating properties of an iodinated Tyr-L-maurocalcine analog, Biochim. Biophys. Acta (2014), http://dx.doi.org/10.1016/j.bbamcr.2014.03.017

F98 cell image to calculate the global volume using the stained plasma membrane boundaries.

2.8. Quantitative evaluation of the cell penetration of ^{125}I-Tyr-L-MCa

F98 cells were incubated with various concentrations of radio-iodinated ^{125}I-Tyr-L-MCa (33 nM to 10 μM) in DMEM F-12 culture medium (200 to 400 μl per well) without serum or antibiotics at 37 °C for 2 h to allow cell penetration. For the estimation of the kinetics of cell entry of the compound, the time of incubation could be shortened as indicated. Each concentration contained 2.5% of ^{125}I-radiolabeled peptide and 97.5% of ^{127}I-labeled peptide to diminish the quantity of radioactive peptide to handle. After incubation, the cells were washed twice with PBS to remove excess extracellular peptide. They were then treated with 0.05% trypsin-EDTA for 5 min at 37 °C to (i) degrade any remaining extracellular ^{125}I-Tyr-L-MCa and (ii) detach F98 cells from the surface. Cells were collected and resuspended in DMEM-F12 with 2% fetal bovine serum. Cells were centrifuged at 800 ×*g* during 5 min. The pellet was resuspended in PBS and cells were then centrifuged a second time in the same conditions. Of note, for each one of the centrifugation and washing steps, resuspended cells were transferred to new tubes to eliminate any extracellular radioiodinated ^{125}I-Tyr-L-MCa or trypsin-induced fragment that may be potentially present by sticking to the plastic. Cells were resuspended in 1 ml of lysis buffer (in mM: Tris 20, NaCl 150, DTT 1, sucrose 250, pH 8.0 along with protease inhibitors) and incubated on ice for 5 min. Next, cells were mechanically disrupted using a potter. Subcellular fractionation was performed as follows. First, the cell lysates were centrifuged at 900 ×*g* for 20 min and the pellet containing the cell nuclei (F98-N) was collected. Next, the supernatant was collected and centrifuged at 50.000 ×*g* for 60 min. The pellet containing the plasma membrane was kept (F98-PM) along with the supernatant that represents the cytoplasm (F98-C). Both pellets were resuspended in 500 μl distilled water for counting. This subcellular fractionation method separates membrane-bound (F98-PM) from intracellular ^{125}I-Tyr-L-MCa (F98-N + F98-C) providing an estimate of cell penetration of the peptide into the cytoplasm. Counting of radioactivity was carried out by gamma-well counter.

2.9. Determination of the intracellular concentration of ^{125}I-Tyr-L-MCa

Knowing the precise cell number per well, the average cell volume and the specific activity of ^{125}I-Tyr-L-MCa, we were able to convert counts per min to intracellular peptide concentration. The concentration of radioiodinated Tyr-L-MCa is provided in μM and was calculated according to the equation $f_0 = (((cpm/cell\ number)/a)/b)/cell\ volume$. The value **a** is a constant value of the gamma-well counter (a = 35515679 to convert cpm values in MBq). The value **b** is the specific activity of Tyr-L-MCa that has been used for the preparation of dilutions. Only the added values of F98-N and F98-C radioactivity were taken into account to quantify cell penetration. F98-PM values were discarded.

2.10. Kinetic of cellular leakage of ^{125}I-Tyr-L-MCa

F98 cells were incubated with 1 μM of ^{125}I-Tyr-L-MCa in DMEM F-12 culture medium without serum or antibiotics at 37 °C for 2 h. The cells were then washed three times with PBS to remove excess extracellular peptide, and then completed with DMEM F-12 medium. At different times (0, 1, 2, 3, 4, 5, 6 and 24 h), a sample of 100 μl of medium was taken for radioactivity counting and replaced by 100 μl of fresh complete medium. The value obtained was corrected by a factor of 4 (100 μl taken out of 400 μl of medium). A control was performed without cells to demonstrate that the plastic of the wells did not release any radioactivity. The quantity of radioactivity released by the cells was evaluated as a ratio of total cell radioactivity as determined previously.

2.11. [^{3}H]-ryanodine binding on ryanodine receptors from skeletal muscle heavy SR vesicles

Heavy sarcoplasmic reticulum (SR) vesicles were prepared as described [11]. Protein concentration was measured by the Biuret method. Heavy SR vesicles (1 mg/ml) were incubated at 37 °C for 2 h in an assay buffer composed of 10 nM [^{3}H]-ryanodine, 150 mM KCl, 2 mM EGTA, 2 mM $CaCl_2$ (pCa = 5), and 20 mM MOPS, pH 7.4. 200 nM L-MCa or Tyr-L-MCa was added prior to the addition of heavy SR vesicles. [^{3}H]-ryanodine bound to heavy SR vesicles was measured by filtration through Whatman GF/B glass filters followed by three washes with 5 ml of ice-cold washing buffer composed of 150 mM NaCl, 20 mM HEPES, pH 7.4. [^{3}H]-ryanodine retained on the filters was measured by liquid scintillation. Nonspecific binding was measured in the presence of 80 μM unlabeled ryanodine. The data are presented as mean ± S.E. Each experiment was performed in triplicate.

3. Results

3.1. Tyr-L-MCa: a functional MCa analog for iodination

L-MCa itself lacks a tyrosine residue for radio-iodination of the peptide. To this end, we produced a new analog of L-MCa with an extra amino-terminal tyrosine residue. Earlier observations had demonstrated that N-terminal-modified analogs of L-MCa could be easily produced since the addition of an extra-biotinylated lysine residue is without impact on the proper folding/oxidation of the peptide [9]. MS analyses (MALDI-TOF technique) of crude and folded/oxidized Tyr-L-MCa provide experimental molecular masses $(M + H)^+$ of 4026.9 and 4020.8 Da, respectively. The shift in experimental molecular mass of 6.1 Da upon folding/oxidation is in agreement with the engagement of all six cysteine residues in the formation of three disulfide bridges. Since the activity of L-MCa is strictly dependent on the proper/folding of the peptide [21] and that this activity is not altered by N-terminal modification [6,9], it is expected that Tyr-L-MCa should have preserved its pharmacological effect. Fig. 1B illustrates that this is indeed the case. As shown, Tyr-L-MCa turned as potent as L-MCa itself in stimulating the binding of [^{3}H]-ryanodine onto skeletal muscle ryanodine receptors from SR vesicles. Next, since Tyr-L-MCa remained functional, the peptide was enzymatically iodinated using the lactoperoxidase/H_2O_2 system. Under the experimental conditions described radiochemical purity higher than 95% was achieved. This was further illustrated in the HPLC profile of the compound (Fig. 1C). ^{125}I-Tyr-L-MCa remained stable for over 24 h. ^{127}I iodination was also used to prepare ^{127}I-Tyr-L-MCa instead of ^{125}I-Tyr-L-MCa to lower the specific activity and the quantity of radioactivity to handle. Modeling experiments illustrates the relative position of the extra iodinated tyrosine residue onto L-MCa (Fig. 2).

3.2. Tyr-L-MCa lacks cell toxicity and is partially degraded by trypsin treatment

We first assessed that Tyr-L-MCa does not induce cell death that may alter the evaluation of cell penetration. For that purpose, we used rat glioma F98 cells because we plan to use L-MCa as a vector for the delivery of chemo-active drugs in later studies. As shown by flow cytometry, incubating F98 cells 2 h with 33 μM Tyr-L-MCa does not induce any specific cell death compared to the control condition (Fig. 1D, E). The control condition contained about 3.3% of dead cells compared to the 2.6% of the Tyr-L-MCa condition. In contrast, 5 min incubation with 0.1% saponin has a drastic effect on cell survival since the proportion of dead cells reached 93.4% (Fig. 1F). Similar results were obtained for a set of Tyr-L-MCa concentration that all indicate that this vector is non-toxic for F98 cells (Fig. 1G). Similar observations were made with F98 cells incubated with ^{125}I-Tyr-L-MCa indicating that gamma radiation did not

Please cite this article as: C. Tisseyre, et al., Quantitative evaluation of the cell penetrating properties of an iodinated Tyr-L-maurocalcine analog, Biochim. Biophys. Acta (2014), http://dx.doi.org/10.1016/j.bbamcr.2014.03.017

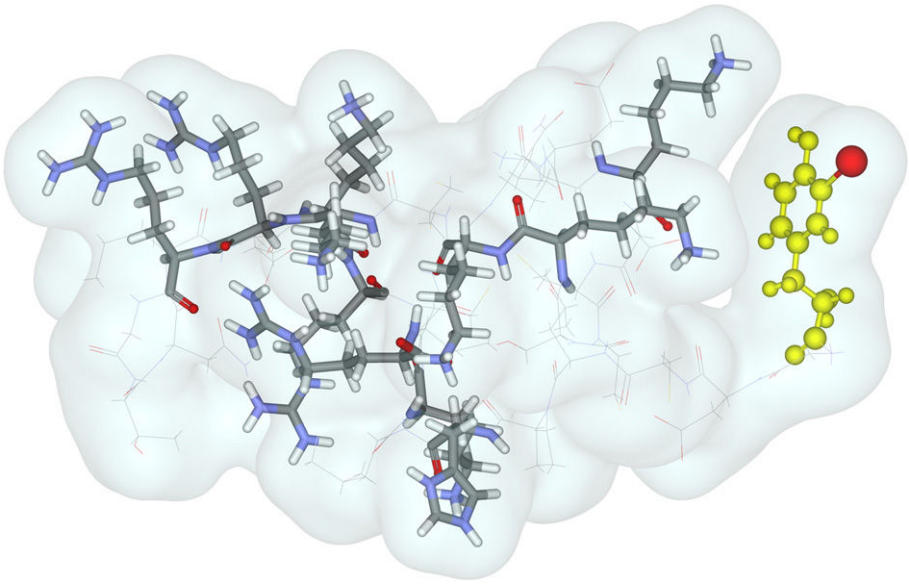

Fig. 2. Modeled 3D structure of ^{125}I-Tyr-L-MCa. The structure was modeled starting with L-MCa as a structural basis (1C6W from the Protein Database). The extra tyrosine residue is in yellow and the iodine on the tryrosine ring in red. The positively charged amino acid residues of L-MCa are also highlighted.

add a layer of cell toxicity in the frame of our experiments (data not shown).

3.3. Cell penetration properties of ^{125}I-Tyr-L-MCa

Production of the ^{125}I-Tyr-L-MCa compound with high radiochemical purity is an opportunity to quantify the cell penetration of L-MCa into cells. Earlier labeling of L-MCa with a fluorescence indicator provided only semi-quantitative information [11]. We first designed a subcellular fractionation protocol that was aimed at minimizing the contribution of any external membrane-attached ^{125}I-Tyr-L-MCa radioactivity associated to F98 cells. This protocol includes trypsin treatment, many cell washes, and a systematic transfer of the biological material to new plastic tubes in order to avoid possible attachment of any external ^{125}I-Tyr-L-MCa to plastic surfaces. Trypsin treatment was kept to the minimum because its first aim is to detach cells from the surface. Longer exposure would result in better external ^{125}I-Tyr-L-MCa degradation but also in cell damaging which is not desirable. Fig. 3 illustrates that indeed a 5 min trypsin digestion after F98 cell incubation with ^{125}I-Tyr-L-MCa results in only limited peptide degradation. The appearance on the HPLC elution profile of a new leftward-shifted peak, which is superimposed to the remnant

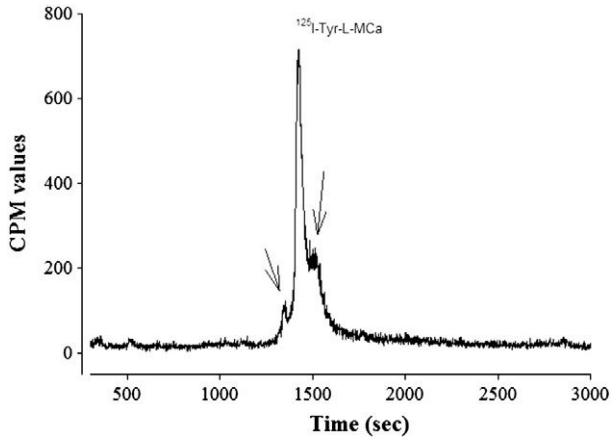

Fig. 3. RP-HPLC profile of ^{125}I-Tyr-L-MCa following 5 min of incubation with trypsin. The major peak is the intact ^{125}I-Tyr-L-MCa, while the peaks denoted by the arrows reflect degraded products.

peak of the original ^{125}I-Tyr-L-MCa compound, indicates that the trypsin-mediated degradation is only partial. To further minimize the potential quantitative contribution of any cell membrane-bound ^{125}I-Tyr-L-MCa, the plasma membrane was quantified as a separate entity and the radioactivity associated to this subcellular fraction was excluded from our calculations of L-MCa cell entry and accumulation. However, as we shall see later, the radioactivity associated with the plasma membrane was extremely low indicating little accumulation of the peptide in membrane fractions which further strengthens the reliance on the protocol used to quantify cell entry.

The entire study was performed on the rat glioblastoma cancer cell line F98 maintained in culture. To assess the cell concentration achieved by the ^{125}I-Tyr-L-MCa, we first determined two important parameters: i) the cell number in each well and ii) the average volume of F98 cells. The cell number in each culture well was established by FACS counting. The average cell number was 403,754 ± 23,434 per well (n = 4 wells). This includes 96.7% of live cells and 3.3% of dead cells as defined in Fig. 1D. Next, we evaluated the average cell volume using two different techniques: DHM and cell volume reconstruction through the acquisition of stacks of confocal images. Fig. 4A illustrates the optical thickness image produced by DHM with gray levels coding for the optical thickness. The surface reconstruction of the optical thicknesses is shown in Fig. 4B. The volume of F98 cells can be obtained by integration of the optical thickness inside the cell areas. A histogram illustrating individual cell volume was constructed (Fig. 4C). Fitting the data provides an average cell volume of $8.9 \times 10^{-7} \pm 0.2 \times 10^{-7}$ μl (n = 130 cells). We also used z-stacks of CM images to reconstruct cell volumes, again by focusing on individual cells. The boundaries of cells were provided by concanavalin-A rhodamine staining of the plasma membranes. Using this CM method instead of DHM, we come up with an average F98 cell volume of 18.9×10^{-7} μl (n = 95 cells). There is thus a 2.12-fold difference in volume estimation using these two methods. DHM is likely a more precise technique for volume estimation and we will rely on the average DHM value to calculate the intracellular concentration of ^{125}I-Tyr-L-MCa. However, when applicable, the concentration values will also be provided using the CM cell volume evaluation method in parentheses.

First, we investigated how dead cells may affect the uptake of ^{125}I-Tyr-L-MCa. The peptide being extremely basic it is possible that dead cells, by exposing their DNA or their protein content, may overly contribute to the measured signal. We therefore purposely compared

Please cite this article as: C. Tisseyre, et al., Quantitative evaluation of the cell penetrating properties of an iodinated Tyr-L-maurocalcine analog, Biochim. Biophys. Acta (2014), http://dx.doi.org/10.1016/j.bbamcr.2014.03.017

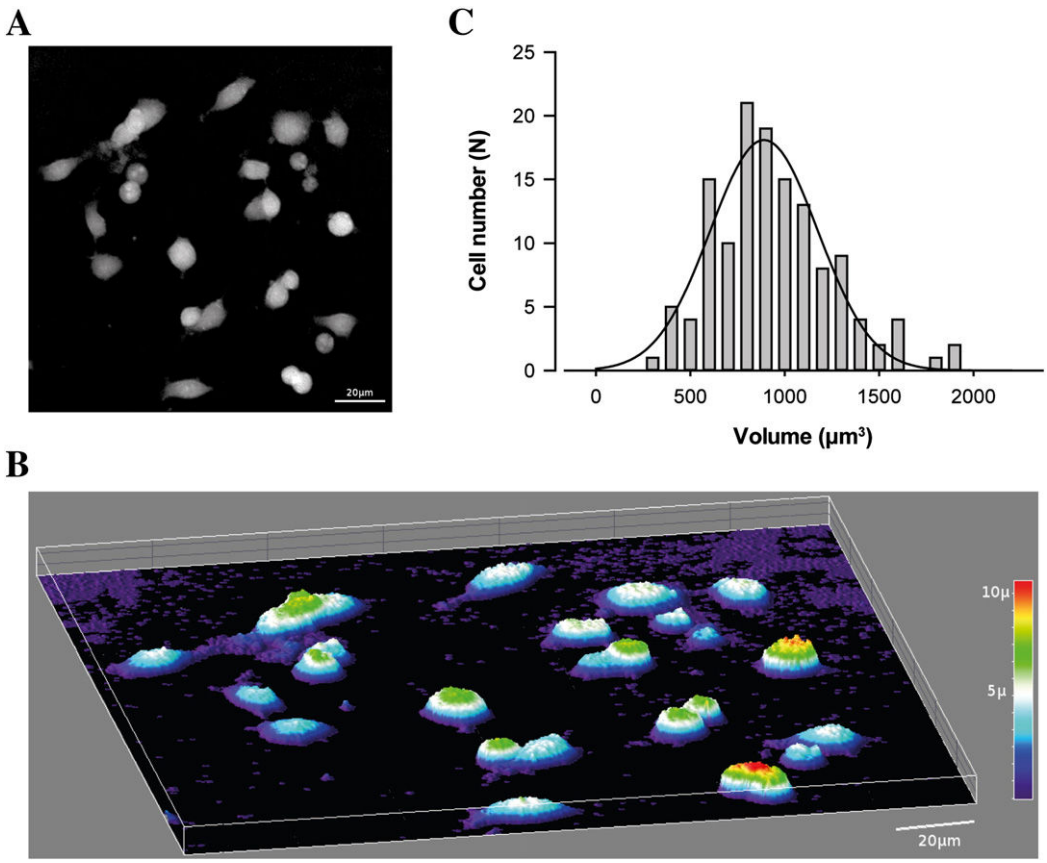

Fig. 4. Estimation of the average volume of F98 glioblastoma cells by DHM. (A) Optical thickness image produced by DHM, the gray levels are coding for the optical thickness. (B) Surface reconstruction of the optical thicknesses. (C) Histogram showing the distribution of individual cell volumes, obtained by integrating the optical thickness inside the cell areas. Only individual cells were used to evaluate cell volumes since touching cells could lead to overestimation. Cell fragments were also avoided for this analysis.

the amount of accumulated radioactivity in live cells incubated 2 h with 33 µM ^{125}I-Tyr-L-MCa with the amount found in dead cells, the cell death being promoted by 0.1% saponin. As shown in Fig. 5A, dead cells accumulate a surprisingly high level of radioactivity in each of the subcellular fractions. In each case however, the level of activity was lower than in live cells, indicating that cell death should not affect the measurements on live cells significantly. Fig. 5A also illustrates that the plasma membrane is the subcellular fraction that accumulates the least radioactivity compared to the cytoplasm and the nucleus. At this external concentration, the plasma membrane represents 9.4% of the accumulated radioactivity. In contrast, the cytoplasm and the nucleus of live cells accumulate each 25.6% and 64.7%, respectively. These proportions were however altered in dead cells with respective accumulations of 15.7% (plasma membrane), 45.1% (cytoplasm) and 32.2% (nucleus). The comparatively good accumulation of ^{125}I-Tyr-L-MCa in the cytoplasmic fraction of dead cells is probably linked to the effect of saponin on the plasma membrane. Since saponin should not affect the membrane of the nucleus, we still observe a quantitative difference in the accumulation of ^{125}I-Tyr-L-MCa radioactivity in dead cells compared to live ones. The result also indicates that the intracellular concentration of ^{125}I-Tyr-L-MCa should not exceed by far the extracellular concentration of the compound since passive accumulation within permeabilized cells resembles the accumulation within live cells.

We examined the concentration-dependent uptake of ^{125}I-Tyr-L-MCa by live F98 cells using extracellular concentrations ranging from 3.3 nM to 10 µM for a 2 hour-incubation time. We then assessed the cumulated radioactivity within each subcellular fraction. As shown in Fig. 5B, evident accumulation of ^{125}I-Tyr-L-MCa occurs essentially within the cytoplasm and the nucleus at a concentration as low as 300 nM. Increasing extracellular concentrations of the ^{125}I-Tyr-L-MCa also produce increasing elevations of the radioactivity within each fraction with similar dose-dependent profiles. In the result shown here, there was almost no accumulation within the plasma membrane fraction. There is no sign of saturation in full agreement with earlier observations using L-MCa tagged with fluorescent dyes [10,11]. The cell count, the average DHM-assessed F98 cell volume and the specific activity of ^{125}I-Tyr-L-MCa have been used to convert the experimental cpm data into average cell concentrations of ^{125}I-Tyr-L-MCa. Only cumulated cpm values from the cytoplasm and the nucleus were taken into account since the radioactivity associated to the plasma membrane fraction could bear some ^{125}I-Tyr-L-MCa from the outer leaflet of the membrane that would not be digested by the trypsin treatment as shown earlier. Obviously, this may lead to underestimation of the total accumulated ^{125}I-Tyr-L-MCa in F98 cells but this was preferable to a slightly overestimated concentration, the plasma membrane accounting for only a small fraction of the total radioactivity (<10% at all concentrations tested and for each experiment we performed). According to the method, we show a close correspondence in the intracellular concentration of ^{125}I-Tyr-L-MCa compared to the extracellular concentration (Fig. 5C). For instance at 1 µM external ^{125}I-Tyr-L-MCa, F98 cells accumulated 2.41 µM of the peptide according to DHM volume estimation (1.14 µM according to CM-based volume estimation). Examining the internal concentration of ^{125}I-Tyr-L-MCa as a function of the external concentration indicates that the concentration ratio (internal/external) is higher at lower external concentrations than at high external concentrations. This was marked at 10 nM where penetration is barely detected with this cell penetrating peptide. Fitting the experimental data with a decreasing exponential curve yields a concentration ratio of 2.45 according to DHM data (or 1.15 according to CM data) (Fig. 5C, inset).

Please cite this article as: C. Tisseyre, et al., Quantitative evaluation of the cell penetrating properties of an iodinated Tyr-L-maurocalcine analog, Biochim. Biophys. Acta (2014), http://dx.doi.org/10.1016/j.bbamcr.2014.03.017

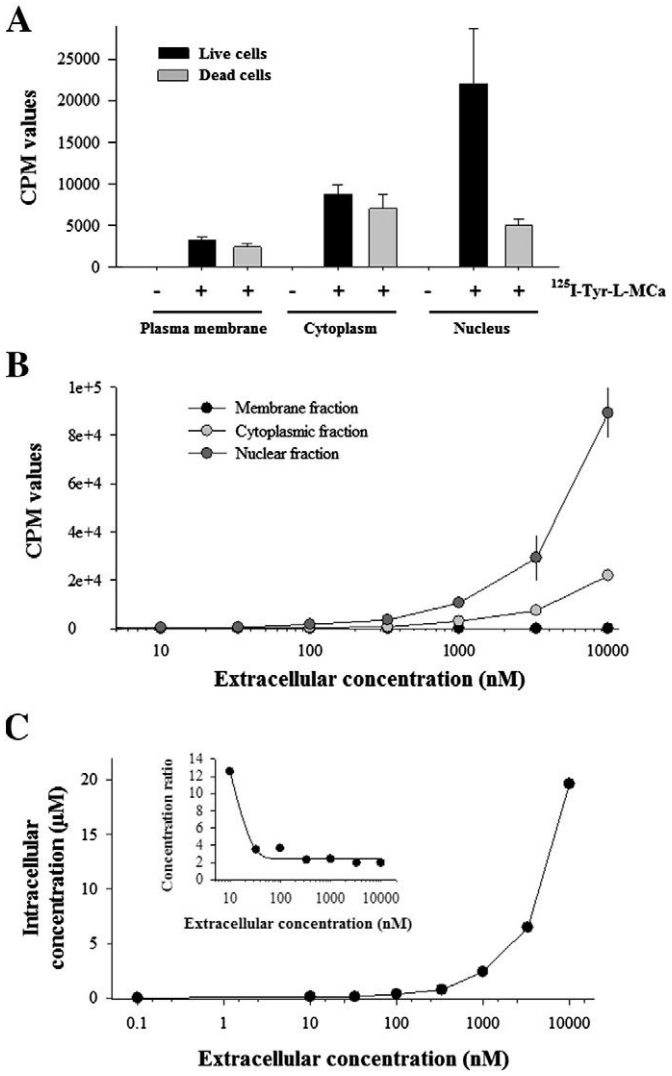

Fig. 5. Estimation of the accumulation properties of ^{125}I-Tyr-L-MCa in F98 cells. (A) Total radioactivity accumulated in subcellular fractions of live and dead cells (plasma membrane, cytoplasm, and nucleus). Radioactivity was also measured for control live cells in the absence of ^{125}I-Tyr-L-MCa. No significant counts could be measured. Extracellular concentration of ^{125}I-Tyr-L-MCa used: 33 µM. 2 h incubation. (B) Concentration dependent accumulation of ^{125}I-Tyr-L-MCa in subcellular fractions of live cells. 2 h of incubation with the radiochemical compound. (C) Evaluation of the internal concentration of ^{125}I-Tyr-L-MCa reached after 2 h incubation of live F98 cells as a function of the external concentration of ^{125}I-Tyr-L-MCa. Inset: ratio of concentration as a function of the external ^{125}I-Tyr-L-MCa. The data were fitted with the following equation $y = y_0 + a.e^{-bx}$ where $y_0 = 2.45 \pm 0.31$, $a = 27.1 \pm 8.6$ and $b = 0.098 \pm 0.031$.

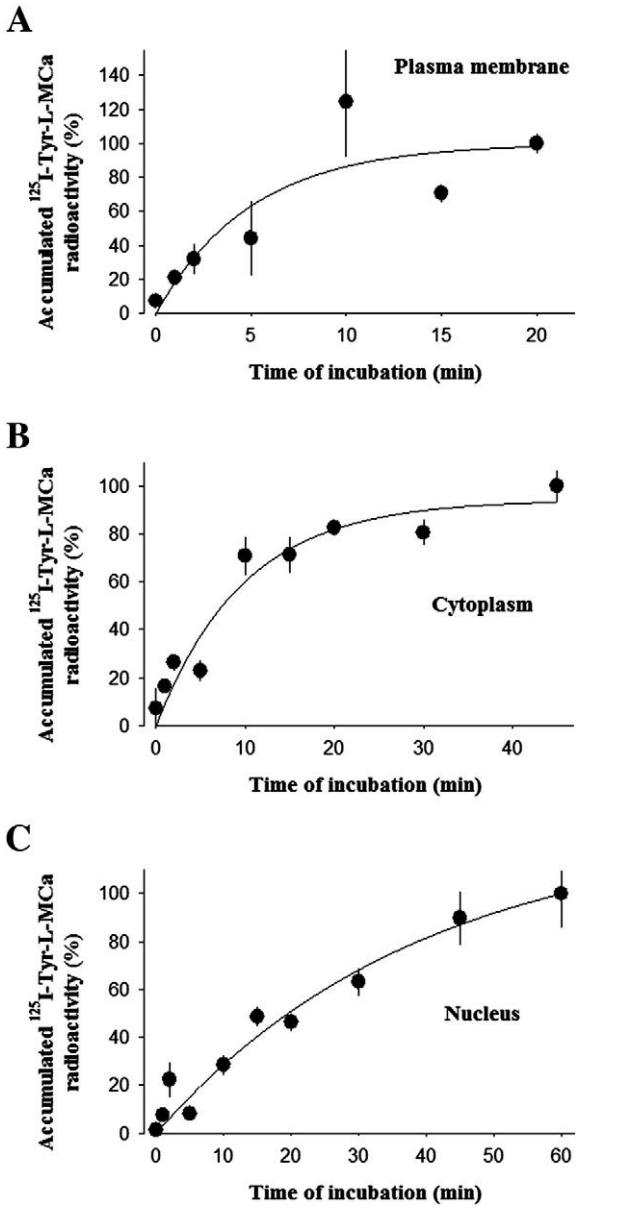

Fig. 6. Kinetics of ^{125}I-Tyr-L-MCa accumulation within the different subcellular compartments of F98 cells. (A) Kinetics of ^{125}I-Tyr-L-MCa accumulation within the plasma membrane fraction of F98 cells. The data were fitted with the equation $y = a \times (1 - e^{-bx})$ where $a = 99.8 \pm 19.7$ and $b = 0.20 \pm 0.12$ min^{-1}. (B) Kinetics of ^{125}I-Tyr-L-MCa accumulation within the cytoplasmic fraction of F98 cells. Parameters after fitting were: $a = 94.2 \pm 8.1$ and $b = 0.10 \pm 0.02$ min^{-1}. (C) Kinetics of ^{125}I-Tyr-L-MCa accumulation within the nuclear fraction of F98 cells. Parameters after fitting were: $a = 127.6 \pm 23.5$ and $b = 0.025 \pm 0.007$ min^{-1}. For all these experiments we used 1 µM of ^{125}I-Tyr-L-MCa.

3.4. Kinetics of entry and exit of ^{125}I-Tyr-L-MCa into and from F98 cells

For a ^{125}I-Tyr-L-MCa accumulation in the nucleus, the peptide needs first to cross the plasma membrane, then to accumulate within the cytoplasm, and should afterwards travel to the nucleus of F98 cells. This sequence of events requires that the kinetics of accumulation within each subcellular fraction should follow a logic time gradient. This point was investigated by incubating F98 cells with 1 µM ^{125}I-Tyr-L-MCa for various durations, fractionating the cells and counting the radioactivity associated to each fraction (Fig. 6). As shown, the time constant for radioactivity accumulation in the plasma membrane is $\tau = 5$ min (Fig. 6A). This value rises to $\tau = 10$ min for the cytoplasm (Fig. 6B), which remains quite rapid, and to $\tau = 20$ min for the accumulation in the nuclear fraction of F98 cells (Fig. 6C).

^{125}I-Tyr-L-MCa is heavily charged (net positive charge = +8) indicating that it may be attracted to the internal face of the plasma membrane because of the existence of the negative membrane potential. It can be envisioned that while the cell entry of the peptide is facilitated because of this membrane potential, the same negative charges residing in the cell may prevent the cell escape of the peptide. We investigated this issue by examining the gradual release of radioactivity within the external medium. As shown, F98 cells are extremely reluctant to release the radioactivity once accumulation has occurred (Fig. 7). It is only after 24 h of washout time that about 8.9% of the radioactivity is released by the cells.

Please cite this article as: C. Tisseyre, et al., Quantitative evaluation of the cell penetrating properties of an iodinated Tyr-L-maurocalcine analog, Biochim. Biophys. Acta (2014), http://dx.doi.org/10.1016/j.bbamcr.2014.03.017

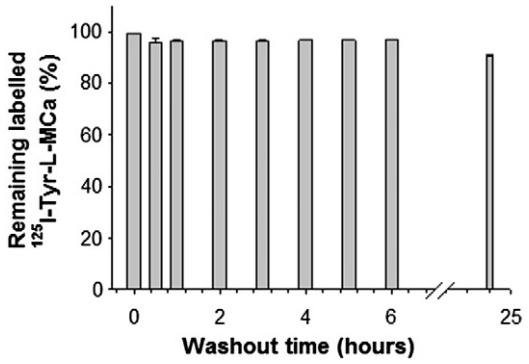

Fig. 7. Kinetics of cell exit rate of ^{125}I-Tyr-L-MCa from F98 cells. Time-dependent exit of ^{125}I-Tyr-L-MCa from F98 cells expressed as a percentage of total intracellular labeled peptide.

4. Discussion

L-MCa is the first example of a folded and oxidized animal peptide toxin acting as a CPP [6,8–12,14,21–24]. Since CPPs hold great promises in the field of drug delivery, it was therefore of great importance to determine the precise cell entry characteristics of L-MCa. Radiolabeling represents the most sensitive and quantitative method to quantify the cell entry of a molecule of interest. To this aim we produced Tyr-L-MCa that, as expected from earlier evidence, preserved proper folding and oxidation, as well as the original pharmacological properties of L-MCa and the resistance to proteolytic cleavage. The position of the extra tyrosine residue ensured that iodination occurred in a convenient way, without accessibility problems and without introducing structural disturbances within the native sequence. Compared to other reporting methods, the addition of an iodinated Tyr residue at the N-terminus of L-MCa keeps structural alterations of the peptide to a minimum.

For the first time, compared to all our earlier investigations using fluorochromes as reporters [10,11,14,21], we were able to extract valuable quantitative information on the cell penetration properties of ^{125}I-Tyr-L-MCa. For that purpose, we used the rat glioblastoma F98 cell line and several critical parameters to assess the penetration properties. First, we precisely defined the specific activity of ^{125}I-Tyr-L-MCa that allowed us to establish a precise correlation between measured cpm values and peptide quantities. Then, we used DHM to evaluate the cell volume and transform peptide quantities into intracellular concentrations. Finally, an adequate biochemical protocol combined to cell sub-fractionation helped defined cell compartments and informed on the relative cell distribution of ^{125}I-Tyr-L-MCa. It was striking to observe that very little radioactivity is associated to the plasma membrane fraction. This is coherent with earlier observations using MCa analogs coupled to fluorescent dyes. These vector/cargo couples were in most cases not observed at the plasma membrane level on images gathered by confocal microscopy, except on some occasions [10]. It was however possible that the lipophilic environment of the membrane could quench the fluorescence of these dyes. Our data using iodinated Tyr-L-MCa demonstrates that the plasma membrane is not a compartment of peptide accumulation on or in the cells. This indicates that the residency time of ^{125}I-Tyr-L-MCa within the plasma membrane is very low, a finding that is consistent with the fast kinetics of cell accumulation within the membrane. While the plasma membrane is an obligatory route of cell entry for ^{125}I-Tyr-L-M, the peptide must use unstable modes of interaction with the plasma membrane components. The transient nature of these interactions argues for a rapid crossing followed by a dilution process within the cytoplasm. The kinetics of accumulation within the cytoplasm is itself quite rapid (time constant of 10 min) but the degree of accumulation is significantly greater than in the plasma membrane. An interesting observation is the accumulation of the peptide within the nucleus, to a great proportion, indicating that the peptide that is transferred from the cytoplasm to the nucleus had to be freely moving in the cytoplasm and could not be trapped within endosomes. This wouldn't have occurred if the majority of the peptide had been captured in F98 cells by a form of endocytosis such as macropinocytosis. We were not able to assess the relative volumes occupied by the cytoplasm and the nucleus. These values would however be meaningless to some extent as both compartments are themselves sub-compartmentalized. However, the values of cpm accumulation within these two compartments were closely related suggesting that most likely passive equilibrium was reached in the concentrations of the labeled peptide. In any case, the finding that the peptide is present in the nucleus contradicts other observations using dyes or proteins as cargoes, as in all cases MCa analogs were mostly confined to the cytoplasmic region presumably because of cargo-oriented trapping into endosomes [8–12,14]. In other cases, however, we found evidence for nuclear accumulation of doxorubicin as cargo [22,25–27], indicating that the matter of nuclear accumulation is cargo dependent. The reason for the accumulation of ^{125}I-Tyr-L-MCa in the nucleus has not been investigated. However, it may be argued that the peptide freely crosses nuclear pores and passively invades the nucleus. Because of its basic nature, it may then be stabilized there by ionic interactions with DNA. This matter may be studied later by using some of the small cell penetrating peptide variants derived from L-MCa that lack the basic nature of the full-length peptide [10,14].

The kinetics of accumulation within the plasma membrane and the cytoplasm deserve another comment. The time constant of a few minutes for the cell penetration of ^{125}I-Tyr-L-MCa is in apparent contrast with the second time scale required for L-MCa to trigger Ca^{2+} release after external application [6]. This difference is unlikely to be due to the extra-tyrosine residue or its labeling with iodine. The ryanodine receptor activation requires less than 10 nM internal concentration. However because of the peculiar location of the binding site of L-MCa on the ryanodine receptor [5], at the interface of the cytoplasm and the plasma membrane, it is possible that local L-MCa elevations may suffice to activate the ryanodine receptor. This would further be exaggerated by the presence of up to four binding sites of L-MCa on the ryanodine receptor, with a single occupancy being sufficient for activation. In addition, significant Ca^{2+} signals are expected with the activation of very few ryanodine receptors. Finally, considering the lipophilic environment of the L-MCa binding site, the reversibility of interaction between L-MCa and the ryanodine receptor is not evident. For all these reasons, we therefore believe that the kinetics of cell entry and Ca^{m} release activation cannot be easily compared.

Regarding peptide concentrations reached within the cell, we found values indicating near passive distribution between the outside and the inside of the cell. Precise estimation of cell concentration of ^{125}I-Tyr-L-MCa is also linked to the precise estimation of cell volume. We purposely used two techniques of cell volume investigation and found closely related values. The close to 2-fold difference suggests that our concentration values can be corrected by a factor of 2 as well. In the worst-case scenario, the global concentration of the peptide inside cells would match the outside concentration of ^{125}I-Tyr-L-MCa. The estimated cell volume is of course the total cell volume and does not take into account the volume loss that should be introduced by the volume of many organelles such as mitochondria, endoplasmic reticulum and the Golgi apparatus for instance, if the peptide does not accumulate into these organelles. If we take this assumption as correct, then we may assume that part of the peptide accumulation may occur against the concentration gradient. Voltage-driven accumulation may well represent one mechanism explaining how cells may cumulate higher peptide concentrations than the outside. Cells are negatively polarized. The net positively charged L-MCa should be attracted by the negative charges located underneath the plasma membrane. A second potential mechanism may be local increases of the peptide concentration at the external side of the plasma membrane. L-MCa interacts with negatively charged glycosaminoglycans [24] or negatively charged lipids [8] and the positive charges of L-MCa may contribute to greater

Please cite this article as: C. Tisseyre, et al., Quantitative evaluation of the cell penetrating properties of an iodinated Tyr-L-maurocalcine analog, Biochim. Biophys. Acta (2014), http://dx.doi.org/10.1016/j.bbamcr.2014.03.017

interactions, thereby locally increasing the peptide concentration. In any case, the finding that the labeled peptide can barely escape the intracellular environment is also evidence for the existence of an accumulation process that is not only linked to passive redistribution of the peptide into the cells. It indicates the existence of a strong asymmetry in the fluxes of Tyr-L-MCa through the membrane. This may be linked to the asymmetric lipid composition or the existence again of a voltage gradient across the plasma membrane.

Acknowledgements

We thank the following platforms (GAIA, Prométhée, and microscopie optique from Université Joseph Fourier) for their collaboration. C. Tisseyre has a fellowship from Région Rhône-Alpes (cluster 11 Handicap, Vieillissement et Neurosciences). MDW thanks the French Agence Nationale de la Recherche (program Nanofret2 and LabEx "Ion Channel Science and Therapeutics", program number: ANR-11-LABX-0015) for financial support.

References

[1] M. Mae, U. Langel, Cell-penetrating peptides as vectors for peptide, protein and oligonucleotide delivery, Curr. Opin. Pharmacol. 6 (2006) 509–514.
[2] M. Pooga, U. Soomets, M. Hallbrink, A. Valkna, K. Saar, K. Rezaei, U. Kahl, J.X. Hao, X.J. Xu, Z. Wiesenfeld-Hallin, T. Hokfelt, T. Bartfai, U. Langel, Cell penetrating PNA constructs regulate galanin receptor levels and modify pain transmission *in vivo*, Nat. Biotechnol. 16 (1998) 857–861.
[3] M. Rhee, P. Davis, Mechanism of uptake of C105Y, a novel cell-penetrating peptide, J. Biol. Chem. 281 (2006) 1233–1240.
[4] A. Mosbah, R. Kharrat, Z. Fajloun, J.G. Renisio, E. Blanc, J.M. Sabatier, M. El Ayeb, H. Darbon, A new fold in the scorpion toxin family, associated with an activity on a ryanodine-sensitive calcium channel, Proteins 40 (2000) 436–442.
[5] X. Altafaj, W. Cheng, E. Esteve, J. Urbani, D. Grunwald, J.M. Sabatier, R. Coronado, M. De Waard, M. Ronjat, Maurocalcine and domain A of the II–III loop of the dihydropyridine receptor Cav 1.1 subunit share common binding sites on the skeletal ryanodine receptor, J. Biol. Chem. 280 (2005) 4013–4016.
[6] E. Esteve, K. Mabrouk, A. Dupuis, S. Smida-Rezgui, X. Altafaj, D. Grunwald, J.C. Platel, N. Andreotti, I. Marty, J.M. Sabatier, M. Ronjat, M. De Waard, Transduction of the scorpion toxin maurocalcine into cells. Evidence that the toxin crosses the plasma membrane, J. Biol. Chem. 280 (2005) 12833–12839.
[7] S. Mouhat, B. Jouirou, A. Mosbah, M. De Waard, J.M. Sabatier, Diversity of folds in animal toxins acting on ion channels, Biochem. J. 378 (2004) 717–726.
[8] S. Boisseau, K. Mabrouk, N. Ram, N. Garmy, V. Collin, A. Tadmouri, M. Mikati, J.M. Sabatier, M. Ronjat, J. Fantini, M. De Waard, Cell penetration properties of maurocalcine, a natural venom peptide active on the intracellular ryanodine receptor, Biochim. Biophys. Acta 1758 (2006) 308–319.
[9] K. Mabrouk, N. Ram, S. Boisseau, F. Strappazzon, A. Rehaim, R. Sadoul, H. Darbon, M. Ronjat, M. De Waard, Critical amino acid residues of maurocalcine involved in pharmacology, lipid interaction and cell penetration, Biochim. Biophys. Acta 1768 (2007) 2528–2540.
[10] C. Poillot, H. Bichraoui, C. Tisseyre, E. Bahemberae, N. Andreotti, J.M. Sabatier, M. Ronjat, M. De Waard, Small efficient cell-penetrating peptides derived from scorpion toxin maurocalcine, J. Biol. Chem. 287 (2012) 17331–17342.
[11] C. Poillot, K. Dridi, H. Bichraoui, J. Pecher, S. Alphonse, B. Douzi, M. Ronjat, H. Darbon, M. De Waard, D-Maurocalcine, a pharmacologically inert efficient cell-penetrating peptide analogue, J. Biol. Chem. 285 (2010) 34168–34180.
[12] T.-N.I., N. Ram, K. Pernet-Gallay, C. Poillot, M. Ronjat, A. Andrieux, C. Arnoult, J. Daou, M. De Waard, *In vitro* and *in vivo* cell delivery of quantum dots by the cell penetrating peptide maurocalcine, Int. J. Biomed. Nanosci. Nanotechnol. 2 (2011) 12–32.
[13] G.J. Stasiuk, S. Tamang, D. Imbert, C. Poillot, M. Giardiello, C. Tisseyre, E.L. Barbider, P.H. Fries, M. de Waard, P. Reiss, M. Mazzanti, Cell-permeable Ln(III) chelate-functionalized InP quantum dots as multimodal imaging agents, ACS Nano 5 (2011) 8193–8201.
[14] C. Tisseyre, E. Bahembera, L. Dardevet, J.M. Sabatier, M. Ronjat, M. De Waard, Cell penetration properties of a highly efficient mini maurocalcine Peptide, Pharm. (Basel) 6 (2013) 320–339.
[15] S. Mitra, T.S. Banerjee, S.K. Hota, D. Bhattacharya, S. Das, P. Chattopadhyay, Synthesis and biological evaluation of dibenz[b, f][1,5]oxazocine derivatives for agonist activity at kappa-opioid receptor, Eur. J. Med. Chem. 46 (2011) 1713–1720.
[16] E. Frampas, C. Maurel, P. Thedrez, P. Remaud-Le Saec, A. Faivre-Chauvet, J. Barbet, The intraportal injection model for liver metastasis: advantages of associated bioluminescence to assess tumor growth and influences on tumor uptake of radiolabeled anti-carcinoembryonic antigen antibody, Nucl. Med. Commun. 32 (2011) 147–154.
[17] Z. Fajloun, R. Kharrat, L. Chen, C. Lecomte, E. Di Luccio, D. Bichet, M. El Ayeb, H. Rochat, P.D. Allen, I.N. Pessah, M. De Waard, J.M. Sabatier, Chemical synthesis and characterization of maurocalcine, a scorpion toxin that activates Ca(2+) release channel/ryanodine receptors, FEBS Lett. 469 (2000) 179–185.
[18] R.B. Merrifield, Solid-phase peptide synthesis, Adv. Enzymol. Relat. Areas Mol. Biol. 32 (1969) 221–296.
[19] E. Cuche, F. Bevilacqua, C. Depeursinge, Digital holography for quantitative phase-contrast imaging, Opt. Lett. 24 (1999) 291–293.
[20] B. Rappaz, P. Marquet, E. Cuche, Y. Emery, C. Depeursinge, P. Magistretti, Measurement of the integral refractive index and dynamic cell morphometry of living cells with digital holographic microscopy, Opt. Express 13 (2005) 9361–9373.
[21] N. Ram, N. Weiss, I. Texier-Nogues, S. Aroui, N. Andreotti, F. Pirollet, M. Ronjat, J.M. Sabatier, H. Darbon, V. Jacquemond, M. De Waard, Design of a disulfide-less, pharmacologically-inert and chemically-competent analog of maurocalcine for the efficient transport of impermeant compounds into cells, J. Biol. Chem. 283 (2008) 27048–27056.
[22] S. Aroui, N. Ram, F. Appaix, M. Ronjat, A. Kenani, F. Pirollet, M. De Waard, Maurocalcine as a non toxic drug carrier overcomes doxorubicin resistance in the cancer cell line MDA-MB 231, Pharm. Res. 26 (2009) 836–845.
[23] A. Jayagopal, Y.R. Su, J.L. Blakemore, M.F. Linton, S. Fazio, F.R. Haselton, Quantum dot mediated imaging of atherosclerosis, Nanotechnology 20 (2009) 165102.
[24] N. Ram, S. Aroui, E. Jaumain, H. Bichraoui, K. Mabrouk, M. Ronjat, H. Lortat-Jacob, M. De Waard, Direct peptide interaction with surface glycosaminoglycans contributes to the cell penetration of maurocalcine, J. Biol. Chem. 283 (2008) 24274–24284.
[25] S. Aroui, S. Brahim, M. De Waard, J. Breard, A. Kenani, Efficient induction of apoptosis by doxorubicin coupled to cell-penetrating peptides compared to unconjugated doxorubicin in the human breast cancer cell line MDA-MB 231, Cancer Lett. 285 (2009) 28–38.
[26] S. Aroui, S. Brahim, M. De Waard, A. Kenani, Cytotoxicity, intracellular distribution and uptake of doxorubicin and doxorubicin coupled to cell-penetrating peptides in different cell lines: a comparative study, Biochem. Biophys. Res. Commun. 391 (2010) 419–425.
[27] S. Aroui, S. Brahim, J. Hamelin, M. De Waard, J. Breard, A. Kenani, Conjugation of doxorubicin to cell penetrating peptides sensitizes human breast MDA-MB 231 cancer cells to endogenous TRAIL-induced apoptosis, Apoptosis 14 (2009) 1352–1365.

Please cite this article as: C. Tisseyre, et al., Quantitative evaluation of the cell penetrating properties of an iodinated Tyr-L-maurocalcine analog, Biochim. Biophys. Acta (2014), http://dx.doi.org/10.1016/j.bbamcr.2014.03.017

4.2 Conclusion

Dans la lignée cellulaire de gliobastome murin F98 *in vitro*, la MCa mono-iodée commence à s'accumuler au sein des cellules à partir de faibles quantités de peptide dans le milieu (100 nM) et ne connaît pas de saturation, en tout cas pour les concentrations extracellulaires testées (10 µM maximum). De plus, la maurocalcine commence à atteindre le cytoplasme après seulement 10 minutes d'incubation et ne sort plus du compartiment intracellulaire : en effet, 90% du signal radioactif est retrouvé après 24h. Enfin, elle tend à s'accumuler légèrement contre son gradient de concentration puisqu'on l'estime 2,45 fois plus présente dans le cytoplasme que dans le milieu extracellulaire.

Cette étude nous a permis de confirmer les propriétés de pénétration remarquables de la maurocalcine native ainsi que sa capacité à s'accumuler au sein des cellules. Nous avons également pu souligner son intérêt comme vecteur de divers cargos *in vivo* : substances thérapeutiques (chimiothérapie, radiothérapie par exemple), agents de contraste pour l'imagerie... La MCa est un CPP prometteur, et il convient de continuer à évaluer l'éventail de ses possibilités.

Chapitre 5

Article 4 : Biodistribution de la L-MCa chez la souris

5.1 Introduction

L'article précédent nous a permis de constater que la maurocalcine native s'accumule contre son gradient de concentration dans les cellules de glioblastome murin. Ce nouveau peptide de pénétration cellulaire est donc *a priori* un outil prometteur pour la délivrance de composés thérapeutiques, particulièrement dans le cas de tumeurs cérébrales. Cependant, il est nécessaire de caractériser la biodistribution de cette toxine avant d'évaluer son intérêt pour de futures applications cliniques.

Afin d'apporter une première réponse à cette problématique, nous avons injecté à des souris CD-1 la MCa native mono-iodée, puis nous avons suivi sa distribution au sein de leur organisme par une technique de nanoSPECT/CT scanning. Enfin, la radioactivité a été comptée au sein de leurs organes après dissection, ceci permettant de quantifier l'accumulation de MCa mono-iodée dans les différents tissus.

In vivo biodistribution of the cell penetrating and drug delivering maurocalcine peptide in CD-1 mice

Cathy Poillot[1,2], Mitra Ahmadi[1,3], Laurent Riou[1,3], Sandrine Martin[1,3], Céline Tisseyre[1,2], Julien Pecher[4], Michel Ronjat[1,2], Jean-Marc Sabatier[5], Daniel Fagret[1,6], Catherine Ghezzi[1,3] & Michel De Waard[1,2,4,*]

[1]Université Joseph Fourier, Grenoble, France.

[2]INSERM U836, Grenoble Institute of Neuroscience, Bâtiment Edmond J. Safra, 38042 Grenoble, France.

[3]INSERM U877, Radiopharmaceutiques Biocliniques, Grenoble, France.

[4]Smartox Biotechnologies, Bâtiment Biopolis, 5, avenue du Grand Sablon, 38700 La Tronche, France.

[5]INSERM UMR1097, Parc scientifique de Luminy, Université Aix-Marseille, 163 Avenue de Luminy, 13288 France.

[6]INSERM 1039, Pôle Imagerie, Clinique Universitaire de Médecine Nucléaire, CHU de Grenoble, 38043 Grenoble, France.

* Send correspondance to MDW: E-mail: michel.dewaard@ujf-grenoble.fr - Phone: +33 4 56 52 05 63 - Fax: +33 4 56 52 06 37

Running title: *In vivo biodistribution of maurocalcine*

Word count: 5080 words

Supported by an ANR grant to MDW

Abstract

Maurocalcine is the first natural cell penetrating peptide discovered in animal venom. It was found to be a powerful vector for the cell penetration of structurally diverse therapeutic compounds. It possesses several distinguishing features that should make it become a peptide of choice for clinical and biotechnological applications. Its binding site on its natural pharmacological target is located in the cytoplasm indicating that membrane translocation and cytoplasmic accumulation rather than endocytosis is the preferred route of cell entry. The peptide is amazingly nontoxic, even at high concentrations, and cell penetration occurs at low peptide concentration. Finally, the peptide is folded within a complex structure thanks to the presence of three disulfide bridges, thereby conferring an unusual stability to the peptide which is a highly desirable property when considering *in vivo* applications. The purpose of this study is to gain essential information about the *in vivo* biodistribution of maurocalcine before envisioning clinical applications for this vector. **A** Tyr-grafted analogue of maurocalcine was chemically synthesized and folded/oxidized. The purified peptide was stably iodinated before examining blood stability and *in vivo* biodistribution in CD-1 mice. The iodinated [^{125}I]-Tyr-maurocalcine is chemically very stable *in vitro*. The peptide is also very stable (over 3 hrs) in mice blood samples *in vitro* and *in vivo* following i.v. injection. We show that the disulfide bridges confer an essential competitive advantage for the *in vivo* stability of the peptide over a non-folded Tyr-grafted maurocalcine. The types of organs targeted by the peptide have been identified as well as the routes of elimination. This information will be important for adequate drug-targeted delivery purposes *in vivo*. In conclusion, maurocalcine appears as an incredibly stable peptide vector for drug delivery applications *in vivo*.

Introduction

Maurocalcine (MCa) is a 33 amino acid peptide that was identified in 2000 by the Institut Pasteur of Tunis out of the venom of the Tunisian scorpion *Scorpio maurus palmatus* (*1*). At that time the peptide was bearing exquisite amino acid sequence resemblance with imperatoxin A, a toxin isolated earlier from *Pandinus imperator*, another scorpion species, and that was found active on the ryanodine receptor type 1 (RyR1) from skeletal muscles (*2*). This observation had prompted us to investigate the interaction of MCa with RyR1 and, sure enough, the peptide was also found active on the channel according to several technical approaches. As a matter of fact, MCa (i) promotes Ca^{2+} efflux from the sarcoplasmic reticulum (*3*), (ii) increases the channel open probability and promotes a long-lasting subconductance level (*4-6*), and (iii) stimulates [^{3}H]-ryanodine binding by virtue of its stimulatory effect on channel activity (*3*). Owing to the fact that RyR1 is a calcium channel expressed within the membrane of the endoplasmic reticulum and that the binding site of MCa on RyR1 is located within a domain predicted to be present in the cytoplasm (*7*), MCa was suspected to cross the plasma membrane and to easily reach the cytoplasm in order to implement its effect on RyR1. In agreement with this hypothesis, external application of MCa onto skeletal myotubes rapidly triggers cytoplasmic Ca^{2+} elevation which also occurs in the absence of external Ca^{2+}. These findings demonstrated that the rise in Ca^{2+} concentration finds its origin from the mobilization of internal Ca^{2+} sources (*8*). Finally, the greatest evidence for cell penetration of MCa was obtained by coupling a biotinylated derivative of MCa to fluorescent streptavidin and showing the accumulation of fluorescence in a variety of cell types. This observation was the first demonstration that MCa could also act as a peptide vector for the cell penetration of a protein cargo (*8*). Further attempts to understand how MCa may proceed to enter into cells and reach its pharmacological target lead to the identification of glycosaminoglycans and negatively charged phospholipids as natural membrane receptors of MCa (*9*). Glycosaminoglycans interact with MCa with affinities in the range of a few micromolar whereas negatively charged lipids show interactions in the high nanomolar range. At the structural level, MCa folds according to an inhibitor cysteine knot motif and contains three well-defined β-strands (*1*). The secondary structures are constrained by three disulfide bridges with a pattern of connectivity forming the

unusual knot. The uniqueness of MCa is that it is heavily charged owing to the presence of many basic amino acid residues (mainly lysine amino acids). This property, along with the fact that MCa has the ability to induce cell penetration of a variety of cargoes (*10-14*), led to the conclusion that MCa was the first identified toxin member of the large structurally-unrelated family of cell penetrating peptides (CPP). CPP are becoming increasingly popular to those that wish to utilize a vector for the cell entry of a cargo that would otherwise not enter cells. As such, MCa demonstrated excellent vector properties for quantum dots, peptides, or drugs, and promising applications are envisioned in oncology (*10, 15-18*). MCa is now recognized as a competitive CPP because of i) its low concentration efficacy, ii) its ability to reach the cytoplasm, where most cargos should be addressed, and iii) its lack of cell toxicity. Many of our efforts have focused on getting MCa analogues deprived of undesirable pharmacological effects but with preserved cell penetration properties. Luckily, this task of designing cell penetrating MCa analogues that are unable to modulated RyR1 activity was considerably eased by the stringent structural requirements for MCa binding onto RyR1. In contrast, the cell penetration properties of MCa are not under a similar structural strictness. Hence, all of the chemical strategies tested so far to produce cell penetrating competent analogues of MCa lacking RyR1 binding were successful: (i) point mutation of MCa (*19*), (ii) impeding with disulfide bridge formation and hence MCa secondary structures (*14*), and (iii) synthesis of a mirror image of MCa, the diastereoisomer D-MCa (*13*).

While the design of good CPP derived from MCa has come to maturity, it now seems obvious that these vectors have great potential for the intracellular delivery of important therapeutic or diagnostic compounds *in vivo*. By essence, venomous toxins are delivered *in vivo* and are tailored to survive enough time within the blood stream of animal preys until the pharmacological potential of these molecules has been fully exploited. The presence of disulfide bridges appears to represent a strong asset for the *in vivo* stability of these molecules. To investigate the *in vivo* properties of MCa, we first synthesized a Tyr-tagged MCa for *in vitro* radio-iodination. We next studied the metabolic stability of the [^{125}I]-labeled peptide in blood both *in vitro* and *in vivo*, and followed its body distribution. We finally investigated the routes of elimination of the peptide. This study helps delineating the type of *in vivo* application in which MCa can

be used for intracellular delivery and the organ that can be targeted. Our data demonstrate the wonderful stability of MCa *in vivo* and further highlight the advantages to use MCa for cell delivery purposes rather than other popular CPP.

Methods

Reagents

N-α-Fmoc-L-aminoacid, Wang-Tentagel resin and reagents used for peptide syntheses were obtained from Iris Biotech. Solvents were analytical grade products from Acros Organics.

Solid-phase peptide syntheses

Chemical synthesis of Tyr-MCa was performed as previously described for other MCa analogues (*13*). Briefly, Tyr-MCa was chemically synthesized by the SPPS method (*20*) using an automated peptide synthesizer (CEM© Liberty). Peptide chain was assembled stepwise on 0.24 mEq of Fmoc-L-Arg(Pbf)-Wang-Tentagel resin using 0.24 mmol of N-α-fluorenylmethyloxycarbonyl (Fmoc) L-amino-acid derivatives. The side-chain protecting groups were: Trityl for Cys and Asn, *tert*-butyl for Ser and Tyr, Thr, Glu and Asp, Pbf for Arg, and *tert*-butylcarbonyl for Lys. Reagents were at the following concentrations: 0.2 M Fmoc-amino-acids (Fmoc-AA-OH in dimethylformamide (DMF)), 0.5 M activator (2-(1H-benzotriazole-1-yl)-1,1,3,3-tetramethyluronium hexafluorophosphate in DMF), 2 M activator base (diisopropylethylamine in N-methyl-pyrrolidone (NMP)) and deprotecting agent (5% piperazine / 0.1 M 1-hydroxybenzotriazole in DMF), as advised by PepDriver (CEM©). After peptide chain assembly, the resin was treated 4 hrs at room temperature with a mixture of trifluoroacetic acid/water/triisopropylsilane (TIS)/1,4-dithiothreitol (DTT) (92.5/2.5/2.5/2.5). The peptide mixture was then filtered (to eliminate the resin) and the filtrate was precipitated by adding cold *t*-butylmethyl ether. The crude peptide was pelleted by centrifugation (10.000 × g, 15 min) and the supernatant was discarded. The reduced Tyr-MCa was submitted to oxidation for disulfide bridge formation in 0.1 M Tris/HCl buffer at pH 8.2 during 3 days at room temperature. Oxidized/folded Tyr-MCa was then purified by HPLC using a Vydac C18 column (218TP1010, 250×10 mm). Elution of the peptide was performed with a 10-60% acetonitrile linear

gradient containing 0.1% trifluoroacetic acid over 40 min. The purity of the purified fraction was analyzed by analytical RP-HPLC (Vydac C18 column 218TP104, 250 × 4.6 mm). Tyr-MCa was characterized by MALDI-TOF mass spectrometry.

MCa radiolabeling and in vitro stability

[^{125}I]-Tyr-MCa was prepared using an oxidation reaction. Briefly, 148 MBq (4.0 mCi; 0.04 mL) of ^{125}I were added to 40 µg of Tyr-MCa in 200 µl of phosphate buffer (50 mM, pH 7.4). The reaction was allowed to proceed for 20 min at room temperature (RT) after addition of 15 µl (1 mg/ml) lactoperoxidase and 40 µl H_2O_2 (1:50,000). Radioiodinated Tyr-MCa was analysed by HPLC using a Vydac 218 TP C18 column, (10 µm, 250 × 4.6 mm). The solvent system consisted of H_2O–TFA 0.1% (solvent A) and acetonitrile 90%–TFA 0.1% (solvent B). Tracer elution was achieved by applying a gradient of 0% B during 8.3 min, 0-1% B during 1 min 40 sec, 1-10% B during 1 min 40 sec, 10-60% B during 33 min 12 sec, 60-100% B during 1 min 40 sec, 100% B during 8 min 18 sec and 100-0% B during 8 min 18 sec (total run time, 65 min) at a flow rate of 1 ml/min. The stability of the radio-labeling was determined by incubation of the complex at room temperature for 24 hrs, following which an HPLC analysis was performed as described above.

The *in vitro* stability of [^{125}I]-Tyr-MCa was evaluated in mouse blood. Twenty MBq of radio-labeled Tyr-MCa was incubated for 15, 30, 60, and 90 min in 0.5 ml of mouse blood at 37°C. At each time point, a 100 µl sample was centrifuged (2,000 g, 5 min) (pellet, fraction #1) and the plasma was filtered through a 10 K Omega™ membrane (Nanosep®; Pall Life Science, NY) at 7,000 g for 20 min (filter, fraction #2; filtered solution, fraction #3) followed by HPLC analyses using the above mentioned conditions. The blood samples were also used for the determination of the relative distribution of radioactivity in fraction #1, 2 and 3, corresponding to blood cells, plasma proteins, and protein-free plasma, respectively.

In vivo experimental protocol

Eight standard CD-1 mice were obtained from Charles River Laboratories (France) and housed for 1 week prior to inclusion in the experimental protocol. Conscious animals were restrained for tracer injection in a tail vein.

In Vivo [^{125}I]-Tyr-MCa Stability – Two animals were dedicated to the evaluation of [^{125}I]-Tyr-MCa *in vivo* stability. The animals were injected with 55 MBq of tracer. At 15 and 30 min (n = 1 each) following injection, the animals were anesthetized using pentobarbital (60 mg/kg, intraperitoneal) and a thoracotomy was performed in order to withdraw a blood sample directly from the LV cavity through a transmural puncture. The blood sample was immediately centrifuged, the plasma was filtered, and the filtered solutions were analyzed by HPLC as described above. In addition, the distribution of radioactivity in fractions obtained as described above (see *METHODS – MCa radiolabeling and in vitro stability* paragraph) was also performed.

Biodistribution – [^{125}I]-Tyr-MCa (1.5 ± 0.0 MBq/g body weight; ~35 MBq total) was injected in the tail vein of 6 conscious and restrained animals (body weight, 23.7 ± 0.3 g). Three out of 6 animals were anesthetized immediately following tracer injection using isoflurane and imaged using a small animal nuclear imaging gamma-camera (nanoSPECT/CT, Bioscan, France). Tomographic *in vivo* images (24 projections, 20 sec / projection) were acquired at 15, 30, and 60 min post-tracer injection using a 15 – 75 keV energy window. A whole body CT acquisition was performed between the 30 and 60 min nuclear image acquisition. Gaseous anesthesia was maintained using isoflurane throughout the experimental imaging protocol.

Post mortem analysis

Sixty min following tracer injection, all 6 anesthetized animals were euthanized by cervical dislocation and samples from the heart, lung, liver, spleen, kidney, stomach, intestine, duodenum, pancreas, salivary glands, thyroid, skin, skeletal muscle, pancreas, thymus, brain, fat, brown fat, spinal cord, blood, and urine were obtained. Organs were quickly rinsed following excision and organ and blood activities of the tracers were assessed using a gamma-well counter (Cobra II, Packard Instruments, Courtaboeuf, France) with a 15–75 keV energy window for ^{125}I. All tissue counts were corrected for background.

Data analysis

The results were expressed as mean ± SEM.

Biodistribution - Organ and blood activities by gamma-well counting were expressed as percent of the

injected dose per gram of wet weight (% ID/g).

Image Analyses - *In vivo* tomographic images were analyzed using dedicated software (InVivoScope). Regions of interest (ROIs) were drawn on the thyroid, liver, kidney, skeletal muscle, stomach, salivary gland, brain, heart, myocardial left ventricle (for blood activity determination) and bladder. Tracer activities were expressed as % ID/cm^3.

Statistical Analysis - Statistical analysis was performed using Systat software. Mean values were compared using unpaired student *t*-test and Kruskall-Wallis non parametric test. A P value < 0.05 was considered significant.

Results

Chemical synthesis, radiolabeling and in vitro stability of maurocalcine analogues **-** MCa amino acid sequence lacks an internal Tyr residue for peptide iodination. To facilitate the labeling of MCa, we therefore chemically synthesized the 34 amino acid Tyr-MCa peptide which contains an additional Tyr residue at the N-terminus of the sequence (Figure 1A). The peptide folded well in spite of the extra Tyr residue. This was expected because MCa has sequence identity with another calcin toxin, hadrucalcin (*20*), which possesses an extended N-terminus compared to MCa. Tyr-MCa keeps the classical disulfide bridging patter of MCa, Cys^3-Cys^{17}, Cys^{10}-Cys^{21} and Cys^{16}-Cys^{32}, demonstrating full folding equivalence (not shown). In addition, the new analogue remained active for RyR1 channel activation (not shown). Next, the peptide was iodinated according to a procedure described earlier (Ahmadi *et al.*, submitted manuscript). RP-HPLC analysis of [^{125}I]-Tyr-MCa immediately following radio-labeling is shown in Figure 1B. The results indicate that the conditions of iodination used yield a single major radioactive specie that elutes at 25 min with radiochemical purity (RCP) > 95%. Mass spectrometry analyses using similar iodination conditions but with ^{127}I reveal that this single peak corresponds to the expected mass for a single iodination on the extra Tyr residue (data not shown). Also, iodination does not occur on MCa that lacks the extra tyrosine residue (not shown). [^{125}I]-Tyr-MCa remained stable (RCP > 95%) at room temperature for at least 24 hrs following radio-labeling as demonstrated by RP-HPLC analysis (Figure

1B). For the subsequent experiments, [^{125}I]-Tyr-MCa was always used within 12 hrs following radio-labeling.

Blood stability of maurocalcine analogues

The *in vitro* distribution pattern of radioactivity after 15, 30, 60 and 90 min of [^{125}I]-Tyr-MCa incubation with whole mouse blood is indicated in Table 1 below. The results indicate that tracer distribution was quite stable over time. The radioactivity was mostly associated with plasma proteins (~60% of total). Blood cells and the protein-free plasma fraction presented similar amounts of radioactivity (~15-20% each). HPLC analyses of radioactive species in the protein-free plasma fraction of mouse blood samples after 15, 30, 60 and 90 min of incubation with the tracer followed by centrifugation and filtration is shown in Table 2. Three peaks were systematically detected. They correspond to free ^{125}I (retention time of 3 min), an iodinated metabolite (retention time of 19 min) and [^{125}I]-Tyr-MCa (retention time of 25 min). The iodinated metabolite represented a minor 2% of the total radioactivity at 15 min and increased to 7% at 90 min, whereas [^{125}I]-Tyr-MCa decreased from 75% at 15 min to 67% at 90 min. The amount of free ^{125}I was stable over time and represented ~20-25% of the protein-free plasma fraction of the tracer, i.e. ~4% of total blood activity assuming that free ^{125}I is present only in the protein-free plasma fraction.

***In Vivo* tracer stability**

The *in vivo* blood distribution pattern of radioactivity at 15 and 30 min following [^{125}I]-Tyr-MCa intravenous injection is indicated in Table 3 below. As observed *in vitro*, the radioactivity was mostly associated with plasma protein (~40-45%), although to a slightly lower level. The remaining activity was equally distributed between blood cells and the protein-free plasma fraction. Analysis of radioactive species in the protein-free plasma fraction of mouse blood at 15 and 30 min post-[^{125}I]-Tyr-MCa injection in mice indicated the presence of 2 peaks with retention times of 3 min and 24 min, which corresponded to free ^{125}I and [^{125}I]-Tyr-MCa, respectively (Figure 2). ^{125}I represented ~60% of the total protein-free plasma radioactivity, a value which did not increase over time. Considering that the protein-free plasma fraction of blood contained ~26% of the total blood activity (Table 3), one can therefore estimate that free ^{125}I represented ~16% of the total circulating activity following *in vivo* injection of the tracer. Rather than

indicating an increased deiodination of the tracer following *in vivo* injection, the apparently higher proportion of free ^{125}I following *in vivo* injection of [^{125}I]-Tyr-MCa (~16% of total blood activity) as compared with results from *in vitro* incubation of the tracer with mouse blood (~3% of total blood activity) was likely due to the fact that unbound [^{125}I]-Tyr-MCa was available for organ distribution following *in vivo* injection in mice whereas it was not the case following *in vitro* blood incubation of the tracer. These observations indicate that [^{125}I]-Tyr-MCa is probably accumulating in cells of various organs, which is expected for a cell penetrating peptide.

Biodistribution

The biodistribution of [^{125}I]-Tyr-MCa in CD-1 mice at 60 min following tracer injection is shown in Figure 3. The tracer was mainly eliminated through the kidneys as shown by the high renal and urinary activities. High activities were also observed in the stomach, salivary gland, and thyroid, which corresponded to ^{125}I uptake by these organs. [^{125}I]-Tyr-MCa did not cross the blood brain barrier as shown by the extremely low brain and cerebellum activities. Figure 3 also compares the *in vivo* biodistribution of [^{125}I]-Tyr-MCa with a pretreatment with the NaI symporter inhibitor, potassium perchlorate, to the condition without this pretreatment. This inhibitor prevents ^{125}I uptake into tissues. The biodistribution patterns were comparable between the two experiments. However, as expected, the presence of potassium perchlorate significantly inhibits ^{125}I uptake by the salivary glands and thyroid, which likely accounts for a significantly increased amount of blood circulating radioactivity.

***In vivo* imaging**

Presented in Figure 4 are representative images acquired in the same animal at 15 min (panel A), 30 min (panel B), and 60 min (panel C) following the intravenous injection of [^{125}I]-Tyr-MCa. The results from *in vivo* image quantification are presented in Figure 5. Noninvasive 60-min image quantification accurately reflected post-mortem organ biodistribution. As shown on images and confirmed following image quantification, there was a progressive accumulation of ^{125}I in the thyroid, stomach, and salivary glands from 0 to 60 min post-injection. Renal elimination of the tracer began immediately following injection and remained stable over time. Hepatic elimination of [^{125}I]-Tyr-MCa was lower than that occurring through

the kidneys and was also stable over time.

Conclusion and future directions

MCa lacks a tyrosine residue within its sequence which prevents its convenient labeling by ^{125}I. An extra-tyrosine has been added to the sequence at the N-terminus of MCa. It does not hamper the proper folding and oxidation of the peptide. Also, it did not prevent the peptide from binding onto its target receptor, RyR1 (data not shown); which was also observed for biotinylated MCa on which an extra lysine residue had been added at the N-terminus (*19*). N-terminal modifications also did not appear to affect cell penetration properties of MCa (*8*) suggesting that labeling at the N-terminus of MCa is a safe strategy to preserve the native properties of the peptide. In many respects, the ^{125}I labeling of a tyrosine residue placed at the N-terminus of peptide sequence appears preferable for preserving intact peptide properties than a labeling that would occur on an internal tyrosine residue, if this one had been present. It is therefore likely that the properties of *in vivo* biodistribution of [^{125}I]-Tyr-MCa, we report in this manuscript, properly describe what the biodistribution of MCa itself could be. The analyses we performed occurred at blood peptide concentrations in the range of 1 µM and are therefore also in good agreement with the effective concentrations required for cell penetration and pharmacological action. The labeling procedure we developed for this peptide produced a stable [125I]-Tyr-MCa molecule, at least within the 24 hrs post-labeling period.

This study led to several interesting conclusions. First, MCa is remarkably stable in blood according to the study we conducted. Apart from deiodination that leads to free ^{125}I, the peptide showed little or no degradation over a period of 90 min. This is in agreement with the expected stability of disulfide-bridged toxins *in vivo*. We hypothesize that, here also, the three disulfide bridges that connect the six internal cysteine residues of MCa confer a relatively high resistance to protease action to this peptide. This finding further reinforces the competitiveness of MCa as a cell delivery vector. Second, this study brings in important conclusions on the fate of the peptide once injected in the blood stream. Both *in vitro* and *in vivo* data provide coherent conclusions. A fraction of the radioactivity (17 to 30% depending on the

time scale) is associated to blood cells, which is a first indication that [^{125}I]-Tyr-MCa has the ability to enter these cell types. What kind of blood cell is preferentially targeted by [^{125}I]-Tyr-MCa will be an interesting question to investigate if applications need to be developed in which targeted blood cell delivery is required. Obviously, most of the radioactivity associates to plasma proteins, and a minor fraction (equivalent to the blood cell fraction) is associated to the protein-free plasma. Interestingly, there is a consistent difference in the proportion of radioactivity associated to plasma proteins and protein-free plasma between the *in vitro* and *in vivo* conditions. *In vivo*, there is approximately a reduction of a third in the amount of radioactivity associated to plasma proteins, as well as a 1.5 to 2-fold increase in radioactivity associated to the protein-free plasma. Both effects can be interpreted by the organ delivery of [^{125}I]-Tyr-MCa (that does not occur *in vitro*) and the proportional increase in free ^{125}I in the protein-free plasma (that does not reflect deiodination). Third, the data clearly demonstrate that [^{125}I]-Tyr-MCa does not reach neural tissues and that therefore the peptide is unlikely to cross the blood brain barrier. This observation will limit the number of application where vector delivery to the brain is required, except maybe in pathological conditions (brain cancers for instance) where disruption of the blood brain barrier is expected to occur. Important labeling is detected in the stomach, the spleen, the skin, lungs, intestine, duodenum, pancreas and liver. Non negligible labeling is observed in heart, skeletal muscle, thymus and brown fat. In some organs, such as salivary glands and thyroid, the accumulation of radioactivity was linked to a preferential accumulation of free ^{125}I. This could readily be suppressed by a treatment with potassium perchlorate.

Fourth, the strong kidney and urine accumulation of radioactivity implies that the kidneys are the main route of elimination of the peptide. Kidney labeling does not change much with time between 15 and 60 min suggesting that we face a rather rapid elimination immediately after IV injection of the peptide. The only organs that showed increased levels of radioactivity with time were those that accumulated free ^{125}I suggesting that [^{125}I]-Tyr-MCa distribution *in vivo* had reached equilibrium rather fast after IV injection (within 15 min).

In summary, this study indicates that MCa is a stable peptide vector *in vivo*, that it targets

peripheral organs mainly with interesting quantitative differences, that blood cells also appear to accumulate the peptide and that the main route of elimination occurs through the kidneys. This study will therefore delimitate the field of applications in which MCa can be used to deliver cargoes into cells *in vivo*.

Acknowledgements

We acknowledge financial support from ANR PNANO on the program Nanofret[2].

References

1. Mosbah A, Kharrat R, Fajloun Z, Renisio JG, Blanc E, Sabatier JM, et al. A new fold in the scorpion toxin family, associated with an activity on a ryanodine-sensitive calcium channel. Proteins. 2000; 40(3):436-42.
2. Zamudio FZ, Gurrola GB, Arevalo C, Sreekumar R, Walker JW, Valdivia HH, et al. Primary structure and synthesis of Imperatoxin A (IpTx(a)), a peptide activator of Ca2+ release channels/ryanodine receptors. FEBS Lett. 1997; 405(3):385-9.
3. Esteve E, Smida-Rezgui S, Sarkozi S, Szegedi C, Regaya I, Chen L, et al. Critical amino acid residues determine the binding affinity and the Ca2+ release efficacy of maurocalcine in skeletal muscle cells. J Biol Chem. 2003; 278(39):37822-31.
4. Fajloun Z, Kharrat R, Chen L, Lecomte C, Di Luccio E, Bichet D, et al. Chemical synthesis and characterization of maurocalcine, a scorpion toxin that activates Ca(2+) release channel/ryanodine receptors. FEBS Lett. 2000; 469(2-3):179-85.
5. Chen L, Esteve E, Sabatier JM, Ronjat M, De Waard M, Allen PD, et al. Maurocalcine and peptide A stabilize distinct subconductance states of ryanodine receptor type 1, revealing a proportional gating mechanism. J Biol Chem. 2003; 278(18):16095-106.
6. Lukacs B, Sztretye M, Almassy J, Sarkozi S, Dienes B, Mabrouk K, et al. Charged surface area of maurocalcine determines its interaction with the skeletal ryanodine receptor. Biophys J. 2008; 95(7):3497-509.
7. Altafaj X, Cheng W, Esteve E, Urbani J, Grunwald D, Sabatier JM, et al. Maurocalcine and domain A of the II-III loop of the dihydropyridine receptor Cav 1.1 subunit share common binding sites on the skeletal ryanodine receptor. J Biol Chem. 2005; 280(6):4013-6.
8. Esteve E, Mabrouk K, Dupuis A, Smida-Rezgui S, Altafaj X, Grunwald D, et al. Transduction of the scorpion toxin maurocalcine into cells. Evidence that the toxin crosses the plasma membrane. J Biol Chem. 2005; 280(13):12833-9.
9. Ram N, Aroui S, Jaumain E, Bichraoui H, Mabrouk K, Ronjat M, et al. Direct Peptide Interaction with Surface Glycosaminoglycans Contributes to the Cell Penetration of Maurocalcine. J Biol Chem. 2008; 283(35):24274-84.
10. Aroui S, Ram N, Appaix F, Ronjat M, Kenani A, Pirollet F, et al. Maurocalcine as a Non Toxic Drug Carrier Overcomes Doxorubicin Resistance in the Cancer Cell Line MDA-MB 231. Pharm Res. 2009; 26(4):836-45.

11. Boisseau S, Mabrouk K, Ram N, Garmy N, Collin V, Tadmouri A, et al. Cell penetration properties of maurocalcine, a natural venom peptide active on the intracellular ryanodine receptor. Biochim Biophys Acta. 2006; 1758(3):308-19.
12. Jayagopal A, Su YR, Blakemore JL, Linton MF, Fazio S, Haselton FR. Quantum dot mediated imaging of atherosclerosis. Nanotechnology. 2009; 20(16):165102.
13. Poillot C, Dridi K, Bichraoui H, Pecher J, Alphonse S, Douzi B, et al. D-Maurocalcine, a pharmacologically inert efficient cell-penetrating peptide analogue. J Biol Chem. 2010; 285(44):34168-80.
14. Ram N, Weiss N, Texier-Nogues I, Aroui S, Andreotti N, Pirollet F, et al. Design of a disulfide-less, pharmacologically-inert and chemically-competent analog of maurocalcine for the efficient transport of impermeant compounds into cells. J Biol Chem. 2008; 283:27048-56.
15. Aroui S, Brahim S, De Waard M, Breard J, Kenani A. Efficient induction of apoptosis by doxorubicin coupled to cell-penetrating peptides compared to unconjugated doxorubicin in the human breast cancer cell line MDA-MB 231. Cancer Lett. 2009; 285(1):28-38.
16. Aroui S, Brahim S, Hamelin J, De Waard M, Breard J, Kenani A. Conjugation of doxorubicin to cell penetrating peptides sensitizes human breast MDA-MB 231 cancer cells to endogenous TRAIL-induced apoptosis. Apoptosis. 2009; 14(11):1352-65.
17. Aroui S, Brahim S, De Waard M, Kenani A. Cytotoxicity, intracellular distribution and uptake of doxorubicin and doxorubicin coupled to cell-penetrating peptides in different cell lines: a comparative study. Biochem Biophys Res Commun. 2010; 391(1):419-25.
18. Aroui S, Mili D, Brahim S, De Waard M, Kenani A. Doxorubicin coupled to penetratin promotes apoptosis in CHO cells by a mechanism involving c-Jun NH2-terminal kinase. Biochem Biophys Res Commun. 2010; 396(4):908-14.
19. Mabrouk K, Ram N, Boisseau S, Strappazzon F, Rehaim A, Sadoul R, et al. Critical amino acid residues of maurocalcine involved in pharmacology, lipid interaction and cell penetration. Biochim Biophys Acta. 2007; 1768(10):2528-40.
20. Schwartz EF, Capes EM, Diego-Garcia E, Zamudio FZ, Fuentes O, Possani LD, et al. Characterization of hadrucalcin, a peptide from Hadrurus gertschi scorpion venom with pharmacological activity on ryanodine receptors. Br J Pharmacol. 2009; 157(3):392-403.

Figure legends

Table 1. *In vitro* blood distribution pattern of radioactivity following [^{125}I]-Tyr-MCa incubation with whole mouse blood.

Table 2. *In vitro* stability analysis of [^{125}I]-Tyr-MCa after 15 to 90 min incubation with mouse blood. HPLC analysis was performed in the protein-free plasma fraction of mouse blood.

Table 3. *In vivo* blood distribution pattern of radioactivity following [^{125}I]-Tyr-MCa intravenous injection.

Figure 1. Radio-labeling of maurocalcine analogues and *in vitro* stability of the iodinated compounds. (A) HPLC chromatogram of [^{125}I]-Tyr-MCa immediately following radio-labelling. (B) HPLC chromatogram of [^{125}I]-Tyr-MCa at 24 hrs following radio-labelling.

Figure 2. *In vivo* stability of the iodinated MCa analogues. (A) HPLC chromatogram of [^{125}I]-Tyr-MCa at 15 min post-injection to mice. (B) HPLC chromatogram of [^{125}I]-Tyr-MCa at 30 min post-injection to mice. Analyses were conducted for the protein-free plasma fraction.

Figure 3. Biodistribution of [^{125}I]-Tyr-MCa in CD-1 mice 60 min post-injection and effect of the NaI symporter inhibitor potassium perchlorate. Biodistributions of [^{125}I]-Tyr-MCa were analyzed 60 min post-injection in CD-1 mice. Mean injected dose for control and potassium perchlorate pretreatment conditions were ~35 and ~17 MBq, respectively. SG, salivary gland; Cereb., cerebellum; Spinal C., Spinal Cord. *, $P \leq 0.05$.

Figure 4. 15-min *in vivo* tomographic whole-body imaging of [^{125}I]-Tyr-MCa biodistribution in CD-1 mice. (A) 15 min i.v. post-injection. (B) 30 min i.v. post-injection. (C) 60 min i.v. post-injection. From left to right, 3D rendering, sagittal, coronal, and transverse views of tracer activity.

Figure 5. Quantification of *in vivo* tomographic images of [^{125}I]-Tyr-MCa whole-body distribution at 15, 30, and 60 min post-injection. *, $P \leq 0.05$ *versus* 15 min condition.

Keywords: Cell penetrating peptide; Maurocalcine; Scorpion toxin; nanoSPECT/CT; Drug delivery; *In vivo* biodistribution.

A

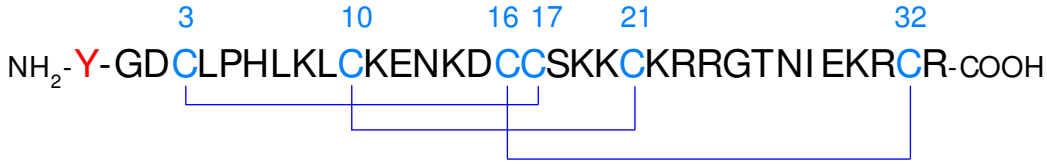
3
10
16 17
21
32
NH2-Y-GDCLPHLKLCKENKDCCSKKCKRRGTNIEKRCR-COOH

B

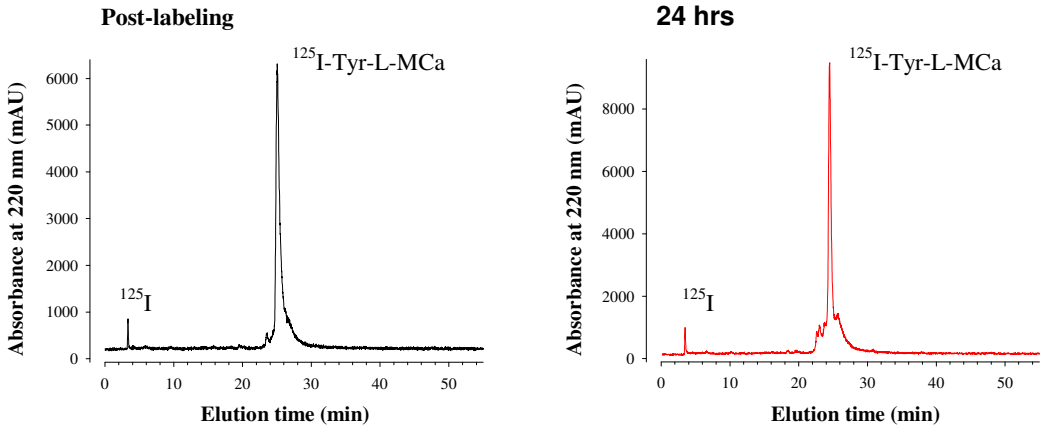
Post-labeling
125I-Tyr-L-MCa
125I
Absorbance at 220 nm (mAU)
Elution time (min)
24 hrs
125I-Tyr-L-MCa
125I
Absorbance at 220 nm (mAU)
Elution time (min)

In vivo plasma

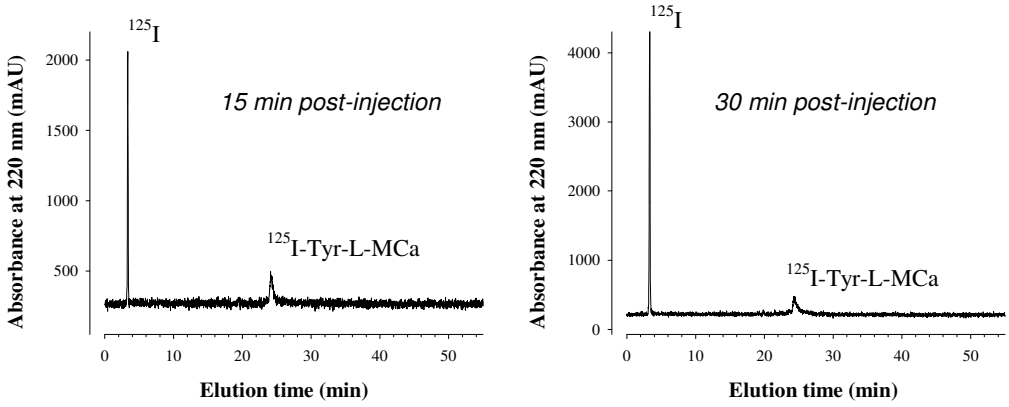

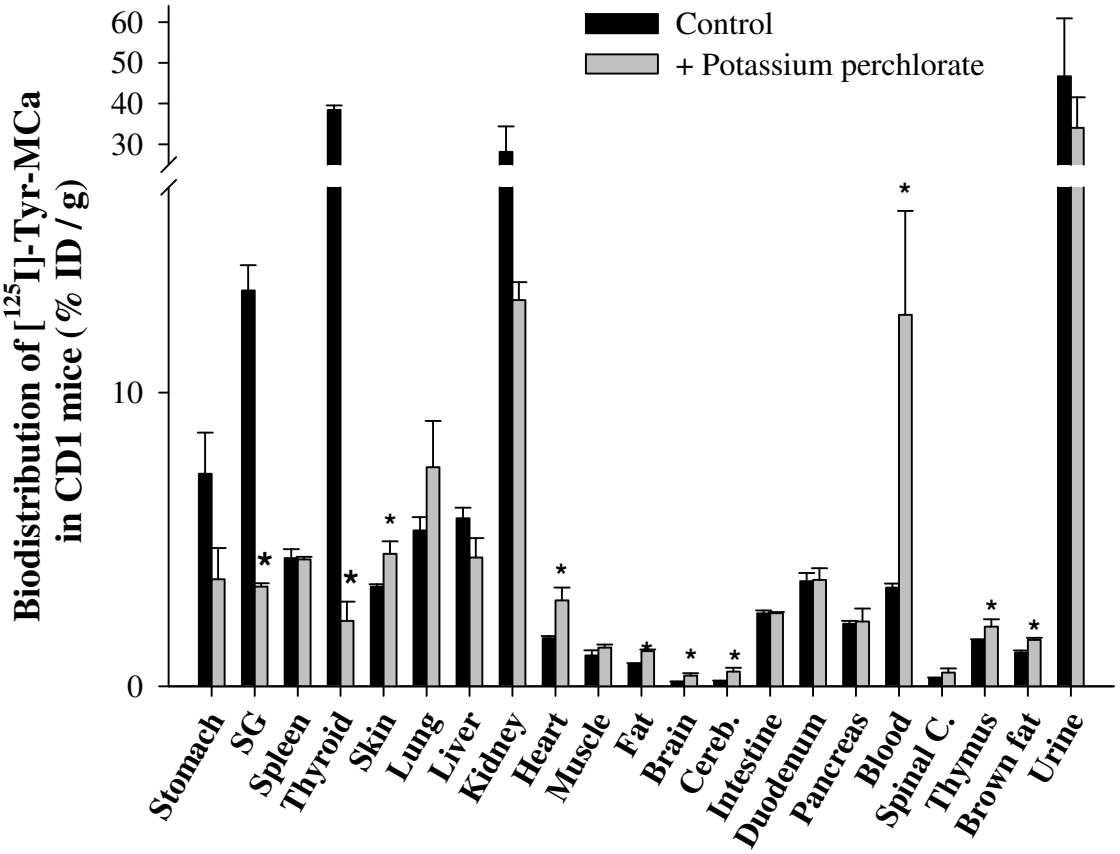
Biodistribution of [125I]-Tyr-MCa
in CD1 mice (% ID / g)
Control
+ Potassium perchlorate
60
50
40
30
10
0
Stomach
SG
Spleen
Thyroid
Skin
Lung
Liver
Kidney
Heart
Muscle
Fat
Brain
Cereb.
Intestine
Duodenum
Pancreas
Blood
Spinal C.
Thymus
Brown fat
Urine

A

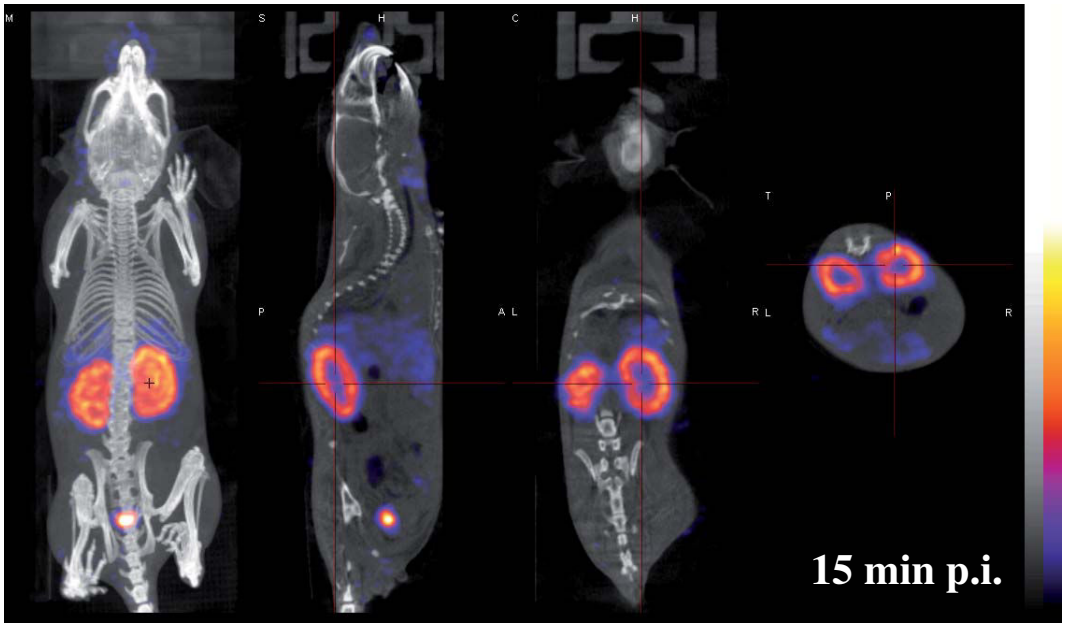

B

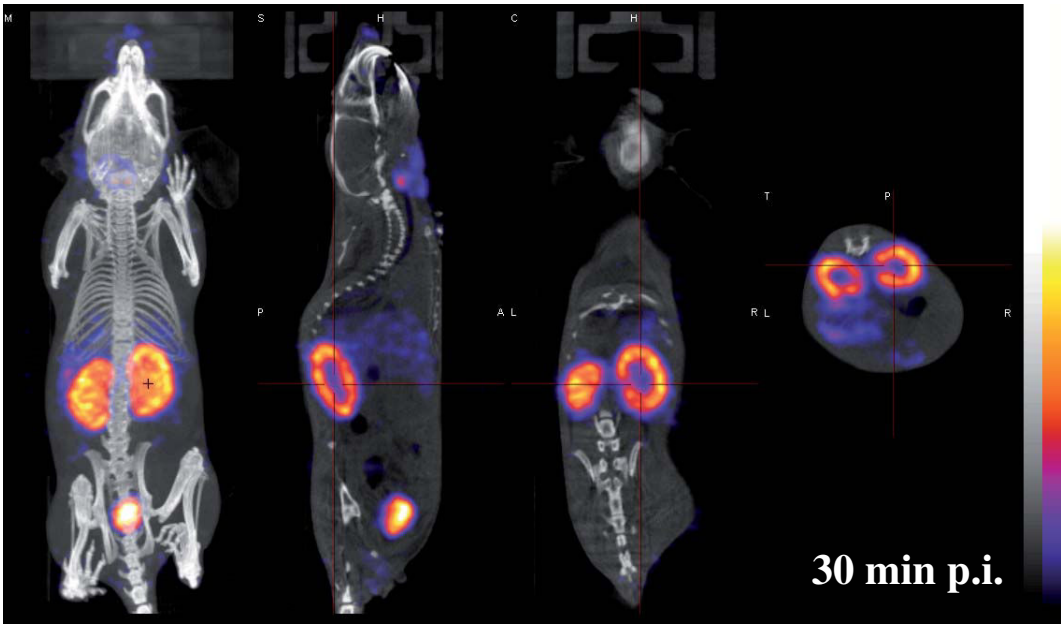

C

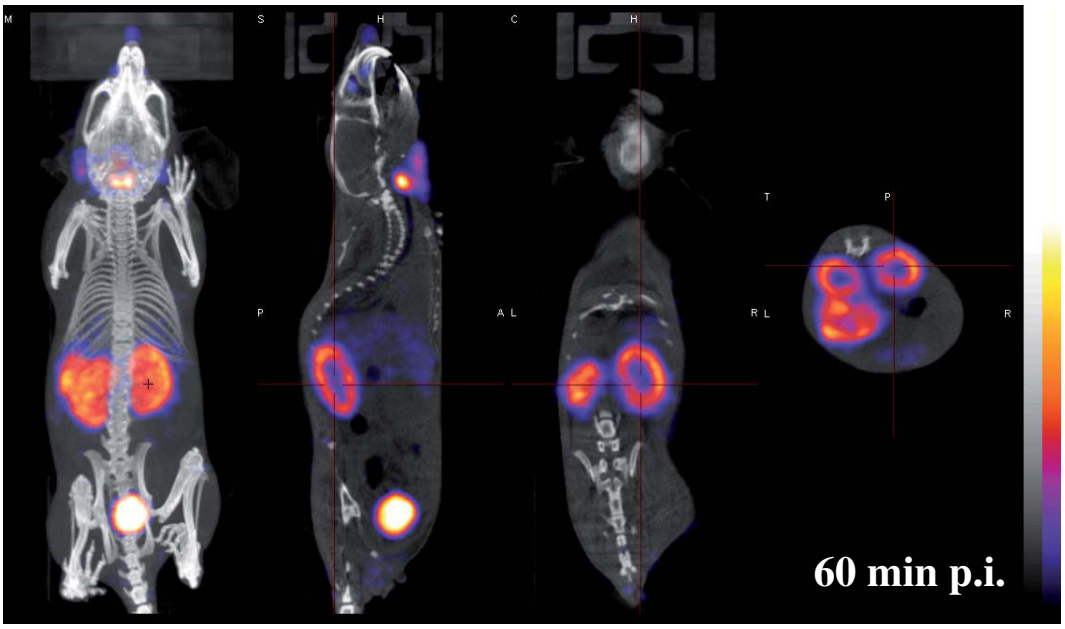

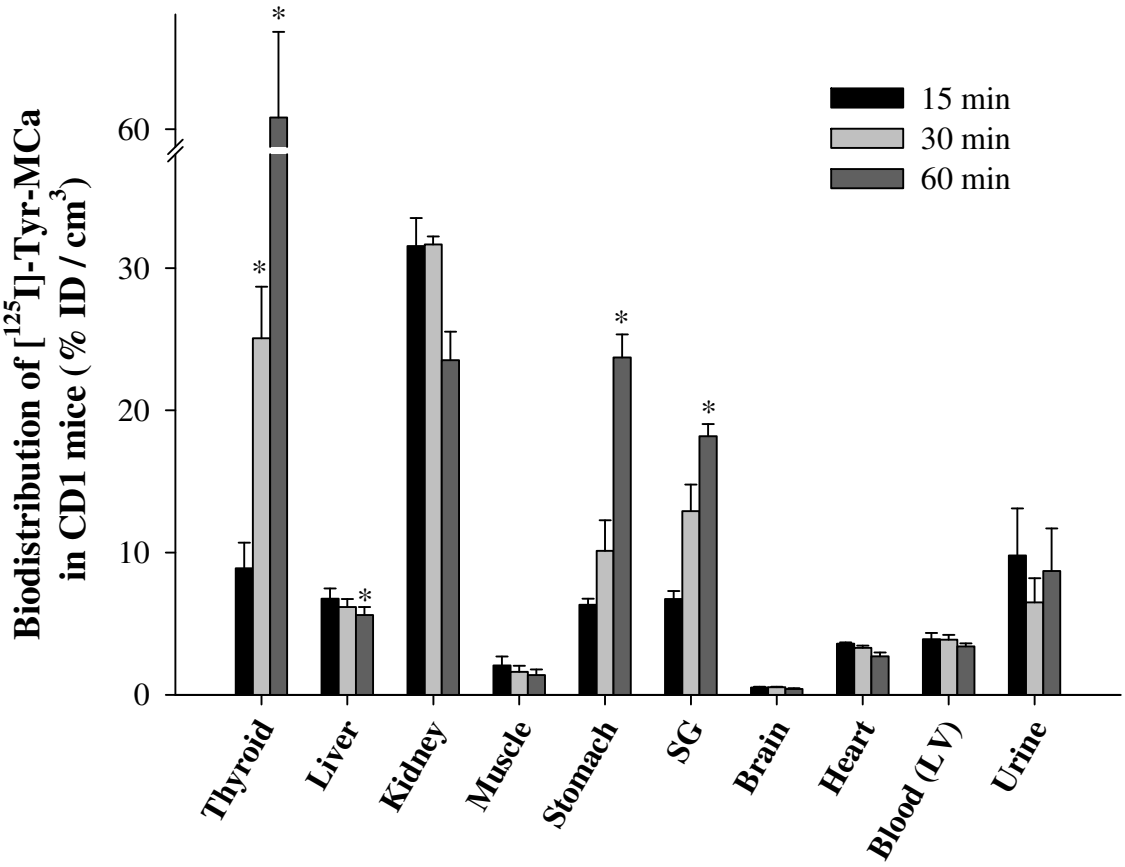
Biodistribution of [125I]-Tyr-MCa in CD1 mice (% ID / cm3)
15 min
30 min
60 min
0
10
20
30
60
*
Thyroid
Liver
Kidney
Muscle
Stomach
SG
Brain
Heart
Blood (LV)
Urine

Table 1. *In vitro* blood distribution pattern of radioactivity following [^{125}I]-Tyr-MCa incubation with whole mouse blood.

	Incubation time (min)			
	15	**30**	**60**	**90**
Blood cells	19%	23%	19%	17%
Plasma proteins	61%	59%	58%	67%
Protein-free plasma	17%	17%	14%	14%

Table 2. *In vitro* stability analysis of [^{125}I]-Tyr-MCa after 15 to 90 min incubation with mouse blood.

	Incubation time (min)			
	15	**30**	**60**	**90**
Free [^{125}I]	22%	20%	24%	24%
[^{125}I]-metabolite	2%	3%	5%	7%
[^{125}I]-Tyr-MCa	75%	75%	70%	67%

Table 3. *In vivo* blood distribution pattern of radioactivity following [^{125}I]-Tyr-MCa intravenous injection.

	Time post-injection (min)	
	15	**30**
Blood cells	24%	30%
Plasma proteins	47%	39%
Protein-free plasma	29%	26%

5.2 Conclusion

La maurocalcine native possède une stabilité remarquable dans le sang après injection intraveineuse, probablement de par la présence de ponts disulfure au sein de sa structure. Les organes principalement ciblés par la toxine sont les reins, l'estomac, la rate, la peau, les poumons, les intestins, le pancréas et le foie. Dans une moindre mesure, le cœur, les muscles squelettiques, le thymus, les cellules sanguines et le tissu adipeux brun retiennent également de grandes quantités de MCa. La grande accumulation de radioactivité dans les reins et les urines indique qu'ils constituent la principale voie d'élimination de la toxine.
Cette étude a donc permis d'établir une première définition des champs d'application de la MCa pour la délivrance intracellulaire de molécules thérapeutiques *in vivo*.

Chapitre 6

Article 5 : Utilité de la L-MCa pour la délivrance d'une sonde d'imagerie multimodale chez le rat

6.1 Introduction

Comme nous avons pu le voir au cours des chapitres précédents, la maurocalcine est un puissant outil pour la délivrance de divers cargos *in vivo*. Nous nous sommes intéressés plus particulièrement à son utilité pour la vectorisation d'agents de contraste IRM. En effet, les agents de contraste habituellement utilisés en clinique possèdent une localisation exclusivement extracellulaire, ce qui peut entraver leur rétention au sein des tissus. Un complexe d'ions gadolinium GdIII a donc été couplé à une nanoparticule luminescente ou quantum dot (QD) ainsi qu'à la maurocalcine native. Cette nouvelle double sonde IRM/optique devrait donc posséder un pouvoir de rétention plus élevé que les agents de contraste classiquement utilisés, et également permettre d'obtenir une information plus précise que les fluorochromes actuellement étudiés, qui eux aussi possèdent une localisation strictement extracellulaire.

ARTICLE

Cell-Permeable Ln(III) Chelate-Functionalized InP Quantum Dots As Multimodal Imaging Agents

Graeme J. Stasiuk,[†] Sudarsan Tamang,[‡] Daniel Imbert,[†] Cathy Poillot,[§] Marco Giardiello,[†] Céline Tisseyre,[§] Emmanuel L. Barbider,[§] Pascal Henry Fries,[†] Michel de Waard,[§] Peter Reiss,[‡] and Marinella Mazzanti[†,*]

[†]CEA-Grenoble, INAC, SCIB, Laboratoire de Reconnaissance Ionique et Chimie de Coordination, UMR-E 3 CEA-UJF, 38054 Grenoble Cedex 9, France, [‡]CEA Grenoble, INAC, SPrAM, Laboratoire d'Electronique Moléculaire, Organique et Hybride, UMR 5819 CEA-CNRS-UJF, France, and [§]Grenoble Institute of Neuroscience, Inserm U836, Site Santé de la Tronche, Bâtiment Edmond J. Safra, Chemin Fortuné Ferrini, BP170, 38042, France

ABSTRACT Quantum dots (QDs) are ideal scaffolds for the development of multimodal imaging agents, but their application in clinical diagnostics is limited by the toxicity of classical CdSe QDs. A new bimodal MRI/optical nanosized contrast agent with high gadolinium payload has been prepared through direct covalent attachment of up to 80 Gd(III) chelates on fluorescent nontoxic InP/ZnS QDs. It shows a high relaxivity of 900 mM^{-1} s^{-1} (13 mM^{-1} s^{-1} per Gd ion) at 35 MHz (0.81 T) and 298 K, while the bright luminescence of the QDs is preserved. Eu(III) and Tb(III) chelates were also successfully grafted to the InP/ZnS QDs. The absence of energy transfer between the QD and lanthanide emitting centers results in a multicolor system. Using this convenient direct grafting strategy additional targeting ligands can be included on the QD. Here a cell-penetrating peptide has been co-grafted in a one-pot reaction to afford a cell-permeable multimodal multimeric MRI contrast agent that reports cellular localization by fluorescence and provides high relaxivity and increased tissue retention with respect to commercial contrast agents.

KEYWORDS: gadolinium · lanthanide complexes · imaging agents · quantum dots · fluorescence · magnetic resonance imaging

Functionalized nanoparticles have become key players for enhancing contrast of images in medical diagnostics and are essential in molecular imaging. Magnetic resonance imaging (MRI) is a powerful, noninvasive diagnostic tool with impressive anatomic resolution and tissue penetration, but applications are limited by its low sensitivity and lack of cell specificity. MRI contrast agents (CAs), primarily gadolinium Gd^{III} complexes, are used to enhance the image contrast. This enhancement is the result of the increase of the water proton relaxation rate, $1/T_1$, induced by the neighboring paramagnetic Gd^{III} ions. The efficiency of current commercial contrast agents, usually expressed in terms of their relaxivity r_1 (mM^{-1} s^{-1}), that is, the increase of $1/T_1$ per mM of added Gd^{III} complexes, is too low for the detection of events at the molecular scale. Moreover, commercial CAs are limited to extracellular applications. A possible approach for increasing MRI sensitivity is the use of multimeric CAs in which a large number of small Gd^{III} chelates are bound to a nanosized carrier allowing for the accumulation of paramagnetic Gd^{III} ions at the site of interest.[1−5]

Another approach consists in combining MRI with a different high-sensitivity imaging modality[6−8] such as fluorescence.[9−13] The accuracy of the analysis can be improved by a combined tissue study by optical microscopy and by MRI, which requires creating a multimodal reporter.[14] The majority of dual (MRI/optical) probes are MRI contrast agents coupled to organic dyes. More recently, dual probes have been identified where the optical reporter is a transition metal, a Ln^{III} complex, or a quantum dot.[10,11,14−16] Quantum dots (QDs) are highly luminescent, photostable semiconductor nanoparticles of size-controlled emission. They are very attractive for use in diagnostic, molecular, and cellular imaging due to their optical properties and their increased photostability as compared to organic dyes.[17−24] Luminescent lanthanide complexes, on the other hand, are characterized by large Stokes shifts and long-lived luminescence, which render them very attractive for applications in cellular imaging.[25−32] Bimodal probes can be obtained simply by mixing luminescent Ln^{III} and Gd^{III} ions complexed by the same ligand due to chemical equivalence (leading to similar biodistribution) of lanthanide complexes.[16,33,34] We have previously shown that the pyridinecarboxylate-based *bpatcn* (H_3bpatcn = 1-(carboxymethyl)-4,7-bis[(6-carboxypyridin-2-yl)methyl]-1,4,7-triazacyclononane) ligand can be used to prepare both a Tb^{III} complex with high luminescence quantum yield and Gd^{III} complex with favorable relaxivity for MRI application.[35] Dual reporters have been demonstrated to be highly valuable in the multimodal imaging[36] studies of animals,

* Address correspondence to marinella.mazzanti@cea.fr.

Received for review July 27, 2011 and accepted September 3, 2011.

Published online 10.1021/nn202839w

allowing the combination of preoperative and intraoperative visualization of tumors,[37] co-validation of CA distribution,[38] and combined tracking of transplanted stem cells.[39] A challenge in the development of MRI CAs for investigating biochemical processes and cellular events is the efficient delivery of agents across cellular membranes. For instance, the monitoring of cell fate and migration *in vivo* will be essential to the development of cell-based therapies. While the development of MRI/optical imaging agents has significantly increased in the past few years, there are only few examples of high Gd^{III} payload dual agents capable of penetrating cells.[9,11,40] QDs provide convenient scaffolds in the development and applications[41−43] of bimodal multimeric Gd-based CAs for molecular MRI.[11,13,14,44] Notably, multiple ligands can be simultaneously attached to the QD surface to promote cell penetration and/or specific targeting. Applications of Gd-chelate-functionalized QDs in molecular imaging have been reported by the groups of Mulder and Backes.[41−43,45] In the reported systems the gadolinium chelates were grafted through an "indirect" method involving the incorporation into a lipid coating or biotin−streptavidin interactions. Moreover, all the reported systems are based on established CdSe/ZnS QDs, whose applications are limited due to the intrinsic toxicity of cadmium.

Here we report a new MRI/optical probe based on nontoxic InP/ZnS QDs, which shows high relaxivity of 900 mM^{-1} s^{-1} at 35 MHz (0.81 T) and 298 K, obtained by the direct covalent attachment of around 80 Gd(bpatcn) complexes to the nanocrystal surface, giving a relaxivity of 13 mM^{-1} s^{-1} per Gd(bpatcn). The versatile synthetic strategy used herein allows the introduction of additional modalities on the QDs. In particular, the simultaneous grafting of the cell-penetrating peptide maurocalcine and of up to 40 gadolinium chelates affords a cell-permeable multimodal multimeric MRI CA. This multimodal agent reports cellular localization by fluorescence and provides bright MRI signal and increased tissue retention with respect to commercial contrast agents. We also demonstrate the covalent attachment of the chemically equivalent visible-emitting Tb- and Eu(bptacn) complexes, which provide a good analytical tool to monitor the grafting process and could be used in the development of different types of Ln-Gd-QD multimodal reporters including Ln-based and QD-based optical modalities.

RESULTS AND DISCUSSION

The previously reported [Ln(bpatcn)] complexes[35] were functionalized for grafting on InP/ZnS QDs according to Scheme 1 and Scheme S1. Complex Ln.1 is an amine-appended derivative of the [Ln(bpatcn)] complexes; Gd.1 has a r_1 of 4.12 mM^{-1} s^{-1} at 200 MHz (4.6T, 298 K), which is comparable to the previously reported bpatcn analogues[16] and commercial CAs.[46,47] Ligand L1 was prepared from 1,4,7-triazacyclononane-1, 4-dibis(methylene)dipicolinic acid and 6-aminohexanoic acid in 62% yield through a multistep synthesis described in the Supporting Information. The amine functionality brings versatility, allowing for further modification. Notably, preliminary studies show that L1 can be directly conjugated through peptide chemistry coupling to different biomolecules such as peptides or oligonucleotides. In this work lipoic acid was successfully reacted with complex Ln.1 to afford the Ln.2 dithiol derivatives in 60% yield. The dithiol linker was chosen to ensure strong binding of the Ln chelates to the outer ZnS shell of the QDs.

InP/ZnS QDs are prepared in octadecene using phosphine gas as the phosphorus precursor and capped with a ZnS shell using a method we reported earlier.[48] Prior to the grafting of the water-soluble CA, a phase transfer reaction is performed using penicillamine at pH 9 in a 1:1 mixture of water and chloroform (reaction time 2 h, transfer yield 60%).[49] The InP/ZnS QDs capped with penicillamine (QD.Pen) provide a versatile platform for grafting of lanthanide chelates and/or other bioprobes.

The dithiol-functionalized lanthanide chelates are reacted overnight in a shaker with the QD.Pen in aqueous media at pH 9 and 20 °C in the presence of the reducing agent tris(carboxyethyl)phosphine (TCEP) to cleave the disulfide bond. This process results in the grafting of 75−80 lanthanide chelates on a single InP/ZnS QD in a 40% yield. The hydrodynamic diameters measured using dynamic light scattering (Table S1) showed an increase from 6.9 nm for the QD.Pen to 8.6−9.2 nm for the lanthanide complex functionalized QDs. This increase of around 2 nm is consistent with the successful coverage of the QD surface by Gd chelates. The strongest indication of successful grafting is the NMRD profile shown in Figure 1. Both Gd.1 and Gd.2 show a classical profile for monoaqua chelates. The Gd.2.QD system, with its larger molecular weight, shows a very different profile, with an increase in r_1 from 3 to 35 MHz (0.07−0.81 T, 298 K) of 10 to 13 mM^{-1} s^{-1}. The NMRD profile provides unambiguous evidence of efficient grafting and shows that the optimum relaxivity for Gd.2.QD is at 30 MHz (0.7 T, 298 K) with r_1 = 13 mM^{-1} s^{-1}. This significant increase in r_1 with respect to the nongrafted chelate is consistent with a slower rotation of the grafted complex due to its larger size. Increasing the molecular weight of Gd complexes by macromolecule and protein binding is an effective way to increase the relaxivity of small Gd chelates in the magnetic field range of 30−100 MHz (0.7−2.3 T, 298 K).[47] Magnetic susceptibility measurements and UV−visible spectroscopy showed the presence of 70−80 chelates grafted onto Gd.2.QD. As a result, the relaxivity per quantum dot reaches 900 mM^{-1} s^{-1}at 35 MHz (0.81 T, 298 K). As expected

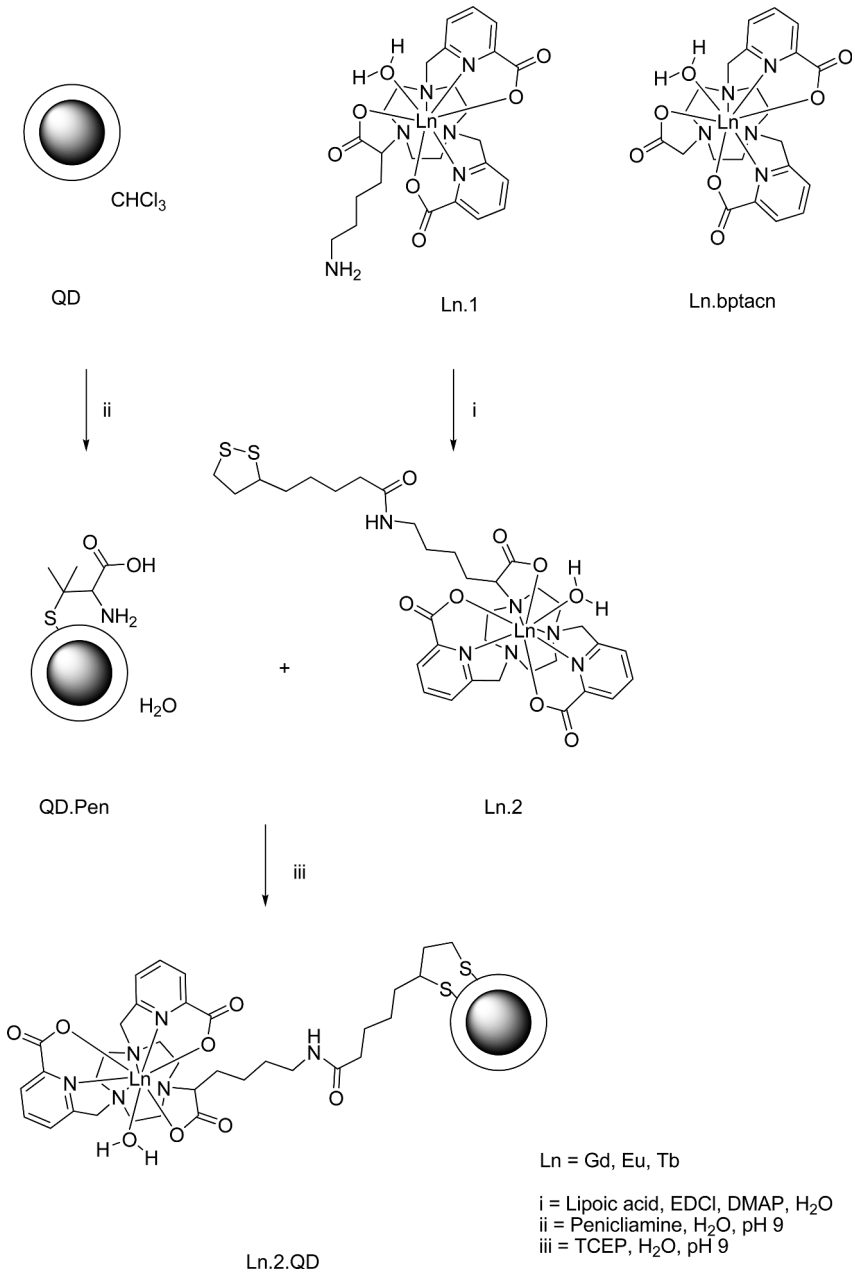

Scheme 1. Synthesis of Ln(III) QDs

from the theory of relaxivity, the slow rotation is not favorable at higher fields (200 MHz) and the relaxivity decreases, yielding a relaxivity per Gd chelate of 4.19 mM^{-1} s^{-1}. However, the relaxivity per quantum dot is still around 200 mM^{-1} s^{-1}, thus providing a very bright contrast agent compared to smaller chelates and commercial agents (r_{1-4} mM^{-1} s^{-1}) (Figure S2).

In order to assess the full potential of Ln.2.QD systems as multimodal (optical/optical and optical/magnetic) contrast agents, we have investigated their photophysical properties. The water-dispersible penicillamine-capped InP/ZnS QDs show a fluorescence quantum yield (QY) of 8.5% in water. A significant decrease in QY (QY in chloroform: 20%) after phase transfer *via* surface ligand exchange is generally observed in the literature.[22] The lack of difference in the emission spectra of QD.Pen and Gd.2.QD (Figure S3) suggests that grafting of the complex does not affect the luminescence of the QDs, resulting in a magnetic and optical dual-mode imaging probe. The InP/ZnS photoluminescence peak is located at 620 nm, and the QY measured at 480 nm for Gd.2.QD in water (6.1%) is comparable to the value of QD-pen (8.5%). Since the picolinate ligand can efficiently sensitize terbium and europium (Figure S4), the grafting of chelates containing these visible-emitting lanthanide ions results in a dual-mode optical probe with emission from both the QD (nanosecond time scale) and the Tb or Eu ions

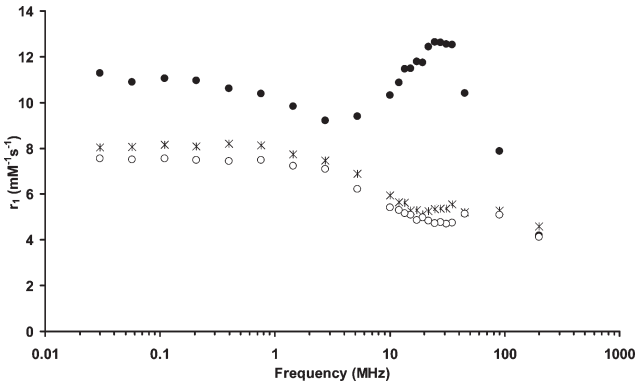

Figure 1. NMRD profile for Gd.1 (hollow circles), Gd.2 (crosses), and Gd.2.QD (full circles), at pH 7.4, 298 K.

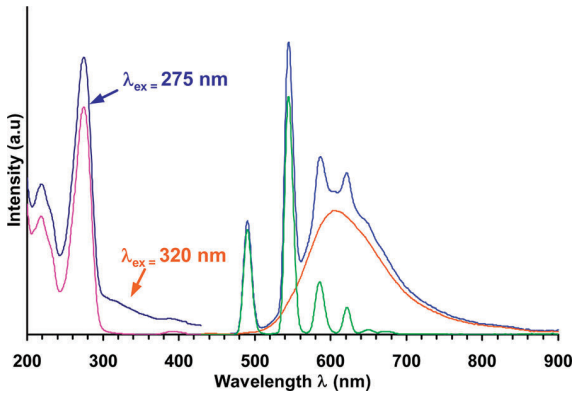

Figure 2. Luminescence of Tb.2.QD. (Left) Excitation spectra with λ_{em} = 546 nm (dark blue: 0 ms and pink: 0.05 ms delay, respectively). (Right) Emission spectra with λ_{ex} = 275 nm (blue: 0 ms and green: 0.05 ms delay, respectively) and 320 nm (orange: 0 ms delay).

(millisecond time scale). Energy transfer from Tb to QDs has been reported by Charbonniere for QDs grafted with Tb chelates through a streptavidine−biotine interaction.[20] In order to obtain dual-color systems, we have chosen QDs with emission matching the emission of the Eu and Tb complexes so that the energy transfer between the emitting centers is prevented. This strategy was successful, as no energy transfer was observed between the Tb or Eu and the QDs in our systems due the small energy gap between their emitting levels. F2 Figure 2 shows the excitation and emission spectra of Tb.2.QD. The excitation spectrum of Tb.2.QD shows a large peak at 275 nm, corresponding to the picolinate ligand absorption, while the excitation corresponding to the QDs extends over the range 200−500 nm. Emission from one or the other of the two emitters or from both can be selectively turned on by a suitable choice of acquisition conditions. Notably, the excitation of Tb.2.QD at 275 nm with 0 ms delay yields dual emission from the QDs and Tb ions at 620 and 546 nm. When a 0.05 ms delay is applied, only the emission from the TbIII ions is observed due to their longer luminescence lifetime with respect to the QDs. Conversely, when Tb.2.QD is excited at 320 nm with 0 ms delay, only emission from the QDs is observed. This provides a dual luminescent probe, which has two defined emission wavelengths on two different time scales, the millisecond and the nanosecond scale. Similar results were obtained for Eu.2.QD (Figure S5).

The direct grafting of the Gd chelate on the QDs provides a bimodal architecture with high relaxivity and bright luminescence in water. The versatile synthetic method can be adapted to introduce on the QD one or several additional functionalities such as targeting and bioactive moieties or cell-penetrating ligands. Cell penetration is crucial for the use of CAs in the monitoring of biological events such as enzyme activity or pH and temperature changes or in the tracking of stems cells, but only few examples of cell-penetrating CAs have been reported. The peptide maurocalcine (MCa) coupled to commercial QDs has shown a great potential for cell penetration in *in vivo* imaging of macrophages as an indicator of atherosclerosis.[50] Therefore, we have used MCa as a cell-penetrating ligand for a further functionalization of our bimodal platform.

We conjugated reproducibly both Gd.2 and the cell-penetrating peptide maurocalcine in its disulfideless version[51] through an additional N-terminal cysteine residue onto the penicillamine-capped InP/ZnS QDs in a one-step synthesis using a QD:Gd.2:TCEP:MCa ratio of

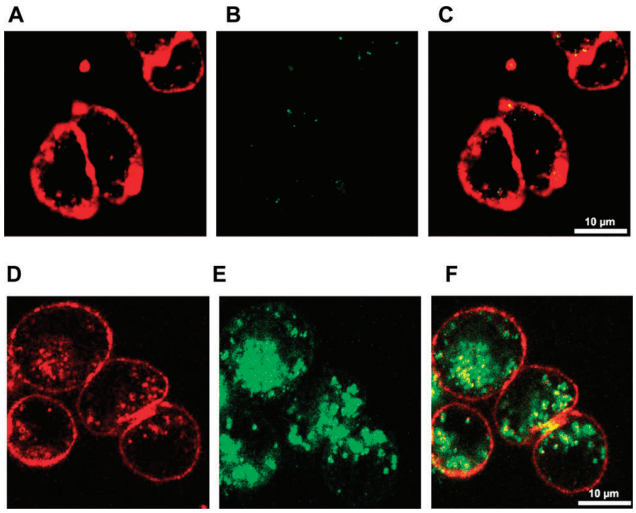

Figure 3. Confocal microscope images (false colors) of two batches of Chinese hamster ovarian cells (CHO). Batch 1: (A) stained with concanavalin A rhodamine (red); (B) incubation with Gd.2.QD (green) for 2 h followed by washing, (C) merge of A and B. Batch 2: (D) CHO cells as in A; (E) incubation with Gd.2.QD.MCa for 2 h followed by washing (green), (F) merge of D and E.

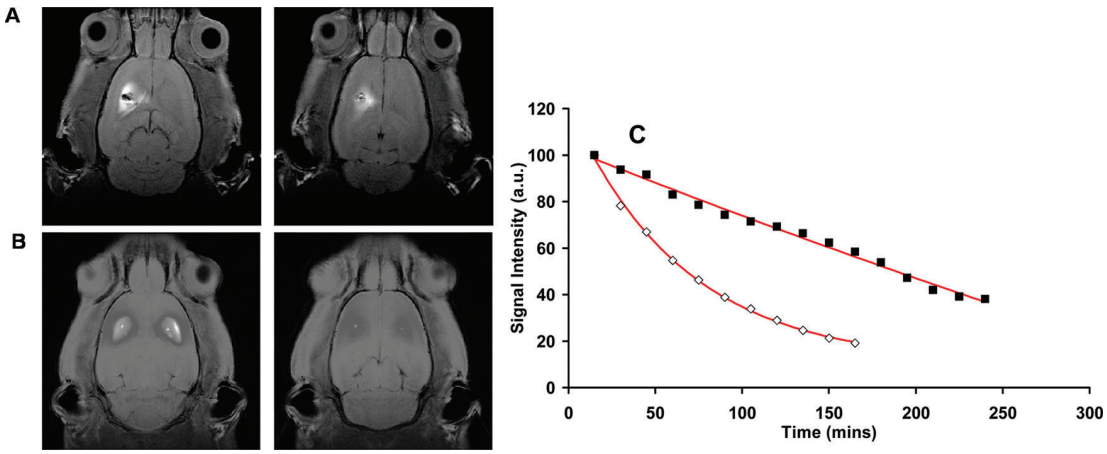

Figure 4. T_1-weighted MRI images of rat brain at 7 T (1 mM, 10 μL). (A) Gd.2.QD.MCa at 15 min and 4 h. (B) Dotarem at 15 min and 4 h. (C) Signal intensity *vs* time; Dotarem (◇) and Gd.2.QD.MCa (■).

1:200:9000:5. TCEP was used at high concentration to cleave the disulfide bridge of Gd.2 and to prevent the formation of undesired disulfide bridges. Magnetic susceptibility measurements[52] and UV−visible spectroscopy showed the presence of 30 to 40 Gd chelates on the MCa QDs.

In order to probe the cell-penetrating ability of this Gd.2.QD MCa dual probe, confocal microscopy images were recorded after incubation of the probe with Chinese hamster ovary (CHO) cells (Figure 3). They clearly show that the MCa-conjugated Gd.2.QDs accumulate within CHO cells during the 2 h incubation time, while no cell penetration is observed in the absence of MCa. Staining appeared as punctuate dots, suggesting that these MCa-functionalized QDs accumulate mostly in endosomes probably through an endocytosis-mediated uptake mechanism. The used resolution scale does not allow for the determination of the specific localization of Gd.2.QD.MCa. Some diffuse staining was also evident, suggesting that direct membrane translocation should not be excluded as one of the possible entry mechanisms. These data are coherent with earlier observations.[53] Importantly, similar experiments conducted with Gd.2.QD did not lead to intracellular accumulation of QD (Figure 3C), confirming that MCa was properly conjugated to Gd.2.QD and demonstrating that MCa is solely responsible for cell penetration of the complex.

The Gd.2Qd.MCa system provides a new, high-relaxivity bimodal probe that can penetrate cells. The cell permeability should lead to an increased retention of this contrast agent in brain tissue with respect to commercial CAs such as Dotarem ([Gd(DOTA)$^-$]). We therefore set out to compare whether Gd.2.QD.MCa provides a competitive advantage over Dotarem with regard to the retention time of the CA within the brain tissue.

To investigate this issue, 10 μL of 1 mM Dotarem or Gd.2.QD.MCa was injected directly into the striatum of 7-week-old rats (Figure 4). Both CAs led to a distinct signal within the injected striatum 15 min after injection. After 4 h, the Dotarem signal almost disappeared, whereas distinct signal intensity was still measurable for Gd.2.QD.MCa (Figure 4A).

Data analysis of the signal intensity over time illustrates that Dotarem concentration decreases rapidly in the striatum, whereas the Gd.2.QD.MCa concentration decrease is significantly slower over the 4 h period (Figure 4C). These data indicate a slower clearance of the Gd.2.QD.MCa with respect to Dotarem, which we attribute to a significant increase in tissue retention. While MCa is probably contributing to some extent to the improved duration of the MRI signal at the injection point, the size of the agents is an important factor limiting the lateral tissue diffusion of the compound.

CONCLUSIONS

Herein we have synthesized a new bimodal MRI/optical probe through direct grafting of gadolinium chelates on fluorescent InP/ZnS QDs. The high payload of gadolinium (up to 80 chelates) results in a high relaxivity of the nanosized contrast agent (900 mM^{-1} s^{-1}, 13 mM^{-1} s^{-1} per Gd ion at 35 MHz (0.81 T, 298 K), 200 mM^{-1} s^{-1}, 4.19 mM^{-1} s^{-1} per Gd ion at 200 MHz (4.6 T 298 K)), while the bright luminescence of the QDs is preserved. Chelates containing visible-emitting lanthanide ions have also been grafted on the QDs, and the absence of energy transfer between lanthanide ions and QDs results in a dual-mode optical probe with emission from the QDs and the Tb or Eu ions on different time scales (nanoseconds for the QDs, milliseconds for the rare earth ions). The versatile synthetic strategy allows the simultaneous grafting of various probes on the QDs. Notably, the protocol could be easily extended to produce a trimodal probe, optical (Tb-chelate)/magnetic (Gd-chelate)/optical (QD), and will be the subject of future work. We have also shown, through the example of the cell-penetrating peptide MCa, that additional targeting ligands can be co-grafted in a one-pot reaction. A new cell-penetrating multimodal probe has been identified that shows bright luminescence, high relaxivity, and excellent tissue retention properties, allowing for longer MRI recording than with commercial CAS.

METHODS

General Procedures. NMR spectra were recorded on Bruker DPX200 500 MHz spectrometers using standard Bruker software. Chemical shifts are reported in ppm with solvent as internal reference. ESMS were recorded on a Thermo Scientific (LXQ) spectrometer. Electronic absorption spectra were recorded on a Varian Cary 50 probe UV/vis spectrometer.

Materials. Solvents and starting materials were obtained from Aldrich, Fluka, Acros, and Alfa. They were used without further purification unless otherwise stated. Solvents were dried over the appropriate drying agents when required. Water and H_2O refer to high-purity water with a resistivity value of 18 MΩ·cm, obtained from the "Millipore/Milli-Q" purification system. Lanthanide chloride salts were purchased from Aldrich. Dotarem was purchased from Guerbet SA (Aulnay-s-bois, France). The precise metal ion content was titrated by colorimetry in acetate buffer (pH = 4.5) using standardized H_2Na_2edta solution (Merck) and xylenol orange indicator.

Ligand and Complex Synthesis. L1 was prepared from 1,4,7-triazacyclononane-1,4-dibis(methylene)dipicolinic acid[35] and 6-aminohexanoic through a multistep synthesis. The lanthanide complexes were formed in water. Synthetic procedures are detailed in the Supporting Information.

Quantum Dot Synthesis. The synthesis follows the protocol given by P. Reiss and co-workers.[54] Briefly, the indium precursor (1 equiv of indium myristate in 1-octadecene) was reacted under an Ar atmosphere with *in situ* generated PH_3 gas at 250 °C for 60 min to form the core InP QDs. For growth of the ZnS shell, 10 equiv of zinc stearate was added into the dispersion of the InP NCs and heated for 4 h to 280 °C to form a Zn^{2+}-rich surface before injecting slowly 2.5 equiv of zinc ethylxanthate at 210 °C during 30 min.

Synthesis of Penicillamine-Capped QDs (QD-pen). Thorough purification of the initial QDs assuring the removal of excess hydrophobic ligands is crucial for the successful phase transfer. Five milliliters of the QDs in organic solvent was mixed with anhydrous ethanol (1:3) and centrifuged at 10 000 rpm (rotations per minute) for 6 min. The clear solution of supernatant was discarded, and the precipitate was redispersed in 15 mL of a 1:3 chloroform/ethanol mixture and centrifuged again. The precipitate was dispersed in a minimum amount of chloroform. The concentration was estimated from the first excitonic peak in the UV−vis spectrum.[23] A 0.2 M solution of penicillamine in degassed Milli-Q water (1 mL) with pH adjusted at 9 with 0.5 M TMAH (tetramethylammonium hydroxide) was mixed with a ~5 μM dispersion of the QDs in chloroform (1.5 mL). The resulting biphasic mixture was stirred vigorously at 1400 rpm for 2 h to afford a fine aqueous suspension of QD-pen, which was separated from the organic layer (yield: 60%).

Synthesis of Gd.2.QD. Solutions of Gd.2 (0.25 mL, 2.1×10^{-3} M) and TCEP (0.046 mL, 0.5 M) in degassed water were added to the suspension of QD-pen (0.5 mL, 5.2×10^{-6} M) in degassed water, and the pH of the resulting suspension was adjusted to 9 with 0.5 M TMAH. The mixture was shaken at 800 rpm overnight at 20 °C. The resulting fine suspension was purified portionwise (200 μL) using PES 30K centrifuge filters at 1400 rpm for 60 s. The obtained nanoparticles were washed with 3 × 150 μL of degassed H_2O/PBS to remove any ungrafted complex. The nanoparticle portions were combined and concentrated to 100 μL, giving a fine orange suspension (yield 40%). This procedure was repeated several times. A gadolinium content in the range 70−80 complexes per QD was determined for independent syntheses by combined magnetic susceptibility measurements and UV−vis spectroscopy.

Synthesis of Gd.2QD.MCa. Solutions of Gd.2 (0.25 mL, 2.1×10^{-3} M), TCEP (0.046 mL, 0.5 M), and maurocalcine (MCa) (0.054 mL, 2.5×10^{-5} M) in degassed water were added to the suspension of QD-pen (0.5 mL, 5.2×10^{-6} M) in degassed water, and the pH of the resulting suspension was adjusted to 9. The mixture was shaken at 800 rpm overnight at 20 °C. The resulting fine suspension was purified portionwise (200 μL) using modified PES 30K centrifuge filters at 1400 rpm for 60 s. The obtained nanoparticles were washed with 3 × 150 μL of degassed H_2O/PBS to remove any ungrafted complex. The nanoparticle portions were combined and concentrated to 100 μL, giving a fine orange suspension. This procedure was

repeated several times. A gadolinium content in the range 30−40 complexes per QD was determined for independent synthesis by combined magnetic susceptibility measurements and UV−vis spectroscopy. The concentration of the samples before phase transfer and after grafting is estimated from the first excitonic peak in the UV−vis spectra using the empirical correlations between the excitonic peak, size, and molar extinction coefficient compiled in ref 23. The concentration of Gd(III) was checked by the chemical shift measurement of HOD induced by the magnetic susceptibility.[52]

Relaxivity Measurements. The Gd.1 and Gd.2 samples were prepared *in situ* by mixing the appropriate amounts of ligand and $GdCl_3 \cdot 6H_2O$ (99.99%; Aldrich) in H_2O followed by adjustment of the pH with NaOH aqueous solution (pH = 7.4). The pH of the Gd2.QD suspension was adjusted for relaxivity measurements at 7.4. The resulting suspension was placed in a 1.7 mm diameter capillary, which was sealed. The absence of free gadolinium was checked in all samples by the xylenol orange test.[55] The NMRD profiles were measured at 298 K in the range 0.1 and 35 Mz, by using a Spinmaster FFC (fast field cycling) NMR relaxometer (Stelar, Italy). The $1/T_1$ measurement was performed on a Bruker Avance 200 spectrometer (200 MHz). The $1/T_1$ measurements at 45 MHz (1.06 T) and 298 K were performed on a BrukerMinispec "mqvar" ND2318. At higher magnetic fields relaxation measurements were performed on conventional high-resolution NMR spectrometers.

Luminescence Spectroscopy. Luminescence data were recorded using a Perkin-Elmer LS50B luminescence spectrometer (using FLWINLAB for Windows v2.2) and a a modular Fluorolog FL3-22 spectrometer from Horiba-Jobin Yvon-Spex. Samples were held in a 10 × 10 nm or 10 × 2 nm quartz Hellma cuvette, and a cutoff filter (450 nm) was used to avoid second-order diffraction effects.

Quantum Yield Measurements. The excitation source was a 450 W Xe arc lamp, and all spectra were corrected for detection and optical spectral response (instrumental functions) of the FL3-22 spectrofluorimeter. It is equipped with a double grating excitation monochromator and a iHR320 imaging spectrometer coupled to a R928P Hamamatsu photomultiplier for visible measurement. The quantum yields were determined at room temperature through an absolute method[56] using a home-modified integrating sphere coupled to the modular Fluorolog FL 3-22 spectrofluorimeter. The values reported are the average of three independent determinations for each sample. The absolute quantum yield was calculated using the following expression:

$$\Phi = \frac{E_c}{L_a - L_c} = \frac{E_c}{L_a \alpha} \text{ and } \alpha = \frac{L_a - L_c}{L_a}$$

where E_c is the emission spectra in the emission range of the sample (ex: if the emission maximum is 620 nm, the range of this spectrum will be from 450 to 750 nm), L_c is the emission spectra of the excitation wavelength of the sample, and L_a is the emission spectra of the excitation wavelength of the reference (quartz capillary tube 4 mm in diameter filled with the solvent used).

Lifetime Measurements and Time-Gated Experiments. Time-gated experiments were recorded using a 0.05 ms delay to remove luminescence from the QD. Excited-state lifetime measurements were made on a Perkin-Elmer LS50B luminescence spectrometer (using FLWINLAB for Windows). Lifetimes were measured by direct excitation (275 nm) of the sample with a short 40 ms pulse of light (500 pulses per point) followed by monitoring the integrated intensity of light (617 nm for Eu and 546 nm for Tb) emitted during a fixed gate time of 0.1 ms, at a delay time later. Delay times were set at 0.1 ms intervals, covering 4 or more lifetimes. Excitation and emission slits were set to 5:5 nm bandpass, respectively. The obtained decay curves were fitted to a simple monoexponential first-order decay curve using Microsoft Excel. *q*-Values were calculated using the following equations:[57]

$$q = 1.2[kH_2O - kD_2O - 0.25] \text{ forEu}$$

$$q = 5[kH_2O - kD_2O - 0.06] \text{ forTb}$$

DLS Measurements. The hydrodynamic diameter of the water-soluble NCs dispersed in water was measured by dynamic light scattering (DLS), using a Malvern Zeta Sizer (NanoZS). The samples have been thoroughly purified with centrifugal filters from VWR (MWCO 30k) and dispersed in Milli-Q water (18 mΩ·cm) prior to the measurements. Given the sensitivity of the instrument, multiple runs (>3) were performed to avoid erroneous results. The spectra have been corrected by the instrument software for viscosity (0.882 mPa·s at 25 °C), absorption (at 532 nm), solvent (water) refractive index (1.33), and material (InP) refractive index (3.1). The data are collected in automatic mode and expressed in number %.

TEM Image. TEM images of Gd.2.QD were taken with a JEOL 4000EX microscope operated at 400 kV. The samples were prepared by evaporating a drop of the colloidal solution on a copper grid supporting a thin carbon film.

Biological Tests. *CHO Cell Culture.* Chinese hamster ovary (CHO) cell line (from ATCC) was maintained at 37 °C in 5% CO_2 in F-12K nutrient medium (InVitrogen) supplemented with 10% (v/v) heat-inactivated fetal bovine serum (InVitrogen) and 10 000 units/mL streptomycine and penicillin (InVitrogen).

Confocal Microscopy. Live CHO cells were incubated for 2 h with 10 μM Gd.QD or Gd.QD-MCa in F-12K cell culture medium without serum. Immediately after a two-time washing procedure with F-12K medium, the cell plasma membrane was stained with 5 μg/mL rhodamin-conjugated concanavalin A for 5 min, and cells were then washed again with F-12K medium. Live cells were immediately analyzed by confocal laser scanning microscopy using a Zeiss LSM 710 (Gd.2.QD or Gd.2.QD.MCa) or a Zeiss AxioVert 200M. Rhodamine (580 nm) and QD (620 nm) were sequentially excited (at 488 nm for rhodamine and 561 nm for QD), and emission fluorescence was collected in *z*-confocal planes of 10−15 nm steps.

***In Vivo* MRI Studies.** All animal experiments were conducted in agreement with the "Principles of Laboratory Animal Care" (NIH publication no. 86-23, revised 1985). The guidelines of the French Ministry of Agriculture (87/848) and of the European Community (86/609/EEC) were also respected. The protocol was submitted for approval to the local neuroscience institute committee to minimize animal suffering and abusive use of animal numbers. OFA 7-week-old rats were anesthetized by 5% isoflurane inhalation in a mixture air/O_2 30% and maintained in anesthesia in 2% isoflurane. Rats were then injected with 10 μL of 1 mM Dotarem or Gd.2.QD.MCa (Dotarem or Gd.2 concentrationwise) in the striatum using a stereotaxic frame (coordinates: 0 mm frontal, 3.5 mm lateral, and 5.5 mm in depth) and at a rate of 2 μL/min. T_1-weighted images (spin−echo, T_R/T_E = 300/27 ms) of rat brain were acquired 15 min after intrastriatal injection and after placing the rats in a 7 T magnet (Bruker BioSpec 70/20 USR AVIII; Preclinical MRI Facility of Grenoble). Sequences of 16 slices (slice thickness: 1 mm each) over a period of 15 min were taken. This sequence was repeated over a 4 h period, thus leading to the total acquisition of 16 sets of 16 slices. The temperature was maintained at 37 °C throughout the experiments.

Data Analyses of MRI Images. Two types of MRI image analyses were performed. In each case, the most intense average T_1 signal was selected from the set of 16 images at T = 15 min and kept for all other times. First, a region of interest (ROI) was drawn (10 pixels) close to the injection point (*x* mm of the injection point), and the average signal intensity calculated over the ROI minus the average intensity of the contra-lateral control area (zone with contrast agent). This type of analysis provides a hint of signal reduction with time. Second, the same type of analysis was conducted by drawing a similar sized ROI at a distance of *y* mm away from the injection point, close to the outer limit of the detectable contrast agent signal. This second type of analysis provides some information about the lateral diffusion process of the contrast agent. Images and image analyses for Gd.2.QD.MCa were compared to Dotarem data.

Acknowledgment. This research was carried out in the frame of the EC COST Action D-38 "Metal-Based Systems for Molecular Imaging Applications" and the European Molecular Imaging Laboratories (EMIL) network. We acknowledge financial support from the French Research Agency (PNANO-07-NANO-044) and from CEA Technologies pour la Santé "TIMO-MA2" and thank L. Plassais for help with synthetic chemistry.

Supporting Information Available: Description of the material, extensive figures, and expanded discussions are available free of charge *via* the Internet at http://pubs.acs.org.

REFERENCES AND NOTES

1. Manus, L. M.; Mastarone, D. J.; Waters, E. A.; Zhang, X. Q.; Schultz-Sikma, E. A.; MacRenaris, K. W.; Ho, D.; Meade, T. J. Gd(III)-Nanodiamond Conjugates for MRI Contrast Enhancement. *Nano Lett.* **2010**, *10*, 484–489.
2. Datta, A.; Hooker, J. M.; Botta, M.; Francis, M. B.; Aime, S.; Raymond, K. N. High Relaxivity Gadolinium Hydroxypyridonate-Viral Capsid Conjugates: Nanosized MRI Contrast Agents. *J. Am. Chem. Soc.* **2008**, *130*, 2546–2552.
3. Castelli, D. D.; Gianolio, E.; Crich, S. G.; Terreno, E.; Aime, S. Metal Containing Nanosized Systems for MR-Molecular Imaging Applications. *Coord. Chem. Rev.* **2008**, *252*, 2424–2443.
4. Moriggi, L.; Cannizzo, C.; Dumas, E.; Mayer, C. R.; Ulianov, A.; Helm, L. Gold Nanoparticles Functionalized with Gadolinium Chelates as High-Relaxivity MRI Contrast Agents. *J. Am. Chem. Soc.* **2009**, *131*, 10828–10829.
5. Hooker, J. M.; Datta, A.; Botta, M.; Raymond, K. N.; Francis, M. B. Magnetic Resonance Contrast Agents from Viral Capsid Shells: A Comparison of Exterior and Interior Cargo Strategies. *Nano Lett.* **2007**, *7*, 2207–2210.
6. Frullano, L.; Catana, C.; Benner, T.; Sherry, A. D.; Caravan, P. Bimodal MR-PET Agent for Quantitative pH Imaging. *Angew. Chem., Int. Ed.* **2010**, *49*, 2382–2384.
7. Choi, J. S.; Park, J. C.; Nah, H.; Woo, S.; Oh, J.; Kim, K. M.; Cheon, G. J.; Chang, Y.; Yoo, J.; Cheon, J. A Hybrid Nanoparticle Probe for Dual-Modality Positron Emission Tomography and Magnetic Resonance Imaging. *Angew. Chem., Int. Ed.* **2008**, *47*, 6259–6262.
8. Tsotsalas, M.; Busby, M.; Gianolio, E.; Aime, S.; De Cola, L. Functionalized Nanocontainers as Dual Magnetic and Optical Probes for Molecular Imaging Applications. *Chem. Mater.* **2008**, *20*, 5888–5893.
9. Song, Y.; Xu, X. Y.; MacRenaris, K. W.; Zhang, X. Q.; Mirkin, C. A.; Meade, T. J. Multimodal Gadolinium-Enriched DNA-Gold Nanoparticle Conjugates for Cellular Imaging. *Angew. Chem., Int. Ed.* **2009**, *48*, 9143–9147.
10. Tu, C. Q.; Ma, X. C.; Pantazis, P.; Kauzlarich, S. M.; Louie, A. Y. Paramagnetic, Silicon Quantum Dots for Magnetic Resonance and Two-Photon Imaging of Macrophages. *J. Am. Chem. Soc.* **2010**, *132*, 2016–2023.
11. Mulder, W. J. M.; Koole, R.; Brandwijk, R. J.; Storm, G.; Chin, P. T. K.; Strijkers, G. J.; Donega, C. D.; Nicolay, K.; Griffioen, A. W. Quantum Dots with a Paramagnetic Coating as a Bimodal Molecular Imaging Probe. *Nano Lett.* **2006**, *6*, 1–6.
12. Howes, P.; Green, M.; Bowers, A.; Parker, D.; Varma, G.; Kallumadil, M.; Hughes, M.; Warley, A.; Brain, A.; Botnar, R. Magnetic Conjugated Polymer Nanoparticles as Bimodal Imaging Agents. *J. Am. Chem. Soc.* **2010**, *132*, 9833–9842.
13. Yang, H. S.; Santra, S.; Walter, G. A.; Holloway, P. H. Gd-III-Functionalized Fluorescent Quantum Dots as Multimodal Imaging Probes. *Adv. Mater.* **2006**, *18*, 2890–2894.
14. Jennings, L. E.; Long, N. J. 'Two is Better than One'-Probes for Dual-Modality Molecular Imaging. *Chem. Commun* **2009**, 3511–3524.
15. Koullourou, T.; Natrajan, L. S.; Bhavsar, H.; Pope, S. J. A.; Feng, J. H.; Narvainen, J.; Shaw, R.; Scales, E.; Kauppinen, R.; Kenwright, A. M.; *et al*. Synthesis and Spectroscopic Properties of a Prototype Single Molecule Dual Imaging Agent Comprising a Heterobimetallic Rhenium-Gadolinium Complex. *J. Am. Chem. Soc.* **2008**, *130*, 2178–2179.
16. Crich, S. G.; Biancone, L.; Cantaluppi, V.; Esposito, D. D. G.; Russo, S.; Camussi, G.; Aime, S. Improved Route for the Visualization of Stem Cells Labeled with a Gd-/Eu-Chelate as Dual (MRI and Fluorescence) Agent. *Magn. Reson. Med.* **2004**, *51*, 938–944.
17. Michalet, X.; Pinaud, F. F.; Bentolila, L. A.; Tsay, J. M.; Doose, S.; Li, J. J.; Sundaresan, G.; Wu, A. M.; Gambhir, S. S.; Weiss, S. Quantum Dots for Live Cells, in Vivo Imaging, and Diagnostics. *Science* **2005**, *307*, 538–544.
18. Lee, J. H.; Lee, K.; Moon, S. H.; Lee, Y.; Park, T. G.; Cheon, J. All-in-One Target-Cell-Specific Magnetic Nanoparticles for Simultaneous Molecular Imaging and SiRNA Delivery. *Angew. Chem., Int. Ed.* **2009**, *48*, 4174–4179.
19. Geissler, D.; Charbonniere, L. J.; Ziessel, R. F.; Butlin, N. G.; Lohmannsroben, H. G.; Hildebrandt, N. Quantum Dot Biosensors for Ultrasensitive Multiplexed Diagnostics. *Angew. Chem., Int. Ed.* **2010**, *49*, 1396–1401.
20. Hildebrandt, N.; Charbonniere, L. J.; Beck, M.; Ziessel, R. F.; Lohmannsroben, H. G. Quantum Dots as Efficient Energy Acceptors in a Time-Resolved Fluoroimmunoassay. *Angew. Chem., Int. Ed.* **2005**, *44*, 7612–7615.
21. Hussain, S.; Won, N.; Nam, J.; Bang, J.; Chung, H.; Kim, S. One-Pot Fabrication of High-Quality InP/ZnS (Core/Shell) Quantum Dots and Their Application to Cellular Imaging. *Phys. Chem. Chem. Phys.* **2009**, *10*, 1466–1470.
22. Yong, K. T.; Ding, H.; Roy, I.; Law, W. C.; Bergey, E. J.; Maitra, A.; Prasad, P. N. Imaging Pancreatic Cancer Using Bioconjugated InP Quantum Dots. *ACS Nano* **2009**, *3*, 502–510.
23. Reiss, P.; Protiere, M.; Li, L. Core/Shell Semiconductor Nanocrystals. *Small* **2009**, *5*, 154–168.
24. Parak, W. J.; Pellegrino, T.; Plank, C. Labelling of Cells with Quantum Dots. *Nanotechnology* **2005**, *16*, R9–R25.
25. Frias, J. C.; Bobba, G.; Cann, M. J.; Hutchison, C. J.; Parker, D. Luminescent Nonacoordinate Cationic Lanthanide Complexes as Potential Cellular Imaging and Reactive Probes. *Org. Biomol. Chem.* **2003**, *1*, 905–907.
26. Botta, M.; Quici, S.; Pozzi, G.; Marzanni, G.; Pagliarin, R.; Barra, S.; Crich, S. G. NMR Relaxometric Study of New Gd-III Macrocyclic Complexes and Their Interaction with Human Serum Albumin. *Org. Biomol. Chem.* **2004**, *2*, 570–577.
27. New, E. J.; Parker, D.; Smith, D. G.; Walton, J. W. Development of Responsive Lanthanide Probes for Cellular Applications. *Curr. Opin. Chem. Biol.* **2010**, *14*, 238–246.
28. Bunzli, J. C. G. Lanthanide Luminescence for Biomedical Analyses and Imaging. *Chem. Rev.* **2010**, *110*, 2729–2755.
29. Song, Y.; Kohlmeir, E. K.; Meade, T. J. Synthesis of Multimeric MR Contrast Agents for Cellular Imaging. *J. Am. Chem. Soc.* **2008**, *130*, 6662–6663.
30. Bunzli, J. C. G. Lanthanide Luminescent Bioprobes (LLBs). *Chem. Lett.* **2009**, *38*, 104–109.
31. Deiters, E.; Song, B.; Chauvin, A. S.; Vandevyver, C. D. B.; Gumy, F.; Bunzli, J. C. G. Luminescent Bimetallic Lanthanide Bioprobes for Cellular Imaging with Excitation in the Visible-Light Range. *Chem.—Eur. J.* **2009**, *15*, 885–900.
32. New, E. J.; Congreve, A.; Parker, D. Definition of the Uptake Mechanism and Sub-Cellular Localisation Profile of Emissive Lanthanide Complexes as Cellular Optical Orobes. *Chem. Sci.* **2011**, *1*, 111–118.
33. Lowe, M. P.; Parker, D.; Reany, O.; Aime, S.; Botta, M.; Castellano, G.; Gianolio, E.; Pagliarin, R. pH-Dependent Modulation of Relaxivity and Luminescence in Macrocyclic Gadolinium and Europium Complexes Based on Reversible Intramolecular Sulfonamide Ligation. *J. Am. Chem. Soc.* **2001**, *123*, 7601–7609.
34. Picard, C.; Geum, N.; Nasso, I.; Mestre, B.; Tisnes, P.; Laurent, S.; Muller, R. N.; Vander Elst, L. A Dual Lanthanide Probe Suitable for Optical (Tb^{3+} Luminescence) and Magnetic Resonance Imaging (Gd^{3+} Relaxometry). *Bioorg. Med. Chem. Lett.* **2006**, *16*, 5309–5312.
35. Nonat, A.; Gateau, C.; Fries, P. H.; Mazzanti, M. Lanthanide Complexes of a Picolinate Ligand Derived from 1,4,7-Triazacyclononane with Potential Application in Magnetic Resonance Imaging and Time-Resolved Luminescence Imaging. *Chem.—Eur. J.* **2006**, *12*, 7133–7150.
36. Frullano, L.; Meade, T. J. Multimodal MRI Contrast Agents. *J. Biol. Inorg. Chem.* **2007**, *12*, 939–949.
37. Kircher, M. F.; Mahmood, U.; King, R. S.; Weissleder, R.; Josephson, L. A Multimodal Nanoparticle for Preoperative Magnetic Resonance Imaging and Intraoperative Optical Brain Tumor Delineation. *Cancer Res.* **2003**, *63*, 8122–8125.
38. Mulder, W. J. M.; Strijkers, G. J.; Habets, J. W.; Bleeker, E. J. W.; van der Schaft, D. W. J.; Storm, G.; Koning, G. A.; Griffioen, A. W.; Nicolay, K. MR Molecular Imaging and Fluorescence Microscopy for Identification of Activated

Tumor Endothelium Using a Bimodal Lipidic Nanoparticle. *Faseb J.* **2005**, *19*, 2008–2010.
39. Modo, M.; Cash, D.; Mellodew, K.; Williams, S. C. R.; Fraser, S. E.; Meade, T. J.; Price, J.; Hodges, H. Tracking Transplanted Stem Cell Migration Using Bifunctional, Contrast Agent-Enhanced, Magnetic Resonance Imaging. *Neuroimage* **2002**, *17*, 803–811.
40. Olson, E. S.; Jiang, T.; Aguilera, T. A.; Nguyen, Q. T.; Ellies, L. G.; Scadeng, M.; Tsien, R. Y. Activatable Cell Penetrating Peptides Linked to Nanoparticles as Dual Probes for in Vivo Fluorescence and MR Imaging of Proteases. *Proc. Natl. Acad. Sci. U. S. A.* **2010**, *107*, 4311–4316.
41. Oostendorp, M.; Douma, K.; Hackeng, T. M.; Post, M. J.; van Zandvoort, M.; Backes, W. H. Gadolinium-Labeled Quantum Dots for Molecular Magnetic Resonance Imaging: R-1 Versus R-2 Mapping. *Magn. Reson. Med.* **2010**, *64*, 291–298.
42. Ostendorp, M.; Douma, K.; Hackeng, T. M.; Dirksen, A.; Post, M. J.; van Zandvoort, M. A. M.; Backes, W. H. Quantitative Molecular Magnetic Resonance Imaging of Tumor Angiogenesis Using cNGR-Labeled Paramagnetic Quantum Dots. *Cancer Res.* **2008**, *68*, 7676–7683.
43. Mulder, W. J. M.; Strijkers, G. J.; Nicolay, K.; Griffioen, A. W. Quantum Dots for Multimodal Molecular Imaging of Angiogenesis. *Angiogenesis* **2009**, *13*, 131–134.
44. Prinzen, L.; Miserus, R.; Dirksen, A.; Hackeng, T. M.; Deckers, N.; Bitsch, N. J.; Megens, R. T. A.; Douma, K.; Heemskerk, J. W.; Kooi, M. E.; *et al*. Optical and Magnetic Resonance Imaging of Cell Death and Platelet Activation Using Annexin A5-Functionalized Quantum Dots. *Nano Lett.* **2007**, *7*, 93–100.
45. van Tilborg, G. A. F.; Vucic, E.; Strijkers, G. J.; Cormode, D. P.; Mani, V.; Skajaa, T.; Reutelingsperger, C. P. M.; Fayad, Z. A.; Mulder, W. J. M.; Nicolay, K. Annexin A5-Functionalized Bimodal Nanoparticles for MRI and Fluorescence Imaging of Atherosclerotic Plaques. *Bioconjugate Chem.* **2006**, *21*, 1794–1803.
46. Powell, H. D.; Ni Dhubhghaill, O. M. N.; Pubanz, D.; Helm, L.; Lebedev, Y. S.; Schlaepfer, W.; Merbach, A. E. Structural and Dynamic Parameters Obtained from 17O NMR, EPR NMRD Studies of Monomeric and Dimeric Gd(III) Complexes. *J. Am. Chem. Soc.* **1996**, *118*, 9333–9346.
47. Merbach, A. E.; Toth, E. *The Chemistry of Contrast Agents in Medical Magnetic Resonance Imaging*; Wiley: Chichester, 2001.
48. Xu, S.; Ziegler, J.; Nann, T. Rapid Synthesis of Highly Luminescent InP and InP/ZnS Nanocrystals. *J. Mater. Chem.* **2008**, *18*, 2653–2656.
49. Jayagopal, A.; Su, Y. R.; Blakemore, J. L.; Linton, M. F.; Fazio, S.; Haselton, F. R. Quantum Dot Mediated Imaging of Atherosclerosis. *Nanotechnology* **2009**, *20*, 165102.
50. Esteve, E.; Mabrouk, K.; Dupuis, A.; Smida-Rezgui, S.; Altafaj, X.; Grunwald, D.; Platel, J. C.; Andreotti, N.; Marty, I.; Sabatier, J. M.; *et al*. Transduction of the Scorpion Toxin Maurocalcine into Cells - Evidence that the Toxin Crosses the Plasma Membrane. *J. Biol. Chem.* **2005**, *280*, 12833–12839.
51. Ram, N.; Weiss, N.; Texier-Nogues, I.; Aroui, S.; Andreotti, N.; Pirollet, F.; Ronjat, M.; Sabatier, J. M.; Darbon, H.; Jacquemond, V.; *et al*. Design of a Disulfide-Less, Pharmacologically Inert, and Chemically Competent Analog of Maurocalcine for the Efficient Transport of Impermeant Compounds into Cells. *J. Biol. Chem.* **2008**, *283*, 27048–27056.
52. Corsi, D. M.; Platas-Iglesias, C.; van Bekkum, H.; Peters, J. A. Determination of Paramagnetic Lanthanide(III) Concentrations from Bulk Magnetic Susceptibility Shifts in NMR Spectra. *Magn. Reson. Chem.* **2001**, *39*, 723–726.
53. Ram, N.; Texier-Nogues, I.; Pernet-Gallay, K.; Poillot, C.; Ronjat, M.; Andrieux, A.; Arnoult, C.; Daou, J.; De Waard, M. In Vitro and In Vivo Intracellular Delivery of Quantum Dots by Maurocalcine. *IJBNN* **2011**, *2*, 12–32.
54. Li, L.; Protiere, M.; Reiss, P. Economic Synthesis of High Quality InP Nanocrystals Using Calcium Phosphide as the Phosphorus Precursor. *Chem. Mater.* **2008**, *20*, 2621–2623.
55. Brunisholz, G.; Randin, M. Sur la Separation des Terres Rares a Laide de Lacide Ethylenediamine-Tetraacetique 0.9. Procede en Cycle pour le Fractionnement des Terres Yttriques. *Helv. Chim. Acta* **1959**, *42*, 1927–1938.
56. deMello, J. C.; Wittmann, H. F.; Friend, R. H. An Improved Experimental Determination of External Photoluminescence Quantum Efficiency. *Adv. Mater.* **1997**, *9*, 230–232.
57. Beeby, A.; Clarkson, I. M.; Dickins, R. S.; Faulkner, S.; Parker, D.; Royle, L.; de Sousa, A. S.; Williams, G. J. A.; Woods, M. Non Radiative Deactivation of the Excited States of Europium Terbium and Ytterbium Complexes by Proximate Energy Matched Oh, Nh, Ch Oscillators: An Improved Luminescence Method for Establishing Solution Hydration States. *J. Chem. Soc., Perkin Trans. 2* **1999**, 493–503.

6.2 Conclusion

Le couplage de la maurocalcine à un complexe de gadolinium ainsi qu'à un quantum dot fluorescent a donné lieu à une nouvelle sonde multimodale qui s'accumule au sein des cellules. Cette sonde permet d'obtenir un signal plus puissant que celui fourni par les agents de contraste utilisés en clinique mais également d'utiliser une détection complémentaire par fluorescence, qui présente une meilleure résolution spatiale. De plus, la présence d'un CPP augmente la rétention du complexe au sein du cytoplasme et donc des tissus, ce qui laisse la possibilité à des acquisitions IRM de plus longue durée. Ceci confirme l'intérêt de l'utilisation de la MCa pour la délivrance de cargos *in vivo* puisque, dans bien des cas, l'accumulation intracellulaire entraîne une potentialisation de leurs effets.

Troisième partie

Conclusion générale

Au cours de cette thèse, je me suis intéressée à la caractérisation des propriétés de pénétration de la maurocalcine et de ses variants, et ce afin d'évaluer leur intérêt comme nouveaux vecteurs de molécules thérapeutiques ou d'imagerie. En effet, de nombreuses études ont mis en évidence les remarquables propriétés de pénétration cellulaire de la maurocalcine native (L-MCa), qui permettent de considérer cette molécule comme faisant partie des peptides de pénétration cellulaire (Esteve *et al.*, 2005; Boisseau *et al.*, 2006; Ram *et al.*, 2008b). Mais la MCa appartient également à la grande famille des produits naturels et plus particulièrement à celle des toxines animales, puisqu'elle est issue du venin du scorpion *Scorpio maurus palmatus*.

L'intérêt des toxines animales en thérapeutique ne cesse d'être démontré, que ce soit grâce à leur activité pharmacologique en tant que telle (Zhang *et al.*, 2007; Soman *et al.*, 2009), leur capacité à cibler certains types cellulaires (Graf *et al.*, 2012) ou, comme pour la MCa, leur capacité à délivrer des cargos au sein des cellules (Gurrola *et al.*, 2010). C'est dans ce contexte que j'ai cherché à parfaire les connaissances déjà acquises au sujet de la L-MCa, mais également à étudier plusieurs de ses variants afin de préciser leurs possibles applications thérapeutiques.

La grande stabilité de L et la D-MCa conférée par leurs ponts disulfures présente un avantage certain, mais leur structure foldée ainsi que leur taille relativement importante complexifient leur synthèse. C'est pourquoi il convient de se pencher sur les variants tronqués (linéaires) de la L-MCa. Pour ce faire, nous avons testé les propriétés de pénétration cellulaire de plusieurs de ces variants. Quelle que soit la partie de la séquence conservée, tous ces analogues de la MCa possèdent la capacité à s'accumuler au sein des cellules. Ceci laisse à penser que plusieurs parties de la séquence sont impliquées dans l'internalisation de la MCa.

J'ai également comparé les propriétés de pénétration des variants tronqués à celles de Tat (fragment de la protéine Trans-Activatrice de la Transcription impliquée dans la transcription du génome du VIH et donc dans sa réplication) et de la pénétratine (dérivée d'un facteur de transcription de l'homéodomaine du gène Antennapedia de la drosophile), tous deux CPP de référence largement utilisés en recherche appliquée. Il en ressort que tous les analogues de la maurocalcine testés ont une capacité à être internalisés bien plus élevée que celle des CPP de référence. C'est notamment le cas du peptide MC$a_{\mathrm{UF1-9}}$ (qui correspond à un domaine hydrophobe de la maurocalcine), détecté à l'intérieur des cellules pour une concentration extracellulaire de 100 nM, alors que Tat et la pénétratine semblent ne s'accumuler qu'à partir de 1 µM. Ce nouveau CPP présente un intérêt pour la délivrance intracellulaire de composés thé-

rapeutiques puisqu'il s'accumule dans le cytoplasme à de faibles concentrations extracellulaires, mais également parce que son temps de rétention est élevé (on évalue à 27% la quantité de peptide toujours présente 34h après lavage).

MC$a_{\mathrm{UF1-9}}$ possédant une distribution punctiforme au sein des cellules, comportement typique d'un peptide favorisant l'endocytose, je me suis intéressée à l'effet de certains inhibiteurs de l'endocytose sur sa pénétration. De façon surprenante, seul l'amiloride (inhibiteur de la macropinocytose) a sensiblement diminué sa capacité à s'accumuler au sein des cellules. Cette capacité n'a pas été amoindrie en présence de methyl-β-cyclodextrin (inhibiteur des voies dépendantes des radeaux lipidiques), de nocodazole (inhibiteur de la formation des microtubules) ou de cytochalasin D (inhibiteur de l'élongation de l'actine-F). Ces données laissent à penser que la distribution punctiforme de MC$a_{\mathrm{UF1-9}}$ ne s'explique pas par le recours à l'endocytose.

L'histidine présente en position 6 de la séquence de MCa_{1-9} contribue en partie à la pénétration cellulaire et est une cible de protonation idéale (donc susceptible d'être sensible au pH environnant). En évaluant la pénétration du peptide dans des cellules de glioblastome murin en fonction du pH extracellulaire, j'ai pu montrer qu'un pH acide favorise son accumulation. Il est à noter qu'en cas de tumeur solide et donc de glioblastome, le pH extracellulaire est légèrement acide (Cardone *et al.*, 2005; Garcia-Martin *et al.*, 2001). Le peptide MC$a_{\mathrm{UF1-9}}$ pourrait donc représenter un avantage stratégique puisqu'il permettrait en partie l'accumulation préférentielle de l'agent thérapeutique dans le tissu tumoral plutôt que dans le tissu sain avoisinant.

Si le nouveau CPP MC$a_{\mathrm{UF1-9}}$ s'est révélé prometteur pour la délivrance intracellulaire de molécules thérapeutiques, l'approfondissement des connaissances au sujet de la maurocalcine native reste une priorité. En effet, la L-MCa n'étant étudiée que depuis une dizaine d'années, la compréhension de ses mécanismes d'action ainsi que des possibilités thérapeutiques qu'elle offre n'est pas exhaustive. La première étape de cette étude a consisté en l'estimation du volume de notre modèle cellulaire (cellules F98, lignée de glioblastome murin). La microscopie holographique digitale (DHM) nous a amené à considérer ce volume comme étant égal à $8{,}9\times10^{-7}\,\mu$L.

Nous nous sommes ensuite intéressés à la quantification de l'accumulation intracellulaire de la L-MCa *in vitro*. Pour ce faire, la toxine a été couplée à de l'iode radioactive (I^{125}) : une molécule d'iode étant couplée à une molécule de MCa, nous avons été en mesure de calculer les quantités de peptide accumulées au sein du cytoplasme et relarguées au cours du temps. Ces travaux ont confirmé que la maurocalcine s'ac-

cumule rapidement (dès 10 minutes d'incubation), à partir de faibles concentrations extracellulaires (100 nM) et contre son gradient de concentration. En effet, on estime les quantités de L-MCa 2,45 fois plus élevées dans le cytoplasme que dans le compartiment extracellulaire. Sa rétention dans le compartiment intracellulaire est également remarquable puisque 90% du signal radioactif sont conservés 24h après lavage.

Après avoir confirmé l'intérêt thérapeutique de la maurocalcine native et caractérisé en partie son accumulation intracellulaire *in vitro*, il convient de se pencher sur sa biodistribution avant d'envisager de potentielles applications *in vivo*. Suite à l'injection intraveineuse de L-MCa mono-iodée (I^{125}) chez la souris CD-1, nous avons constaté la présence du marqueur radioactif et donc de la toxine au niveau des reins, de l'estomac, de la rate, de la peau, des poumons, des intestins, du pancréas et du foie. De façon moins prononcée, la MCa s'accumule également au sein du cœur, des muscles squelettiques, du thymus, des cellules sanguines et du tissu adipeux brun. Les reins et les urines, quant à eux, constituent sa principale voie d'élimination. Cette compréhension de la biodistribution est primordiale pour la mise en place de projets impliquant la délivrance de cargos *in vivo* par la maurocalcine.

Si l'impact de la biodistribution de la MCa est important dans le cas de l'administration de la toxine par injection intraveineuse, il devient minime lorsque l'on s'intéresse à une application nécessitant une injection réalisée directement au sein d'un organe. En effet, ce CPP possède une capacité de rétention intracellulaire élevée et n'est donc pas *a priori* soumis au phénomène de diffusion. C'est ce que nous avons pu confirmer en utilisant la L-MCa afin de vectoriser des agents de contraste IRM. Nous avons injecté dans le cerveau de rats une molécule chimère formée par la maurocalcine, un complexe de gadolinium (agent de contraste), et une nanoparticule luminescente (quantum dot). En comparaison aux agents de contrastes classiquement utilisés, cette nouvelle sonde multimodale a généré un signal plus puissant et moins diffus. Ce signal possède également un temps de rétention plus élevé, ce qui laisse donc la possibilité à des acquisitions IRM de plus longue durée. En outre, la présence d'un fluorochrome lui confère un avantage supplémentaire, l'imagerie optique permettant une meilleure résolution spatiale. Les propriétés de pénétration cellulaire remarquables de la maurocalcine ainsi que son pouvoir de rétention élevé permettent de ce fait de repousser les limites inhérentes à la localisation strictement extracellulaire des agents de contraste et des fluorochromes utilisés en clinique.

Ces travaux de thèse ont donc apporté quelques précisions au sujet d'un CPP déjà connu, la maurocalcine, mais ont également permis la mise en évidence d'un nouveau CPP d'intérêt, le petit peptide MC$a_{\mathrm{UF1-9}}$. La toxine native présente l'avantage d'une plus grande stabilité *in vivo* du fait de la présence de ponts disulfure au sein de sa structure, ainsi que d'une meilleure rétention intracellulaire. Son analogue tronqué, en revanche, est plus simple à synthétiser (donc moins coûteux), et sensible au pH environnant puisque sa capacité de pénétration cellulaire se révèle accrue en milieu acide. Il convient par conséquent de définir l'application la plus appropriée pour chaque outil selon qu'il est plus intéressant d'avoir un vecteur de taille relativement imposante et complexe à synthétiser mais possédant une grande stabilité *in vivo*, ou un vecteur plus petit, mais moins stable. Notons toutefois que lorsque l'utilisation du peptide entier sera privilégiée, on préférera à la maurocalcine native son analogue synthétisé à partir d'acides aminés D (D-MCa) qui possède une structure identique mais permet de s'affranchir des effets pharmacologiques liés à la L-MCa.

Afin de préciser l'intérêt particulier de chaque CPP, certaines études restent à mener. Tout d'abord, les voies d'entrée de ces molécules au sein des cellules sont encore méconnues, et leur mise en évidence constitue l'une des priorités liées à la suite de ce projet. Ensuite, l'évaluation de la toxicité *in vivo* de ces CPP ainsi que de la biodistribution de MC$a_{\mathrm{UF1-9}}$ est une étape incontournable à la mise en place de tests *in vivo* et, éventuellement, d'études précliniques. Enfin, ces CPP étant, *a priori*, en mesure de pénétrer tout type cellulaire, un projet de couplage de la maurocalcine native à une séquence de ciblage a été mis en place. Il s'agira en effet de permettre la délivrance d'agents anticancéreux au sein de cellules tumorales gliales. Pour cela, la molécule thérapeutique sera couplée à la D-MCa ainsi qu'à tout ou partie de la chlorotoxine, issue du venin du scorpion *Leiurus quinquestriatus* et connue pour se fixer spécifiquement à la membrane de cellules de gliome (Graf *et al.*, 2012). Ceci vise à surmonter l'une des difficultés majeures rencontrées lors de l'administration de chimiothérapies dans le cas de gliomes : la grande résistance des cellules tumorales, non seulement capables d'expulser les molécules thérapeutique hors de leur cytoplasme mais également difficiles à atteindre à cause du phénomène de surpression existant au niveau de la tumeur. Ainsi, nous espérons tirer profit des remarquables propriétés d'accumulation et de rétention de la MCa au sein du compartiment intracellulaire mais également de la spécificité cellulaire de la chlorotoxine afin de mettre au point une molécule chimère plus efficace que les antitumoraux actuellement utilisés.

Cette thèse confirme, s'il en était besoin, l'immense potentiel thérapeutique des produits naturels et des toxines animales en particulier. Il est tout à fait légitime d'imaginer évaluer d'ici quelques années les effets d'une molécule chimère constituée uniquement de toxines animales couplées entre elles. Il pourrait s'agir par exemple de la maurocalcine (ou du petit CPP MC$a_{\mathrm{UF1-9}}$) à laquelle se grefferait à la fois à une toxine ciblant un type cellulaire particulier comme la chlorotoxine, et une toxine possédant une activité antitumorale intrinsèque telle que la melittine (Soman *et al.*, 2009). Il m'apparaît par conséquent primordial de poursuivre l'étude de la maurocalcine et de ses variants en tant que vecteurs de composés thérapeutiques.

Annexe

Utilité de l'hadrucalcine (toxine issue du venin du scorpion *Hadrurus gertschi*) pour la délivrance intracellulaire d'un nanobiosenseur de calcium

NANO LETTERS

Letter

pubs.acs.org/NanoLett

Cell-Penetrating Nanobiosensors for Pointillistic Intracellular Ca^{2+}-Transient Detection

Alsu I. Zamaleeva,[†,‡,§] Mayeul Collot,[∥,⊥,¶] Eloi Bahembera,[○,●] Céline Tisseyre,[○,●] Philippe Rostaing,[†,‡,§] Aleksey V. Yakovlev,[†,‡,§] Martin Oheim,[□,■] Michel de Waard,[○,●] Jean-Maurice Mallet,[∥,⊥,¶] and Anne Feltz*[,†,‡,§]

[†]Ecole Normale Supérieure, Institut de Biologie de l'ENS (IBENS), Paris F-75005, France

[‡]INSERM U1024, Paris F-75005, France

[§]CNRS UMR 8197, Paris F-75005, France

[∥]UPMC Université Paris 06, Ecole Normale Supérieure (ENS), Paris, F-75005 France

[⊥]CNRS UMR 7203, Paris F-75005, France

[¶]Laboratory of Biomolecules (LBM), Paris F-75005, France

[□]Brain Physiology Laboratory, Université Paris Descartes, PRES Sorbonne Paris Cité, Paris F-75006, France

[■]CNRS UMR 8118, Paris F-75006, France

[○]Inserm U836, Grenoble Neuroscience Institute, Research Group 3, LabEx Ion Channel Science and Therapeutics, BP170, 38042 Grenoble Cedex 09, France

[●]Université Joseph Fourier, Grenoble, France

Supporting Information

ABSTRACT: Small-molecule chemical calcium (Ca^{2+}) indicators are invaluable tools for studying intracellular signaling pathways but have severe shortcomings for detecting local Ca^{2+} entry. Nanobiosensors incorporating functionalized quantum dots (QDs) have emerged as promising alternatives but their intracellular use remains a major challenge. We designed cell-penetrating FRET-based Ca^{2+} nanobiosensors for the detection of local Ca^{2+} concentration transients, using commercially available CANdot565QD as a donor and CaRuby, a custom red-emitting Ca^{2+} indicator, as an acceptor. With Ca^{2+}-binding affinities covering the range of 3−20 μM, our CaRubies allow building sensors with a scalable affinity for detecting intracellular Ca^{2+} transients at various concentrations. To facilitate their cytoplasmic delivery, QDs were further functionalized with a small cell-penetrating peptide (CPP) derived from hadrucalcin (Had_{UF1-11}: H11), a ryanodine receptor-directed scorpion toxin identified within the venom of *Hadrurus gertschi*. Efficient internalization of QDs doubly functionalized with PEG5-CaRuby and H11 (in a molar ratio of 1:10:10, respectively) is demonstrated. In BHK cells expressing a *N*-methyl-D-aspartate receptor (NMDAR) construct, these nanobiosensors report rapid intracellular near-membrane Ca^{2+} transients following agonist application when imaged by TIRF microscopy. Our work presents the elaboration of cell-penetrating FRET-based nanobiosensors and validates their function for detection of intracellular Ca^{2+} transients.

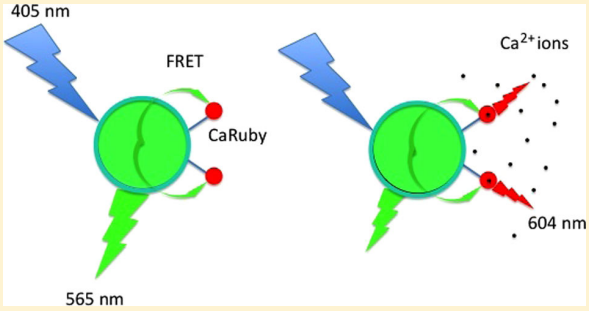

KEYWORDS: *Quantum dot biosensors, nanoparticle surface chemistry, FRET-based calcium probes, red-emitting calcium indicator, intracellular calcium fluorimetry, cell penetrating peptide*

Free calcium (Ca^{2+}) acts as a ubiquitous second messenger in numerous intracellular signaling pathways. Ca^{2+} controls cell metabolism, gene expression, vesicular trafficking and exocytosis to name a few functions. Ca^{2+} signals gain specificity by acting on different spatial and temporal scales. However, detecting fast and local Ca^{2+} concentration ($[Ca^{2+}]$) changes presents a major experimental challenge for microfluorimetric Ca^{2+} measurements with conventional Ca^{2+} indicators because only a few indicator molecules are localized in the small near-membrane volume invaded by local Ca^{2+} signaling events (see ref 1 for a measure of the external juxtacellular $[Ca^{2+}]$). Also, the intracellular diffusion of both the Ca^{2+} ions and the fluorescent Ca^{2+} indicator contributes to the rapid equilibration of Ca^{2+} gradients. Therefore, immobilizing and up-concentrat-

Received: November 12, 2013
Revised: April 16, 2014
Published: April 23, 2014

Table 1. Physical Parameters of QDs

QD donor	surface ligand	core/2 shells/surface ligand radius (nm)	QY %	ε^a (M^{-1} cm^{-1})	R_0 (Å) with CaRuby	r^e (Å) with PEG5 kDa
CANdot 565 organic	HDA/TOP/TOPO	~1.47[a] + 0.6[b] + ~1.2 = ~ 3.27	68	303764@405 nm 99040@543 nm		
CANdot 565-KC	50% pC/(pC + pK)	~1.8 ± 0.25[c]+	56	303764@405 nm	45	54
	85% pC/(pC + pK)	~2[d] = ~3.8	51	99040@543 nm		

[a]CdSe core estimated from the 543 nm first-exciton.[31] [b]CdS/ZnS shell.[32] [c]CdSe/CdS/ZnS by TEM (Supporting Information Figure S2). [d](pC+ pK) from ref 29 [e]See Figure 2b.

ing the Ca^{2+} sensitive dye, for example, by binding several molecules to a slowly diffusing dextran or nanoparticle is expected to report local [Ca^{2+}] transients more accurately.

The development of fluorescent inorganic colloidal nanoparticles (quantum dots, QDs, with a core diameter of 2−10 nm) that combine high brightness, photostability, and narrow emission spectra has been a breakthrough for single-particle imaging.[2,3] QDs are being used as molecular beacons to monitor enzymatic reactions,[2,4,5] track single vesicles following their endocytic uptake,[6] or for studying membrane diffusion of individual QD-tagged receptors,[6−9] all of which are experiments in which QDs report molecular position. Adding a sensing functionality to this localization information, for example, via Förster resonance energy transfer (FRET) opens new tracks for developing powerful tools in the fields of toxin detection, cell physiology, and pathology.[10−12]

Despite the synthesis and characterization of several nanobiosensors in vitro, their intracellular use is still challenging. Two major obstacles have impeded cell studies with FRET-based QD sensors: (i) in our experience, Ca^{2+} indicators that display low basal fluorescence and high sensitivity alone often show a disappointing performance once linked to a QD donor, and (ii) getting across the plasma membrane in a noninvasive way is another difficult step. Cationic liposomes yield generally low transfection rates while further inducing damaging cellular stress. The demonstration that ferromagnetic beads linked to Tat-derived cell penetrating peptides (CPPs) enter cells points to a potentially more efficient delivery strategy.[13] Besides penetratin, a peptide from the insect homeotic protein Antennapedia,[14,15] natural CPPs have been derived from scorpion toxins targeted toward the ryanodine receptor.[16−18] In contrast to the widely used positively charged CPPs,[19−21] these latter peptides efficiently drive internalization at nanomolar concentrations even if they are not charged.[22]

QDs functionalized with these peptides enter cells, the most potent ones delivering them into the cytoplasm rather than getting stuck in the endosomal pathway.[23,24] To date, no ionic nanobiosensor having both sensing and cell-penetrating function has been reported. The synthesis of such a nanobiosensor is complicated by the fact that QDs must be rendered water-soluble in a first step, bound to the Ca^{2+} indicator in a controlled manner (stoichiometry, donor/acceptor distance), and the CPPs linked to the surface as well.

Here, we design and validate both in vitro and in situ, a FRET-based cell-penetrating Ca^{2+} nanobiosensor combining a green fluorescent CdSe/CdS/ZnS (core/2 shells) QD donor with a red-fluorescent Ca^{2+} indicator of 3 μM affinity for Ca^{2+} binding (CaRubyMe).[25]

Our sensor is also functionalized with a H11 CPP from a scorpion toxin to facilitate its cytoplasmic entry. By building on the recently developed toolbox[25−27] of CaRuby Ca^{2+} indicators with affinities for Ca^{2+} binding ranging from 3 to 20 μM, Ca^{2+} biosensors with a similar architecture can be generated that will cover the entire biologically relevant range of local Ca^{2+} signals.

Results and Discussion. *Preparation of Hydrophilic Peptide-coated Quantum Dots.* We worked with a single, large batch of CANdots that combine high quantum yield (QY: 68%) and narrow peak emission at 565 ± 8 nm with a fwhm of 50 nm, that is, small size variability. With the first exciton peak at 543 nm, their emission overlaps with the absorption spectrum of our CaRubies (Supporting Information Figure S1), yielding a calculated Förster radius of 4.5 nm. We used a single batch, kept in hexane at 4 °C, that was stable over two years of experimentation.

To obtain hydrophilic QDs we used ligand exchange of the passivating trioctylphosphine/trioctylphosphine oxide (TOP/TOPO) layer by short phytochelatin-related peptides that bind by metal-affinity of a cysteine-rich $(FCC)_3$ adhesive domain to the CdZnSe QD surface.[28] The number of peptides that can be accommodated on a ~600 nm emitting QD is ~25−30 for the phytochelatin-like peptides[29,30] ensuring valence control. This amphiphilic peptide coating provides small diameter, monodisperse, negatively charged, hydrophilic nanoparticles with a high colloidal stability. Using transmission electron microscopy, we estimated their size and obtained a mean radius of 1.8 ± 0.25 nm (Supporting Information Figure S2). We showed that the average size of the core/2 shells particles remained the same while the total size of QDs slightly increased after the ligand exchange (Table 1).

To facilitate binding of biomolecules to the QDs we first introduced mixed SH-terminated and NH_2-terminated phytochelatin-like peptides (pC and pK, respectively, see legend of Figure 1 and Supporting Information Material and Methods) in a 1:1 ratio, half of them, the pCs, to be engaged in a SH/

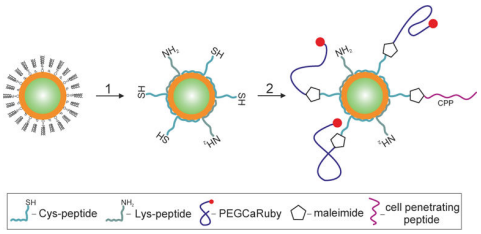

Figure 1. FRET-based Ca^{2+} biosensors. (Step 1) The QD TOP/TOPO passivating layer was replaced by a peptide coating made by mixing cysteine (SH function) and lysine (NH_2 function) terminated peptides (pC, Ac-CGSESGGSESG$(FCC)_3$F-amide; and pK, NH_2-KGSESGGSESG$(FCC)_3$F-amide respectively). Both components (hydrophobic QDs and peptides) were first dissolved in their respective solvents, pyridine and DMSO.[32] After mixing, surfactant exchange and peptide binding were initiated by raising the pH. (Step 2) Nanoparticles were further functionalized by adding CaRuby (red dots) and cell-penetrating peptides (CPP, purple wiggle) onto peptide-coated QDs using a SH/maleimide linking reaction.

dx.doi.org/10.1021/nl500733g | Nano Lett. 2014, 14, 2994−3001

maleimide linking reaction for further ligands conjugation[32] (Figure 1). The resulting constructs retained the photophysical properties of the original hydrophobic QDs (Table 1) with an only minor decrease of the fluorescence QY by ~12%. Because we aimed additionally at rendering the QDs membrane permeable by grafting CPPs, we considered increasing the relative number of pC peptides, but pC-only decorated QDs displayed a dramatically reduced QY. In contrast, by adding peptides in a 85:15% pC/pK ratio, some 25 SH sites are available for further conjugation[30] while keeping the QY at 51% (Table 1). We could thus investigate the properties of the FRET QDs-CaRuby pairs when varying acceptor to donor molar ratio (A/D).

Building of QD−CaRuby FRET pairs. CaRuby, the red-emitting Ca^{2+} indicator used here, is an extended rhodamine linked to a Ca^{2+}-chelating BAPTA moiety and having an additional linker arm (fluorescence excitation and emission peaks near 586 and 604 nm, respectively). Its Ca^{2+}-dependent fluorescence results from photoinduced electron transfer (PET) quenching. Ca^{2+} binding relieves PET and the fluorophore lights up.[26]

To functionalize QDs and avoid performing multiple reaction steps, we decided to synthesize a NH_2-terminated-PEG-CaRuby. The CaRuby PEGylation was efficiently performed with a commercially available NH_2-PEG-alkyne and CaRuby-N_3 by copper-catalyzed click chemistry. This compound was then transformed by a GMBS reaction into a maleimide-PEG-CaRuby for linkage. After binding maleimide-PEG-CaRuby to pC-sites of the QDs surface in a chosen QD/CaRuby stoichiometric ratio, the excess of unbound molecules of the dye was removed by dialysis (Supporting Information Figure S3).

Once assembled, we explored the spectral properties of the QD-CaRuby complexes in a 2 mM Ca^{2+} containing medium where FRET from the QD core to the rhodamine moiety is revealed. As illustrated in Figure 2 for QD-PEG5-CaRuby, FRET between the QD donor (D) and the CaRuby acceptor (A) increased with the number of CaRuby molecules, as expected for multiacceptor FRET.[33] We determined the A/D ratio by linear unmixing of the absorption spectra of the assembly using the pure A and D spectra. The A/D ratio was very close to the expected one, after correction for the fact that only 80% of the PEGs were labeled, implying an almost complete reaction. FRET efficiency ($E = 1 - F'_D/F_D$, where F'_D and F_D are the donor fluorescence intensities in the presence and absence of the acceptor, respectively) increased up to 80% while acceptor sensitization plateaued at 20% when the number of PEG5-CaRuby was increased up to 10. With a Förster radius of 4.5 nm, data of FRET efficiency (E) were well described by $E = nR_0^6/(nR_0^6 + r^6)$. Fit yielded a center-to-center distance r between donor and acceptor of 5.4 nm. This value results from the long 5 kDa PEG linker (black line in Figure 2b).

Ca^{2+} Sensing. Increasing the FRET efficiency should maximize the signal-to-noise ratio (SNR) for detecting Ca^{2+} transients. This can be achieved either by increasing A/D ratio (Figure 2a) or by reducing the D to A distance. To test the latter strategy, we prepared PEG-CaRubies of variable lengths: a custom-synthesized short <0.3 kDa NH_2-PEG-alkyne (see Supporting Information Materials and Methods, PEG0.3) and commercial 5 kDa (PEG5) and 10 kDa (PEG10) NH_2-PEG-alkyne. After coupling these CaRuby derivatives to the QDs, we systematically investigated the Ca^{2+}-sensitivity of the resulting FRET pairs with fluorimetric titrations in which we switched from a nominally Ca^{2+}-free solution (zero Ca^{2+} and 10 mM EGTA, peak photoluminescence, PL = F_0) to saturating (2 mM) Ca^{2+}: peak PL = F, and we used the relative increase in CaRuby fluorescence (dynamic range DR = $(F - F_0)/F_0$) as an index of sensitivity.

Although CaRuby retained a high Ca^{2+}-sensitivity after binding to PEG by click chemistry (DR = 60), unexpectedly, QD-CaRuby pairs built from short PEG0.3-CaRuby were largely Ca^{2+}-insensitive (DR = 0.5, n = 2). This was not due to the absence of FRET as evidenced by the donor quenching in the FRET pair (Figure 3b). Prasuhn et al.[34] obtained a Ca^{2+}-sensitive FRET signal when linking CaRuby to a QD through a short linker attached to a 6-His-terminated peptide composed of 2 α-helix turns. However, this signal was absent when a DHLA-PEG0.75 was intercalated instead of the peptide. This observation led us hypothesize that excessive proximity of the CaRuby to the QD surface perturbed Ca^{2+}-sensing. This should

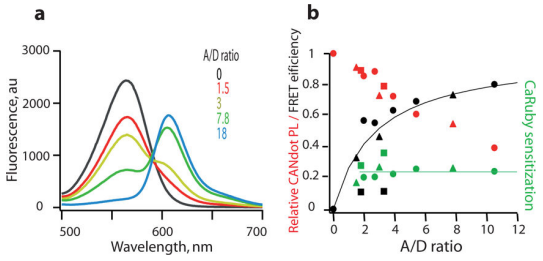

Figure 2. FRET upon 350 nm donor excitation, measured as donor quenching and acceptor sensitization, as a function of A/D ratio, at a constant $[Ca^{2+}]$ of 2 mM. (a) Series of mixed spectra obtained by increasing the number of PEG5-CaRubyMe while keeping QD concentration constant. A/D ratio was measured by absorbance at 407 and 581 nm to evaluate QD and CaRuby concentrations, respectively. (b) Relative donor quenching (QD photoluminescence, red) and FRET efficiency (black) after linear unmixing. Acceptor sensitization (F_{CaRuby} (exc@350 nm) $-F_{QD}$ (exc@350 nm)/(F_{CaRuby} (exc@535 nm) is also reported (green). Symbols ▲, ●, ■ show results from 3 experiments; black line: fit with $E = nR_0^6/(nR_0^6 + r^6)$ with R_0 = 45.5 Å and variable r = 54.2 ± 1.6 Å. The line in green shows average acceptor sensitization for A/D ratio between 2 and 12 (~22%).

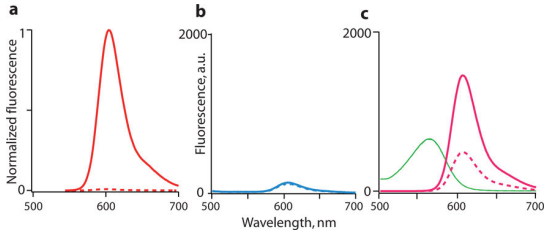

Figure 3. Emission spectra of FRET pairs in the presence (solid) and absence (dotted) of Ca^{2+}. (a) Normalized emission spectra of free PEG5-CaRuby. (b) Emission spectra of QD-PEG0.3-CaRuby with A/D = 18.8 (blue). (c) Spectra of QD-PEG5-CaRuby with A/D = 7.8. Acceptor and donor contribution to the spectra was separated by linear unmixing. FRET, estimated from QDs contribution to the spectrum, is unchanged (traces of QDs emission in 2 mM Ca^{2+} and 10 mM EGTA are superimposed). In panels b and c, QDs alone with no dye yielded a peak emission of about 2500 in both cases so allowing for direct comparison. In panel c, the same batch as in Figure 2 dark green trace.

dx.doi.org/10.1021/nl500733g | Nano Lett. 2014, 14, 2994−3001

not be the case when intercalating PEG5 or PEG10. However, even for these longer spacers the DR of the QD-CaRuby pair, while improving, remained quite low. At a 1:1 molar ratio, DR was ~1, as if CaRuby was still close to the QD surface, possibly due to the flexible PEG molecule backing upon itself. We therefore instead aimed at increasing the DR by systematically increasing the A/D ratio of PEG-CaRuby molecules bound onto a single QD, constructing stiffer "hairy ball" geometry.

Red fluorescence emission of QD-PEG5-CaRuby, either in response to direct excitation or via FRET, slowly but steadily increased with growing A/D ratio from 1 to 15 (Figure 4a; see

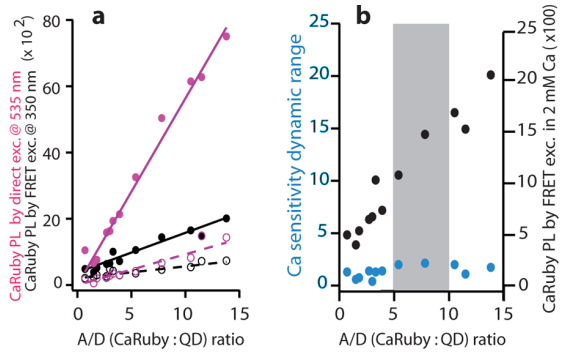

Figure 4. Ca^{2+} sensitivity of QD-PEG5-CaRuby as a function of A/D ratio. (a) CaRuby emission upon FRET excitation at 350 nm (in black) and direct excitation at 535 nm (in purple). Filled circles refer to measurements in a 2 mM Ca^{2+} and empty circles to measurements in 10 mM EGTA. FRET emission and PL obtained by direct excitation as well, linearly increase with an A/D ratio in the range 1−15 (PL by FRET in Ca^{2+} = 380 + 119 A/D ratio; FRET in EGTA = 200 + 36 A/D ratio). With CaRuby direct excitation, PL in Ca = 200 + 540 A/D ratio; in EGTA = 2 + 92 A/D ratio. (b) Summary graph displaying FRET absolute value increase (in 2 mM Ca^{2+}; black circles) whereas DR (blue dots) is constant when molar ratio was varied between 0 and 15. All data refer to the same QDs concentration. Data from 4 batches of QD-PEG5-CaRuby.

Supporting Information Figure S4 for QD-PEG10-CaRuby). In the same range, between 1 and 15 A/D, FRET efficiency (measured in 10 mM EGTA) also increased. As a result, the DR from the FRET-activated CaRuby was constant but low at ~2 (Figure 4b). With direct excitation, the DR was about twice as large but it never exceeded 5. Thus, while the DR of CaRuby is much reduced once linked to QDs, an A/D ratio in the range of 5−15 produces a Ca^{2+}-dependent fluorescence large enough to allow efficient Ca^{2+}-sensing (Figure 4b). As we aimed at visualizing and hence localize nanobiosensors inside the cell, even at resting intracellular $[Ca^{2+}]$, we finally retained an A/D ratio of 5−10 as a compromise for in situ experiments. Noticeably, these constructs proved to be stable over at least 2 months.

Next, we examined if the Ca^{2+}-binding affinity of CaRubyMe was changed by the nanosensor assembly. Samples of QD-PEG5-CaRubyMe (A/D ratio = 9) prepared at concentrations of 0.5 μM CaRuby were mixed with Ca^{2+} concentrations increasing from 0.1 up to 1000 μM (Figure 5a). Hill fit with fluorescence peaks from two separate experiments confirmed a K_d of 2.9 ± 0.3 μM (Figure 5b), not distinguishable from the 3.4 ± 0.5 μM, previously reported for CaRubyMe alone. Thus, despite its attachment in proximity of the highly charged QDs surface, CaRubyMe affinity for Ca^{2+} was unaltered. Furthermore, the k_{on} for Ca^{2+} binding to the nanobiosensors

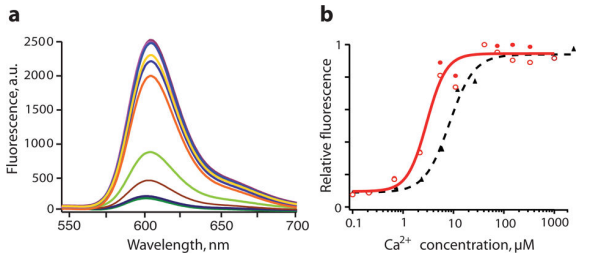

Figure 5. Fluorimetric titration against $[Ca^{2+}]$ of QD-PEG5-CaRubyMe complexes (A/D ratio = 9; buffer containing (in mM): 100 KCl and 30 MOPS, pH 7.2). (a) Superimposed fluorescence curves in the presence of increasing concentrations of Ca^{2+} as plotted in the dose−response curve on the right (red dots: direct excitation of CaRuby at 535 nm). (b) Peak fluorescence versus $[Ca^{2+}]$ for two independent titrations, filled and empty red dots, respectively. Red continuous line is Hill fit of all in cuvette data points, K_d = 2.9 ± 0.3 μM. Black triangles and dotted line show in cell-Ca2+ calibration using flow cytometry yielding a K_d of 7.6 ± 1.4 μM.

(calculated from the K_d and stopped-flow measurement of the k_{off}: ~150 s^{-1}) was of the order of 10^8 M^{-1} s^{-1}, as expected for BAPTA-based Ca^{2+} chelator.[35,36] This high k_{on} value makes our sensors an adequate tool for detecting fast $[Ca^{2+}]_i$ transients (Supporting Information Figure S5).

Internalization of Nanobiosensors. To promote the intracellular translocation of functionalized QDs, we used CPPs of specially high efficiency that we recently identified, derived from toxins targeted against the intracellular ryanodine receptor.[22] Uptake of H11 (Smartox Biotechnology, Saint Martin d'Hères, France), a CPP derived from the scorpion toxin hadrucalcin, was already significant at a concentration as low as 500 nM (Supporting Information Figure S6). Incubation of cells with 100 nM QDs functionalized with 5−10 CPPs brings CPP local concentration in this range. Baby hamster kidney cells (BHK-21) were incubated for 2 h with 100 nM QDs doubly functionalized with PEG5-CaRuby and H11 in the molar ratio 1:10:10 and the internalization efficiency was evaluated by live-cell confocal imaging. The nucleus and the plasma membrane were counterstained to better assess the cytoplasmic location of the QDs (Figure 6a).

As seen on the confocal section shown in Figure 6b, QD-CaRuby-H11 complexes penetrated inside the cells and were distributed throughout the cytoplasm. However, compared to conventional chemical Ca^{2+} indicators our sensors have a pointillistic distribution. This pointillistic distribution of our sensors provides a localized read-out of $[Ca^{2+}]$ at discrete points where the CaRuby has been up-concentrated. Internalization of functionalized QDs occurred without damaging side effects (Supporting Information Figure S7).

Because the number of internalized QDs varied from cell to cell, a first quantification of the internalized QDs was carried out using imaging flow cytometry. For the analysis QDs located in close vicinity to the plasma membrane were subtracted whether on its extracellular or intracellular sides. A number of QDs without CPPs were internalized; QDs internalization, however, as illustrated in Figure 6c, is almost doubled by CPPs addition, with no further improvement when going from 5 to 10 CPPs.

Electron micrographs of BHK cells loaded with QD-CaRuby-H11 complexes show groups of ~15−20 QDs dispersed over an area of ~500 nm diameter probably corresponding to the spots observed in confocal microscopy. Though at this point we

dx.doi.org/10.1021/nl500733g | Nano Lett. 2014, 14, 2994−3001

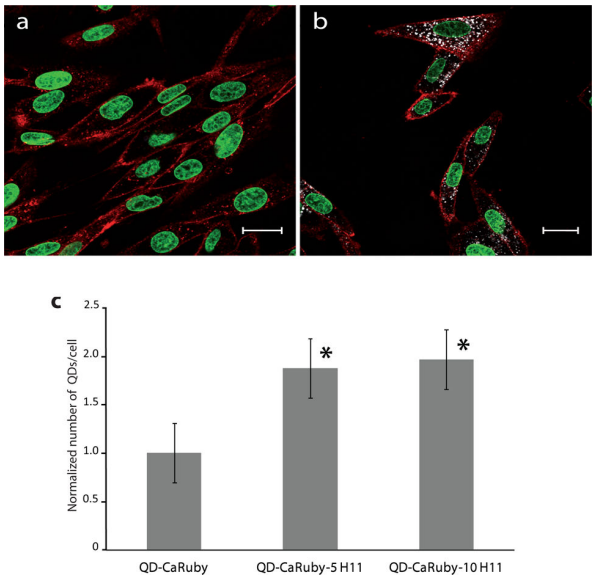

Figure 6. Cell penetration of QDs doubly functionalized with CaRuby and cell penetrating peptide H11. (a) Confocal microscopy section of live BHK-21 cells with Hoechst nuclear staining (green) and concanavalin-Alexa 647 membrane staining (red). (b) BHK-21 cells with internalized QDs. Gray dots show QDs-CaRuby-H11 emission upon direct excitation of CaRuby at 561 nm. Scale bar, 20 μm. (c) Imaging flow cytometry analysis of QDs penetration. Normalized average number of internalized QDs per cell for QD-CaRuby alone, QD-CaRuby-5H11, and QD-CaRuby-10H11 complexes, respectively. Measurements made upon CaRuby direct excitation at 561 nm. Data show mean ± s.e.m for 100 cells of each sample; *—p < 0,05 compared to QD-CaRuby.

do not know their exact path for cell entry, we show QDs to be not enclosed in a membrane-delimited compartment (Figure 7). This is the conclusion attained with a TEM image poorly contrasted to better see the small size QDs (Figure 7) and as well of an TEM image where the contrast has been increased to the point when some uranyl acetate deposits are formed (Supporting Information Figure S8). Thus, our nanobiosensors are exposed to the intracellular medium and hence should be able to report the local cytoplasmic Ca^{2+} concentration.

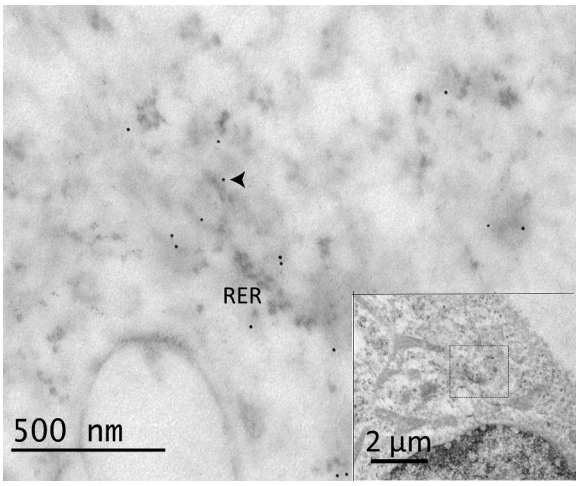

Figure 7. EM micrograph of QD-CaRuby-H11 complexes internalized in aBHK cell. Image shows zoom on the region of interest identified on the inset image. Individual QDs (arrow) appear as electron-dense spots of ~5 nm diameter, dispersed throughout the cytoplasm. Larger and less dense punctiform structures are the rough endoplasmic reticulum (RER) and ribosomes.

Intracellular Ca^{2+} Nanobiosensing. To demonstrate the Ca^{2+}-sensing ability of our sensors inside live cells we used HEK293 cells expressing *N*-methyl-D-aspartate receptors (NMDARs). These are plasma membrane cation-permeable channels mediating Ca^{2+} influx upon activation by agonist binding. Our nanobiosensors were loaded as described above, followed by the resuspension of the cells in a HEPES-buffered medium for time-lapse fluorescence measurements. External $[Ca^{2+}]$ was raised to 10 mM to maximize Ca^{2+} entry upon receptors activation.

After loading of QD-CaRuby-H11 complexes, some QDs remained attached to the external side of plasma membrane, which resulted in a high background fluorescence. This background was efficiently reduced by adding to the extracellular saline 40 μM Cu^{2+}, an effective QDs and CaRuby quencher.[25,37] The Ca^{2+} binding affinity (K_d) to the nanosensor was slightly increased, an effect described for other Ca^{2+} indicators and possibly related to the higher viscosity of the intracellular medium (see Figure 5b dotted line).

Injection to the cell suspension of the NMDAR agonists glutamate and glycine in the presence of external Ca^{2+} produced an increase of the CaRuby fluorescence (Figure 8c, red trace), as expected from the NMDAR-mediated Ca^{2+} influx (Figure 8a), confirming the intracellular responsiveness of our Ca^{2+} nanobiosensors.

Preincubation of the cells with APV, a NMDAR antagonist, (Figure 8b) almost completely abolished the agonist-evoked

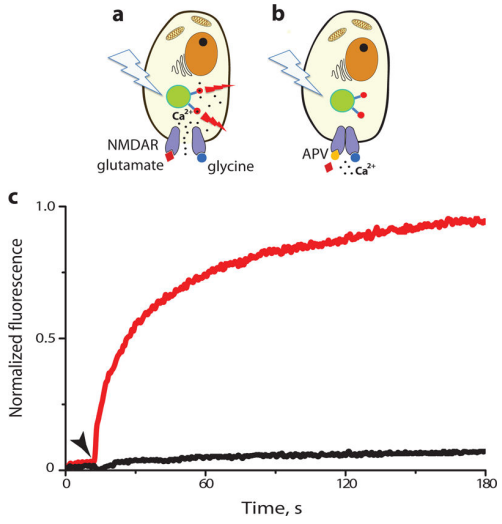

Figure 8. Intracellular $[Ca^{2+}]$ measurement in a suspension of HEK293 cells transfected with NMDARs and incubated with 100 nM nanobiosensors. Schematic representation of (a) NMDAR activation by coapplication of agonists (100 μM glutamate and 20 μM glycine) followed by Ca^{2+} influx into the cell and (b) of the NMDAR blockade by an antagonist (100 μM APV) preventing Ca^{2+} influx upon application of the agonists. (c) Intracellular Ca^{2+}-dependent acceptor fluorescence as a function of time. Arrowhead marks application of agonists in absence of antagonist or after blocking NMDAR by APV, red and black traces, corresponding to conditions (a) and (b) respectively (2 replicates in 3 independent experiments).

dx.doi.org/10.1021/nl500733g | *Nano Lett.* 2014, 14, 2994−3001

Ca^{2+} response (Figure 8c, black trace). Likewise, no fluorescence increase was observed when applying agonists in Ca^{2+} free medium (data not shown). The Ca^{2+} response of our sensors is similar to that obtained using conventional dyes and cells, expressing the same subunits of NMDA receptor-channels.[38] We thus show that our QD-based Ca^{2+} nanobiosensors can specifically detect Ca^{2+} changes in a biologically relevant paradigm of receptor activation.

Finally, to demonstrate the ability of developed nanobiosensors to detect local subcellular Ca^{2+} signals in live cells, we loaded QD-CaRuby-H11 nanobiosensors into BHK cells stably expressing the NR1 and NR2 subunits of the NMDAR.[38] To visualize near-membrane QD sensors, we used total internal reflection fluorescence (TIRF) microscopy, simultaneously detecting in the green and red channel upon 405 and 568 nm evanescent-wave excitation on a custom prism-type VA TIRF microscope,[39] (Supporting Information Figure S9). To reduce noise caused by extracellularly attached QDs, QD-loaded cells were trypsinized and replated on quartz coverslips displaying a low autofluorescence. After trypsinization, transient $CuSO_4$ addition to BHK cells is not necessary unless an improved signal-to-noise ratio is sought (see Supporting Information Figure S10 illustrating the characteristics of the Cu^{2+} effect).

Evanescent-wave illumination allowed visualizing only those nanosensors close to the basal cell membrane with a high contrast, permitting readout of the fluorescence emitted by QD-sensors (Figure 9a,b). Ca^{2+} transients were evoked by NMDAR activation (100 μM glutamate, 20 μM glycine and 5 mM $CaCl_2$) and responses continuously recorded at 4 Hz during 3 min before and during agonists application. Figure 9c shows the Ca^{2+} transients detected at single sites, after background subtraction and correction for photobleaching, expressed as F/F_0, where F_0 is the (local) basal value before NMDAR activation. Our nanosensors read out local $[Ca^{2+}]$ transients that were distinct both, between cells (cell 1 and cell 2 in Figure 9c,d) and at the subcellular level, some displaying an F/F_0 up to 2.0 whereas some sensors nearby were silent and others show intermediary values.

Interestingly among the detected Ca^{2+} transients, the F/F_0 peak value read in a single cell at saturating concentration of agonists here applied was 2.2 ± 0.9 (ranging from 1.4 to 4.7, n = 14 cells, on 6 distinct coverslips from 4 distinct batches of cells). In cell 1, time constants at three regions of interest were 500, 700, and 900 ms, from top to bottom, respectively. In addition to variability in the agonist application, the distance from the biosensor to the Ca^{2+} source may account for such local variations. Along this line, the nonresponsiveness of red-emitting QDs is coherent with a localization in a cytoplasmic region ensuing no change in $[Ca^{2+}]$, but also alternatively with a localization in endosomes because this structure has a $[Ca^{2+}]$ saturating for the probe. Average kinetics of fluorescence transients recorded with QD-CaRuby-H11 were similar to those obtained with a conventional bulk-loaded small-molecule chemical Ca^{2+} indicator, X-rhod-1, AM, when the same cell was stimulated again following dye loading at the end of the experiment (Supporting Information Figure S10). Control applications in Ca^{2+}-free extracellular saline failed to produce measurable fluorescence changes.

Taken together, these experiments comfort our interpretation that QD-CaRuby-H11 sensors indeed detect cytoplasmic Ca^{2+} transients evoked by NMDAR-mediated Ca^{2+} influx across the plasma membrane. Furthermore, sequential applications of

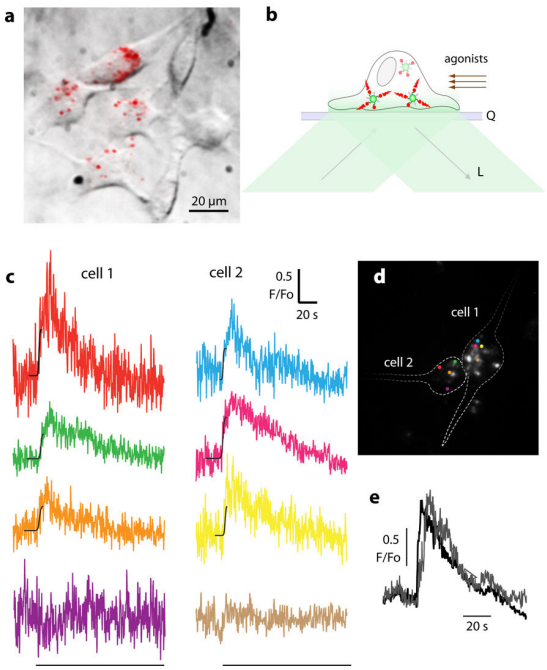

Figure 9. Read-out of local Ca^{2+} transients. (a) Localization of internalized biosensors (QD-CaRuby-H11 in a ratio 1:10:10) on the superimposed bright-field and time-averaged TIRF image of cultured BHK cells. (b) Schematic representation of the TIRF imaging of Ca^{2+} nanobiosensors. Confinement of excitation light (L) excites only fluorophores present in a ~100 nm layer above the quartz coverslip (Q). Among the three nanosensors schematized, only two are fluorescent while the third one is out-of-reach of the evanescent wave. (c) Local Ca^{2+} detection. Traces show simultaneously acquired transients in distinct spots in response to bath application of saturating concentrations of NMDAR agonists (during bottom black line) at various points in two neighboring cells "1" and "2" (left and right columns respectively); 700 images, t_{exp} = 250 ms. (d) Pseudocolor-overlay of spot positions on the cell outline. (e) Repetitive simulation evokes reversible Ca^{2+} transients. Superimposed traces, recorded at a same point, are responses to two successive bath applications of NMDAR agonists at a saturating concentration within between a 15 min long continuous bath perfusion of CTR saline for recovery from desensitization. Ca^{2+} signals were recorded with (c) and without (e) a previous transient application of Cu^{2+}.

NMADR agonists produced stereotyped reversible Ca^{2+} transients at the same site as expected (Figure 9e).

Compared to classical chemical Ca^{2+} indicators, FRET-based nanobiosensors are attractive for probing microdomain Ca^{2+} signals because, (i) QD-based, they combine high brightness with low cytoplasmic mobility[40−43] and low photobleaching compared to organic Ca^{2+} probes. (ii) They further allow localizing by green fluorescence candidate sites even at resting Ca^{2+}. (iii) With conventional chemical small-molecule Ca^{2+} indicators and genetically encoded Ca^{2+} indicators (GECIs), only a few indicator molecules are localized in the small near-membrane volume invaded by local Ca^{2+} signaling events.[44] Here, covalently linking the Ca^{2+} sensor to the QD surface locally up-concentrates the indicator up to the approximately millimolar range, a concentration that cannot be attained by simple aqueous dilution, thus (iv) permitting to attain signal-to-noise ratios favorable for the detection of fast and local Ca^{2+} transients. (v) Average cytoplasmic concentrations is maintained low, and hence exogenous Ca^{2+} buffer capacity. (vi)

dx.doi.org/10.1021/nl500733g | Nano Lett. 2014, 14, 2994−3001

Compared to other red-emitting low-affinity Ca^{2+} probes like Xrhod-5F or CaRuby-Cl alone, their large molecular weight prevents mitochondrial internalization and light-induced cytotoxicity.

Here, using a commercial QD donor, our CaRuby as a red-emitting Ca^{2+}-sensitive acceptor and a cell-penetrating peptide-derived cytoplasmically active toxin to facilitate cell entry, our Ca^{2+} nanobiosensors combine ease of synthesis, controlled stoichiometric assembly, high colloidal stability and efficient cytoplasmic delivery. Added to the extracellular saline, these Ca^{2+} nanobiosensors are internalized within 2 h to display a punctate cytoplasmic distribution when imaged with TIRF microscopy on the day thereafter, after replating. In a cell line stably expressing the Ca^{2+}-permeable NMDA receptor channel, we detected heterogeneous intracellular Ca^{2+} transients following receptor-activation with specific agonists, thus providing the first validation of Ca^{2+} nanobiosensors for subcellular biological Ca^{2+} imaging in live cells.

The next logical step is the targeting of our sensor by its further functionalization with specific antibodies to a high-conductivity Ca^{2+} channel such as the RyRs (400 pS) or NMDARs (50 pS) and perform optical single-channel recording.

■ ASSOCIATED CONTENT

Supporting Information

Eleven supplementary figures and their legends, detailed materials and methods, and abbreviations. This material is available free of charge via the Internet at http://pubs.acs.org.

■ AUTHOR INFORMATION

Corresponding Author

*E-mail: anne.feltz@ens.fr.

Present Addresses

(M.C.) UMR 7213 CNRS, Laboratoire de Biophotonique et Pharmacologie 74 route du Rhin, CS 60024, F - 67401 Illkirch 67400, France.

(A.V.Y) Biology Faculty, Kazan Federal University, Kazan, Russia

(A.I.Z., secondary address) Biomaterials and Nanomaterials Group, Department of Microbiology, Kazan Federal University, Kazan, Republic of Tatarstan, RF, 420008.

Author Contributions

The manuscript was written through contributions of all authors. All authors have given approval to the final version of the manuscript.

A.I.Z. and M.C. contributed equally to the work.

Notes

The authors declare no competing financial interest.

■ ACKNOWLEDGMENTS

We want to thank Institut Curie for giving us access to its Flow Cytometry platform, and especially to Mrs. Z. Maciorowski for her help in initiating us to this technique. O. Hernandez-Cubero helped us in the analysis of the TEM images. Christian Boudier (UMR7213 Laboratoire de Biophotonique et Pharmacologie, Strasbourg) a permis les expériences de "stopped flow". We thank Pierre Paoletti's group (IBENS, Paris) for providing the NMDAR (NR1 and NR2B) plasmids. We specially thank Dr. H. Bräuner-Osborne and J. Egebjerg (University of Copenhagen) for providing the BHK cell line stably expressing NR1 and NR2 subunits of the NMDA receptor that also proved to be strongly adherent to quartz coverslips making possible the present TIRF experiments. This work has received support under the program "Investissements d'Avenir" launched by the French government and implemented by the ANR (ANR-10-LABX-54 MEMO LIFE, ANR-11-IDEX-001-02-PSL). This work was supported by the French Agence National de la Recherche (ANR P3N, nanoFRET^2 grant, to A.F., J.M.M., M.d.W., M.O.) and the European Union (FP6 STRP AUTOSCREEN grant and FP7 ERA-NET NeuronNANOSYN grant to M.O.). M.O. is supported by the FranceBioImaging initiative (FBI).

■ REFERENCES

(1) Etter, E. F.; Kuhn, M. A.; Fay, F. S. *J. Biol. Chem.* **1994**, *269*, 10141−9.

(2) Alivisatos, A. P.; Gu, W.; Larabell, C. *Annu. Rev. Biomed Eng.* **2005**, *7*, 55−76.

(3) Michalet, X.; Pinaud, F. F.; Bentolila, L. A.; Tsay, J. M.; Doose, S.; Li, J. J.; Sundaresan, G.; Wu, A. M.; Gambhir, S. S.; Weiss, S. *Science* **2005**, *307*, 538−44.

(4) Biebricher, A.; Wende, W.; Escude, C.; Pingoud, A.; Desbiolles, P. *Biophys. J.* **2009**, *96*, L50−2.

(5) Lidke, D. S.; Nagy, P.; Heintzmann, R.; Arndt-Jovin, D. J.; Post, J. N.; Grecco, H. E.; Jares-Erijman, E. A.; Jovin, T. M. *Nat. Biotechnol.* **2004**, *22*, 198−203.

(6) Zhang, Q.; Li, Y.; Tsien, R. W. *Science* **2009**, *323*, 1448−53.

(7) Dahan, M.; Levi, S.; Luccardini, C.; Rostaing, P.; Riveau, B.; Triller, A. *Science* **2003**, *302*, 442−5.

(8) Saint-Michel, E.; Giannone, G.; Choquet, D.; Thoumine, O. *Biophys. J.* **2009**, *97*, 480−9.

(9) Triller, A.; Choquet, D. *Neuron* **2008**, *59*, 359−74.

(10) Delehanty, J. B.; Susumu, K.; Manthe, R. L.; Algar, W. R.; Medintz, I. L. *Anal. Chim. Acta* **2012**, *750*, 63−81.

(11) Sapsford, K. E.; Berti, L.; Medintz, I. L. *Angew. Chem., Int. Ed.* **2006**, *45*, 4562−89.

(12) Wang, Y.; Chen, L. *Nanomedicine* **2011**, *7*, 385−402.

(13) Josephson, L.; Tung, C. H.; Moore, A.; Weissleder, R. *Bioconjugate Chem.* **1999**, *10*, 186−191.

(14) Derossi, D.; Joliot, A. H.; Chassaing, G.; Prochiantz, A. *J. Biol. Chem.* **1994**, *269*, 10444−50.

(15) Joliot, A.; Pernelle, C.; Deagostini-Bazin, H.; Prochiantz, A. *Proc. Natl. Acad. Sci. U.S.A.* **1991**, *88*, 1864−8.

(16) Esteve, E.; Smida-Rezgui, S.; Sarkozi, S.; Szegedi, C.; Regaya, I.; Chen, L.; Altafaj, X.; Rochat, H.; Allen, P.; Pessah, I. N.; Marty, I.; Sabatier, J. M.; Jona, I.; De Waard, M.; Ronjat, M. *J. Biol. Chem.* **2003**, *278*, 37822−31.

(17) Poillot, C.; Bichraoui, H.; Tisseyre, C.; Bahembera, E.; Andreotti, N.; Sabatier, J. M.; Ronjat, M.; De Waard, M. *J. Biol. Chem.* **2012**, *287*, 17331−17342.

(18) Poillot, C.; Dridi, K.; Bichraoui, H.; Pecher, J.; Alphonse, S.; Douzi, B.; Ronjat, M.; Darbon, H.; De Waard, M. *J. Biol. Chem.* **2010**, *285*, 34168−80.

(19) Derossi, D.; Chassaing, G.; Prochiantz, A. *Trends Cell Biol.* **1998**, *8*, 84−7.

(20) Boeneman, K.; Delehanty, J. B.; Blanco-Canosa, J. B.; Susumu, K.; Stewart, M. H.; Oh, E.; Huston, A. L.; Dawson, G.; Ingale, S.; Walters, R.; Domowicz, M.; Deschamps, J. R.; Algar, W. R.; Dimaggio, S.; Manono, J.; Spillmann, C. M.; Thompson, D.; Jennings, T. L.; Dawson, P. E.; Medintz, I. L. *ACS Nano* **2013**, *7*, 3778−96.

(21) Walrant, A.; Vogel, A.; Correia, I.; Lequin, O.; Olausson, B. E.; Desbat, B.; Sagan, S.; Alves, I. D. *Biochim. Biophys. Acta* **2012**, *1818*, 1755−63.

(22) Tisseyre, C.; Bahembera, E.; Dardevet, L.; Sabatier, J. M.; Ronjat, M.; De Waard, M. *Pharmaceuticals* **2013**, *6*, 320−339.

(23) Ram, N.; Texier-Nogues, I.; Pernet-Gallay, K.; Poillot, C.; Ronjat, M.; Andrieux, A.; Arnoult, C.; Daou, J.; De Waard, M. *Int. J. Biomed. Nanosci. Nanotechnol.* **2011**, *2*, 12−32.

dx.doi.org/10.1021/nl500733g | *Nano Lett.* 2014, 14, 2994−3001

(24) Ram, N.; Weiss, N.; Texier-Nogues, I.; Aroui, S.; Andreotti, N.; Pirollet, F.; Ronjat, M.; Sabatier, J. M.; Darbon, H.; Jacquemond, V.; De Waard, M. *J. Biol. Chem.* **2008**, *283*, 27048−56.
(25) Collot, M.; Loukou, C.; Yakovlev, A. V.; Wilms, C. D.; Li, D.; Evrard, A.; Zamaleeva, A.; Bourdieu, L.; Leger, J. F.; Ropert, N.; Eilers, J.; Oheim, M.; Feltz, A.; Mallet, J. M. *J. Am. Chem. Soc.* **2012**, *134*, 14923−31.
(26) Gaillard, S.; Yakovlev, A.; Luccardini, C.; Oheim, M.; Feltz, A.; Mallet, J. M. *Org. Lett.* **2007**, *9*, 2629−32.
(27) Luccardini, C.; Yakovlev, A. V.; Pasche, M.; Gaillard, S.; Li, D.; Rousseau, F.; Ly, R.; Becherer, U.; Mallet, J. M.; Feltz, A.; Oheim, M. *Cell Calcium* **2009**, *45*, 275−83.
(28) Pinaud, F.; Michalet, X.; Bentolila, L. A.; Tsay, J. M.; Doose, S.; Li, J. J.; Iyer, G.; Weiss, S. *Biomaterials* **2006**, *27*, 1679−87.
(29) Clarke, S.; Pinaud, F.; Beutel, O.; You, C.; Piehler, J.; Dahan, M. *Nano Lett.* **2010**, *10*, 2147−54.
(30) Iyer, G.; Pinaud, F.; Tsay, J.; Weiss, S. *Small* **2007**, *3*, 793−8.
(31) Yu, W. W.; Qu, L.; Guo, W.; Peng, X. *Chem. Mater.* **2003**, *15*, 2854−2860.
(32) Pinaud, F.; King, D.; Moore, H. P.; Weiss, S. *J. Am. Chem. Soc.* **2004**, *126*, 6115−23.
(33) Yakovlev, A. V.; Zhang, F.; Zulqurnain, A.; Azhar-Zahoor, A.; Luccardini, C.; Gaillard, S.; Mallet, J. M.; Tauc, P.; Bro chon, J. C.; Parak, W. J.; Feltz, A.; Oheim, M. *Langmuir* **2009**, *25*, 3232−9.
(34) Prasuhn, D. E.; Feltz, A.; Blanco-Canosa, J. B.; Susumu, K.; Stewart, M. H.; Mei, B. C.; Yakovlev, A. V.; Loukov, C.; Mallet, J. M.; Oheim, M.; Dawson, P. E.; Medintz, I. L. *ACS Nano* **2010**, *4*, 5487−97.
(35) Kao, J. P.; Tsien, R. Y. *Biophys. J.* **1988**, *53*, 635−9.
(36) Jackson, A. P.; Timmerman, M. P.; Bagshaw, C. R.; Ashley, C. C. *FEBS Lett.* **1987**, *216*, 35−9.
(37) Xie, H.-Y.; Liang, J.-G.; Zhang, Z.-L.; Liu, Y.; He, Z.-K.; Pang, D.-W. *Spectrochim. Acta, Part A* **2004**, *60*, 2527−2530.
(38) Hansen, K. B.; Brauner-Osborne, H.; Egebjerg, J. *Comb Chem. High Throughput Screening* **2008**, *11*, 304−15.
(39) van't Hoff, M.; Reuter, M.; Dryden, D. T.; Oheim, M. *Phys. Chem. Chem. Phys.* **2009**, *11*, 7713−7720.
(40) Courty, S.; Luccardini, C.; Bellaiche, Y.; Cappello, G.; Dahan, M. *Nano Lett.* **2006**, *6*, 1491−5.
(41) Grünwald, D.; Hoekstra, A.; Dange, T.; Buschmann, V.; Kubitscheck, U. *ChemPhysChem* **2006**, *7*, 812−815.
(42) Yum, K.; Na, S.; Xiang, Y.; Wang, N.; Yu, M. F. *Nano Lett.* **2009**, *9*, 2193−2198.
(43) Delehanty, J. B.; Bradburne, C. E.; Susumu, K.; Boeneman, K.; Mei, B. C.; Farrell, D.; Blanco-Canosa, J. B.; Dawson, P. E.; Mattoussi, H.; Medintz, I. L. *J. Am. Chem. Soc.* **2011**, *133*, 10482−10489.
(44) Oheim, M.; van't Hoff, M.; Feltz, A.; Zamaleeva, A.; Mallet, J. M.; Collot, M. *Biochim. Biophys. Acta* **2014**.

Bibliographie

Bibliographie

Altafaj, X., France, J., Almassy, J., Jona, I., Rossi, D., Sorrentino, V., Mabrouk, K., De Waard, M., & Ronjat, M. 2007. Maurocalcine interacts with the cardiac ryanodine receptor without inducing channel modification. *Biochem. J.*, **406**(2), 309–315. [PubMed Central :PMC1948973] [DOI :10.1042/BJ20070453] [PubMed :17537000]. *Cité page 23*

Aroui, S., Ram, N., Appaix, F., Ronjat, M., Kenani, A., Pirollet, F., & De Waard, M. 2009. Maurocalcine as a non toxic drug carrier overcomes doxorubicin resistance in the cancer cell line MDA-MB 231. *Pharm. Res.*, **26**(4), 836–845. [PubMed Central :PMC2820506] [DOI :10.1007/s11095-008-9782-1] [PubMed :19083085]. *Cité page 26*

Arya, S. K., Guo, C., Josephs, S. F., & Wong-Staal, F. 1985. Trans-activator gene of human T-lymphotropic virus type III (HTLV-III). *Science*, **229**(4708), 69–73. [PubMed :2990040]. *Cité page 10*

Boisseau, S., Mabrouk, K., Ram, N., Garmy, N., Collin, V., Tadmouri, A., Mikati, M., Sabatier, J. M., Ronjat, M., Fantini, J., & De Waard, M. 2006. Cell penetration properties of maurocalcine, a natural venom peptide active on the intracellular ryanodine receptor. *Biochim. Biophys. Acta*, **1758**(3), 308–319. [DOI :10.1016/j.bbamem.2006.02.007] [PubMed :16545341]. *2 citations pages 24 et 121*

Boucrot, E., & McMahon, H. T. 2011. [Nucleation of clathrin-coated pits - « membrane sculptors » at work]. *Med Sci (Paris)*, **27**(2), 122–125. [DOI :10.1051/medsci/2011272122] [PubMed :21382316]. *3 citations pages , 14, et 15*

Cantelmo, A. R., Cammarota, R., Noonan, D. M., Focaccetti, C., Comoglio, P. M., Prat, M., & Albini, A. 2010. Cell delivery of Met docking site peptides inhibit angiogenesis and vascular tumor growth. *Oncogene*, **29**(38), 5286–5298. [PubMed Central :PMC3007100] [DOI :10.1038/onc.2010.267] [PubMed :20603611]. *Cité page 20*

Cardone, R. A., Casavola, V., & Reshkin, S. J. 2005. The role of disturbed pH dynamics and the Na+/H+ exchanger in metastasis. *Nat. Rev. Cancer*, **5**(10), 786–795. [DOI :10.1038/nrc1713] [PubMed :16175178]. *2 citations pages 47 et 122*

Castle, N. A., London, D. O., Creech, C., Fajloun, Z., Stocker, J. W., & Sabatier, J. M. 2003. Maurotoxin : a potent inhibitor of intermediate conductance Ca2+-activated potassium channels. *Mol. Pharmacol.*, **63**(2), 409–418. [PubMed :12527813]. *Cité page 5*

Catterall, W. A. 2000. From ionic currents to molecular mechanisms : the structure and function of voltage-gated sodium channels. *Neuron*, **26**(1), 13–25. [PubMed :10798388]. *Cité page 4*

Conner, S. D., & Schmid, S. L. 2003. Regulated portals of entry into the cell. *Nature*, **422**(6927), 37–44. [DOI :10.1038/nature01451] [PubMed :12621426]. *Cité page 14*

Cragg, G. M., & Newman, D. J. 2013. Natural products : a continuing source of novel drug leads. *Biochim. Biophys. Acta*, **1830**(6), 3670–3695. [PubMed Central :PMC3672862] [DOI :10.1016/j.bbagen.2013.02.008] [PubMed :23428572]. *Cité page 3*

DeBin, J. A., Maggio, J. E., & Strichartz, G. R. 1993. Purification and characterization of chlorotoxin, a chloride channel ligand from the venom of the scorpion. *Am. J. Physiol.*, **264**(2 Pt 1), C361–369. [PubMed :8383429]. *Cité page 6*

Derossi, D., Joliot, A. H., Chassaing, G., & Prochiantz, A. 1994. The third helix of the Antennapedia homeodomain translocates through biological membranes. *J. Biol. Chem.*, **269**(14), 10444–10450. [PubMed :8144628]. *Cité page 11*

Derossi, D., Calvet, S., Trembleau, A., Brunissen, A., Chassaing, G., & Prochiantz, A. 1996. Cell internalization of the third helix of the Antennapedia homeodomain is receptor-independent. *J. Biol. Chem.*, **271**(30), 18188–18193. [PubMed :8663410]. *Cité page 11*

Deshane, J., Garner, C. C., & Sontheimer, H. 2003. Chlorotoxin inhibits glioma cell invasion via matrix metalloproteinase-2. *J. Biol. Chem.*, **278**(6), 4135–4144. [DOI :10.1074/jbc.M205662200] [PubMed :12454020]. *Cité page 7*

Dias, D. A., Urban, S., & U., Roessner. 2012. A Historical Overview of Natural Products in Drug Discovery. *Metabolites*, **2**(2), 303–336. *2 citations pages 3 et 4*

Esteve, E., Smida-Rezgui, S., Sarkozi, S., Szegedi, C., Regaya, I., Chen, L., Altafaj, X., Rochat, H., Allen, P., Pessah, I. N., Marty, I., Sabatier, J. M., Jona, I., De Waard, M., & Ronjat, M. 2003. Critical amino acid residues determine the binding affinity and the Ca2+ release efficacy of maurocalcine in skeletal muscle cells. *J. Biol. Chem.*, **278**(39), 37822–37831. [DOI :10.1074/jbc.M305798200] [PubMed :12869557]. *Cité page 23*

Esteve, E., Mabrouk, K., Dupuis, A., Smida-Rezgui, S., Altafaj, X., Grunwald, D., Platel, J. C., Andreotti, N., Marty, I., Sabatier, J. M., Ronjat, M., & De Waard, M. 2005. Transduction of the scorpion toxin maurocalcine into cells. Evidence that the toxin crosses the plasma membrane. *J. Biol. Chem.*, **280**(13), 12833–12839. [PubMed Central :PMC2713311] [DOI :10.1074/jbc.M412521200] [PubMed :15653689]. *3 citations pages 24, 26, et 121*

Fajloun, Z., Kharrat, R., Chen, L., Lecomte, C., Di Luccio, E., Bichet, D., El Ayeb, M., Rochat, H., Allen, P. D., Pessah, I. N., De Waard, M., & Sabatier, J. M. 2000. Chemical synthesis and characterization of maurocalcine, a scorpion toxin that activates Ca(2+) release channel/ryanodine receptors. *FEBS Lett.*, **469**(2-3), 179–185. [PubMed :10713267]. *3 citations pages 6, 21, et 22*

Frankel, A. D., & Pabo, C. O. 1988. Cellular uptake of the tat protein from human immunodeficiency virus. *Cell*, **55**(6), 1189–1193. [PubMed :2849510]. *Cité page 10*

Fu, Y. J., Yin, L. T., Liang, A. H., Zhang, C. F., Wang, W., Chai, B. F., Yang, J. Y., & Fan, X. J. 2007. Therapeutic potential of chlorotoxin-like neurotoxin from the Chinese scorpion for human gliomas. *Neurosci. Lett.*, **412**(1), 62–67. [DOI :10.1016/j.neulet.2006.10.056] [PubMed :17166663]. *Cité page 7*

Garcia-Martin, M. L., Herigault, G., Remy, C., Farion, R., Ballesteros, P., Coles, J. A., Cerdan, S., & Ziegler, A. 2001. Mapping extracellular pH in rat brain gliomas in vivo by 1H magnetic resonance spectroscopic imaging : comparison with maps of metabolites. *Cancer Res.*, **61**(17), 6524–6531. [PubMed :11522650]. *2 citations pages 68 et 122*

Gauldie, J., Hanson, J. M., Rumjanek, F. D., Shipolini, R. A., & Vernon, C. A. 1976. The peptide components of bee venom. *Eur. J. Biochem.*, **61**(2), 369–376. [PubMed :1248464]. *Cité page 8*

Gehring, W. J., Qian, Y. Q., Billeter, M., Furukubo-Tokunaga, K., Schier, A. F., Resendez-Perez, D., Affolter, M., Otting, G., & Wuthrich, K. 1994. Homeodomain-DNA recognition. *Cell*, **78**(2), 211–223. [PubMed :8044836]. *Cité page 11*

Graf, N., Mokhtari, T. E., Papayannopoulos, I. A., & Lippard, S. J. 2012. Platinum(IV)-chlorotoxin (CTX) conjugates for targeting cancer cells. *J. Inorg. Biochem.*, **110**(May), 58–63. [PubMed Central :PMC3350571] [DOI :10.1016/j.jinorgbio.2012.02.012] [PubMed :22465700]. *3 citations pages 8, 121, et 124*

Gurrola, G. B., Capes, E. M., Zamudio, F. Z., Possani, L. D., & Valdivia, H. H. 2010. Imperatoxin A, a Cell-Penetrating Peptide from Scorpion Venom, as a Probe of Ca-Release Channels/Ryanodine Receptors. *Pharmaceuticals (Basel)*, **3**(4), 1093–1107. [PubMed Central :PMC2910439] [DOI :10.3390/ph3041093] [PubMed :20668646]. *2 citations pages 12 et 121*

Hannon, H. E., & Atchison, W. D. 2013. Omega-conotoxins as experimental tools and therapeutics in pain management. *Mar Drugs*, **11**(3), 680–699. [PubMed Central :PMC3705365] [DOI :10.3390/md11030680] [PubMed :23470283]. *Cité page 6*

Harvey, A. L. 2008. Natural products in drug discovery. *Drug Discov. Today*, **13**(19-20), 894–901. [DOI :10.1016/j.drudis.2008.07.004] [PubMed :18691670]. *Cité page 3*

Heitz, F., Morris, M. C., & Divita, G. 2009. Twenty years of cell-penetrating peptides : from molecular mechanisms to therapeutics. *Br. J. Pharmacol.*, **157**(2), 195–206. [PubMed Central :PMC2697800] [DOI :10.1111/j.1476-5381.2009.00057.x] [PubMed :19309362]. *Cité page 16*

Hockaday, D. C., Shen, S., Fiveash, J., Raubitschek, A., Colcher, D., Liu, A., Alvarez, V., & Mamelak, A. N. 2005. Imaging glioma extent with 131I-TM-601. *J. Nucl. Med.*, **46**(4), 580–586. [PubMed :15809479]. *Cité page 8*

Hood, J. L., Jallouk, A. P., Campbell, N., Ratner, L., & Wickline, S. A. 2013. Cytolytic nanoparticles attenuate HIV-1 infectivity. *Antivir. Ther. (Lond.)*, **18**(1), 95–103. [DOI :10.3851/IMP2346] [PubMed :22954649]. *2 citations pages et 9*

Hugues, M., Romey, G., Duval, D., Vincent, J. P., & Lazdunski, M. 1982. Apamin as a selective blocker of the calcium-dependent potassium channel in neuroblastoma cells : voltage-clamp and biochemical characterization of the toxin receptor. *Proc. Natl. Acad. Sci. U.S.A.*, **79**(4), 1308–1312. [PubMed Central :PMC345952] [PubMed :6122211]. *Cité page 5*

Jayagopal, A., Su, Y. R., Blakemore, J. L., Linton, M. F., Fazio, S., & Haselton, F. R. 2009. Quantum dot mediated imaging of atherosclerosis. *Nanotechnology*, **20**(16),

165102. [PubMed Central :PMC2718756] [DOI :10.1088/0957-4484/20/16/165102] [PubMed :19420562]. *Cité page 26*

Jenkinson, D. H. 2006. Potassium channels–multiplicity and challenges. *Br. J. Pharmacol.*, **147 Suppl 1**(Jan), 63–71. [PubMed Central :PMC1760724] [DOI :10.1038/sj.bjp.0706447] [PubMed :16402122]. *Cité page 5*

Joliot, A., Pernelle, C., Deagostini-Bazin, H., & Prochiantz, A. 1991. Antennapedia homeobox peptide regulates neural morphogenesis. *Proc. Natl. Acad. Sci. U.S.A.*, **88**(5), 1864–1868. [PubMed Central :PMC51126] [PubMed :1672046]. *Cité page 11*

Kerkis, A., Kerkis, I., Radis-Baptista, G., Oliveira, E. B., Vianna-Morgante, A. M., Pereira, L. V., & Yamane, T. 2004. Crotamine is a novel cell-penetrating protein from the venom of rattlesnake Crotalus durissus terrificus. *FASEB J.*, **18**(12), 1407–1409. [DOI :10.1096/fj.03-1459fje] [PubMed :15231729]. *2 citations pages 11 et 12*

Kharrat, R., Mabrouk, K., Crest, M., Darbon, H., Oughideni, R., Martin-Eauclaire, M. F., Jacquet, G., el Ayeb, M., Van Rietschoten, J., Rochat, H., & Sabatier, J. M. 1996. Chemical synthesis and characterization of maurotoxin, a short scorpion toxin with four disulfide bridges that acts on K+ channels. *Eur. J. Biochem.*, **242**(3), 491–498. [PubMed :9022673]. *Cité page 5*

Kingston, D. G. 2007. The shape of things to come : structural and synthetic studies of taxol and related compounds. *Phytochemistry*, **68**(14), 1844–1854. [PubMed Central :PMC1979092] [DOI :10.1016/j.phytochem.2006.11.009] [PubMed :17184797]. *Cité page 3*

Knapp, O., McArthur, J. R., & Adams, D. J. 2012. Conotoxins targeting neuronal voltage-gated sodium channel subtypes : potential analgesics ? *Toxins (Basel)*, **4**(11), 1236–1260. [PubMed Central :PMC3509706] [DOI :10.3390/toxins4111236] [PubMed :23202314]. *Cité page 5*

Kumari, S., Mg, S., & Mayor, S. 2010. Endocytosis unplugged : multiple ways to enter the cell. *Cell Res.*, **20**(3), 256–275. [DOI :10.1038/cr.2010.19] [PubMed :20125123]. *Cité page 15*

Lewis, R. J., Dutertre, S., Vetter, I., & Christie, M. J. 2012. Conus venom peptide pharmacology. *Pharmacol. Rev.*, **64**(2), 259–298. [DOI :10.1124/pr.111.005322] [PubMed :22407615]. *Cité page 6*

Lim, K. J., Sung, B. H., Shin, J. R., Lee, Y. W., Kim, D. J., Yang, K. S., & Kim, S. C. 2013. Correction : A Cancer Specific Cell-Penetrating Peptide, BR2, for the Efficient Delivery of an scFv into Cancer Cells. *PLoS ONE*, **8**(11). [PubMed Central :PMC3829981] [DOI :10.1371/annotation/fb854e6a-cc9e-4446-b50a-5318cffb68c5] [PubMed :24260084]. *Cité page 19*

Ma, Z., Kong, J., Gordon, D., Gurevitz, M., Azam, L., & Kallen, R. G. 2012. Direct Evidence that Scorpion α-Toxins (Site-3) Modulate Sodium Channel Inactivation by Hindrance of Voltage-Sensor Movements. *Plos One.*, **8**(11). *Cité page 5*

Mabrouk, K., Ram, N., Boisseau, S., Strappazzon, F., Rehaim, A., Sadoul, R., Darbon, H., Ronjat, M., & De Waard, M. 2007. Critical amino acid residues of maurocalcine involved in pharmacology, lipid interaction and cell penetration. *Biochim. Biophys. Acta*, **1768**(10), 2528–2540. [DOI :10.1016/j.bbamem.2007.06.030] [PubMed :17888395]. *Cité page 24*

Margus, H., Padari, K., & Pooga, M. 2012. Cell-penetrating peptides as versatile vehicles for oligonucleotide delivery. *Mol. Ther.*, **20**(3), 525–533. [PubMed Central :PMC3293609] [DOI :10.1038/mt.2011.284] [PubMed :22233581]. *Cité page 18*

Mayer, A. M., Glaser, K. B., Cuevas, C., Jacobs, R. S., Kem, W., Little, R. D., McIntosh, J. M., Newman, D. J., Potts, B. C., & Shuster, D. E. 2010. The odyssey of marine pharmaceuticals : a current pipeline perspective. *Trends Pharmacol. Sci.*, **31**(6), 255–265. [DOI :10.1016/j.tips.2010.02.005] [PubMed :20363514]. *Cité page 4*

McCleskey, E. W., Fox, A. P., Feldman, D. H., Cruz, L. J., Olivera, B. M., Tsien, R. W., & Yoshikami, D. 1987. Omega-conotoxin : direct and persistent blockade of specific types of calcium channels in neurons but not muscle. *Proc. Natl. Acad. Sci. U.S.A.*, **84**(12), 4327–4331. [PubMed Central :PMC305078] [PubMed :2438698]. *Cité page 6*

McGivern, J. G. 2007. Ziconotide : a review of its pharmacology and use in the treatment of pain. *Neuropsychiatr Dis Treat*, **3**(1), 69–85. [PubMed Central :PMC2654521] [PubMed :19300539]. *Cité page 8*

Mehta, A., Shervington, A., Howl, J., Jones, S., & Shervington, L. 2013. Can RNAi-mediated hsp90Î± knockdown in combination with 17-AAG be a therapy for glioma? *FEBS Open Bio*, **3**, 271–278. [PubMed Central :PMC3722647] [DOI :10.1016/j.fob.2013.06.002] [PubMed :23905009]. *Cité page 19*

Mohandessi, S., Rajendran, M., Magda, D., & Miller, L. W. 2012. Cell-penetrating peptides as delivery vehicles for a protein-targeted terbium complex. *Chemistry*, **18**(35), 10825–10829. [PubMed Central :PMC3729426] [DOI :10.1002/chem.201201805] [PubMed :22807190]. *Cité page 17*

Morris, M. C., Vidal, P., Chaloin, L., Heitz, F., & Divita, G. 1997. A new peptide vector for efficient delivery of oligonucleotides into mammalian cells. *Nucleic Acids Res.*, **25**(14), 2730–2736. [PubMed Central :PMC146800] [PubMed :9207018]. *Cité page 11*

Morris, M. C., Depollier, J., Mery, J., Heitz, F., & Divita, G. 2001. A peptide carrier for the delivery of biologically active proteins into mammalian cells. *Nat. Biotechnol.*, **19**(12), 1173–1176. [DOI :10.1038/nbt1201-1173] [PubMed :11731788]. *Cité page 11*

Mosbah, A., Kharrat, R., Fajloun, Z., Renisio, J. G., Blanc, E., Sabatier, J. M., El Ayeb, M., & Darbon, H. 2000. A new fold in the scorpion toxin family, associated with an activity on a ryanodine-sensitive calcium channel. *Proteins*, **40**(3), 436–442. [PubMed :10861934]. *Cité page 22*

Newman, D. J., & Cragg, G. M. 2012. Natural products as sources of new drugs over the 30 years from 1981 to 2010. *J. Nat. Prod.*, **75**(3), 311–335. [PubMed Central :PMC3721181] [DOI :10.1021/np200906s] [PubMed :22316239]. *Cité page 3*

Olson, E. S., Jiang, T., Aguilera, T. A., Nguyen, Q. T., Ellies, L. G., Scadeng, M., & Tsien, R. Y. 2010. Activatable cell penetrating peptides linked to nanoparticles as dual probes for in vivo fluorescence and MR imaging of proteases. *Proc. Natl. Acad. Sci. U.S.A.*, **107**(9), 4311–4316. [PubMed Central :PMC2840175] [DOI :10.1073/pnas.0910283107] [PubMed :20160077]. *Cité page 20*

Padari, K., Saalik, P., Hansen, M., Koppel, K., Raid, R., Langel, U., & Pooga, M. 2005. Cell transduction pathways of transportans. *Bioconjug. Chem.*, **16**(6), 1399–1410. [DOI :10.1021/bc050125z] [PubMed :16287236]. *Cité page 11*

Park, C. B., Kim, M. S., & Kim, S. C. 1996. A novel antimicrobial peptide from Bufo bufo gargarizans. *Biochem. Biophys. Res. Commun.*, **218**(1), 408–413. [DOI :10.1006/bbrc.1996.0071] [PubMed :8573171]. *Cité page 19*

Poillot, C., Dridi, K., Bichraoui, H., Pecher, J., Alphonse, S., Douzi, B., Ronjat, M., Darbon, H., & De Waard, M. 2010. D-Maurocalcine, a pharmacologically inert efficient

cell-penetrating peptide analogue. *J. Biol. Chem.*, **285**(44), 34168–34180. [PubMed Central :PMC2962515] [DOI :10.1074/jbc.M110.104919] [PubMed :20610396]. *3 citations pages , 22, et 25*

Pooga, M., Hallbrink, M., Zorko, M., & Langel, U. 1998. Cell penetration by transportan. *FASEB J.*, **12**(1), 67–77. [PubMed :9438412]. *2 citations pages 11 et 13*

Pooga, M., Kut, C., Kihlmark, M., Hallbrink, M., Fernaeus, S., Raid, R., Land, T., Hallberg, E., Bartfai, T., & Langel, U. 2001. Cellular translocation of proteins by transportan. *FASEB J.*, **15**(8), 1451–1453. [PubMed :11387254]. *Cité page 11*

Pringos, E., Vignes, M., Martinez, J., & Rolland, V. 2011. Peptide neurotoxins that affect voltage-gated calcium channels : a close-up on Ï‰-agatoxins. *Toxins (Basel)*, **3**(1), 17–42. [PubMed Central :PMC3210452] [DOI :10.3390/toxins3010017] [PubMed :22069688]. *Cité page 6*

Qian, Y. Q., Billeter, M., Otting, G., Muller, M., Gehring, W. J., & Wuthrich, K. 1989. The structure of the Antennapedia homeodomain determined by NMR spectroscopy in solution : comparison with prokaryotic repressors. *Cell*, **59**(3), 573–580. [PubMed :2572329]. *Cité page 11*

Ram, N., Weiss, N., Texier-Nogues, I., Aroui, S., Andreotti, N., Pirollet, F., Ronjat, M., Sabatier, J. M., Darbon, H., Jacquemond, V., & De Waard, M. 2008a. Design of a disulfide-less, pharmacologically inert, and chemically competent analog of maurocalcine for the efficient transport of impermeant compounds into cells. *J. Biol. Chem.*, **283**(40), 27048–27056. [PubMed Central :PMC2652642] [DOI :10.1074/jbc.M804727200] [PubMed :18621738]. *Cité page 25*

Ram, N., Aroui, S., Jaumain, E., Bichraoui, H., Mabrouk, K., Ronjat, M., Lortat-Jacob, H., & De Waard, M. 2008b. Direct peptide interaction with surface glycosaminoglycans contributes to the cell penetration of maurocalcine. *J. Biol. Chem.*, **283**(35), 24274–24284. [PubMed Central :PMC2701444] [DOI :10.1074/jbc.M709971200] [PubMed :18603532]. *2 citations pages 25 et 121*

Ransom, C. B., O'Neal, J. T., & Sontheimer, H. 2001. Volume-activated chloride currents contribute to the resting conductance and invasive migration of human glioma cells. *J. Neurosci.*, **21**(19), 7674–7683. [PubMed :11567057]. *Cité page 6*

Regaya, I., Beeton, C., Ferrat, G., Andreotti, N., Darbon, H., De Waard, M., & Sabatier, J. M. 2004. Evidence for domain-specific recognition of SK and Kv channels by MTX and HsTx1 scorpion toxins. *J. Biol. Chem.*, **279**(53), 55690–55696. [DOI :10.1074/jbc.M410055200] [PubMed :15498765]. *Cité page 5*

Richard, J. P., Melikov, K., Vives, E., Ramos, C., Verbeure, B., Gait, M. J., Chernomordik, L. V., & Lebleu, B. 2003. Cell-penetrating peptides. A reevaluation of the mechanism of cellular uptake. *J. Biol. Chem.*, **278**(1), 585–590. [DOI :10.1074/jbc.M209548200] [PubMed :12411431]. *Cité page 10*

Richard, J. P., Melikov, K., Brooks, H., Prevot, P., Lebleu, B., & Chernomordik, L. V. 2005. Cellular uptake of unconjugated TAT peptide involves clathrin-dependent endocytosis and heparan sulfate receptors. *J. Biol. Chem.*, **280**(15), 15300–15306. [DOI :10.1074/jbc.M401604200] [PubMed :15687490]. *Cité page 10*

Shai, Y., & Oren, Z. 2001. From "carpet" mechanism to de-novo designed diastereomeric cell-selective antimicrobial peptides. *Peptides*, **22**(10), 1629–1641. [PubMed :11587791]. *2 citations pages et 13*

Shiraishi, T., & Nielsen, P. E. 2011. Peptide nucleic acid (PNA) cell penetrating peptide (CPP) conjugates as carriers for cellular delivery of antisense oligomers. *Artif DNA PNA XNA*, **2**(3), 90–99. [PubMed Central :PMC3324339] [PubMed :22567192]. *Cité page 17*

Sodroski, J., Patarca, R., Rosen, C., Wong-Staal, F., & Haseltine, W. 1985. Location of the trans-activating region on the genome of human T-cell lymphotropic virus type III. *Science*, **229**(4708), 74–77. [PubMed :2990041]. *Cité page 10*

Soman, N. R., Baldwin, S. L., Hu, G., Marsh, J. N., Lanza, G. M., Heuser, J. E., Arbeit, J. M., Wickline, S. A., & Schlesinger, P. H. 2009. Molecularly targeted nanocarriers deliver the cytolytic peptide melittin specifically to tumor cells in mice, reducing tumor growth. *J. Clin. Invest.*, **119**(9), 2830–2842. [PubMed Central :PMC2735896] [DOI :10.1172/JCI38842] [PubMed :19726870]. *3 citations pages 9, 121, et 125*

Spratt, B. G. 2012. The 2011 Garrod Lecture : From penicillin-binding proteins to molecular epidemiology. *J. Antimicrob. Chemother.*, **67**(7), 1578–1588. [PubMed Central :PMC3370820] [DOI :10.1093/jac/dks109] [PubMed :22457311]. *Cité page 4*

Suzuki, T., Futaki, S., Niwa, M., Tanaka, S., Ueda, K., & Sugiura, Y. 2002. Possible existence of common internalization mechanisms among arginine-rich peptides. *J. Biol.*

Chem., **277**(4), 2437–2443. [DOI :10.1074/jbc.M110017200] [PubMed :11711547]. *Cité page 10*

Temsamani, J., & Vidal, P. 2004. The use of cell-penetrating peptides for drug delivery. *Drug Discov. Today*, **9**(23), 1012–1019. [DOI :10.1016/S1359-6446(04)03279-9] [PubMed :15574317]. *Cité page 17*

Terlau, H., & Olivera, B. M. 2004. Conus venoms : a rich source of novel ion channel-targeted peptides. *Physiol. Rev.*, **84**(1), 41–68. [DOI :10.1152/physrev.00020.2003] [PubMed :14715910]. *Cité page 6*

van den Bogaart, G., Guzman, J. V., Mika, J. T., & Poolman, B. 2008. On the mechanism of pore formation by melittin. *J. Biol. Chem.*, **283**(49), 33854–33857. [PubMed Central :PMC2662212] [DOI :10.1074/jbc.M805171200] [PubMed :18819911]. *Cité page 8*

van Rietschoten, J., Granier, C., Rochat, H., Lissitzky, S., & Miranda, F. 1975. Synthesis of apamin, a neurotoxic peptide from bee venom. *Eur. J. Biochem.*, **56**(1), 35–40. [PubMed :1175625]. *Cité page 5*

Vives, E., Brodin, P., & Lebleu, B. 1997. A truncated HIV-1 Tat protein basic domain rapidly translocates through the plasma membrane and accumulates in the cell nucleus. *J. Biol. Chem.*, **272**(25), 16010–16017. [PubMed :9188504]. *Cité page 10*

Waszkielewicz, A. M., Gunia, A., Szkaradek, N., Sloczynska, K., Krupinska, S., & Marona, H. 2013. Ion channels as drug targets in central nervous system disorders. *Curr. Med. Chem.*, **20**(10), 1241–1285. [PubMed Central :PMC3706965] [PubMed :23409712]. *3 citations pages 4, 5, et 6*

Wender, P. A., Mitchell, D. J., Pattabiraman, K., Pelkey, E. T., Steinman, L., & Rothbard, J. B. 2000. The design, synthesis, and evaluation of molecules that enable or enhance cellular uptake : peptoid molecular transporters. *Proc. Natl. Acad. Sci. U.S.A.*, **97**(24), 13003–13008. [PubMed Central :PMC27168] [DOI :10.1073/pnas.97.24.13003] [PubMed :11087855]. *Cité page 10*

Zhang, M. M., Green, B. R., Catlin, P., Fiedler, B., Azam, L., Chadwick, A., Terlau, H., McArthur, J. R., French, R. J., Gulyas, J., Rivier, J. E., Smith, B. J., Norton, R. S., Olivera, B. M., Yoshikami, D., & Bulaj, G. 2007. Structure/function characterization of micro-conotoxin KIIIA, an analgesic, nearly irreversible blocker of mammalian neuronal sodium channels. *J. Biol. Chem.*, **282**(42), 30699–30706. [DOI :10.1074/jbc.M704616200] [PubMed :17724025]. *2 citations pages 5 et 121*

Résumé

La maurocalcine (MCa) est une toxine de 33 acides aminés initialement issue du venin du scorpion *Scorpio maurus palmatus*, et est considérée comme faisant partie de la famille des CPP (Cell Penetrating Peptides) depuis de nombreuses années déjà. La MCa présente donc un intérêt thérapeutique certain dans le domaine de la délivrance intracellulaire de cargos, et les travaux exposés ici cherchent à caractériser au mieux les propriétés de pénétration de la molécule native ainsi que celle de certains de ses variants.

Après avoir quantifié l'internalisation de plusieurs variants tronqués (linéaires), j'ai pu mettre en évidence le fait que tous ces analogues testés ont une capacité à être internalisés bien plus élevée que celle des CPP de référence (notamment Tat et la pénétratine). Parmi ces variants, l'analogue MC$a_{\mathrm{UF1-9}}$ présente l'avantage d'un temps de rétention relativement élevé au sein des cellules, ainsi que d'une accumulation légèrement accrue en environnement acide (ce qui advient lors de la formation tumeurs solides). Ce nouveau CPP possède donc un certain potentiel thérapeutique mais l'étude de la MCa native, remarquablement stable *in vivo*, reste plus que jamais d'actualité.

Mots clés : maurocalcine, toxine animale, peptides de pénétration cellulaire

Abstract

Maurocalcine (MCa) is a 33-mer toxin originally isolated from the venom of the scorpio *Scorpio maurus palmatus*, and has been considered as a cell-penetrating peptide (CPP) for several years. MCa presents a therapeutic interest for the intracellular delivery of cargoes, and this thesis aims to characterise the cell penetration properties of the native molecule as well as some of its variants'.

After quantifying several truncated (linear) variants' internalisation, I have been able to highlight the fact that all of those analogs possess a higher internalization ability than those of standard CPP (especially Tat and penetratin). Among those variants, the analog MC$a_{\mathrm{UF1-9}}$ has a relatively high rentention time within cells, as well as a slightly increased accumulation when in an acidic environment (which occurs during solid tumours formation). This new CPP shows a certain therapeutic potential but the study of native MCa, remarkably stable *in vivo*, remains a priority.

Keywords : maurocalcine, animal toxin, cell-penetrating peptides